Seizures, spreading depolarizations and sudden death

Jansen, N.A.

Seizures, spreading depolarizations and sudden death

Nico Adrian Jansen

Seizures, spreading depolarizations and sudden death

Nico Adrian Jansen

Seizures, spreading depolarizations and sudden death
PhD thesis, Leiden University, Leiden, The Netherlands, 2025

ISBN: 978-94-6496-522-3
Cover design and lay-out: Miranda Pouw, Mirakels Ontwerp
Printing: Gildeprint

The research presented in this thesis was supported by grants of the Dutch National Epilepsy Foundation (2017-10), CURE SUDEP (280560), EU IAPP Program BRAINPATH (612360), the European Innovation Council EIC Pathfinder Program Project MICROVASC (101070917), EU Joint Program REBALANCE (10510062210003) and the Medical Delta program "Medical NeuroDelta: Ambulant Neuromonitoring for Prevention and Treatment of Brain Disease". The funding agencies had no role in the design or conduct of the studies.

Seizures, spreading depolarizations and sudden death

Proefschrift

ter verkrijging van
de graad van doctor aan de Universiteit Leiden,
op gezag van rector magnificus prof. dr. S. de Rijcke,
volgens besluit van het college voor promoties
te verdedigen op woensdag 11 maart 2026
klokke 13.00 uur

door

Nico Adrian Jansen

geboren te Town of Urbana, Verenigde Staten
in 1991

PROMOTOR(ES), CO-PROMOTOR(ES), LEDEN PROMOTIECOMMISSIE

Promotor

Prof. dr. A.M.J.M. van den Maagdenberg

Co-promotor

Dr. E.A. Tolner

Promotiecommissie

Prof. dr. J.J.G.M. Verschuuren	
Prof. dr. ir. L. van der Weerd	
Prof. dr. C.I. de Zeeuw	Erasmus Medisch Centrum Rotterdam
Prof. dr. M.J.A.M. van Putten	Universiteit Twente

Voor Olivier
en mijn lieve meisjes

CONTENTS

Chapter 1

General introduction

GENERAL INTRODUCTION

The brain and its episodic disorders

The structure of the brain and the dynamics it produces to drive thought and behavior are complex. Naturally, brain dynamics – often studied by the electrical fields they produce – require time to be expressed, and over time these dynamics show recurring patterns, or *periodicity*. This periodicity has been hypothesized to allow the brain to guide behaviors and anticipate perturbations, in effect functioning as a "foretelling device".[1] To achieve this, recurring patterns produced by oscillators far removed from one another in the brain need to synchronize. The architecture required to produce such synchronization however may result in an inherent susceptibility to episodic neurological disorders. These disorders are characterized by recurring changes in brain dynamics that cause episodes of neurological dysfunction. Two episodic neurological disorders that are associated with particularly dramatic changes in electrical fields are epilepsy and migraine with aura, which will be the focus of this thesis. Paradoxically, the same architecture that allows hard-to-predict epileptic seizures and migraine episodes to occur, is believed to allow the brain to function as a "foretelling device".

The structure of the brain and spinal cord (together referred to as the central nervous system) was at first considered a continuum – that is, it was believed to lack membrane boundaries. Since the late 19th and early 20th century, the "neuron doctrine" became the dominant theory, dictating that the central nervous system is composed of individual cells.[2] Although neurons have received most attention in the literature, glial cells – which support neuronal functioning and include astrocytes, oligodendrocytes and microglia – have become of growing interest later over the course of the 20th and 21st century (Figure 1).

A neuron may be conceptualized as a battery: its plasma membrane is polarized, which is brought about by an unequal distribution of cations and anions on either side. Similar to a battery, this chemical energy can be "utilized" by the neuron to generate electric potentials or action potentials, which are considered the dominant mode of neuronal communication. The neuronal plasma membrane is more permeable to K^+ than to other cations, resulting in a net outflow of K^+ and hence a negative membrane potential. During an action potential, the membrane is depolarized by small ion fluxes through opening of specific (mainly Na^+) ion channels. Repolarization is mainly achieved by opening of K^+ channels, allowing even more outflow of K^+. Although action potentials are an efficient means of communications by having relatively little effect on ion concentrations in the bulk intra- and extracellular space,[3] this efficiency relies on fast recovery of these ion distributions. This is mainly achieved by the Na^+/K^+ ATPase pump, which transports Na^+ out and K^+ into neurons, with the chief aim to maintain a polarized membrane (i.e. excitability). In addition, to control the (gradual) buildup of extracellular K^+ due to neuronal activity, Na^+/K^+ ATPase pumps in glial cells are required. By opposing the concentration gradients of these cations, this process costs approximately 50% of the total energy consumed by the brain.[4]

FIGURE 1. Trends in usage of the term *neuron* and three subtypes of glial cells from English sources contained in the Google Books corpus.

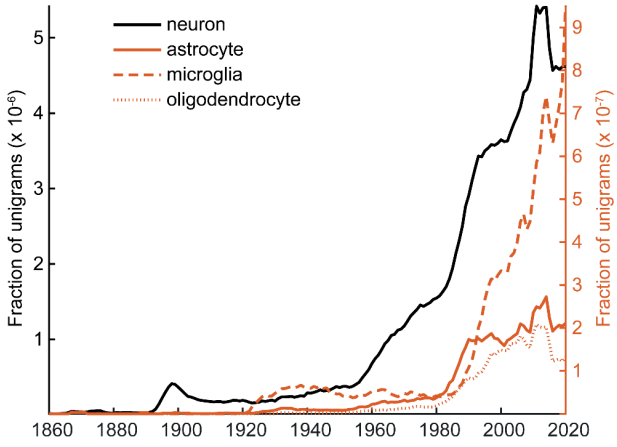

Note that the term *neuron* increased in frequency from the late 19th century onward, while the other terms followed later. Source: Google Books Ngram Viewer.

Excessive neuronal activity, seizures and spreading depolarizations

These electrochemical characteristics underlying membrane potential changes allow neurons to "fire" action potentials at high metabolic efficiency. A potential downside of this high efficiency is that neurons can become excessively activated and, by recruiting sufficient neurons through synchronization, produce *seizures*.[5] Seizures can be induced in a large variety of experimental (animal) models.[6] Seizures that occur in humans and in these models show similar features and are therefore considered naturally inherent to brain tissue.[7]

Almost 80 years ago, the pioneering Brazilian neuroscientist Aristides Leão attempted to characterize the electrical activity associated with cortical seizures in rabbits. When creating conditions of high excitability in the cortex, he surprisingly found a lasting reduction in spontaneous neuronal activity.[8] This decrease in activity was associated with a slow negative voltage shift in the recordings, which he could replicate by occlusion of the major brain arteries.[9] Later studies showed that this phenomenon was caused by sustained depolarization of neurons,[10] resulting from a profound decrease in ion gradients across their membrane.[11] This sustained depolarization propagated slowly through brain tissue, at a rate of a few millimeters per minute, and is therefore now referred to as a *spreading depolarization* (SD). The lasting reduction in spontaneous activity that was already observed by Leão was termed *spreading depression*,[8] that is initiated by the sustained depolarization exceeding the inactivation threshold of action potential-generating membrane channels.[12, 13] These characteristics of SD are fundamentally different from those of a seizure: in

general, seizures propagate at much faster rates throughout the brain, while neurons affected by it maintain their ability to fire action potentials. In keeping with the neuron-battery analogy: while a seizure-state is equivalent to a battery discharging in tandem, an SD-state corresponds to it being short-circuited.[14]

Despite these fundamental differences, both seizures and SDs result from conditions of high neuronal excitability. Similar factors promote seizures and SD, including high concentrations of K^+ and glutamate receptor agonists, low concentrations of Mg^{2+}, and electrical stimulation.[6, 15, 16] In addition, seizures and SDs have been observed in close association under experimental conditions,[17-20] as well as in the human brain for instance following trauma.[21] The deleterious effects of seizures and SDs on functioning of neuronal populations underscore the need to understand the mechanisms of these phenomena in episodic neurological disorders. In epilepsy and migraine with aura, the role of seizures and SD, respectively, are already well-established. Therefore, the remaining paragraphs of this introduction outline the involvement of seizures and SD in the pathophysiology of these two common episodic neurological disorders.

Spreading depolarizations in migraine with aura and epilepsy

Hyperexcitability within neuronal populations may result in SD that, in contrast to seizures, can only be appreciated using direct current (DC) coupled recordings,[22] which reliably capture the "infraslow" (<0.1 Hz) nature of the SD (Figure 2).

Spreading depolarizations are considered a very relevant aspect in the pathophysiology of migraine, as it is believed to be the underlying substrate of the aura phase.[23] Migraine is characterized by recurrent episodes of severe unilateral headache accompanied by nausea, photophobia and phonophobia.[24] Two main types of migraine are distinguished: migraine with aura, and migraine without aura.[24] The term "aura" refers to focal symptoms that are characteristically of visual nature, but may involve other sensory, phatic, motor or brainstem functions. These symptoms often show a characteristic spreading pattern, such as a scintillating scotoma that slowly expands within a visual field. SD was hypothesized to be the underlying cause of the aura symptoms already soon after its discovery,[25] and this hypothesis became (albeit many years later) widely accepted.[26, 27] Experimental evidence indicates that SD can activate trigeminal nociceptive pathways, potentially producing migraine headache.[28] As such, understanding the origin of SD in migraine is believed to allow improvement of migraine treatment.

FIGURE 2. DC recordings are required to reliably detect SD.

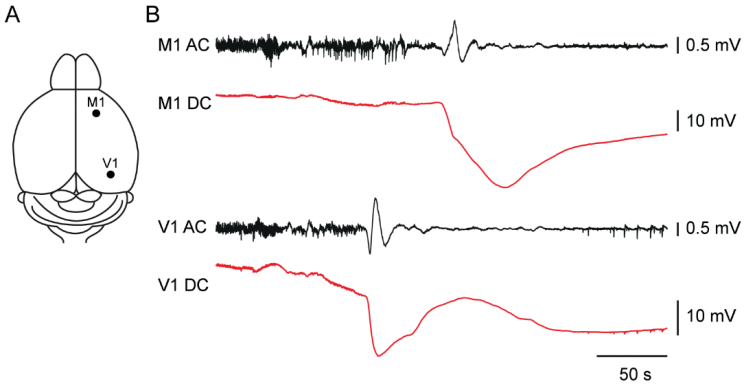

Example of a spontaneous SD recorded in a mouse model of familial hemiplegic type 2, detected by microelectrodes implanted in the primary motor (M1) and visual (V1) cortex **(A)**. Simultaneous alternating current (AC, bandpass filtered at 0.05 – 500 Hz) and DC (lowpass filtered at 500 Hz) recordings at these locations show slow potential changes during SD **(B)**. DC recordings show the magnitude of the depolarization that is lost in the AC recordings, despite the relatively wide bandpass filter settings. Note the suppression of AC signal following SD, representing the spreading depression. Source: Jansen NA et al., Spontaneous spreading depolarizations originate subcortically in a novel mouse model of familial hemiplegic migraine type 2, Neurobiology of Disease 2024;202:106714. Image reproduced with permission of the rights holder, Elsevier.

Experimental models of spreading depolarizations

An SD is an all-or-none depolarizing wave that propagates through gray matter.[15] The fact that it is an all-or-none phenomenon can be explained by the net cation flux across the neuronal membrane that turns persistently inward.[13] This inward current is generated by voltage-gated channels and/or increased extracellular K^+. SD can be initiated by depolarization of neurons via two major mechanisms: activation of neuronal voltage-gated Na^+ and/or Ca^{2+} channels, or inactivation of the Na^+/K^+ ATPase pump that is present on both neurons and astrocytes.[15, 29] Experimental stimuli that induce SD via (in)direct involvement of voltage-gated channels include chemical/pharmacological (with agents such as KCl, glutamate or N-methyl-D-aspartate (NMDA) receptor agonists), electrical or mechanical stimuli.[15, 30] On the other hand, experimental ischemia and/or hypoxia may induce SD via impairment of the Na^+/K^+ pump, which provides a mechanism for the observation of SD and the associated neuronal suppression in stroke.[14, 31] Although these experimental studies have informed us on diverse potential mechanisms of SD, they fail to faithfully model migraine-related SD, since this would require a model in which SDs occur spontaneously.

Genetic models of migraine and neuronal hyperexcitability

Relatives of migraine patients have an increased risk for the same disorder.[32] Whereas polymorphisms in many different genes in concert with environmental factors contribute to common forms of migraine, mutations in single genes underlie forms of familial hemiplegic migraine (FHM), a

subtype of migraine characterized by particularly severe aura, which may include hemiparesis, decreased consciousness, and coma.[33, 34] In the majority of hemiplegic migraine cases, a mutation in one of three genes is found: *CACNA1A* (FHM1), which encodes the pore-forming α1 subunit of $Ca_V2.1$ voltage-gated calcium channels expressed in neurons, *ATP1A2* (FHM2), which encodes the α2 subunit of the Na^+/K^+ ATPase pump, which is almost exclusively expressed in astrocytes in the adult brain, and *SCN1A* (FHM3), which encodes the α1 subunit of voltage-gated $Na_V1.1$ sodium channels expressed in neurons. The discovery of these pathogenic mutations has allowed the translational study of mechanisms underlying migraine-associated symptoms in model systems.[35] For all three FHM subtypes, specific mutations have been found in patients presenting both with migraine and epilepsy,[34, 36] providing a genetic target for research on these often comorbid disorders. In FHM1, the *CACNA1A* S218L missense mutation has been reported to cause both hemiplegic migraine and (lethal) seizures.[37] In FHM2, certain missense mutations in the *ATP1A2* gene can result in hemiplegic migraine and childhood epilepsy.[38] For FHM3, several missense mutations in *SCN1A* have been reported to cause childhood epilepsy,[39] in addition to hemiplegic migraine. Most importantly, increased susceptibility to experimentally induced cortical SD has been demonstrated in mouse models of FHM1[40, 41] and FHM2 (e.g.[42]). Such findings are attributed to enhanced neuronal excitability, albeit via different mechanisms (Figure 3). Similarly, common migraine is generally considered a condition characterized by hyperexcitability, which it shares with epilepsy. [43]

Why model spontaneous spreading depolarizations?

Similar to seizures in epilepsy, SD may be considered a paroxysmal manifestation of neuronal hyperexcitability underlying the aura phase in migraine. Yet, whereas spontaneous seizures have been widely reported in animal models of epilepsy, spontaneous SDs have not been reported in animal models of migraine. That this is a relevant shortcoming may be appreciated by reviewing recent progress in the field of epilepsy research. For example, inhibitory activity was found to be paradoxically increased prior to seizures in various epilepsy models,[44-46] which was also found in a model of Dravet syndrome (DS)[47], a severe epilepsy syndrome that in a majority of cases is caused by a mutation in the *SCN1A* gene. This illustrates that a theoretical framework that may provide a convincing explanation for hyperexcitability (in the case of DS, a decrease in GABAergic inhibition by *SCN1A*-encoded $Na_V1.1$ loss-of-function) may not be sufficient to explain the initiation of a seizure. Similarly, the initiation of an SD may not be accurately explained by enhanced release or impaired uptake of glutamate and/or K^+. Studying the conditions prior to spontaneous SD events could first of all allow a better understanding of how attacks of migraine (in particular those preceded by an aura) initiate. Second, it could help us understand why hyperexcitability sometimes results in seizures, but not in SD, and *vice versa*. And finally, the apparently intricate relation between seizures and SD could be better understood.

FIGURE 3. Affected proteins underlying neuronal hyperexcitability at the glutamatergic and GABAergic synapse in three FHM subtypes.

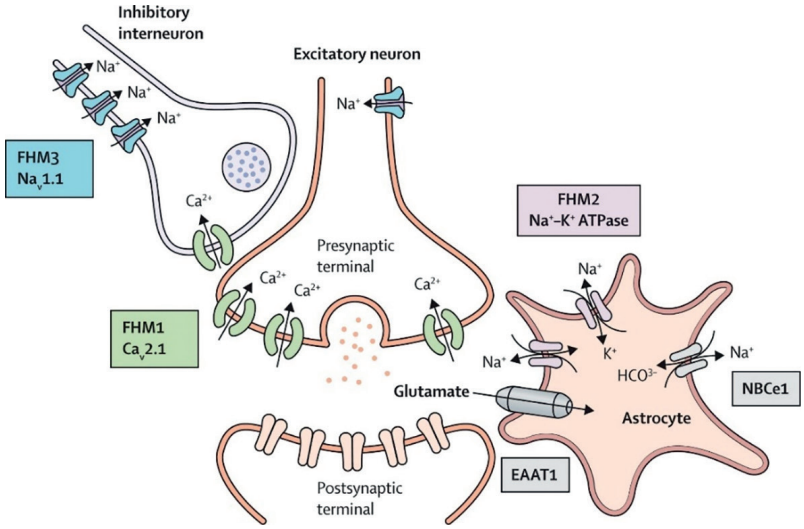

Source: Russell MB et al., Sporadic and familial hemiplegic migraine: pathophysiological mechanisms, clinical characteristics, diagnosis, and management, The Lancet Neurology 2011;10:457-470. Image reproduced with permission of the rights holder, The Lancet Neurology.

Spreading depolarizations in epilepsy

In its first description, SD-related spreading depression was already associated with seizure activity.[8] Since then, various studies have reported SD following induction of seizure activity in animal models,[18, 48-52] as well as following seizures in patients with cortical damage.[21] In addition, SD may occur following spontaneous seizures, as was shown for a DS mouse model.[53] It is important to note that although results from intracranial alternating current (AC) recordings are usually described in epilepsy animal models, direct current (DC) recordings much more rarely are. In addition, technical difficulties in acquiring a stable DC signal from scalp-EEG may explain the current lack of clinical evidence for seizure-related SD in epilepsy patients. It is thus very well possible that SD is a ubiquitous phenomenon in the seizing brain. The fact that SD is followed by neuronal inactivity is of potential benefit in this regard, since it may promote termination of seizure activity, although this has only been tested for chemically-induced prolonged seizure activity.[54] However, SD could be associated with adverse outcome if vital functions, that are otherwise preserved in the seizing brain, may become affected by it. A lethal consequence of such adverse outcome is *Sudden Unexpected Death in Epilepsy* (SUDEP).

Sudden Unexpected Death in Epilepsy

SUDEP is a post-mortem diagnosis defined as an unexpected non-traumatic and non-drowning death of a patient with epilepsy, in the absence of a structural or toxicological cause of death.[55] SUDEP can be diagnosed regardless of the presence of a seizure immediately preceding death, but prolonged seizures lasting ≥30 minutes are regarded as *status epilepticus*, an exclusion criterion for SUDEP.[56] The incidence rate of SUDEP has been established at 1.16 per 1,000 epilepsy patients,[57] but this is likely an underestimation: SUDEP reports mostly rely on death certificates, and incidence rates were found to be higher when medical charts and autopsy reports were available and taken into consideration.[58] Occurrence of generalized tonic-clonic seizures is the most important SUDEP risk factor, and thus development of treatment strategies to limit such seizures is considered to contribute to mitigating SUDEP risk.[59]

Mechanisms of Sudden Unexpected Death in Epilepsy

In the field of forensic medicine, the *cause* of death is distinguished from the *mechanism* of death. Whereas the first entails the disease, trauma or substance causing death, the latter entails the physiological sequence that results in death. In that sense, the knowledge gap between the cause and mechanism of death is substantial for SUDEP. Filling this gap is complicated by the fact that (1) SUDEP is rarely witnessed or recorded, and (2) measurement modalities are limited.

To address the former problem, studies have relied on data from non-lethal seizures to infer hypotheses on SUDEP mechanisms. Since cardiac arrythmias and changes in blood pressure are relatively common during seizures, failure of cardiac function was initially considered as the primary mechanism for SUDEP.[60] Later, a study that included a (relatively) large collection of SUDEP recordings – resulting from a collaborative effort involving epilepsy monitoring units around the world – collated electroencephalogram (EEG), respiratory and electrocardiogram (ECG) activity from 16 definite SUDEP cases.[61] Two important findings emerged from this study: (1) most SUDEP cases had proven seizure activity immediately prior to death, and (2) terminal apnea preceded cardiac arrest in all patients with sufficient quality cardiorespiratory recordings. A later study suggested postictal apnea as a promising biomarker for SUDEP risk.[62] Although seizure activity may not always be evident prior to SUDEP,[63] these recordings favor respiratory failure over cardiac arrythmia/arrest as a primary SUDEP mechanism.

Nevertheless, clinical SUDEP studies are severely limited by the measurement modalities employed, which is inherent to their retrospective nature. Development of preclinical models of SUDEP may help address this problem, since it allows measurements that are ethically or practically difficult to obtain clinically. Although in various models induced seizures can be lethal, animal models should ideally present spontaneous seizures to reproduce clinical SUDEP.[64]

Sudden Death in Epilepsy: a role for spreading depolarizations?

Various animal models have been developed that display fatal and non-fatal seizures. The DS mouse model is interesting in this regard since clinical DS is associated with an unusually high incidence

of seizure-related mortality and SUDEP.[65, 66] DS mice display a SUDEP phenotype that was initially explained by seizure-related severe bradycardia.[67] However, later this was refuted when parallel recordings of respiratory activity showed that apnea preceded bradycardia in DS mice.[68]

Although the ultimate "effector" of SUDEP may have shifted from cardiac to respiratory arrest, the effectual trigger is unknown. A focus on cardiac mechanisms and findings of mutated genes that are expressed in both brain and heart, explains why terms such as "neuro-cardiac channelopathies"[69] and "arrhythmogenic epilepsy"[70] have emerged that propose a mechanism for SUDEP by suggesting a predilection to cardiac arrythmias exacerbated by seizures. However, DS mice in which disruption the *Scn1a* gene was limited to brain tissue could still display fatal seizures.[67] Similarly, disruption of *Kcna1* – which was proposed to increase SUDEP risk by yielding a greater risk for cardiac arrythmias[71] – could still result in fatal seizures when expressed only in brain tissue.[72] Thus, seizure-related failure of neuronal control over vital functions is of increasing interest for SUDEP research.

FIGURE 4. The pre-Bötzinger complex is critical for respiratory rhythmogenesis.

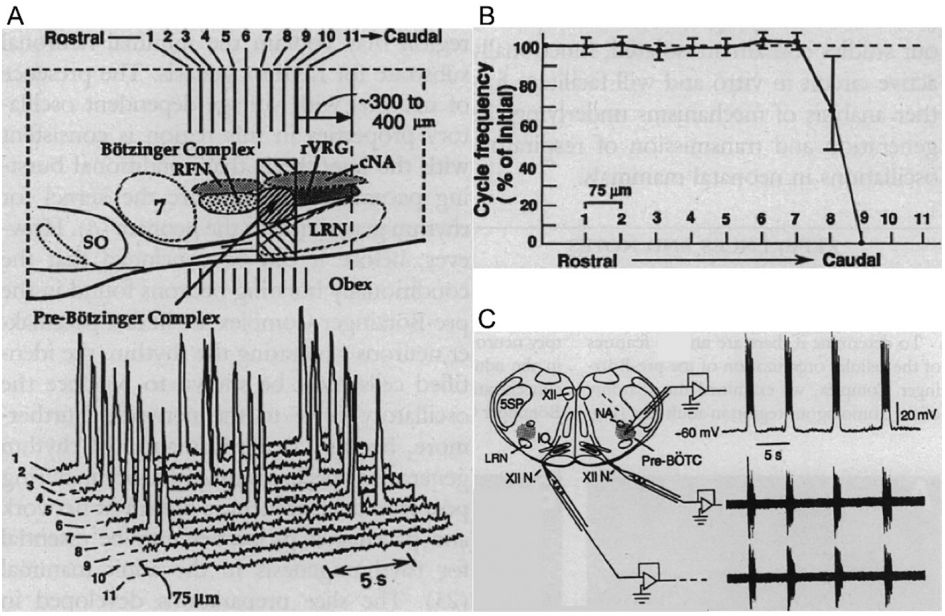

(A) Sagittal view of the rat medulla showing the level of serial microsections performed in a rostral to caudal direction (numbered) and their corresponding effect on breathing rhythm as recorded from phrenic motoneurons from C4 spinal ventral roots. Note the disruption (at location 8) and cessation (from location 9) of breathing rhythm, also shown in **(B)**. **(C)** Recordings in a thick medullary slice that include the pre-Bötzinger complex show respiratory rhythmogenesis, measured by motor output from the nucleus hypoglossus (XII N.). Source: Smith JC et al. Pre-Bötzinger complex: a brainstem region that may generate respiratory rhythm in mammals, Science 1991;254:726-729. Image reproduced with permission of the rights holder, The American Association for the Advancement of Science.

Whereas the (extracranial) sinoatrial node is the pacemaker of the cardiac rhythm, an intracranial structure is required for respiratory rhythmogenesis: the brainstem ventral respiratory column.[73, 74] At the core of this "central pattern generator" lies the pre-Bötzinger complex, which is both necessary and sufficient to produce the inspiratory phase of the breathing cycle (**Figure 4**).[74, 75] Disturbance of the rhythmic bursting of this small population of neurons may have disastrous consequences. Indeed, suppression of its glutamatergic neurons can induce fatal apnea in anaesthetized rats.[76] Intriguingly, also *awake* rats did not resume breathing up to the point of severe hypoxia that required mechanical ventilation, indicating that also voluntary breathing control was completely blocked.[76]

The brainstem is crucially involved in "low-level" control of cardiorespiratory function. Seizures may affect brainstem function by recruiting local neurons, and/or by the release of neuromodulators. Although obtaining local electrophysiology from brainstem structures is practically constrained in humans, blood flow in brainstem regions is increased during tonic-clonic seizures.[77] Interestingly, clonic seizure components require forebrain circuitry, but brainstem circuitry is sufficient to produce the tonic component.[78, 79] The tonic seizure component is strongly associated with post-ictal EEG suppression,[80] a proposed SUDEP risk factor,[81] and monitored SUDEP cases all showed a tonic-clonic seizure prior to death in another study.[61] As such, spread of seizures – and seizure-associated SD – to vital brainstem areas may contribute to SUDEP.

Epileptogenesis and the origin of seizures in epilepsy

Epilepsy (from ἐπιλαμβανω, "to seize") is characterized by the propensity of brain areas to spontaneously generate seizures.[82] Seizures that are restricted to a limited area of the brain are referred to as *focal* seizures, whereas seizures that involve large, bilateral, areas of the brain are referred to as *bilateral tonic-clonic* (in case of focal onset) or *generalized* (in the absence of focal onset) seizures.[83] The process by which the healthy brain develops into one that generates spontaneous seizures is termed *epileptogenesis.*[84]

The study of epileptogenesis is a relatively recent affair. The importance of a proper understanding of why and how epilepsy develops is reflected in the limited efficacy of treatments in a large proportion of patients up until recently: approximately one-third of epilepsy patients have seizures that are poorly controlled by medication,[85] a proportion that has barely changed in almost 50 years.[86, 87] Classical anticonvulsive drugs are suitable for the termination and prevention of seizures, but are ineffective at preventing epileptogenesis,[88] which may explain the lack of improvement in treatment efficacy. A more thorough understanding of epileptogenesis is thus critical to advance epilepsy treatment in coming years.

Traditionally, epilepsy is regarded as a brain disorder resulting from an imbalance between excitatory and inhibitory neurotransmission.[89] The structurally very similar molecules glutamate and γ-aminobutyric acid (GABA; Figure 5), which are respectively excitatory and inhibitory neurotransmitters, mediate the majority of neuronal synaptic communication.[90] Furthermore, removal of these neurotransmitters from the extracellular space by astrocytes is essential for effective synaptic transmission.[91]

FIGURE 5. The chemical structure of GABA (left) and (L-)glutamate (right).

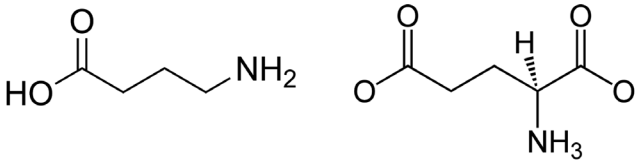

Inhibitory GABAergic neurons are vastly outnumbered by excitatory glutamatergic neurons as it is estimated that only ~15-20% of cortical neurons are GABAergic.[92, 93] Rather than simply opposing the effects of excitatory neurotransmission, inhibitory neurotransmission controls the transfer of information.[90] This is classically illustrated by the research of Charles Sherrington, who observed that a stimulus that induces muscle contraction in parallel inhibits its antagonist muscle.[94] Since cortical excitatory and inhibitory neurons are reciprocally connected, increases in excitatory and inhibitory neurotransmission occur in concert, with changes in inhibitory neuronal function causing pronounced effects on a large number of connected excitatory neurons.[95] Selectively decreasing inhibitory function by specific manipulations therefore results in pathological activity such as seizures.[96] Inhibitory dysfunction is considered importantly implicated in the mechanisms underlying epileptogenesis and seizure generation.[97]

Inhibitory dysfunction in epileptogenesis and epilepsy

Epilepsy can be *acquired*, i.e. caused by an injury in a healthy brain, or *genetic*, i.e. resulting from a genetic mutation. The most common acquired epilepsy in adults is temporal lobe epilepsy (TLE), in which seizures originate from the temporal lobe. It is believed that a precipitating factor – such as a prolonged initial seizure, infection, ischemia, head trauma or a tumor – is the underlying trigger for the development of this epilepsy syndrome. Mesial temporal sclerosis often develops, in which part of the temporal lobe, in particular the hippocampus, is affected by gliosis and atrophy. Both the electroclinical phenotype of TLE and the associated mesial temporal sclerosis have been replicated in various animal models.[88] In such animal models, loss of hippocampal somatostatin-positive GABAergic interneurons is a consistent finding.[98, 99] Notably, this finding has been confirmed in the hippocampus of TLE patients,[100] suggesting impaired inhibition as a mechanism for epileptogenesis in TLE.

Modeling genetic epilepsy syndromes provides another means to study epileptogenesis. Genetic manipulations allow us to examine whether inhibitory dysfunction is necessary and/or sufficient (that is, without the presence of another precipitating factor) to cause epilepsy. For example, genetic modification of a gene involved in regulating the development of cortical and hippocampal interneurons resulted in impaired inhibition and epilepsy in mice.[101] Genes that are predominantly

or specifically expressed in inhibitory interneurons and affect their excitability, which include various genes encoding voltage-gated channels, have been implicated in epilepsy syndromes. Disruption of *KCNA1*, a gene encoding a voltage-gated potassium channel that importantly modulates the excitability of parvalbumin-positive (PV) GABAergic interneurons,[102] results in epilepsy in mice[103] and patients.[104] On the other hand, recruiting PV interneurons using optogenetic activation effectively terminated seizures in a TLE mouse model.[105] Studying how modulation of GABAergic interneuron excitability affects network activity and seizure susceptibility may thus allow a better understanding of epileptogenesis.

Inhibitory dysfunction in Dravet syndrome

Dravet syndrome (DS) is a severe epilepsy syndrome in which inhibitory dysfunction has been particularly well described. Seizures usually initiate within the first year of life,[106] and are followed by cognitive and behavioral deficits later during development.[107] In the majority of cases, a loss-of-function mutation is found in the *SCN1A* gene.[108, 109] This gene encodes the pore-forming α1 subunit of voltage-gated sodium channel type 1 ($Na_V1.1$). In the hippocampus and cortex, $Na_V1.1$ expression appears restricted to PV GABAergic interneurons.[110] Since Na_V channels are critical for the initiation and propagation of action potentials, $Na_V1.1$ loss of function would be expected to specifically result in hypoexcitability of GABAergic interneurons, which indeed was demonstrated for hippocampal interneurons.[111] Decreased versus intact excitability in inhibitory compared to excitatory neuronal populations, respectively, have since been demonstrated in the hippocampus and cortex in DS mouse models.[112-114] These data suggest that network hyperexcitability and seizure activity in DS result from impaired inhibitory functioning. This was further supported by evidence showing that an interneuron-specific knockout of *Scn1a* resulted in spontaneous seizures.[115] In fact, such interneuron-specific knockout may result in a more severe phenotype than observed in mice with global knockout of *Scn1a*, since additional deletion of $Na_V1.1$ in excitatory neurons ameliorated the DS-related phenotype.[116]

Yet, loss-of-function mutations in *SCN1A* do not always result in the severe phenotype associated with DS. As an example, the same *SCN1A* mutation was associated with a mild epilepsy phenotype (without developmental delay) in one family[117] but with DS in another.[118] In addition, carriers without any symptoms were found in both families. Hence, the genotype does not necessarily predict the phenotype. In order to improve disease prediction and allow early treatment, a better understanding of how inhibitory dysfunction may affect network dynamics and promote epileptogenesis in DS is required.

Signatures of inhibitory functioning in local field potential

Neuronal excitation and inhibition are "as thick as thieves", as in, both are recruited during evoked and spontaneous activity, resulting in patterns of feed-forward and feed-back inhibition. In contrast to the many cortical excitatory neurons that have axons projecting to distant brain areas, the majority of inhibitory neurons form local synapses.[95] As a consequence of reciprocal connections

within anatomically well-organized networks, neuronal networks composed of excitatory and inhibitory neurons produce oscillatory activity that can be recorded using extracellular recording electrodes that measure *local field potential* (LFP). Different frequencies of these oscillations have been defined, that span from low frequencies in the delta range (0.5-4 Hz) to high frequencies in the (high) gamma range (30 Hz and above). When a sufficient proportion of neurons fire action potentials in a synchronized and regular manner this will produce membrane potential fluctuations in postsynaptic target neurons,[119] resulting in an oscillation of a certain dominant frequency that can be detected in the LFP signal. At the cellular level, these membrane potential oscillations may remain below the threshold to produce an action potential, but at the network level they do result in temporal windows of increased/decreased excitability.

Excitatory and GABAergic inhibitory synapses differently contribute to oscillatory activity. In particular, GABA is critical for the production of local field gamma oscillations: blockade of $GABA_A$ receptors (i.e. GABA receptors that are fast-responding) abolishes gamma oscillations in the hippocampus.[120, 121] In contrast, antagonists of the AMPA receptor, a glutamate receptor, are ineffective[120, 121] or only partially inhibit gamma oscillations.[122, 123] Thus, gamma oscillations are of particular interest to probe inhibitory functioning. More specifically, PV fast-spiking interneurons are critical for gamma oscillations[119]: they fire phase-locked and with high fidelity to gamma oscillations.[17] As their name suggests, PV fast-spiking interneurons can fire action potentials at high rates, in the range of several hundred Hz.[124] Also, since PV interneurons are widely interconnected, their ability to synchronize their own activity makes them well-positioned to generate (high) gamma oscillations.[119] In addition to gamma, PV interneurons fire phase-locked to theta oscillations[17] and importantly contribute to theta rhythm generation.[125] Therefore, these neurons are considered crucial for another phenomenon that may assist in neuronal communication across brain regions: cross-frequency coupling.

Theta-gamma coupling, inhibition and epileptogenesis

Gamma oscillations are typically very localized. Their amplitude may be modulated by the phase of lower frequencies, which was suggested to underlie the coordination of activity in neuronal populations that are distant from one another.[126] This mode of cross-frequency coupling is termed *phase-amplitude coupling*, which is considered an efficient way of neuronal communication across multiple spatial scales.[127] A ubiquitous form of phase-amplitude coupling in the brain is the coupling of gamma amplitude to theta phase (Figure 6). For example, hippocampal theta modulates both local gamma oscillations,[17, 128] as well as gamma oscillations in distant cortical areas.[129]

FIGURE 6. Cross-frequency coupling of gamma amplitude to theta phase.

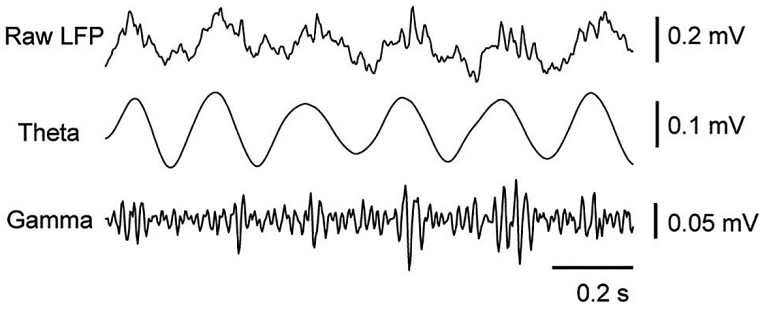

LFP recorded from mouse visual cortex (upper) and the results of bandpass-filtering this signal in the theta (5-10 Hz, middle) and gamma (40-160 Hz, lower) ranges. Note that gamma frequency amplitude tends to increase in the midcycle (or ~180°) of the theta frequency wave. Source: Jansen NA et al., Impaired θ-γ coupling indicates inhibitory dysfunction and seizure risk in a Dravet syndrome mouse model, Journal of Neuroscience 2021;41(3);524-537. Image reproduced with permission of the rights holder, Society for Neuroscience.

Such theta-gamma coupling is considered to underlie cognitive processes including memory function.[126, 130] Since dysfunction of PV interneurons may disrupt theta-gamma phase amplitude coupling,[131] and dysfunctional PV interneurons have been implicated in memory dysfunction in Alzheimer's disease,[132] theta-gamma phase-amplitude coupling may be a sensitive readout for PV interneuron functioning. Impaired functioning and/or loss of PV interneurons have been demonstrated for patients with TLE[133] and animal models of TLE[134, 135] and DS.[112-114] In addition, selective impairment of PV interneurons is sufficient to induce spontaneous seizures in mice.[136] As such, theta-gamma phase-amplitude coupling may hold promise as a measure to monitor epileptogenesis.

Outline of the thesis

The general aim of this thesis is to characterize brain network dynamics underlying spontaneous spreading depolarizations (I), as well as sudden death (II) and epileptogenesis (III) in genetic animal models of migraine and epilepsy.

To study the effects of cortical spreading depolarizations, these events are generally locally induced by suprathreshold stimuli, which poorly model the spontaneous events that are thought to underlie the migraine aura. This approach inherently complicates the study of spreading depolarization initiation mechanisms. We introduced the FHM type 3-associated *Scn1a*^{L263V} mutation in a mouse model, predicted to result in aberrant neuronal $Na_V1.1$ sodium channel functioning, to examine whether spreading depolarization could occur spontaneously in these animals (**Chapter 2**). To generalize the results to FHM, we established a mouse model of FHM2

with a genetic mutation affecting the Na^+/K^+ adenosine triphosphatase (ATPase) pump, which is chiefly expressed in astrocytes in the adult brain. This approach allowed us to evaluate whether pharmacologic modulations could differently affect spreading depolarization initiation and propagation (**Chapter 3**).

The mechanisms of *sudden unexpected death in epilepsy* (SUDEP) and *sudden infant syndrome* (SIDS) remain elusive and may be better understood by the development of animal models of spontaneous (seizure-related) death. In **Chapters 4 and 5**, we present a mouse model of spontaneous seizure-related sudden death. We used ambulatory recordings to relate brain activity to seizure-induced death (**Chapter 4**). We performed further recordings of cardiorespiratory and brainstem activity in these mice to evaluate whether vital functions may be impaired by aberrant brainstem functioning and whether pharmacological modulation thereof may prevent death (**Chapter 5**). In a translational study, we combined data from a clinical case and a mouse model to study the mechanisms of life-threatening apnea in the absence of seizure activity associated with the *SCN1A*^{L263V} mutation (**Chapter 6**).

Epileptogenesis is mostly studied in experimental models following an induced status epilepticus or brain-damaging insult, as opposed to genetic models that would better model genetic epilepsy syndromes. On the other hand, the same genetic mutation may or may not result in an epilepsy syndrome. We developed a mouse model of Dravet syndrome to study the epileptogenic potential of global *versus* local cortical or hippocampal *Scn1a* knockout (**Chapter 7**). We further used this model to identify potential electrophysiological metrics of seizure risk in Dravet syndrome (**Chapter 8**).

A general discussion of these chapters will follow in **Chapter 9.**

REFERENCES

1. Buzsaki, G., Rhythms of the Brain. 2006: Oxford university press.
2. Jones, E.G., Colgi, Cajal and the Neuron Doctrine. *J Hist Neurosci*, 1999. 8(2): p. 170-8.
3. Alle, H., A. Roth, and J.R. Geiger, Energy-efficient action potentials in hippocampal mossy fibers. *Science*, 2009. 325(5946): p. 1405-8.
4. Harris, J.J., R. Jolivet, and D. Attwell, Synaptic energy use and supply. *Neuron*, 2012. 75(5): p. 762-77.
5. Jiruska, P., et al., Synchronization and desynchronization in epilepsy: controversies and hypotheses. *J Physiol*, 2013. 591(4): p. 787-97.
6. Raol, Y.H. and A.R. Brooks-Kayal, Experimental models of seizures and epilepsies, in Progress in molecular biology and translational science. 2012, *Elsevier*. p. 57-82.
7. Jirsa, V.K., et al., On the nature of seizure dynamics. *Brain*, 2014. 137(Pt 8): p. 2210-30.
8. Leao, A.A., Spreading depression of activity in the cerebral cortex. *Journal of neurophysiology*, 1944. **7**(6): p. 359-390.
9. Leao, A.A., Further observations on the spreading depression of activity in the cerebral cortex. *J Neurophysiol*, 1947. 10(6): p. 409-14.
10. Canals, S., et al., Longitudinal depolarization gradients along the somatodendritic axis of CA1 pyramidal cells: a novel feature of spreading depression. *J Neurophysiol*, 2005. 94(2): p. 943-51.
11. Kraig, R.P. and C. Nicholson, Extracellular ionic variations during spreading depression. *Neuroscience*, 1978. 3(11): p. 1045-59.
12. Haglund, M.M. and P.A. Schwartzkroin, Role of Na-K pump potassium regulation and IPSPs in seizures and spreading depression in immature rabbit hippocampal slices. *J Neurophysiol*, 1990. 63(2): p. 225-39.
13. Kager, H., W.J. Wadman, and G.G. Somjen, Conditions for the triggering of spreading depression studied with computer simulations. *J Neurophysiol*, 2002. 88(5): p. 2700-12.
14. Dreier, J.P., The role of spreading depression, spreading depolarization and spreading ischemia in neurological disease. *Nat Med*, 2011. 17(4): p. 439-47.
15. Somjen, G.G., Mechanisms of spreading depression and hypoxic spreading depression-like depolarization. *Physiol Rev*, 2001. 81(3): p. 1065-96.
16. de Curtis, M., et al., Potassium dynamics and seizures: Why is potassium ictogenic? *Epilepsy Res*, 2018. 143: p. 50-59.
17. Bragin, A., et al., Gamma (40-100 Hz) oscillation in the hippocampus of the behaving rat. *J Neurosci*, 1995. 15(1 Pt 1): p. 47-60.
18. Mody, I., J.D. Lambert, and U. Heinemann, Low extracellular magnesium induces epileptiform activity and spreading depression in rat hippocampal slices. *J Neurophysiol*, 1987. 57(3): p. 869-88.
19. Eickhoff, M., et al., Spreading depression triggers ictaform activity in partially disinhibited neuronal tissues. *Exp Neurol*, 2014. 253: p. 1-15.
20. Gorji, A. and E.J. Speckmann, Spreading depression enhances the spontaneous epileptiform activity in human neocortical tissues. *Eur J Neurosci*, 2004. 19(12): p. 3371-4.
21. Fabricius, M., et al., Association of seizures with cortical spreading depression and peri-infarct depolarisations in the acutely injured human brain. *Clin Neurophysiol*, 2008. 119(9): p. 1973-84.

22. Dreier, J.P., et al., Recording, analysis, and interpretation of spreading depolarizations in neurointensive care: Review and recommendations of the COSBID research group. *J Cereb Blood Flow Metab*, 2017. 37(5): p. 1595-1625.
23. Hadjikhani, N., et al., Mechanisms of migraine aura revealed by functional MRI in human visual cortex. *Proc Natl Acad Sci U S A*, 2001. 98(8): p. 4687-92.
24. Headache Classification Committee of the International Headache Society (IHS) The International Classification of Headache Disorders, 3rd edition. *Cephalalgia*, 2018. 38(1): p. 1-211.
25. Leao, A. and R. Morison, Propagation of spreading cortical depression. *Journal of Neurophysiology*, 1945. 8(1): p. 33-45.
26. Lauritzen, M., Pathophysiology of the migraine aura. The spreading depression theory. *Brain*, 1994. 117 (Pt 1): p. 199-210.
27. Pietrobon, D. and M.A. Moskowitz, Chaos and commotion in the wake of cortical spreading depression and spreading depolarizations. *Nat Rev Neurosci*, 2014. 15(6): p. 379-93.
28. Pietrobon, D. and M.A. Moskowitz, Pathophysiology of migraine. *Annu Rev Physiol*, 2013. 75: p. 365-91.
29. Dreier, J.P. and C. Reiffurth, The stroke-migraine depolarization continuum. *Neuron*, 2015. 86(4): p. 902-922.
30. Harriott, A.M., et al., Spreading depression as a preclinical model of migraine. *J Headache Pain*, 2019. 20(1): p. 45.
31. Strong, A.J., et al., *S*preading and synchronous depressions of cortical activity in acutely injured human brain. *Stroke*, 2002. 33(12): p. 2738-43.
32. Russell, M.B. and J. Olesen, Increased familial risk and evidence of genetic factor in migraine. *BMJ*, 1995. 311(7004): p. 541-4.
33. van de Ven, R.C., et al., Genetic models of migraine. *Arch Neurol*, 2007. 64(5): p. 643-6.
34. Russell, M.B. and A. Ducros, Sporadic and familial hemiplegic migraine: pathophysiological mechanisms, clinical characteristics, diagnosis, and management. *Lancet Neurol*, 2011. 10(5): p. 457-70.
35. Ferrari, M.D., et al., Migraine pathophysiology: lessons from mouse models and human genetics. *Lancet Neurol*, 2015. 14(1): p. 65-80.
36. Hasirci Bayir, B.R., et al., Epilepsy in patients with familial hemiplegic migraine. *Seizure*, 2021. 88: p. 87-94.
37. Stam, A.H., et al., Early seizures and cerebral oedema after trivial head trauma associated with the CACNA1A S218L mutation. *J Neurol Neurosurg Psychiatry*, 2009. 80(10): p. 1125-9.
38. Vanmolkot, K.R., et al., Novel mutations in the Na+, K+-ATPase pump gene ATP1A2 associated with familial hemiplegic migraine and benign familial infantile convulsions. *Ann Neurol*, 2003. 54(3): p. 360-6.
39. Dichgans, M., et al., Mutation in the neuronal voltage-gated sodium channel SCN1A in familial hemiplegic migraine. *Lancet*, 2005. 366(9483): p. 371-7.
40. van den Maagdenberg, A.M., et al., A Cacna1a knockin migraine mouse model with increased susceptibility to cortical spreading depression. *Neuron*, 2004. 41(5): p. 701-10.
41. van den Maagdenberg, A.M., et al., High cortical spreading depression susceptibility and migraine-associated symptoms in Ca(v)2.1 S218L mice. *Ann Neurol*, 2010. 67(1): p. 85-98.
42. Leo, L., et al., Increased susceptibility to cortical spreading depression in the mouse model of familial hemiplegic migraine type 2. *PLoS Genet*, 2011. 7(6): p. e1002129.

43. Rogawski, M.A., Common pathophysiologic mechanisms in migraine and epilepsy. *Arch Neurol*, 2008. 65(6): p. 709-14.
44. Miri, M.L., et al., Altered hippocampal interneuron activity precedes ictal onset. *Elife*, 2018. 7.
45. Grasse, D.W., S. Karunakaran, and K.A. Moxon, Neuronal synchrony and the transition to spontaneous seizures. *Exp Neurol*, 2013. 248: p. 72-84.
46. Toyoda, I., et al., Unit Activity of Hippocampal Interneurons before Spontaneous Seizures in an Animal Model of Temporal Lobe Epilepsy. *J Neurosci*, 2015. 35(16): p. 6600-18.
47. Tran, C.H., et al., Interneuron desynchronization precedes seizures in a mouse model of Dravet syndrome. *Journal of Neuroscienc*e, 2020. 40(13): p. 2764-2775.
48. Bragin, A., M. Penttonen, and G. Buzsaki, Termination of epileptic afterdischarge in the hippocampus. *J Neurosci*, 1997. 17(7): p. 2567-79.
49. Herreras, O., et al., Role of neuronal synchronizing mechanisms in the propagation of spreading depression in the in vivo hippocampus. *J Neurosci*, 1994. 14(11 Pt 2): p. 7087-98.
50. Wadman, W.J., et al., Current source density of sustained potential shifts associated with electrographic seizures and with spreading depression in rat hippocampus. *Brain Res*, 1992. 570(1-2): p. 85-91.
51. Koroleva, V.I. and J. Bures, Cortical penicillin focus as a generator of repetitive spike-triggered waves of spreading depression in rats. *Exp Brain Re*s, 1983. 51(2): p. 291-7.
52. Zakharov, A., et al., Segregation of seizures and spreading depolarization across cortical layers. *Epilepsia*, 2019. 60(12): p. 2386-2397.
53. Aiba, I., Y. Ning, and J.L. Noebels, A hyperthermic seizure unleashes a surge of spreading depolarizations in Scn1a-deficient mice. *JCI Insigh*t, 2023. 8(15).
54. Tamim, I., et al., Spreading depression as an innate antiseizure mechanism. *Nat Commun*, 2021. 12(1): p. 2206.
55. Nashef, L., et al., Apnoea and bradycardia during epileptic seizures: relation to sudden death in epilepsy. *J Neurol Neurosurg Psychiatry*, 1996. 60(3): p. 297-300.
56. Nashef, L., et al., Unifying the definitions of sudden unexpected death in epilepsy. *Epilepsia*, 2012. **53**(2): p. 227-33.
57. Thurman, D.J., D.C. Hesdorffer, and J.A. French, Sudden unexpected death in epilepsy: assessing the public health burden. *Epilepsia*, 2014. 55(10): p. 1479-85.
58. Sveinsson, O., et al., The incidence of SUDEP: A nationwide population-based cohort study. *Neurology*, 2017. 89(2): p. 170-177.
59. Harden, C., et al., Practice guideline summary: Sudden unexpected death in epilepsy incidence rates and risk factors: Report of the Guideline Development, Dissemination, and Implementation Subcommittee of the American Academy of Neurology and the American Epilepsy Society. *Neurology*, 2017. 88(17): p. 1674-1680.
60. Surges, R., et al., Sudden unexpected death in epilepsy: risk factors and potential pathomechanisms. *Nat Rev Neurol*, 2009. 5(9): p. 492-504.
61. Ryvlin, P., et al., Incidence and mechanisms of cardiorespiratory arrests in epilepsy monitoring units (MORTEMUS): a retrospective study. *Lancet Neurol*, 2013. 12(10): p. 966-77.

62. Vilella, L., et al., Postconvulsive central apnea as a biomarker for sudden unexpected death in epilepsy (SUDEP). *Neurology*, 2019. 92(3): p. e171-e182.
63. Lhatoo, S.D., et al., Nonseizure SUDEP: Sudden unexpected death in epilepsy without preceding epileptic seizures. *Epilepsia*, 2016. 57(7): p. 1161-8.
64. Massey, C.A., et al., Mechanisms of sudden unexpected death in epilepsy: the pathway to prevention. *Nat Rev Neurol*, 2014. 10(5): p. 271-82.
65. Shmuely, S., et al., Mortality in Dravet syndrome: A review. *Epilepsy Behav*, 2016. 64(Pt A): p. 69-74.
66. Dravet, C., et al., Severe myoclonic epilepsy in infancy: Dravet syndrome. *Adv Neurol*, 2005. 95: p. 71-102.
67. Kalume, F., et al., Sudden unexpected death in a mouse model of Dravet syndrome. *J Clin Invest*, 2013. 123(4): p. 1798-808.
68. Kim, Y., et al., Severe peri-ictal respiratory dysfunction is common in Dravet syndrome. *J Clin Invest*, 2018. 128(3): p. 1141-1153.
69. Moghimi, N. and S.D. Lhatoo, Sudden unexpected death in epilepsy or voodoo heart: analysis of heart/brain connections. *Curr Cardiol Rep*, 2013. 15(12): p. 424.
70. Goldman, A.M., et al., Arrhythmia in heart and brain: KCNQ1 mutations link epilepsy and sudden unexplained death. *Sci Transl Med*, 2009. 1(2): p. 2ra6.
71. Glasscock, E., et al., Kv1.1 potassium channel deficiency reveals brain-driven cardiac dysfunction as a candidate mechanism for sudden unexplained death in epilepsy. *J Neurosci*, 2010. 30(15): p. 5167-75.
72. Trosclair, K., et al., Neuron-specific Kv1.1 deficiency is sufficient to cause epilepsy, premature death, and cardiorespiratory dysregulation. *Neurobiol Dis*, 2020. 137: p. 104759.
73. Smith, J.C., et al., Brainstem respiratory networks: building blocks and microcircuits. *Trends Neurosci*, 2013. 36(3): p. 152-62.
74. Del Negro, C.A., G.D. Funk, and J.L. Feldman, Breathing matters. *Nat Rev Neurosci*, 2018. 19(6): p. 351-367.
75. Smith, J.C., et al., Pre-Botzinger complex: a brainstem region that may generate respiratory rhythm in mammals. *Science*, 1991. 254(5032): p. 726-9.
76. Tan, W., et al., Silencing preBotzinger complex somatostatin-expressing neurons induces persistent apnea in awake rat. *Nat Neurosci*, 2008. 11(5): p. 538-40.
77. Blumenfeld, H., et al., Cortical and subcortical networks in human secondarily generalized tonic-clonic seizures. *Brain*, 2009. 132(Pt 4): p. 999-1012.
78. Kreindler, A., et al., Electro-clinical features of convulsions induced by stimulation of brain stem. *J Neurophysiol*, 1958. 21(5): p. 430-6.
79. Browning, R.A. and D.K. Nelson, Modification of electroshock and pentylenetetrazol seizure patterns in rats after precollicular transections. *Exp Neurol*, 1986. 93(3): p. 546-56.
80. Alexandre, V., et al., Risk factors of postictal generalized EEG suppression in generalized convulsive seizures. *Neurology*, 2015. 85(18): p. 1598-603.
81. Lhatoo, S.D., et al., An electroclinical case-control study of sudden unexpected death in epilepsy. *Ann Neurol*, 2010. 68(6): p. 787-96.
82. Fisher, R.S., et al., ILAE official report: a practical clinical definition of epilepsy. *Epilepsia*, 2014. 55(4): p. 475-82.

83. Fisher, R.S., et al., Instruction manual for the ILAE 2017 operational classification of seizure types. *Epilepsia*, 2017. 58(4): p. 531-542.
84. Pitkanen, A. and J. Engel, Jr., Past and present definitions of epileptogenesis and its biomarkers. *Neurotherapeutics*, 2014. 11(2): p. 231-41.
85. Kwan, P. and J.W. Sander, The natural history of epilepsy: an epidemiological view. *J Neurol Neurosurg Psychiatry*, 2004. 75(10): p. 1376-81.
86. Loscher, W. and D. Schmidt, Modern antiepileptic drug development has failed to deliver: ways out of the current dilemma. *Epilepsia*, 2011. 52(4): p. 657-78.
87. Coatsworth, J.J., Studies on the clinical efficacy of marketed antiepileptic drugs. 1971: National Institutes of Health;[for sale by the Supt. of Docs., US Govt.
88. Goldberg, E.M. and D.A. Coulter, Mechanisms of epileptogenesis: a convergence on neural circuit dysfunction. Nat Rev Neurosci, 2013. 14(5): p. 337-49.
89. Paz, J.T. and J.R. Huguenard, Microcircuits and their interactions in epilepsy: is the focus out of focus? *Nat Neurosci*, 2015. 18(3): p. 351-9.
90. Fishell, G. and B. Rudy, Mechanisms of inhibition within the telencephalon: "where the wild things are". *Annu Rev Neurosci*, 2011. 34: p. 535-67.
91. Araque, A., et al., Tripartite synapses: glia, the unacknowledged partner. *Trends Neurosci*, 1999. 22(5): p. 208-15.
92. Meinecke, D.L. and A. Peters, GABA immunoreactive neurons in rat visual cortex. *J Comp Neurol*, 1987. 261(3): p. 388-404.
93. Beaulieu, C., Numerical data on neocortical neurons in adult rat, with special reference to the GABA population. *Brain Res*, 1993. 609(1-2): p. 284-92.
94. Sherrington, C., Inhibition as a coordinative factor. *Nobelprize*. org, 1932.
95. Isaacson, J.S. and M. Scanziani, How inhibition shapes cortical activity. *Neuron*, 2011. **72**(2): p. 231-43.
96. Dudek, F.E. and T.P. Sutula, Epileptogenesis in the dentate gyrus: a critical perspective. *Prog Brain Res*, 2007. 163: p. 755-73.
97. Cardin, J.A., Inhibitory Interneurons Regulate Temporal Precision and Correlations in Cortical Circuits. *Trends Neurosci*, 2018. 41(10): p. 689-700.
98. Sloviter, R.S., Decreased hippocampal inhibition and a selective loss of interneurons in experimental epilepsy. *Science*, 1987. 235(4784): p. 73-6.
99. Buckmaster, P.S. and F.E. Dudek, Neuron loss, granule cell axon reorganization, and functional changes in the dentate gyrus of epileptic kainate-treated rats. *J Comp Neurol*, 1997. 385(3): p. 385-404.
100. de Lanerolle, N.C., et al., Hippocampal interneuron loss and plasticity in human temporal lobe epilepsy. *Brain Res*, 1989. 495(2): p. 387-95.
101. Cobos, I., et al., Mice lacking Dlx1 show subtype-specific loss of interneurons, reduced inhibition and epilepsy. *Nat Neurosci*, 2005. 8(8): p. 1059-68.
102. Goldberg, E.M., et al., K+ channels at the axon initial segment dampen near-threshold excitability of neocortical fast-spiking GABAergic interneurons. *Neuron*, 2008. 58(3): p. 387-400.
103. Smart, S.L., et al., Deletion of the K(V)1.1 potassium channel causes epilepsy in mice. *Neuron*, 1998. 20(4): p. 809-19.

104. Eunson, L.H., et al., Clinical, genetic, and expression studies of mutations in the potassium channel gene KCNA1 reveal new phenotypic variability. *Ann Neurol*, 2000. 48(4): p. 647-56.
105. Krook-Magnuson, E., et al., On-demand optogenetic control of spontaneous seizures in temporal lobe epilepsy. *Nat Commun*, 2013. 4: p. 1376.
106. Cetica, V., et al., Clinical and genetic factors predicting Dravet syndrome in infants with SCN1A mutations. *Neurology*, 2017. 88(11): p. 1037-1044.
107. Wolff, M., C. Casse-Perrot, and C. Dravet, Severe myoclonic epilepsy of infants (Dravet syndrome): natural history and neuropsychological findings. *Epilepsia*, 2006. 47 Suppl 2: p. 45-8.
108. Hattori, J., et al., A screening test for the prediction of Dravet syndrome before one year of age. *Epilepsia*, 2008. 49(4): p. 626-33.
109. Ohmori, I., et al., Nonfunctional SCN1A is common in severe myoclonic epilepsy of infancy. *Epilepsia*, 2006. 47(10): p. 1636-42.
110. Ogiwara, I., et al., Nav1.1 localizes to axons of parvalbumin-positive inhibitory interneurons: a circuit basis for epileptic seizures in mice carrying an Scn1a gene mutation. *J Neurosci,* 2007. 27(22): p. 5903-14.
111. Yu, F.H., et al., Reduced sodium current in GABAergic interneurons in a mouse model of severe myoclonic epilepsy in infancy. *Nat Neurosci*, 2006. 9(9): p. 1142-9.
112. Tai, C., et al., Impaired excitability of somatostatin- and parvalbumin-expressing cortical interneurons in a mouse model of Dravet syndrome. *Proc Natl Acad Sci U S A*, 2014. 111(30): p. E3139-48.
113. Favero, M., et al., A Transient Developmental Window of Fast-Spiking Interneuron Dysfunction in a Mouse Model of Dravet Syndrome. *J Neurosci*, 2018. 38(36): p. 7912-7927.
114. De Stasi, A.M., et al., Unaltered Network Activity and Interneuronal Firing During Spontaneous Cortical Dynamics In Vivo in a Mouse Model of Severe Myoclonic Epilepsy of Infancy. *Cereb Cortex*, 2016. 26(4): p. 1778-94.
115. Cheah, C.S., et al., Specific deletion of NaV1.1 sodium channels in inhibitory interneurons causes seizures and premature death in a mouse model of Dravet syndrome. *Proc Natl Acad Sci U S A*, 2012. 109(36): p. 14646-51.
116. Ogiwara, I., et al., Nav1.1 haploinsufficiency in excitatory neurons ameliorates seizure-associated sudden death in a mouse model of Dravet syndrome. *Hum Mol Genet*, 2013. 22(23): p. 4784-804.
117. Escayg, A., et al., Mutations of SCN1A, encoding a neuronal sodium channel, in two families with GEFS+2. *Nat Genet*, 2000. 24(4): p. 343-5.
118. Depienne, C., et al., Mechanisms for variable expressivity of inherited SCN1A mutations causing Dravet syndrome. *J Med Genet*, 2010. 47(6): p. 404-10.
119. Bartos, M., I. Vida, and P. Jonas, Synaptic mechanisms of synchronized gamma oscillations in inhibitory interneuron networks. *Nat Rev Neurosci*, 2007. 8(1): p. 45-56.
120. Whittington, M.A., R.D. Traub, and J.G. Jefferys, Synchronized oscillations in interneuron networks driven by metabotropic glutamate receptor activation. *Nature*, 1995. 373(6515): p. 612-5.
121. Fisahn, A., et al., Distinct roles for the kainate receptor subunits GluR5 and GluR6 in kainate-induced hippocampal gamma oscillations. *J Neurosci*, 2004. 24(43): p. 9658-68.
122. Fisahn, A., et al., Cholinergic induction of network oscillations at 40 Hz in the hippocampus in vitro. *Nature*, 1998. 394(6689): p. 186-9.

123. LeBeau, F.E., et al., Fast network oscillations induced by potassium transients in the rat hippocampus in vitro. *J Physiol*, 2002. 542(Pt 1): p. 167-79.
124. Wang, B., et al., Firing Frequency Maxima of Fast-Spiking Neurons in Human, Monkey, and Mouse Neocortex. *Front Cell Neurosci*, 2016. 10: p. 239.
125. Amilhon, B., et al., Parvalbumin Interneurons of Hippocampus Tune Population Activity at Theta Frequency. *Neuro*n, 2015. 86(5): p. 1277-89.
126. Buzsaki, G. and X.J. Wang, Mechanisms of gamma oscillations. *Annu Rev Neurosci*, 2012. 35: p. 203-25.
127. Buzsaki, G., Neural syntax: cell assemblies, synapsembles, and readers. *Neuron*, 2010. 68(3): p. 362-85.
128. Schomburg, E.W., et al., Theta phase segregation of input-specific gamma patterns in entorhinal-hippocampal networks. *Neuron*, 2014. 84(2): p. 470-85.
129. Sirota, A., et al., Entrainment of neocortical neurons and gamma oscillations by the hippocampal theta rhythm. *Neuron*, 2008. 60(4): p. 683-97.
130. Canolty, R.T. and R.T. Knight, The functional role of cross-frequency coupling. *Trends Cogn Sci*, 2010. 14(11): p. 506-15.
131. Wulff, P., et al., Hippocampal theta rhythm and its coupling with gamma oscillations require fast inhibition onto parvalbumin-positive interneurons. *Proc Natl Acad Sci U S A*, 2009. 106(9): p. 3561-6.
132. Verret, L., et al., Inhibitory interneuron deficit links altered network activity and cognitive dysfunction in Alzheimer model. *Cell*, 2012. 149(3): p. 708-21.
133. Andrioli, A., et al., Quantitative analysis of parvalbumin-immunoreactive cells in the human epileptic hippocampus. *Neuroscience*, 2007. 149(1): p. 131-43.
134. Knopp, A., et al., Loss of GABAergic neurons in the subiculum and its functional implications in temporal lobe epilepsy. *Brain*, 2008. 131(Pt 6): p. 1516-27.
135. Dinocourt, C., et al., Loss of interneurons innervating pyramidal cell dendrites and axon initial segments in the CA1 region of the hippocampus following pilocarpine-induced seizures. *J Comp Neurol*, 2003. 459(4): p. 407-25.
136. Drexel, M., et al., Selective Silencing of Hippocampal Parvalbumin Interneurons Induces Development of Recurrent Spontaneous Limbic Seizures in Mice. *J Neurosci*, 2017. 37(34): p. 8166-8179.

Part I

Spontaneous spreading depolarizations

Chapter 2

First FHM3 mouse model shows spontaneous cortical spreading depolarizations

Nico A. Jansen
Anisa Dehghani
Margot M.L. Linssen
Cor Breukel
Else A. Tolner
Arn M.J.M. van den Maagdenberg

Ann Clin Transl Neurol 2020;7(1):132-138

ABSTRACT

Here we show, for the first time, spontaneous cortical spreading depolarization (CSD) events – the electrophysiological correlate of the migraine aura – in animals by using the first generated familial hemiplegic migraine type 3 (FHM3) transgenic mouse model. The mutant mice express L263V-mutated α1 subunits in voltage-gated $Na_V1.1$ sodium channels (*Scn1a*^{L263V}). CSDs consistently propagated from visual to motor cortex, recapitulating what has been shown in patients with migraine with aura. This model may be valuable for the preclinical study of migraine with aura and other diseases in which spreading depolarization is a prominent feature.

INTRODUCTION

Cortical spreading depolarization (CSD) has been implicated in various human diseases, not only in migraine with aura and its monogenic subtype familial hemiplegic migraine, but also in stroke and traumatic brain injury.[1] Most of the evidence linking CSD with migraine comes from animal studies, but until now CSD events, without exemption, need to be evoked by stimulating the cortex of the animal. The lack of evidence for spontaneous events in animals hampers the study of CSD initiation.

FHM3, an autosomal dominant migraine with aura subtype with severe aura symptoms, is caused by specific missense mutations in the *SCN1A* gene that encodes the α1 subunit of voltage-gated $Na_V1.1$ sodium channels.[2] The overwhelming majority of mutations in *SCN1A* cause Dravet syndrome, a childhood epilepsy phenotype, due to loss of channel function.[3] FHM3 mutations instead seem associated with gain of $Na_V1.1$ channel properties, as was demonstrated in heterologous expression studies.[4-6] The FHM3 L263V mutation resulted in impaired channel inactivation, accelerated recovery from inactivation and greater channel availability of the mutant channels in tsA-201 cells.[6]

To study *in vivo* effects of the L263V mutation, and assess whether mutant mice exhibit spontaneous CSD, we generated the first FHM3 knock-in mouse model by introducing the mutation into the endogenous *Scn1a* gene using a CRISPR/Cas9 approach. We present the *Scn1a*^{L263V} mouse model as a promising mouse model to further the understanding of disease mechanisms in which spreading depolarizations are involved.

METHODS

Generation of *Scn1a*^{L263V} mice

A 1.3 kb dsDNA fragment containing a C to G transition at nucleotide position 787 in exon 7, resulting in a leucine to valine (L263V) amino acid change, of the *Scn1a* gene was used as a template for CRISPR/Cas9-mediated homologous recombination, and introduced in JM8 (C57BL/6J) embryonic stem cells. Clones carrying the correct mutation were injected in C57BL/6J blastocysts to generate chimeric mice. The L263V mutation was transmitted through the germline by breeding chimeric mice with C57BL/6J mice and the subsequent line was maintained on the same genetic background. As maintaining other *Scn1a* mutants on a 129/SvJ background increased survival,[7] we also interbred our mutants with 129/SvJ mice. On either background success of breeding was greatly enhanced by feeding male heterozygous *Scn1a*^{L263V} mice chow that contained GS967 (8 mg/kg chow; Research Diets, New Brunswick, NJ), as previously used.[8, 9] During the mating period, males were given standard chow, just as female wildtype (WT) mice. Hence all experimental mice were exclusively exposed to standard chow. Experiments were approved by local and national ethical committees conforming to the recommendations of the European Communities Council

Directive (2010/63/EU) and carried out in accordance with ARRIVE guidelines. For behavioral phenotyping, naïve *Scn1a*^{L263V} and WT mice were videotaped from P21 – P28 for 2 months or until death.

Surgery for electrophysiology

Prior to surgery, all surgical instruments and electrodes were disinfected with 70% ethanol. ECoG (silver balltips; 75 µm, AG5493; Advent Research Materials, Oxford, UK) or intracortical electrodes (75 µm platinum/iridium, PT6718) were implanted in *Scn1a*^{L263V} (n = 15 and n = 9, respectively) and WT (n = 8 and n = 5, respectively) mice (P21 – P28) under isoflurane anesthesia (4% for induction; 1.5% for maintenance) bilaterally in the primary visual cortex (V1; -3.5/2.0/0.5; mm relative to bregma; anterior, lateral and ventral, respectively) and primary motor cortex (M1; +1.5/1.8/0.5). In a subset of animals (14/24 *Scn1a*^{L263V} and 9/13 WT mice), an additional electrode was implanted in the right hippocampus (-2.2/1.5/1.7).

In a further 8 *Scn1a*^{L263V} mice, epicranial electrodes were placed by thinning of the skull overlying V1 and M1, followed by attachment of silver balltips using conductive carbon-based glue (Anders Products, Melrose, MA).

Electrical threshold for CSD was established by cortical stimulation in *Scn1a*^{L263V} (n = 9) and WT (n = 10) mice. Bipolar stimulation electrodes were implanted bilaterally in caudal V1 (-3.8/2.3/0.5), with recording electrodes in rostral V1 (-2.5/2.4/0.5), M1 and the right hippocampus.

Data acquisition and analyses

Following surgery, animals were connected to a custom-made 7-channel system for continuous video-EEG recordings. Data were acquired as described previously.[10] CSD was defined as a transient negative DC-shift of >5 mV measured at two locations with a delay, associated with a decrease in AC amplitude. Cortical DC-shifts in only one electrode accompanied by decreased AC amplitude were never observed. DC-recordings were inspected for CSDs during 2 weeks postoperatively, or until death of the animal. For all *Scn1a*^{L263V} mice, abnormal behavior, such as seizures, were studied for the whole recording period using AC-recordings and video.

For CSD induction, cathodal pulses of increasing intensities (1 – 5000 µC) were delivered every 3 minutes, until a CSD was observed, and propagation speed between electrodes in V1 and M1 was calculated. Two stimulations were performed per animal, at 24 and 48 hours after surgery (once in either hemisphere), and threshold and propagation rate were averaged for analyses.

Statistical testing was performed in Graphpad Prism (GraphPad Software, La Jolla, CA). A p-value of <0.05 was considered significant.

Immunohistochemistry

Mice were perfused with PBS and 4% PFA. Brains were post-fixed, cryoprotected and coronally sectioned (20 µm) on a cryostat. Antigen retrieval in 10 mM citrate buffer in 0.05% Tween was followed by blocking in 10% normal goat serum for 90 minutes and double-labeling with rabbit anti-$Na_v1.1$ (1:200; Alomone Labs, Jerusalem, Israel) and mouse anti-GAD67 (1:200; Millipore Sigma, St. Louis, MO) antibodies overnight at 4°C. Incubation in goat anti-rabbit Cy2 (1:200) and goat anti-mouse Cy3 (1:200; Jackson Immunoresearch, Cambridgeshire, UK) antibodies was performed for 2 hours. Sections were mounted in medium containing 1 µL/mL Hoechst-33258 and examined using confocal microscopy.

RESULTS

Generation of *Scn1a*^{L263V} mice

CRISPR/Cas9-mediated homologous recombination was used to introduce the human FHM3 L263V missense *SCN1A* mutation in the orthologous mouse gene, generating *Scn1a*^{L263V} mice (Fig 1A). Cortical expression of $Na_V1.1$ protein was observed, mostly in GABAergic interneurons, in WT and heterozygous *Scn1a*^{L263V} mice at P21 (Fig 1E), and in WT, heterozygous and homozygous *Scn1a*^{L263V} mice at P14 (Fig 1F) with no overt difference between genotypes.

Survival of *Scn1a*^{L263V} mice

Heterozygous *Scn1a*^{L263V} mice died at juvenile to young adult age, irrespective of the genetic background (C57BL/6J or mixed (50:50) C57BL/6J/129/SvJ) (Fig 1D). Video recordings of both naïve (n = 11; 8 females) and implanted (n = 24; 17 females) animals revealed that fatality was preceded by limited abnormal behavior lasting 1 – 14 seconds characterized by hindlimb jerks and/or tonic hindlimb extension sometimes preceded by sudden wild running, or occurred directly from sleep (n = 3). No seizure-related or other abnormal behaviors were observed over the recording period preceding death.

FIGURE 1A-1D. Generation, molecular characterization and survival of *Scn1a*^{L263V} mice.

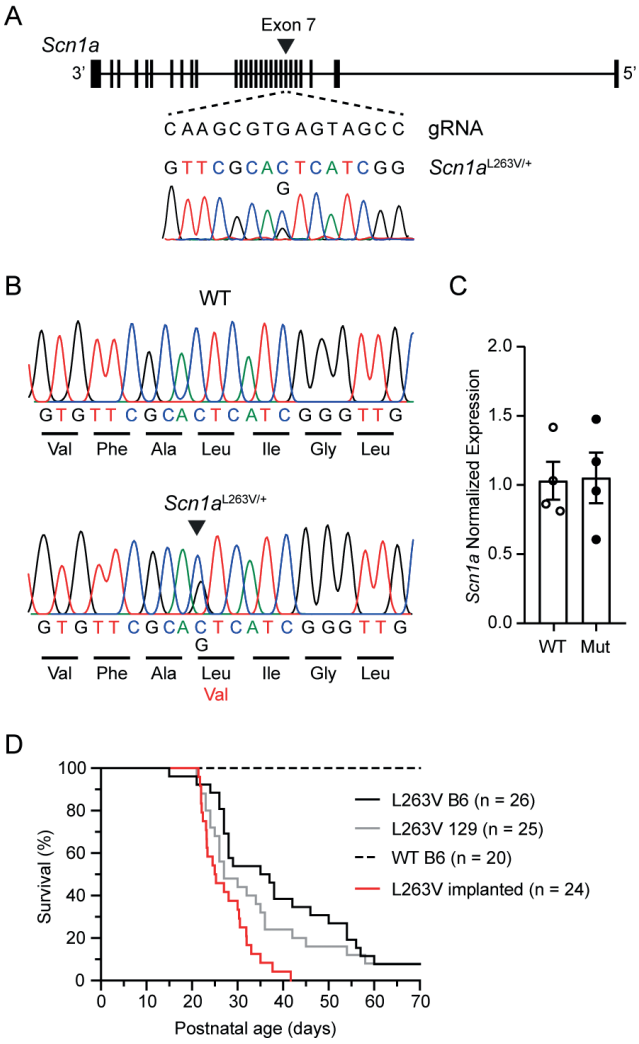

(A) Genomic structure of the *Scn1a* allele and guide RNA used to induce the L263V mutation in exon 7 (indicated by the arrowhead) and the electropherogram of the modified DNA sequence. **(B)** Sequencing analysis of RT-PCR products from whole brain mRNA isolated from WT and heterozygous *Scn1a*^{L263V} mice. **(C)** Normalized expression of *Scn1a* mRNA in WT and *Scn1a*^{L263V} (Mut) mice. **(D)** Survival of naïve (not implanted) *Scn1a*^{L263V} mice on a C57BL/6J (B6; black) and mixed (50:50) C57BL/6J/129/SvJ (B6/129; grey) background was not significantly different ($p = 0.152$, Log-rank test). Implanted C57BL/6J *Scn1a*^{L263V} mice (red) had a significantly decreased survival ($p < 0.001$, Log-rank test), whereas no early mortality was observed in implanted WT mice ($n = 9$; not shown).

FIGURE 1E-1F. Generation, molecular characterization and survival of *Scn1a*^{L263V} mice.

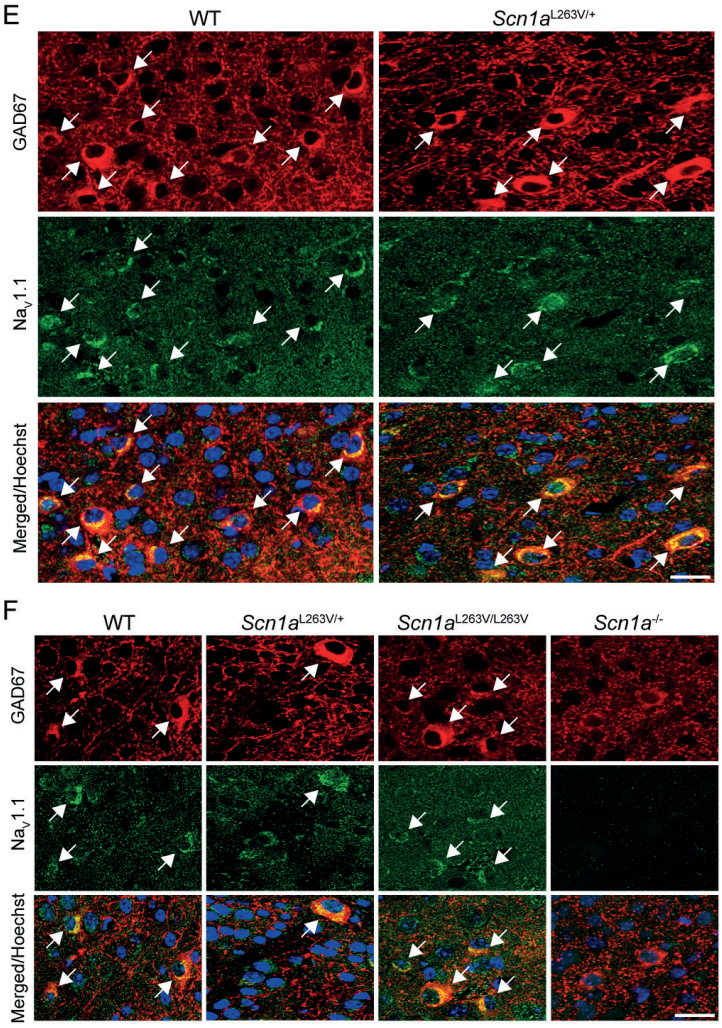

(E,F) Immunofluorescence of $Na_V1.1$ protein in V1 (primary visual cortex) of P21 WT and heterozygous *Scn1a*^{L263V} **(E)** and P14 WT, heterozygous and homozygous *Scn1a*^{L263V} **(F)** mice showed strong overlap in expression with GAD67, a marker for inhibitory interneurons (white arrows indicating double-labelled neurons) that was similar between genotypes. Scale bars, 20 µm.

Spontaneous and induced CSD in *Scn1a*^{L263V} mice

In a subset of *Scn1a*^{L263V} mice (9/24; 6 females; ECoG in 5/9, intracortical in 4/9), a total of 50 spontaneous CSD events were observed in 601 hours of recording (compared to 0/13 WT mice; $\chi^2(1) = 6.442$, $p = 0.011$). The survival time of mice with spontaneous CSDs was not different from mice without CSDs (67 ± 24 hours versus 108 ± 35 hours respectively; $p = 0.327$, unpaired *t*-test). In animals with more than one CSD ($n = 6$; range 2 – 33 CSDs), time between consecutive CSDs ranged from 28 minutes – 31.2 hours. CSD events generally occurred in isolation; only one CSD event consisted of 2 DC-shifts in each cortical electrode separated by approximately 3 minutes. Notably, all CSDs spread from V1 to M1 (Fig 2A and B). In 6/9 mice with spontaneous CSDs, hippocampal DC-potential was measured. Spread of CSDs to the ipsilateral hippocampus was observed in only one animal (Fig 2B). In 3/9 animals with a hippocampal electrode, downward spikes of moderate amplitude (0.5 – 1.5 mV) were observed most often in V1, sometimes in M1, but never in hippocampus. These spikes occurred every few seconds, had a duration of 20 – 50 milliseconds and were not associated with behavioral abnormalities. M1, V1 and hippocampal recordings did not reveal seizure bursts during the fatal event or preceding recording period (total recording time of 2,228 hours, $n = 24$; 17 females). No overt CSD-related behavioral abnormalities, including previously reported wet dog shakes or freezing behavior,[11] were observed. A subset of CSDs occurred during sleep (21/50) and were accompanied by awakening of the animal (9/21), roughly coinciding with spread to M1 (example in Fig 2B).

Although absence of spontaneous CSD in WT mice suggests that this phenomenon is specific to *Scn1a*^{L263V} mice, we additionally tested whether spontaneous CSDs occurred in the absence of cortical damage induced by implantation of intracortical and/or ECoG electrodes. To this end, we measured DC-potential in *Scn1a*^{L263V} mice using epicranial electrodes that did not penetrate the skull. In 2/8 chronically recorded *Scn1a*^{L263V} mice, 3 CSDs were detected in 146 hours of recording (Fig 2D and E).

Cortical cathodal stimulation of V1 was performed in a separate group of freely behaving mice ($n = 9$ *Scn1a*^{L263V}, 5 females; $n = 10$ WT, 4 females). CSD threshold was significantly lower in *Scn1a*^{L263V} mice than in WT littermates, whereas no difference was observed for propagation rate (Fig 3).

FIGURE 2. Spontaneous cortical spreading depolarization (CSD) in *Scn1a*^{L263V} mice with propagation from visual to motor cortex.

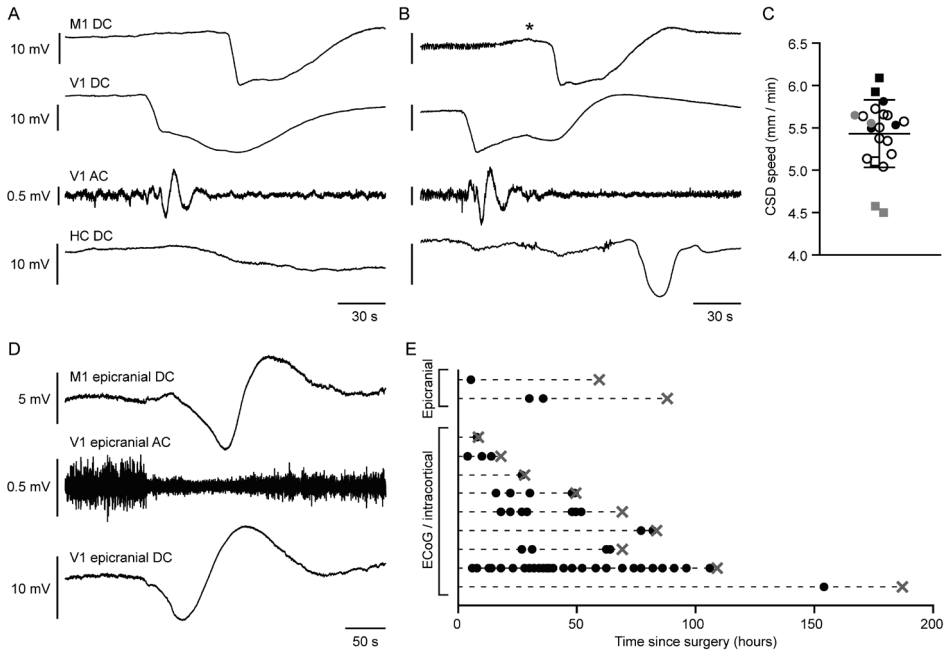

(A,B) Examples of a spontaneous CSD during wakefulness in an *Scn1a*^{L263V} mouse, without evidence of spread to the ipsilateral hippocampus (HC) **(A)** and during sleep, with spread to the ipsilateral HC **(B)** (M1 = primary motor cortex; V1 = primary visual cortex). In the example in B, the animal awoke during the CSD (indicated by an asterisk), but no overt abnormal behavior was observed. **(C)** Propagation rate of spontaneous CSDs occurring >24 hours following surgery. Every symbol represents a single CSD, grouped per animal (squares represent males, total $n = 21$ CSDs in 6 mice). **(D)** Example of a spontaneous CSD detected by epicranial electrodes in an *Scn1a*^{L263V} mouse. **(E)** Incidence of spontaneous CSDs recorded with ECoG, intracortical or epicranial electrodes. Each row represents one mouse, with individual CSDs indicated by black dots and death indicated by a gray cross. With respect to the time since surgery, CSD incidence was similar between the first and second half of recordings (26 and 27 CSDs, respectively). Note that epicranial recordings were not included in the analysis of CSD propagation speed **(C)**, as onset of the DC-shift appeared more gradual. For time series of V1 AC recordings **(A,B,D)** a bandpass filter of 0.5 – 100 Hz was used.

FIGURE 3. Reduced threshold for cortical spreading depolarization (CSD) induced by electrical stimulation in freely behaving *Scn1a*^{L263V} mice.

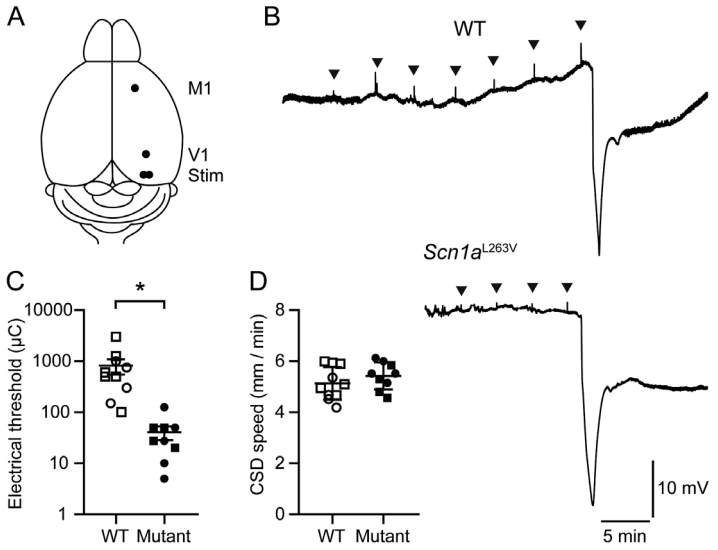

(A) Top view of experimental approach for electrical stimulation of the visual cortex (Stim; M1 = primary motor cortex; V1 = primary visual cortex). **(B)** Example of DC-signal in primary motor cortex of a WT and *Scn1a*^{L263V} mouse, showing that more stimulations of increased intensity (arrowheads) were required to induce CSD in WT mice. **(C,D)** Group analyses showed a reduced electrical threshold for CSD in *Scn1a*^{L263V} mice (*$p < 0.001$, Mann-Whitney test), while CSD propagation rate was not different ($p = 0.29$, Welch's *t*-test). Squares represent males.

DISCUSSION

Investigation into the mechanisms involved in initiation of CSD events is hampered by the fact that such events need to be evoked as there is no animal model, yet, that shows spontaneous occurrence of CSD in metabolically intact tissue. Here, we report that mice expressing the human *SCN1A*^{L263V} mutation, that was shown to cause FHM3 in humans, exhibit spontaneous CSDs that propagate from visual to motor cortex.

Functional consequences of FHM3-related *SCN1A* mutations in transfected cells indicate an overall gain of function of $Na_V1.1$ channels.[4-6] This sharply contrasts with the loss of function observed with mutations causing Dravet syndrome, resulting in loss of $Na_V1.1$ expression predominantly affecting GABAergic interneurons.[7, 12-14] In mice, this loss of function results in spontaneous seizures and large-amplitude interictal spikes, which we did not observe in *Scn1a*^{L263V} mice. As $Na_V1.1$ is predominantly localized in inhibitory interneurons,[7, 14] the present data suggest that the prominent CSD phenotype in *Scn1a*^{L263V} mice results from hyperexcitable cortical inhibitory interneurons. This mechanism seems counterintuitive in light of reports that GABA-A receptor activation could inhibit, not facilitate, CSD.[15, 16, 17] Still, a recent *in silico* study indeed suggested that intense firing of inhibitory interneurons may induce CSD, because of accumulation of extracellular potassium.[18] Of note, increased sodium currents have also been reported in excitatory neurons of loss-of-function *Scn1a* mutants[19] and increased persistent sodium currents, which may contribute to CSD,[20] have been reported in transfected cells that expressed *SCN1A* mutations associated with Dravet syndrome[21] and FHM3.[6] Clearly, the cellular substrate underlying CSD susceptibility in *Scn1a*^{L263V} mice remains to be determined.

Unexpectedly, all *Scn1a*^{L263V} mice died prematurely with peak mortality between P21 – 35. Contrary to previous studies on loss-of-function *Scn1a* mutants,[7, 22] genetic background, i.e. maintaining the mutation on either a pure C57BL/6J or the mixed (50:50) C57BL/6J/ 129/SvJ background, had no significant impact on survival of *Scn1a*^{L263V} mice. Timing of peak mortality, however, seems to overlap with that of loss-of-function *Scn1a* mutants.[23] This may be related to a developmental peak in $Na_V1.1$ expression in this age range.[14] In addition, spreading depolarization susceptibility is particularly high in this developmental time window[24, 25] and was found to induce lethal apnea in an FHM1 mouse model.[10, 26] However, as death is seizure-related in FHM1 mutants[10, 26] and loss-of-function *Scn1a* mutants,[23] the mechanism of death in *Scn1a*^{L263V} mice may be different.

Notably, in *Scn1a*^{L263V} mice all spontaneous CSDs spread from visual to motor cortex, which is in line with rare observations of visual aura features from neuroimaging in patients with migraine with aura,[27] commonly attributed to the occurrence of CSD. Together, these data indicate that *Scn1a*^{L263V} may serve as a valuable model to study mechanisms underlying initiation of spreading depolarizations, which may be relevant for disorders including migraine with aura, stroke and traumatic brain injury.

Acknowledgments

This research was supported by the Dutch National Epilepsy Foundation (2017-10, E.A.T., A.M.J.M.v.d.M.), EU-funded FP7 "EUROHEADPAIN" grant (6026337, A.M.J.M.v.d.M), and EU IAPP Program "BRAINPATH" (612360, E.A.T., A.M.J.M.v.d.M.). We thank M. Schenke for experimental assistance, K. Vonk for assistance with molecular analyses and Dr. L. Clemens-Daxinger for advice on CRISPR/Cas9-related issues.

REFERENCES

1. Dreier JP. The role of spreading depression, spreading depolarization and spreading ischemia in neurological disease. *Nat Med* 2011;17:439-47.
2. Dichgans M, Freilinger T, Eckstein G, et al. Mutation in the neuronal voltage-gated sodium channel SCN1A in familial hemiplegic migraine. *Lancet* 2005;366:371-7.
3. Oakley JC, Kalume F, Catterall WA. Insights into pathophysiology and therapy from a mouse model of Dravet syndrome. *Epilepsia* 2011;52 Suppl 2:59-61.
4. Dhifallah S, Lancaster E, Merrill S, et al. Gain of Function for the SCN1A/hNav1.1-L1670W Mutation Responsible for Familial Hemiplegic Migraine. *Front Mol Neurosci* 2018;11:232.
5. Cestele S, Schiavon E, Rusconi R, et al. Nonfunctional NaV1.1 familial hemiplegic migraine mutant transformed into gain of function by partial rescue of folding defects. *Proc Natl Acad Sci U S A* 2013;110:17546-51.
6. Kahlig KM, Rhodes TH, Pusch M, et al. Divergent sodium channel defects in familial hemiplegic migraine. *Proc Natl Acad Sci U S A* 2008;105:9799-804.
7. Yu FH, Mantegazza M, Westenbroek RE, et al. Reduced sodium current in GABAergic interneurons in a mouse model of severe myoclonic epilepsy in infancy. *Nat Neurosci* 2006;9:1142-9.
8. Anderson LL, Hawkins NA, Thompson CH, et al. Unexpected Efficacy of a Novel Sodium Channel Modulator in Dravet Syndrome. *Sci Rep* 2017;7:1682.
9. Baker EM, Thompson CH, Hawkins NA, et al. The novel sodium channel modulator GS-458967 (GS967) is an effective treatment in a mouse model of SCN8A encephalopathy. *Epilepsia* 2018;59:1166-76.
10. Loonen ICM, Jansen NA, Cain SM, et al. Brainstem spreading depolarization and cortical dynamics during fatal seizures in *Cacna1a* S218L mice. *Brain* 2019;142:412-25.
11. Akcali D, Sayin A, Sara Y, Bolay H. Does single cortical spreading depression elicit pain behaviour in freely moving rats? *Cephalalgia*. 2010;30:1195-206.
12. Han S, Tai C, Westenbroek RE, et al. Autistic-like behaviour in *Scn1a*$^{+/-}$ mice and rescue by enhanced GABA-mediated neurotransmission. *Nature* 2012;489:385-90.
13. Tai C, Abe Y, Westenbroek RE, et al. Impaired excitability of somatostatin- and parvalbumin-expressing cortical interneurons in a mouse model of Dravet syndrome. *Proc Natl Acad Sci U S A* 2014;111:E3139-48.
14. Ogiwara I, Miyamoto H, Morita N, et al. $Na_v1.1$ localizes to axons of parvalbumin-positive inhibitory interneurons: a circuit basis for epileptic seizures in mice carrying an Scn1a gene mutation. *J Neurosci* 2007;27:5903-14.
15. Aiba I, Shuttleworth CW. Characterization of inhibitory GABA-A receptor activation during spreading depolarization in brain slice. *PLoS One* 2014;9:e110849.
16. Wang M, Li Y, Lin Y. GABAA receptor alpha2 subtype activation suppresses retinal spreading depression. *Neuroscience* 2015;298:137-44.
17. Hoffmann J, Akerman S, Goadsby PJ. Efficacy and mechanism of anticonvulsant drugs in migraine. *Expert Rev Clin Pharmacol* 2014;7:191-201.

18. Desroches M, Faugeras O, Krupa M, Mantegazza M. Modeling cortical spreading depression induced by the hyperactivity of interneurons. *J Comput Neurosci* 2019;DOI: 10.1007/s10827-019-00730-8
19. Mistry AM, Thompson CH, Miller AR, et al. Strain- and age-dependent hippocampal neuron sodium currents correlate with epilepsy severity in Dravet syndrome mice. *Neurobiol Dis* 2014;65:1-11.
20. Somjen GG, Muller M. Potassium-induced enhancement of persistent inward current in hippocampal neurons in isolation and in tissue slices. *Brain Res* 2000;885:102-10.
21. Volkers L, Kahlig KM, Verbeek NE, et al. $Na_v1.1$ dysfunction in genetic epilepsy with febrile seizures-plus or Dravet syndrome. *Eur J Neurosci* 2011;34:1268-75.
22. Rubinstein M, Westenbroek RE, Yu FH, et al. Genetic background modulates impaired excitability of inhibitory neurons in a mouse model of Dravet syndrome. *Neurobiol Dis* 2015;73:106-17.
23. Kalume F, Westenbroek RE, Cheah CS, et al. Sudden unexpected death in a mouse model of Dravet syndrome. *J Clin Invest* 2013;123:1798-808.
24. Hablitz JJ, Heinemann U. Alterations in the microenvironment during spreading depression associated with epileptiform activity in the immature neocortex. *Brain Res Dev Brain Res* 1989;46:243-52.
25. Maslarova A, Alam M, Reiffurth C, et al. Chronically epileptic human and rat neocortex display a similar resistance against spreading depolarization in vitro. *Stroke*. 2011;42:2917-22.
26. Jansen NA, Schenke M, Voskuyl RA, et al. Apnea associated with brainstem seizures in *Cacna1a*^{S218L} mice is caused by medullary spreading depolarization. *J Neurosci*. 2019;1713-19.
27. Hadjikhani N, Sanchez Del Rio M, Wu O, et al. Mechanisms of migraine aura revealed by functional MRI in human visual cortex. *Proc Natl Acad Sci U S A* 2001;98:4687-92.

Chapter 3

Spontaneous spreading depolarizations originate subcortically in a novel mouse model of familial hemiplegic migraine type 2

Nico A. Jansen
Chelsey Linnenbank
Maarten Schenke
Rob A. Voskuyl
Maria S. Jorge
Georgii Krivoshein
Cor Breukel
Margot M. Linssen
Jill W.C. Claassens
Conny Brouwers
Sandra H. van Heiningen
Anders Heuck
Karin Lykke-Hartmann
Else A. Tolner
Arn M.J.M. van den Maagdenberg

Neurobiol Dis 2024;202:106714

ABSTRACT

The mechanisms of initiation of spreading depolarization (SD) are understudied due to a paucity of disease models with spontaneously occurring events. We here present a novel mouse model of familial hemiplegic migraine type 2 (FHM2), expressing the missense T345A-mutated a2 subunit of the Na^+/K^+ adenosine triphosphatase pump (*Atp1a2*^{T345A}). Homozygous *Atp1a2*^{T345A} mice showed regular spontaneous SDs that exhibit a diurnal rhythm and typically originate from the hippocampus. Heterozygous *Atp1a2*^{T345A} mice rarely exhibited spontaneous SDs and, for electrically induced SDs, only showed an increased propagation speed, whereas homozygotes showed both increased propagation and decreased threshold. Remarkably, despite hippocampal hyperexcitability, spontaneous SDs in *Atp1a2*^{T345A} mice were only rarely associated with epileptic behavior, and seizure expression during kindling was decreased. Spontaneous SDs could be prevented by modulation of persistent sodium currents. Hippocampal SDs occurred in the presence of an NMDA-receptor antagonist, but these events did not reach the cortex, suggesting that initiation and propagation of SD depend on different mechanisms in this model.

INTRODUCTION

Spreading depolarization (SD) is an electrophysiological phenomenon characterized by prolonged depolarization of brain cells that propagates through grey matter, followed by depression of neuronal activity that lasts for minutes.[1] Cortical SD is considered the neurophysiological phenomenon underlying the migraine aura, a transient focal symptom that precedes headache in one-third of migraine patients.[2] Although different triggers can initiate SD under experimental conditions, a paucity of models of spontaneous SD limits our understanding and treatment of this phenomenon.

Familial hemiplegic migraine type 2 (FHM2) is a rare subtype of migraine with severe auras caused by loss-of-function mutations in the *ATP1A2* gene.[3] *ATP1A2* encodes the α2 subunit of the Na^+/K^+ adenosine triphosphatase (α_2NKA), which acts as a Na^+/K^+-ATPase pump that in adult mice is predominantly expressed in astrocytes.[4] Loss of α_2NKA function has previously been studied in heterozygous knock-in mice expressing missense mutations W887R and G301R. Both *Atp1a2*^{W887R} [5] and *Atp1a2*^{G301R} mice[6] show increased susceptibility to experimentally induced cortical SD, which in *Atp1a2*^{W887R} mice was found associated with a reduced rate of K^+ and glutamate clearance by cortical astrocytes.[7] Of note, also *Atp1a2*$^{+/-}$ mice showed an increased susceptibility to cortical SD[8], although this was not confirmed in another study that showed only a tendency for increased propagation when SDs were evoked under anesthesia.[9]

Notably, homozygous FHM2 mutant mice of the various strains that lack expression of α_2NKA die at or around birth,[5] similar to *Atp1a2*$^{-/-}$ mice that die due to absent respiratory activity immediately after birth.[10] In rare clinical cases of *ATP1A2* homozygous loss-of-function mutations, the absence of α_2NKA protein also led to respiratory distress immediately after birth and subsequent death.[11, 12]

In contrast to FHM2 mutations that lead to absence of α_2NKA protein, the FHM2 *ATP1A2* T345A missense mutation was suggested to result in a decreased affinity for K^+ to mutated Na^+/K^+-ATPase pumps in some,[13] but not all[14, 15] cellular heterologous overexpression studies. Such discrepancy seems due to inherent difficulties with such studies that also produced inconsistent results for other FHM2 mutations. Regardless, the T345A mutation seems to mildly affect Na^+/K^+ ATPase function, compared to the W887R[16] and G301R[17] mutations. Here we generated heterozygous and homozygous *Atp1a2*^{T345A} mice to study *in vivo* effects of the T345A mutation on brain function. We found that homozygous *Atp1a2*^{T345A} mice were viable and had no apparent impairment of mobility, but showed decreased survival and increased susceptibility to cortically induced SD. Moreover, spontaneous cortical SD events occurred in homozygous mutants, with remarkably regular intervals and consistent propagation from visual to motor cortex, and typically originated from the hippocampus. In heterozygous mutants, spontaneous SDs were rarely observed, whereas no such events occurred in wildtype mice. Electrical stimulation of the hippocampus in homozygous mutants resulted in SD that propagated to cortical regions, but, in contrast to wildtype mice, repeated stimulation (i.e., kindling) did not result in the development of seizures. Finally, initiation of spontaneous SD in *Atp1a2*^{T345A} mice was modulated by a preferential inhibitor of persistent

sodium currents. An NMDA receptor (NMDAR) antagonist failed to prevent hippocampal SDs, but effectively blocked propagation to the cortex, suggesting different mechanisms for initiation and propagation of spontaneous SDs in this model. Our findings indicate that spontaneous SDs in the *Atp1a2*^{T345A} mouse model originate from the hippocampus, with demonstrable consequences for strategies to prevent SD.

MATERIALS AND METHODS

Generation of *Atp1a2*^{T345A} mice

A 12 kb targeting construct containing a loxP-PGK-Neo-pA-loxP cassette in intron 8 harboring the human FHM2 T345A missense mutation in exon 9 (Fig. 1A) was used as template for CRISPR/Cas9-mediated homologous recombination, and was introduced in JM8N4 (subcloned from JM8 parental line derived from C57BL/6N[18]) embryonic stem cells by electroporation of the DNA construct and the pX459 plasmid containing cas9 and the CRISPR guide sequence (Int8): aactgtcgctatttcctgct. The obtained embryonic stem cell clones were analyzed, selected for homologous recombination and correct karyotype after which the targeted JM8 ES cells were injected into a C57BL/6J mouse background. Obtained male chimeras were bred to C57BL/6J females to achieve germline transmission. To remove the Neo cassette, mice of the F1 generation were crossed to Cre-deleter mice (strain: B6.Cg-Tg(EIIa-cre)C5379Lmgd/Jlumc; the Jackson Laboratory, Stock number 003724). For further maintenance breeding, C57BL/6J mice were used. Male and female heterozygous and homozygous *Atp1a2*^{T345A} mice and wildtype (WT) littermates were used for the experiments. Mice were kept under standard housing conditions (temperature of 22 ± 1.5 °C, 12-h light/12-h dark cycle) with free access to water and food. Experiments were approved by the local and national ethical committees according to ARRIVE guidelines and recommendations of the European Communities Council Directive (2010/63/EU). All efforts were made to minimize discomfort of experimental animals.

Western blot analysis

Fresh brain tissue isolation of the right hemisphere of 1.5- to 2-month-old WT, heterozygous and homozygous *Atp1a2*^{T345A} mice was performed on ice. Tissues were homogenized in ice-cold lysis buffer, containing 1% sodium dodecylsulfate (SDS), 1 mM Na_3VO_4, protease inhibitor cocktail (cOmplete, mini, EDTA-free) and 10 mM Tris (pH 7.4) using a MagNalyzer (Roche Diagnostics, Almere, the Netherlands) for 20 s at 7000 rpm. Lysates were centrifuged for 2 min at 1000 g at 4 °C and supernatant was stored at -80 °C until western blot analysis. Protein expression was analyzed by TruPage on 4-12% precast gels in MOPS running buffer, followed by wet transfer to PVDF membranes. Membranes were blocked in 5% porcine serum in PBS-T and probed with primary antibody mouse anti-α1 Na^+/K^+ ATPase (1:60, a6F; Developmental Studies Hybridoma Bank, Iowa City, IA, USA), rabbit anti-α2 Na^+/K^+ ATPase (1:500; 07–674; Millipore, Burlington, MA, USA)

or mouse anti-β-Actin (1:5000, A5441; Sigma-Aldrich, St. Louis, MO, USA) diluted 1:1 in PBS-T blocking buffer. Primary antibodies were detected using HRP-conjugated secondary antibody (Li-Cor Biosciences, Lincoln, NE, USA) and ECL reaction with ImageQuant LAS400 mini system (GE Healthcare Bio-Sciences AB, Uppsala, Sweden).

Immunohistochemistry

Mice were perfused with PBS and 4% PFA. Brains were post-fixed for 2 h, followed by a serial incubation in 10% and 30% sucrose (each 12 h) for cryoprotection, and frozen in OCT tissue freezing medium (Tissue-Tek; Sakura Finetek, Los Angeles, CA, USA). Tissues were coronally sectioned at 10-µm thickness on a cryostat. Prior to staining, slides were heated in 10 mM citrate buffer (pH 6.0) for antigen retrieval and sections were permeabilized with 1% Triton X-100. Sections were then incubated with blocking serum (10% normal horse serum in PBS containing 0.05% Triton X-100) for 60 min and followed by double labelling with rabbit anti-a2 Na^+/K^+ ATPase (1:200, 07-674; Millipore) or chicken anti-GFAP (1:500, ab134014; Abcam, Cambridge, UK) antibody overnight at 4 ^{0}C in PBS with 2% normal horse serum and 0.4% Triton X-100. Incubation with secondary antibody Alexa 647 goat anti-rabbit (1:200, A21245; Invitrogen, Waltham, MA, USA) or Alexa 488 donkey anti-chicken (1:200, 703-545-155; Jackson ImmunoResearch, West Grove, PA, USA) was performed for 2 h. Sections were cover slipped in Vectashield hard mounting medium (Vectorlabs, Newark, NJ, USA) containing 1 µL/mL Hoechst-33258 and examined by confocal SP8 microscopy.

Pathology

For pathological examination, various tissues (including brain, muscle, heart and lung) were collected from 1.5- to 2-month-old WT, heterozygous and homozygous *Atp1a2*^{T345A} mice. Tissues were freshly isolated and post-fixed and processed for paraffin-sectioning or frozen for cryosectioning, followed by hematoxyline-eosine staining.

Surgery

For recordings of spontaneous brain activity, animals (postnatal (P) 32-50) were implanted with local field potential (LFP) electrodes (75 µm platinum/iridium; PT6718; Advent Research Materials, Oxford, UK) under isoflurane anaesthesia (induction 4%; maintenance 1.5%). Four electrode configurations were used (in mm relative to bregma, anterior/lateral/ventral, respectively): (1) bilateral primary motor cortex (M1; 1.5/1.8/0.5) and primary visual cortex (V1; -3.5/2.4/0.5); (2) right M1, V1, caudal V1 (V1c; -4.2/2.4/0.5) and dorsal hippocampus (dHC; -2.5/2.0/1.2), and for a subset of mice also ventral hippocampus (vHC; -2.8/2.8/2.6); (3) right M1, V1, and caudal, medial (-3.5/1.1/0.5) and lateral (-3.5/3.7/0.5) to V1; and (4) for recordings of respiratory functioning, a subset of animals were also equipped with a thermistor probe (MEAS-G22K7MCD419, Measurement Specialties Inc., Hampton, VA, USA) inserted in a hollow space overlying the epithelium of the anterior nasal cavity, as described previously,[19] in addition to a silver ball tip electrode (75 µm, AG5493; Advent Research Materials) on the dura overlying V1. For cortical SD electrical threshold

experiments, a separate group of 2- to 4-month-old WT and homozygous *Atp1a2*^{T345A} mice was implanted under isoflurane anesthesia with bipolar stimulation electrodes in bilateral caudal V1 (-3.8/2.3/0.5), with recording electrodes in bilateral rostral V1 (-2.5/2.4/0.5), M1, and the right dorsal HC (-2.2/1.5/1.7). In the latter experiments an additional 400-µm diameter laser doppler probe (403 probe and Periflux System 5000, Perimed Järfälla-Stockholm, Stockholm, Sweden) was placed bilaterally on the parietal skull (-1.5/2/0).

Cortical SD threshold assessment

For cortical SD induction in freely behaving mice, two stimulations were performed per animal (once in each hemisphere) one week after surgery with at least a 24-h interval. Cathodal pulses of increasing intensities (1–5000 µC) were delivered every 3 min until a cortical SD was observed, similar as reported previously,[20] and the propagation speed between electrodes in V1 and M1 was calculated. The additional laser doppler signal served to confirm spread of SD in case of technical issues with one of the direct current (DC)-recordings.

Hippocampal kindling

For hippocampal kindling experiments, a bipolar stimulation electrode was implanted in the left ventral hippocampal CA3 region (-3.0/3.0/2.8) in 2- to 4-month-old animals. Unipolar electrodes were implanted in right dorsal CA3, CA1 (-2.5/2.0/1.2) and V1. Following one day of baseline recording, a train of 1-ms bipolar current pulses (60 Hz for 2 s) was delivered through the hippocampal CA3 electrode every 5 min with increasing current intensities (10-µA steps), until afterdischarges (ADs) lasting ≥5 s were observed. This current intensity was used to trigger ADs twice daily (8-9 AM and 6-8 PM) for the subsequent 15 days. The first hippocampal stimulation session was used for comparing evoked SD features between dorsal CA3 and CA1.

Pharmacology

To test for possible effects of NMDA antagonism on spontaneous events, homozygous *Atp1a2*^{T345A} mice received intraperitoneal injections of either MK-801 (Sigma-Aldrich; 0.5 mg/kg body weight) or vehicle twice daily (8 A.M. and 6 P.M.) for three days, followed by the other treatment, by an experimenter blinded to the treatment. In a second group of homozygous *Atp1a2*^{T345A} mice, the effect of the sodium channel modulator GS967 (also known as PRAX-330) on spontaneous events was tested. Following a baseline recording period of one week, standard chow was replaced by chow containing 8 mg/kg GS967 (Research diets Inc., New Brunswick, NJ, USA), a dose that was previously shown to not cause overt behavioral effects.[21] After one week, GS967-compounded chow was replaced with standard chow for an additional recording period of one week.

Data acquisition and analyses

Wildtype, heterozygous and homozygous *Atp1a2*^{T345A} mice were videotaped at age P24-P54 in a PhenoTyper cage (Model 3000, Noldus Information Technology, Wageningen, the Netherlands) for 24 h. For tracking, mice were placed in the cage between 2:00 PM-4:00 PM. Video tracking and analysis of locomotor activity was performed offline using EthoVision software (Ethovision XT version 11.5, Noldus Information Technology). Locomotor activity was assessed in 1-h time bins and analyzed for the 12th h (i.e., dark period) and 24th h (i.e., light period) by determining total distance moved and mean velocity.

Animals that received surgery were allowed to recover for at least 2 days (for recordings of spontaneous activity) or 7 days (for cortical or hippocampal stimulation), after which they were connected to a 7-channel commutator in a Faraday cage for continuous recording of video, LFP and/or respiratory activity. Data were acquired and digitized as described previously.[22]

For power spectral density (PSD) analyses, alternating current (AC) LFP was artefact-rejected, digitally lowpass filtered (Chebyshev IIR 8th-order filter) and down-sampled to 500 Hz. PSD between 2-100 Hz was calculated using a fast Fourier transform with a Hamming window of 1 s with 50% overlap, and normalized to the average PSD within this range in the 30 s preceding stimulation (pre-stimulus). For post hoc assessment of AD duration, the time the PSD remained 2 (for hippocampus) or 1.5 (for V1) times above pre-stimulus total power was used. For V1 LFP, the reference signal and data from an infrared motion detection sensor were analyzed per 5-s epoch to establish the animal's vigilance state, for a 24-h period starting 7 days after surgery. Epochs without locomotor activity or motion artefacts were considered NREM or REM sleep based on V1 LFP PSD: epochs with a theta (5 – 10 Hz) to delta (1 – 4 Hz) power ratio of >2.5 were defined as REM sleep, while epochs with a high delta power were defined as NREM sleep. Analyses were performed using custom-written MATLAB scripts (version 2019b, Mathworks, Cambridge, UK).

For spontaneous SDs, video-recorded behavior was analyzed before and after the start of the event (i.e., the start of the burst or the start of the DC shift in case of an SD without prior burst activity) using Observer software (Observer XT version 15). Detection of burst activity required the burst amplitude to exceed 2X the value of the averaged root mean square of baseline LFP.

Statistical analysis

Data are presented as mean ± SEM (for time series) or mean ± SD (other). Statistical testing was performed in MATLAB or Graphpad Prism (Graphpad Software, San Diego, CA, USA). Data were compared using a Wilcoxon signed-rank or Mann-Whitney U test for single comparisons. For multiple comparisons, dependent on a prior analysis whether data were normally distributed, a two-way ANOVA, Kruskal-Wallis, Brown-Forsythe, or Welch's ANOVA test was used, followed by a post hoc Tukey's test or unpaired *t*-test with Welch's correction.

RESULTS

Generation of homozygous *Atp1a2*^{T345A} mice and expression of the Na^+/K^+-ATPase α2 subunit

CRISPR/Cas9-mediated homologous recombination was used to successfully introduce the human FHM2 T345A missense mutation in exon 9 of the orthologous mouse *Atp1a2* gene, generating heterozygous and homozygous *Atp1a2*^{T345A} mice (Fig. 1A-C). Western blot quantification of the α1 and α2 isoforms showed expression of both isoforms in the brains of *Atp1a2*^{T345A} and WT mice (Fig. 1D). Immunofluorescence revealed astrocytic expression of the Na^+/K^+-ATPase α2 subunit in hippocampal neurons of *Atp1a2*^{T345A} mice and WT mice (Fig. 1E). Pathological macroscopic and microscopic examination of brain, muscle (gastrocnemius and masseter), heart and various other tissues (lung and diaphragm, liver, spleen, kidney, adrenal gland and thymus) of *Atp1a2*^{T345A} mice revealed no overt abnormalities.

Homozygous *Atp1a2*^{T345A} mice are viable and show an increased susceptibility to cortical SD

In contrast to other FHM2 knock-in models[5, 23] homozygous *Atp1a2*^{T345A} mice were viable, although animals died prematurely from postnatal week 3 onwards (Fig. 2A). Despite early mortality, the animals had a normal appearance, albeit with a reduction in body weight and size that was evident throughout development into adulthood (Supplementary Fig. S1 A-C). Gross behavioral activity of homozygous *Atp1a2*^{T345A} mice seemed unimpaired, as evidenced by total distance moved and mean velocity (Supplementary Fig. S1 D-F).

To study the effects of the mutation on SD susceptibility, we assessed the threshold and propagation speed of induced cortical SD in WT, heterozygous and homozygous *Atp1a2*^{T345A} mice. Following cortical electrical stimulation, homozygous mutants showed a decreased threshold (Fig. 2B) and an increased propagation speed of SD (Fig. 2C) when compared to WT mice. SD propagation speed, but not electrical threshold, was significantly affected in heterozygous mutants compared to WT animals (Fig. 2B and 2C). DC shift duration of the evoked cortical SDs did not differ between homozygous *Atp1a2*^{T345A} mutants (67.1 ± 8.3 seconds; $n = 6$), heterozygous *Atp1a2*^{T345A} mutants (59.8 ± 4.7 seconds; $n = 13$) and wildtype mice (48.9 ± 4.7 seconds; $n = 10$; $p = 0.12$; Kruskal-Wallis test).

FIGURE 1A-1D. Generation, molecular characterization, and α2NKA expression in knock-in (KI) *Atp1a2*^{T345A} mice.

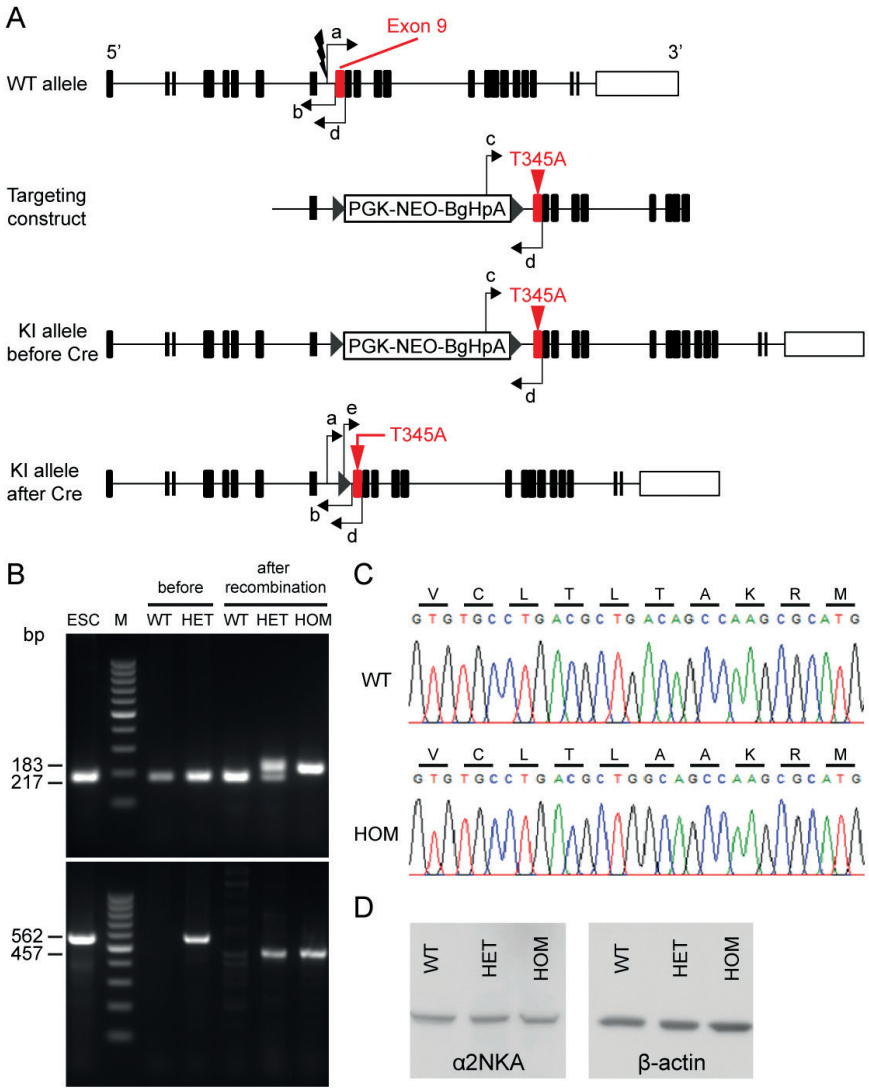

(A) Genomic structure of the wildtype (WT) *Atp1a2* allele, targeting construct containing a loxP-PGK-Neo-pA-loxP cassette (PGK-NEO-BgHpA) in intron 8, structure of the KI allele after homologous recombination (KI allele before Cre), and after Cre-mediated deletion of the cassette (KI allele after Cre). For introduction of the T345A missense mutation in exon 9 (red), a targeting construct combined with a Cas9 containing plasmid and the Crispr guide sequence were used. Positions and direction of the primers used to verify correct targeting of the T345A mutation are indicated by arrows. Sequences of the primers: a: 5'-ctttcttccgggcgtttacc-3'; b: 5'-aaaagggccaagtcgagagt-3', c: 5'-gacagcaaggggaggattg-3'; d: 5'-gagcatttcataccccagga-3'; and e: 5'-gctatttcctgctagataattcg-3'. **(B)** PCR products for primer combinations ab (183 bp (WT allele and before Cre recombination) and 217 bp (after Cre recombination)), cd (562 bp (before Cre recombination), and ed (457 bp after recombination)). **(C)** Sequencing analysis of RT-PCR product of hippocampus of WT and homozygous *Atp1a2*^{T345A} (HOM) mice. **(D)** Western blot of brain (cortex) protein lysate isolated from WT, heterozygous *Atp1a2*^{T345A} (HET) and HOM mice probed for a2NKA (~100 KDa) or β-actin (~42 KDa) protein shows equal expression levels of a2NKA protein in all three genotypes.

FIGURE 1E. Generation, molecular characterization, and α2NKA expression in knock-in (KI) *Atp1a2*^{T345A} mice.

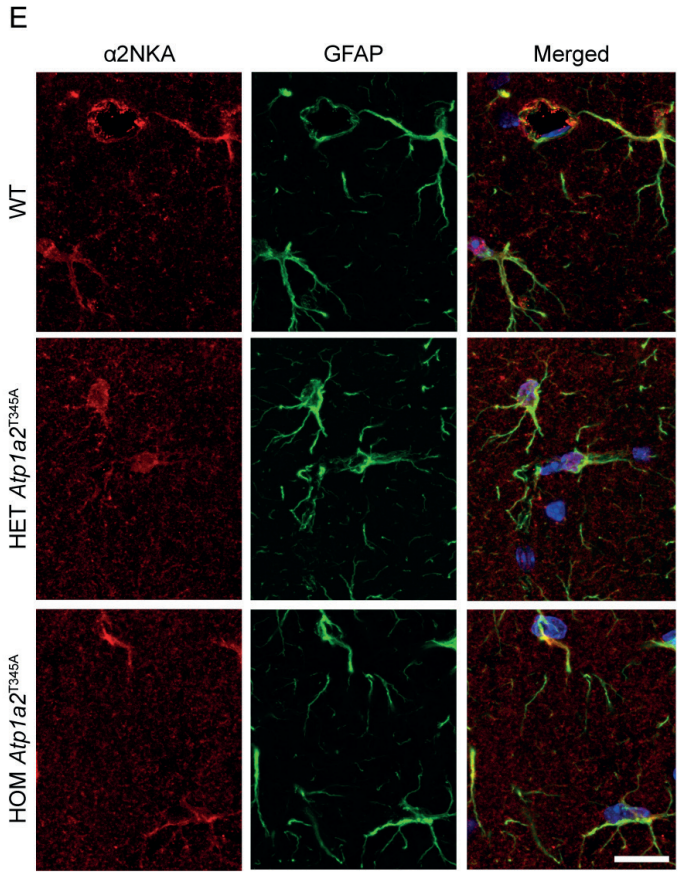

(E) Representative fluorescent images from hippocampal sections of WT, HET and HOM mice showing similar expression of 2NKA (red) in astrocytes stained with GFAP (green). Scale bar: 25 µm.

FIGURE 2. Decreased survival and reduced threshold and increased propagation speed for cortical SD induced by electrical stimulation in *Atp1a2*^{T345A} mice.

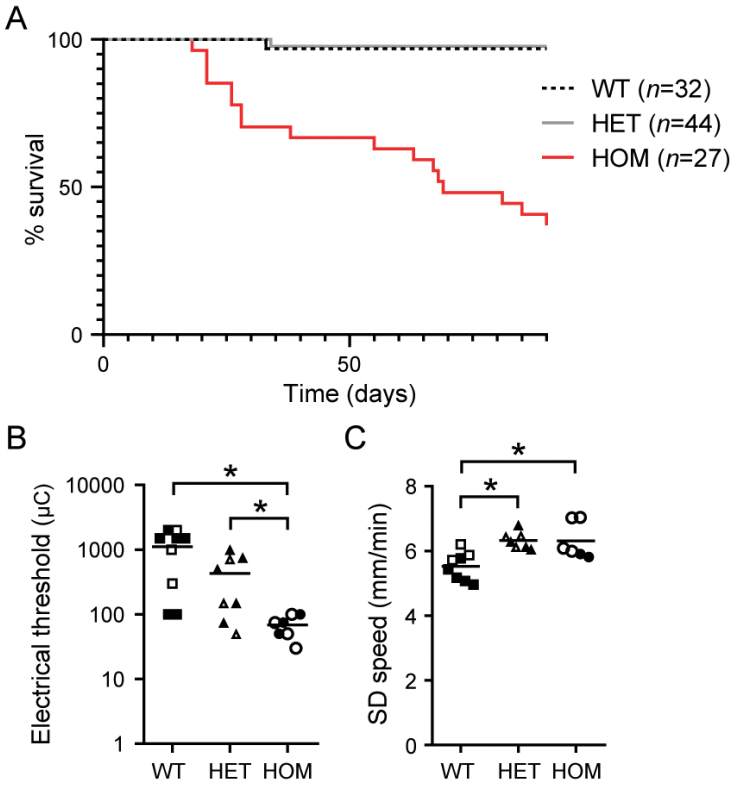

(A) Early mortality occurred from the 3rd postnatal week in homozygous *Atp1a2*^{T345A} mice. Survival was significantly decreased in homozygous *Atp1a2*^{T345A} compared to heterozygous *Atp1a2*^{T345A} and WT mice ($p < 0.001$, Log-rank test). **(B, C)** Electrical stimulation in the right and left hemisphere (closed and open symbols, respectively) resulted in significantly different SD thresholds (B; $p = 0.0004$ and 0.0499 for HOM vs WT and HET, respectively, Kruskal-Wallis and post-hoc Dunn's test) and propagation speeds between V1 and M1 cortex (C; $p = 0.0020$ and 0.0221 for HET and HOM vs WT, respectively, Kruskal-Wallis and post-hoc Dunn's test) in WT ($n = 6$; 9 experiments), HET ($n = 5$; 8 experiments) and HOM ($n = 5$; 7 experiments) *Atp1a2*^{T345A} mice ($n = 6$; 9 experiments). Analyses concern grouped SD data from both hemispheres. For 1 experiment in all genotypes, propagation rate could not be reliably measured due to instability of 1 of the two DC channels.

Homozygous *Atp1a2*^{T345A} mice show abnormal behavior immediately prior to apnea-associated death

To investigate possible causes for the early mortality in homozygous *Atp1a2*^{T345A} mice, five mice were continuously videotaped from P24 onwards, which revealed apparent normal behavior in the hours before death. However, in the seconds preceding terminal behavioral immobility, tonic extension of the hindlimbs occurred, which was preceded by a running bout of 1 – 3 s duration in three animals. In addition, handling of homozygous *Atp1a2*^{T345A} mice occasionally resulted in sudden hindlimb extension and behavioral immobility (6 such events were recorded in the (repetitive) handling of 49 homozygous *Atp1a2*^{T345A} mice) from which some animals did not recover. Recordings of video-encephalography (EEG) and respiratory activity showed that sudden apnea occurred during spontaneous and provoked events (n = 5; example in Fig. 3). In two events respiratory activity did not restore leading to the death of the animal. During one of the events moderate amplitude epileptiform bursts were observed in the EEG. This epileptiform activity had no clear behavioral correlate and continued after terminal behavioral arrest (Fig. 3B). Contamination of the EEG by cardiac electrical activity could still be observed minutes after apnea onset (Fig. 3C). These data indicate that homozygous *Atp1a2*^{T345A} mice are viable, but show early mortality that appears mediated by sudden apnea.

FIGURE 3. Non-fatal and fatal sudden apnea in homozygous *Atp1a2*^{T345A} mice.

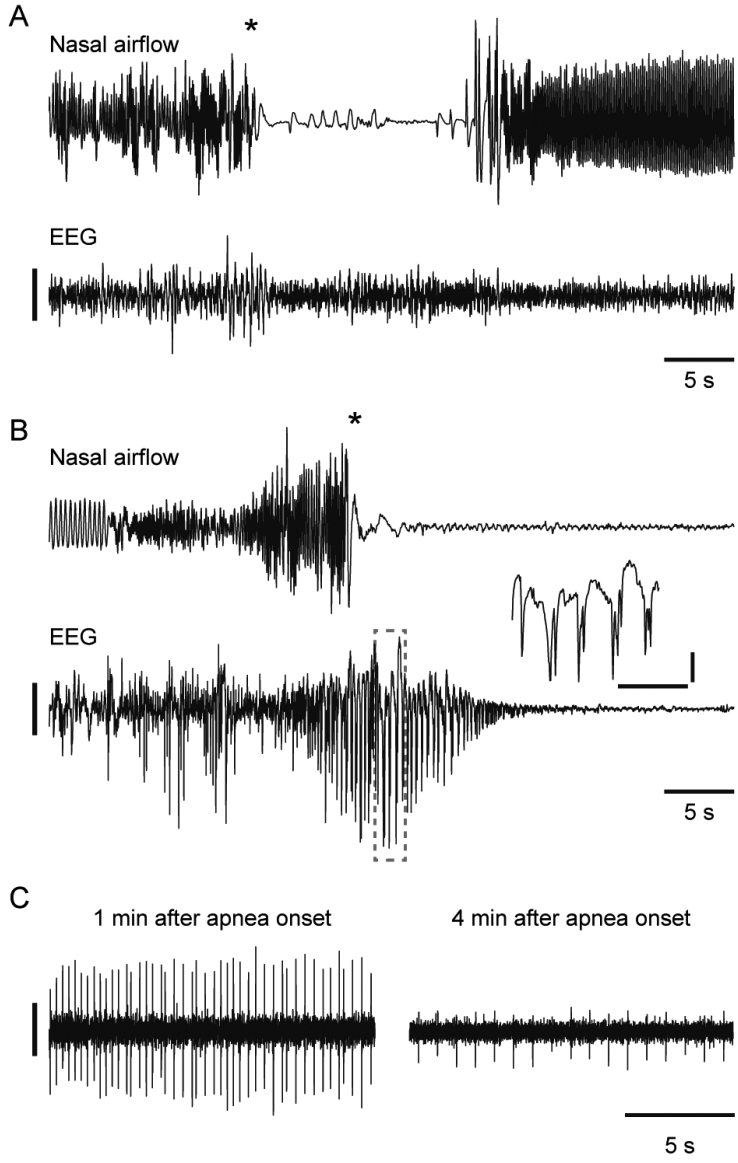

(A) Example of an episode of sudden non-fatal apnea in a homozygous *Atp1a2*^{T345A} mouse, that lasted ~15 s. Onset of apnea coincided with stretching of the hindlimbs (asterisk). The EEG, recorded from primary visual cortex, showed no epileptiform activity. **(B)** Example trace of sudden lethal apnea in a homozygous *Atp1a2*^{T345A} mouse. The EEG showed epileptiform bursts of moderate amplitude (detailed in inset, horizontal scale bar indicating 1 s) that initiated prior to apnea onset, but that had no behavioral correlate. **(C)** Contamination of the near-isoelectric EEG signal by ECG activity showed that cardiac activity was still present minutes after apnea onset. Digital filtering was performed with a highpass filter of 0.5 Hz (for EEG, in A and B) and with a bandpass filter of 10-500 Hz (for ECG, in C). Vertical scale bars indicate 0.5 mV (in A and B) and 20 μV (in C).

Atp1a2^{T345A} mice show spontaneous spreading depolarizations that typically originate from the hippocampus

In other FHM2 knock-in models[5, 23] no spontaneous SDs were reported in heterozygous mutants whereas homozygous mutants could not be investigated due to perinatal death. Here, we were able to record cortical LFP in homozygous *Atp1a2*^{T345A} mice (n = 3) continuously for 7 days, as these mice survive well past weaning (Fig. 4). Spontaneous SDs in the cortex were observed in all 3 animals, and in total 13 SDs were detected (range 3 – 6 SDs per animal). SDs exclusively propagated from V1 to M1 (example in Fig. 4A-C), and the time between SDs ranged from 8 – 51 hrs. Strikingly, in 8 of 13 events, cortical SDs were detected in both hemispheres almost simultaneously: the absolute delay between SD onset in left and right V1 was 13.0 ± 6.3 s, suggesting either a common subcortical source and/or synchronizing activity underlying SD onset. Inspection of LFP revealed epileptiform bursts of moderate amplitude and 20- to 30-s duration that were visible in both V1 and M1, and preceded V1 SD onset by 71 – 101 s.

We hypothesized that the hippocampus may represent a common source for the observed burst activity that preceded cortical SD. To study this, we implanted 19 homozygous *Atp1a2*^{T345A} mice with electrodes in the cortex, dorsal and, for a subset of mice (n = 12/19) also ventral hippocampus, and continuously recorded LFP for a total duration of 162.4 days, averaging 8.6 ± 5.4 (range 2 – 20) days per animal. In total, 1 – 26 SDs were observed per animal, totaling 149 SDs. For one event, the SD was first detected in the cortex, but the remaining 148 SDs were first observed in the hippocampus. Hippocampal LFP showed burst activity directly preceding SD in 90% (134/149) of the events (example in Supplementary Fig. S2), whereas no such abnormal activity was observed for the other 15 events. High-amplitude spikes in the hippocampal LFP occurred synchronously with lower amplitude spikes in cortical LFP, suggesting electric field transmission. The majority of hippocampal SDs (79%; 117/148) propagated to the uni- or bilateral cortex, from V1 to M1 (example in Fig. 4D), with a cortical propagation speed of 5.3 ± 0.5 (range 2.9 – 7.7) mm/min. Additional LFP recordings from different positions relative to V1 (Fig. 4E) confirmed that SDs propagated in a caudal-to-rostral pattern (Fig. 4F). Bilateral neocortical LFP was available during 52% of the events (77/149), allowing confirmation of bilateral, unilateral, or absence of, neocortical SD (Table 1). Hippocampal SD always occurred bilaterally preceding bilateral neocortical SD (39/39). For unilateral events, hippocampal and neocortical SD always occurred ipsilateral (7/7). These data indicate that cortical SDs in homozygous *Atp1a2*^{T345A} mice have a predominant hippocampal origin, with a cortical caudal to rostral propagation pattern. Propagation speed of spontaneous cortical SDs did not differ from that of the above-described induced SD events (p = 0.11).

Recordings of local oxygen partial pressure (PO_2) in the hippocampus of homozygous *Atp1a2*^{T345A} mice (n = 2, 6 spontaneous SD events) showed local hippocampal PO_2 of 21.4 ± 5.3 (range 17.2 – 30.1) mmHg at the time of SD onset (Supplementary Figure S3), mostly within ranges previously reported as "normoxic" for hippocampal recordings [24]. PO_2 starts decreasing during the hippocampal burst activity, but only reaches severe hypoxia (< 10 mm Hg PO_2) after SD onset,

indicating that neuronal activity causes local tissue hypoxia in homozygous *Atp1a2*^{T345A} mice, rather than vice versa.

Long-term hippocampal and cortical recordings in 8 heterozygous *Atp1a2*^{T345A} mice for a total duration of 52 days (6.5 ± 2.3 (range 2 – 9) days per animal) revealed two spontaneous SDs, detected in two animals. One event was preceded by hippocampal burst activity, followed by hippocampal and cortical SD spreading from V1 to M1, similar to homozygous mutants. The other event did not involve the hippocampus, but spread unilaterally from V1 to M1.

FIGURE 4. Cortical SDs occur spontaneously in homozygous *Atp1a2*^{T345A} mice and display a stereotypical spreading pattern.

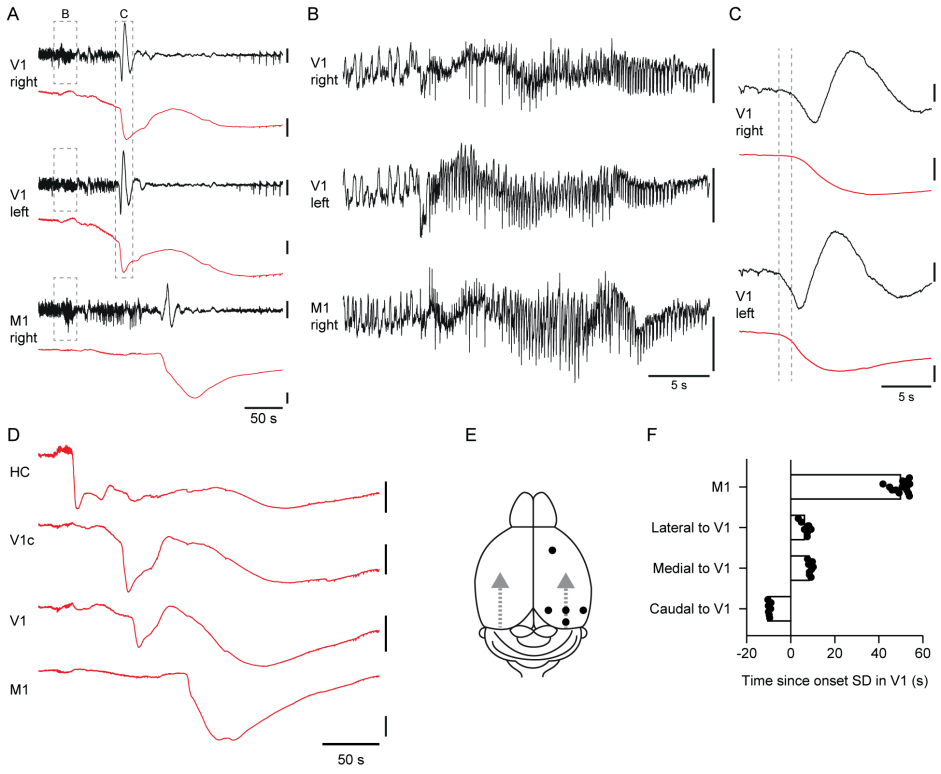

(A) Example of a spontaneous cortical SD in a homozygous *Atp1a2*^{T345A} mouse, with alternating current (AC) signals in black and direct current (DC) LFP signals in red. Vertical scale bars indicate 0.5 and 10 mV for AC and DC signals, respectively. **(B)** A synchronized burst of activity of moderate amplitude (inset from A) occurred approximately 74 s prior to SD onset in the primary visual cortex (V1). **(C)** Cortical SD onset was not synchronous in V1 of both hemispheres (inset from A), since the DC shift in left V1 preceded that in right V1 by approximately 1 s (dashed lines indicate SD onset). **(D)** Typical DC signals recorded from one hemisphere in a homozygous *Atp1a2*^{T345A} mouse during a spontaneous SD event with DC shifts occurring sequentially in hippocampus (HC), caudal V1 (V1c), V1, and primary motor cortex (M1). **(E)** Schematic of the neocortical sites recorded during spontaneous SD events, using three electrode configurations (described in the Materials and Methods). **(F)** SD timings in these areas indicated a caudal-to-rostral spreading pattern.

TABLE 1. Fraction of events that showed SD and/or hippocampal burst activity in homozygous *Atp1a2*^{T345A} mice that had LFP recorded bilaterally from the cortex (n = 77 events) and cortex and hippocampus (n = 39 events).

SD in cortex	Proportion of total SD events	Hippocampal SD		Epileptiform burst
		Unilateral	Bilateral	
Bilateral	51% (39/77)	0% (0/39)	100% (39/39)	100% (39/39)
Unilateral	30% (23/77)	30% (7/23)	70% (16/23)	70% (16/23)
None	19% (15/77)	27% (4/15)	73% (11/15)	47% (7/15)

Spontaneous spreading depolarizations in *Atp1a2*^{T345A} mice exhibit a diurnal rhythm and preferentially initiate during sleep

Homozygous *Atp1a2*^{T345A} mice showed an average SD frequency of 0.95 ± 0.41 (range 0.47 – 2.2) SDs per day. The mean and median time between subsequent SDs was 26.4 and 24.7 h, respectively (Fig. 5A), suggesting that a diurnal pattern was present. Indeed, SDs were more likely to occur in the evening (Fig. 5B and C). Vigilance state analyses showed that mice were asleep immediately prior to 84% (128/153) of events, which was significantly more often than expected based on the average time animals were asleep over 24 h (51 ± 5%; $p < 0.01$, Grubbs' test). All animals were awake during the first minute after SD onset, with locomotor activity increasing from 13 ± 21% to 83 ± 13% (mean ± S.D.) during the minute preceding and following SD onset, respectively.

Since the majority of spontaneous SDs were preceded by LFP burst activity (139/153 events), we studied the animals' behavior during SDs in more detail. Seizure behavior occurred during 5% (8/153) of events (n = 7 with Racine stage 3, n = 1 with Racine stage 5) and only for events preceded by LFP burst activity. Following SD, body stretches, backward and sideward movements, body rotations and head turns and/or waving were observed in 90% (138/153) of events, in the first 4 minutes after SD onset. The most frequently observed SD-related behaviors were stretching (73%; 111/153 events), head waving (63%; 97/153 events) and body rotations (52%; 79/153 events), with stretching typically preceding body rotations and head waving.

FIGURE 5. Spontaneous spreading depolarizations (SDs) in homozygous *Atp1a2*^{T345A} mice occurred preferably during early hours of the dark period.

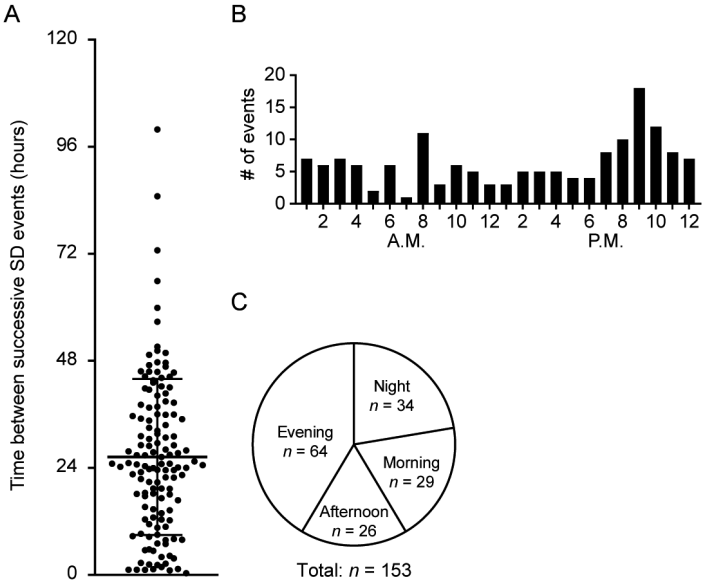

(A) Interval between spontaneous SD events in homozygous *Atp1a2*^{T345A} mice (n = 20, 2 – 10 days per animal). Each dot corresponds to a time interval between 2 successive SDs. **(B)** The distribution of spontaneous SD events during the day, counted per 1-h time bin. (C) SDs were more likely to occur in the evening ($\chi^2_{(3)} = 22.8$, $p < 0.001$).

Subregion-specific hippocampal hyperexcitability in homozygous *Atp1a2*^{T345A} mice

Interictal spikes occurred regularly in hippocampal CA1 and CA3 region in homozygous *Atp1a2*^{T345A} mice, specifically during NREM sleep. These high-amplitude spikes had only a low-amplitude correlate in the cortical LFP (Fig. 6A), suggesting a local origin. Since throughout development NKA activity is increased in CA3 when compared to CA1,[24] we tested whether the *Atp1a2*^{T345A} mutation affects SD susceptibility differently in these hippocampal areas. In the WT immature hippocampus, the CA3 region was previously shown to have a higher threshold for K^+-induced SD when compared to CA1.[25] To compare the SD susceptibility of the CA1 and CA3 in WT and homozygous *Atp1a2*^{T345A} mice, we electrically stimulated the ventral left CA3 region (1-ms bipolar pulses at 60 Hz for 2 s) while recording LFP in right CA1 and CA3 in the dorsal hippocampus. We observed Ads followed by SD in both WT (n = 9) and homozygous *Atp1a2*^{T345A} (n = 4) mice. However, a different pattern was observed for the various genotypes: CA3 SD followed CA1 SD in the majority (6/9) of WT mice, whereas it preceded CA1 SD in all homozygous *Atp1a2*^{T345A} mice (Fig. 6B). Similarly, CA3 SD preceded CA1 SD during 3 spontaneous events that were observed

in 3 of the 4 homozygous *Atp1a2*^{T345A} mice with implanted CA1 and CA3 electrodes (Fig. 6C). Irrespective of the hippocampal subregion, homozygous *Atp1a2*^{T345A} mice showed an increased duration of the negative DC-shift, when compared to WT mice (Fig. 6D). These data further support a role for hippocampal hyperexcitability in the phenotype of *Atp1a2*^{T345A} mice, affecting the CA3 subregion most evidently.

Atp1a2^{T345A} mice show decreased seizure propagation and reduced susceptibility to hippocampal kindling

Homozygous *Atp1a2*^{T345A} mice showed seizure-related behavior for only a small minority of the spontaneous SD events. We therefore evaluated whether seizure progression is affected in these animals. Stimulation of the left ventral hippocampus (1-ms bipolar pulses at 60 Hz for 2 s) resulted in Ads followed by SD in the right hippocampus of WT, heterozygous and homozygous *Atp1a2*^{T345A} mice (example traces in Fig. 7A), which propagated to the cortex in all (7/7) homozygous, a fraction (2/12) of heterozygous, and none (0/11) of the WT mice. The duration and power of the Ads in hippocampal LFP were comparable (Fig. 7B), but were both significantly reduced in V1 of both heterozygous and homozygous mutant mice, and more so for homozygous mutant mice (Fig. 7C). Moreover, whereas the threshold for eliciting Ads was comparable between the genotypes (Fig. 7D), postictal normalized LFP power in V1 was reduced in homozygous mutant when compared to WT mice (preceding SD arrival; Fig. 7E). Twice daily repetitive stimulation at the AD threshold current over the course of 15 days showed reduced seizure expression during kindling in heterozygous and homozygous mutants when compared to WT mice following stimulations 9 to 30, while seizure expression was significantly impaired in homozygous mutant when compared to heterozygous mutant mice following stimulations 18 to 30 (Fig. 7F).

FIGURE 6. Hippocampal hyperexcitability in homozygous *Atp1a2*^{T345A} mice disproportionately affects the CA3 region.

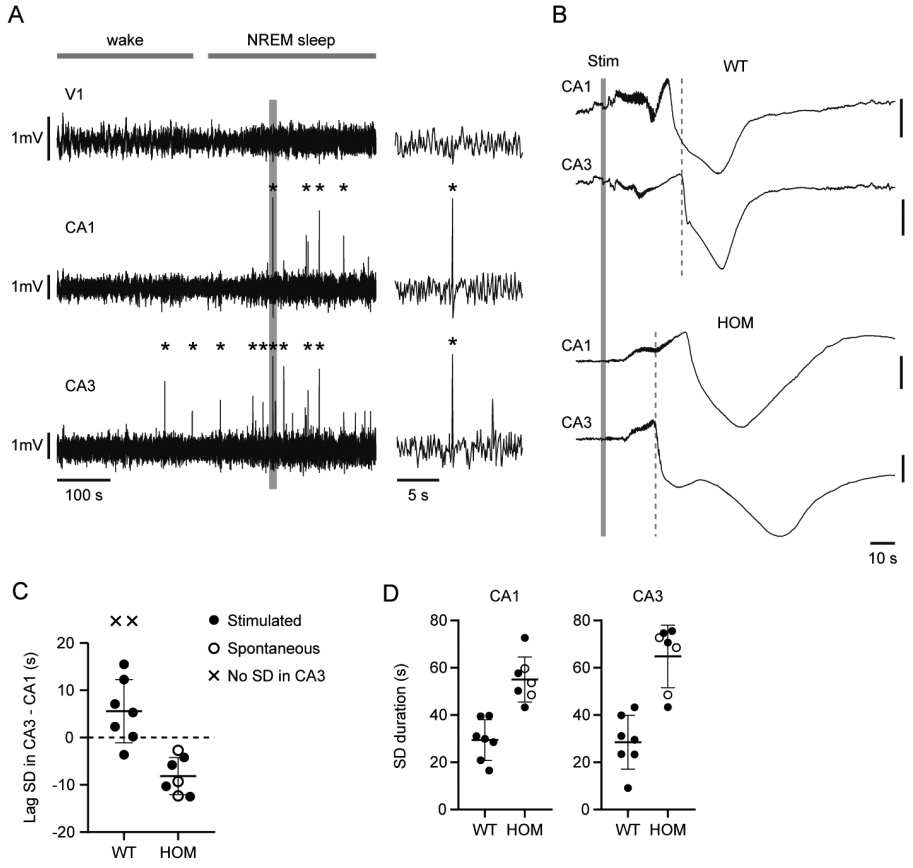

(A) Example LFP recordings in a homozygous *Atp1a2*^{T345A} mouse showing interictal spikes (indicated by asterisks) in hippocampal CA1 and CA3 during NREM sleep, that in the primary visual cortex (V1) was of similar amplitude as background activity. **(B)** Example DC signals from the right CA1 and CA3 region of a wildtype (WT, top) and homozygous *Atp1a2*^{T345A} mouse (HOM, bottom), showing afterdischarges followed by SD, after electrical stimulation (Stim) of the left CA3 region. Note the different spreading pattern of SD in the 2 genotypes: CA3 SD followed CA1 SD in the WT mouse, whereas it preceded CA1 SD in the homozygous *Atp1a2*^{T345A} mouse. Vertical scale bars indicate 10 mV. **(C)** Lag between SD initiation in CA3 *vs* CA1 (i.e. positive values indicate CA1 preceding CA3). In contrast to WT mice, in homozygous *Atp1a2*^{T345A} mice CA3 SD events are more likely to precede CA1 SD events ($p = 0.0012$, Mann-Whitney U test; data from stimulated and spontaneous SD events were grouped for *Atp1a2*^{T345A} mice; WT animals in which no CA3 SD occurred were excluded). **(D)** SD duration in both CA1 and CA3 was significantly greater for homozygous *Atp1a2*^{T345A} mice when compared to WT mice (both $p < 0.001$, Mann-Whitney U test; data from stimulated and spontaneous SD events were grouped for *Atp1a2*^{T345A} mice).

FIGURE 7. Seizure expression and kindling rates are decreased in *Atp1a2*^{T345A} mice.

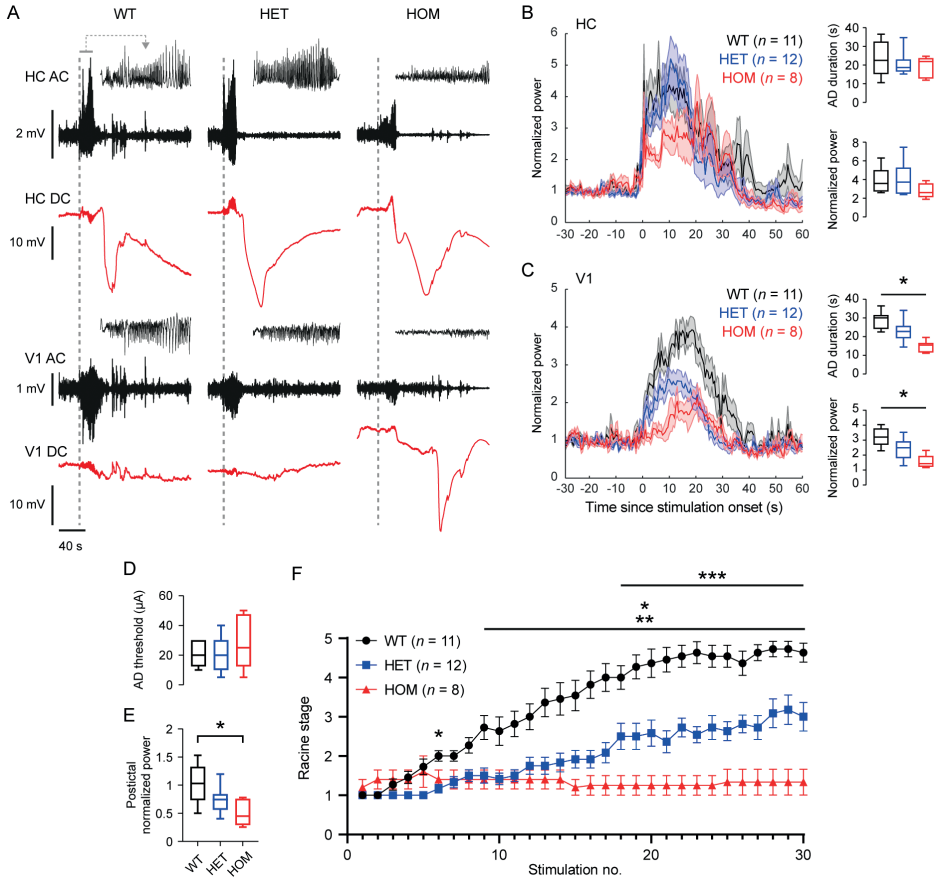

(A) Example LFP signals (AC in black, DC in red) obtained in right hippocampal CA3 (HC) and primary visual cortex (V1) following electrical stimulation of the left HC (dashed line) for wildtype (WT), heterozygous (HET) and homozygous (HOM) *Atp1a2*^{T345A} mice. Insets detail the first 20 s after stimulation. **(B)** Time series of HC LFP power normalized to baseline (30 s preceding stimulation) relative to stimulation onset (at $t = 0$ s). HC afterdischarge (AD) duration and power was similar across genotypes (*right*). **(C)** Time series of V1 LFP power normalized to baseline, demonstrating significant differences in V1 AD duration and power between all genotypes (*right*; $^*p < 0.01$; Welch's ANOVA test followed by unpaired *t* tests with Welch's correction). **(D)** AD threshold was comparable between genotypes ($p = 0.50$; Kruskal-Wallis test). **(E)** Postictal (i.e. after termination of the AD) HC LFP power was significantly reduced in HET and HOM mutant mice when compared to WT ($^*p = 0.047$, $^{**}p = 0.004$; Welch's ANOVA test followed by unpaired *t* tests with Welch's correction). **(F)** Seizure-related behavior, assessed using the Racine scale, during hippocampal kindling achieved by repetitive of stimulation of the HC at the AD threshold (twice daily for 15 days). Seizure-related behavior was decreased in mutant mice, showing a gene-dosage effect over the course of the kindling paradigm (*WT *vs* HET, **WT *vs* HOM, ***HET *vs* HOM; $p < 0.05$; two-way ANOVA with Tukey's multiple comparisons test).

Blockade of persistent sodium currents but not NMDA receptors limits hippocampal initiation of spontaneous spreading depolarizations in homozygous *Atp1a2*^{T345A} mice

Since spontaneous SD occurred regularly in homozygous *Atp1a2*^{T345A} mice, we next assessed whether these SDs could be pharmacologically modulated. NMDA receptor (NMDAR) antagonists, including the non-selective NMDAR antagonist MK801, are potent inhibitors of SD initiation.[26,27] We tested whether twice daily intraperitoneal injections with 0.5 mg/kg MK801, a dose that was previously shown to decrease the number of cortical SDs following cortical KCl application,[28] could decrease spontaneous hippocampal and cortical SD occurrence in homozygous *Atp1a2*^{T345A} mice. In 6 homozygous *Atp1a2*^{T345A} mice, 17 hippocampal SDs occurred over the course of 3 days of MK801 treatment, compared to 15 SDs during vehicle treatment. Cortical appearance of SD followed the majority of hippocampal SDs during vehicle treatment (13/15), but were effectively blocked by MK801 treatment (0/17; example trace in Fig. 8A), indicating effective suppression of SD propagation from hippocampus to cortex. However, MK801 failed to affect the number of spontaneous hippocampal SDs within the 3-day treatment period (Fig. 8B). In fact, MK801 tended to lead to a faster occurrence of an SD event after injection (range 480 – 50,150 s) when compared to vehicle (range 2670 – 50,350 s) (Fig. 8C). Since the dosage of MK801 required to block SD initiation may be higher for hippocampal regions,[29] we additionally tested repeated doses of 2.5 (10 injections in 2 mice), 3.5 (4 injections in 1 mouse) and 5.0 (1 injection in 1 mouse) mg/kg. These doses resulted in abnormal behavior of the animal (loss of posture, immobility) and even early death (4/15 injections). Following the majority of injections (10/15), a hippocampal SD occurred shortly after injection (Fig. 8C). Since the regime was not well tolerated in the mutant mice, no additional experiments with repeated high doses of MK801 were performed.

Decreased effectiveness of NMDAR antagonism in SD initiation may be explained by increased extracellular K^+,[30] which could also ignite SD in the hippocampus by a positive feedback loop involving K^+-induced increases in persistent sodium currents.[31] We therefore tested whether treatment with GS967, a preferential inhibitor of persistent sodium currents, affected SD occurrence in *Atp1a2*^{T345A} mice (n = 8). After one week of baseline recordings, standard chow was replaced by chow containing GS967 (8 mg/kg of chow, estimated to result in a daily dose of 1.5 mg/kg[21]) for one week, again replaced by standard chow for one week of recovery (Fig. 8D). The number of spontaneous hippocampal SD events decreased during GS967 treatment (Fig. 8E). However, GS967 did not prevent spread of SD to the cortex (cortical SD in 15/15 events, compared to 60/65 events during baseline/recovery, $\chi^2_{(1)} = 1.1$, $p < 0.267$) nor did the compound affect the time delay between hippocampal and V1 SD (61 ± 21 s during GS967 treatment vs 66 ± 28 s during baseline; $p = 0.56$). These data suggest that persistent sodium currents but not NMDAR-mediated currents contribute to spontaneous hippocampal SD initiation in homozygous *Atp1a2*^{T345A} mice.

FIGURE 8. Blockade of persistent sodium currents, but not NMDA receptor antagonism, decreased initiation of spontaneous SDs in homozygous *Atp1a2*^{T345A} mice.

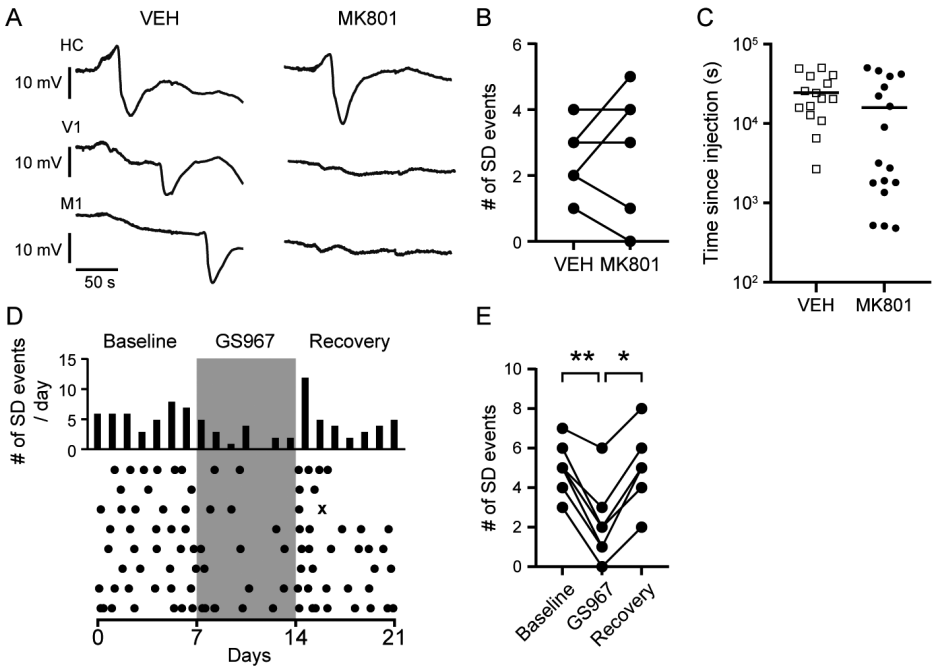

(A) Example LFP DC recordings in hippocampus (HC), primary visual cortex (V1) and primary motor cortex (M1) of a homozygous *Atp1a2*^{T345A} mouse during treatment with vehicle (VEH) or MK801 (0.5 mg/kg, twice daily over the course of 3 days). **(B)** Although MK801 did prevent SD propagation to cortex, it did not affect spontaneous hippocampal event rate ($n = 8$; $p = 0.50$, Wilcoxon signed-rank test). **(C)** Time between injection of 0.5 m/kg MK801 or vehicle and the first hippocampal SD ($p = 0.0637$, Mann-Whitney U test). Following MK801, no propagation to the cortex was observed. **(D)** Raster plot with dots indicating spontaneous hippocampal SD events in homozygous *Atp1a2*^{T345A} mice ($n = 8$) while fed standard chow (baseline and recovery) or GS967-compounded chow (shaded area); superimposed a histogram showing the total event count per 24 h. Note that one animal died during the 21-day recording period, indicated by a cross. **(E)** Spontaneous SD events in homozygous *Atp1a2*^{T345A} mice were significantly less likely to occur during GS967 treatment (*$p = 0.016$ and **$p = 0.008$, Wilcoxon signed-rank rest; $n = 7$; the animal that died during the recovery period was not included in the analysis).

DISCUSSION

In this study, we present a novel FHM2 knock-in mouse model with the *Atp1a2*^{T345A} mutation. Homozygous mutant mice are viable and demonstrate regular spontaneous SD. SD events typically originated from the hippocampus and propagated to the visual cortex and then in a caudal-to-rostral pattern. Hippocampal PO_2 measurements indicated that the spontaneous SD events were not caused by hypoxia. Heterozygous mutant mice rarely exhibit spontaneous SD. Whereas heterozygotes only show an increased propagation speed of electrically evoked cortical SD, homozygotes also show a decreased threshold for such events. Hence, whereas the heterozygous *Atp1a2*^{T345A} mice show certain features relevant to patients, who have one mutant gene copy, the homozygotes provide the unique opportunity to investigate spontaneous SD events. Inhibition of persistent sodium currents reduced the occurrence of spontaneous SD in homozygotes, without affecting SD propagation. Notably, NMDAR antagonism did not inhibit hippocampal SD initiation but blocked subsequent appearance of SD in the cortex in homozygotes. These findings indicate that modelling spontaneous SD allows differentiation of its initiation and propagation mechanisms, potentially impacting treatment strategies.

Spontaneous SDs have not been reported in existing FHM2 mouse models including the *Atp1a2*^{W887R} [5, 7, 32] and *Atp1a2*^{G301R} [23] strains. Homozygous mice of these mouse strains die at birth, similar to *Atp1a2*$^{-/-}$ mice.[4, 33] In the present study, homozygous *Atp1a2*^{T345A} mice show a normal expression level of α_2NKA protein. The location of the T345A missense mutation on the cytoplasmic stalk domain adjacent to transmembrane segment 4 suggests it would affect Na^+/K^+ ATPase functioning. Cellular studies have shown different consequences of the T345A mutation including decreased K^+ affinity,[16] lower maximum turnover rate,[14] or even preserved Na^+/K^+ATPase functioning for the parameters tested.[15] In contrast, the W887R[16] and G301R[17] mutants fail to show any ATPase activity and do not support cell growth. Thus, available data reflect the phenotype of *Atp1a2* mutants, with *Atp1a2*^{T345A} being the mildest. A gene dosage effect for the T345A mutation was evidenced by a relatively high incidence of spontaneous SDs and decreased electrical threshold for induced SDs, in homozygous *versus* heterozygous *Atp1a2*^{T345A} mice. Comparison of results from heterozygous *Atp1a2*^{T345A} mice with *in vivo* SD susceptibility data of heterozygous mutants from published FHM2 mouse models[5, 6, 32, 34] remains qualitative as a direct comparison is hampered by differences in methodology, including differences in SD induction methods (e.g. electrical stimulation and KCl) and brain state during these experiments (i.e. awake freely behaving in our study, versus anesthetized or head-fixed awake in studies in other models). Nevertheless, the enhanced susceptibility to evoked cortical SDs in heterozygous and homozygous *Atp1a2*^{T345A} mice underscores the role of astrocytic buffering in SD susceptibility in the context of FHM2, as nicely illustrated for mice of the *Atp1a2*^{W887R} strain by reduced rates of clearance of glutamate and K^+ by cortical astrocytes during neuronal activity.[7, 32] The observation of sudden apnea preceding early mortality in homozygous *Atp1a2*^{T345A} mice suggests that besides in the hippocampus, local or spreading depolarizations may also occur in the brainstem, as was demonstrated in FHM1[35, 36]

and FHM3[37] mouse models. Regardless, the high incidence and regularity of spontaneous SDs in homozygous *Atp1a2*^{T345A} mice is especially of interest to advance the study of mechanisms and consequences of SD initiation.

In all homozygous *Atp1a2*^{T345A} mice studied, spontaneous SD events were recorded. SD events showed a diurnal rhythm and preferably initiated during sleep. Clinical studies have demonstrated a similar circadian periodicity in attacks both for migraine with and without aura, with attacks occurring preferably during the early morning,[38, 39] although peaks at the middle of the day have also been reported.[40] The majority of patients report migraine attacks upon awakening,[41] which we also observed for homozygous *Atp1a2*^{T345A} mice. Astrocytic activity contributes to the transition from sleep to wakefulness.[42] Considering the role of astrocytes in K^+ clearance and the changes in brain extracellular K^+ levels over the sleep-wake cycle,[43-45] sudden surges in extracellular K^+ during the sleep-wake transition may facilitate SD initiation.

A majority of hippocampal SDs in homozygous *Atp1a2*^{T345A} mice was preceded by epileptiform bursts of relatively short duration and moderate amplitude. The typical observation of hippocampal burst activity followed by SD in homozygous *Atp1a2*^{T345A} mice is in line with preclinical and modeling data showing that SD can initiate from a short localized burst of network activity[46, 47] (for reviews see Somjen 2001[1]; Ayata and Lauritzen 2015[48]). The observation that the amplitude of the epileptiform bursts was always higher in hippocampus compared to cortex, seems further support of a hippocampal origin of the events. Notably, overt seizure-related behavior was absent during most of the spontaneous events, while both heterozygous and homozygous *Atp1a2*^{T345A} mice displayed decreased hippocampal kindling. Such inverse relationship between epileptic kindling and SD incidence has been reported previously.[49] The start of the burst activity preceded hippocampal SD by tens of seconds, which would allow sufficient time for seizure activity to spread and cause seizure-related behaviors. Indeed, in wildtype mice hippocampal SD also occurred during kindling experiments, and it was already preceded by epileptic activity in both LFP and behavior. We thus consider it less likely that reduced seizure expression in *Atp1a2*^{T345A} mice is mediated by the suppressive effects of SD. Previous work has shown that seizure propagation relies on connectivity and synaptic transmission.[50, 51] We thus hypothesize that the decreased amplitudes and duration of ADs in the cortex of *Atp1a2*^{T345A} mice result from less efficient synaptic and/or electric field transmission in these mice, which could hamper seizure generalization.

Impaired glutamate uptake resulting in activation of NMDARs has been shown a critical mechanism underlying SD initiation in *Atp1a2*^{W887R} mice.[7, 32] Such facilitation of cortical SD has been attributed to impaired glutamate clearance by cortical astrocytes, indicating that astrocytic α_2NKA regulates glutamate uptake through coupling with glutamate transporters.[7] Although various studies report that blocking NMDARs effectively blocks experimentally induced SD (for reviews see Klass et al., 2018[27]; Telles et al., 2021), it remains unclear whether this effect is caused by inhibition of SD initiation or propagation mechanisms, or both.[29] Contrasting conclusions may arise from the location of recordings relative to the SD initiation site, for example when comparing the role of NMDARs in hippocampal SD[52] *versus* cortical SD.[53] Alternatively, SD initiation mechanisms

(and related susceptibility to NMDAR modulation) may differ across brain regions and animal models, and might also be influenced by the experimental approach, including the choice for *in vivo* (under anesthesia or awake) or *ex vivo* experimentation. For example, blocking NMDARs did not prevent KCl-induced SD onset in the hippocampus of anesthetized rats,[54] contrasting various reports of suppressing effects of NMDAR blockers on cortical SD, either induced by KCl in cortical slices,[53, 55, 56] by KCl or electrical stimulation in anesthetized mice[28] or rats,[26, 57-60] or by optogenetics in awake mice.[61] Overall, SD initiation mechanisms may be ideally studied in disease models where they occur spontaneously, in the absence of anesthesia. Here, MK801 (0.5 mg/kg i.p.) failed to decrease the frequency of spontaneous hippocampal SDs in homozygous *Atp1a2*^{T345A} mice, while preventing appearance in cortex. While high doses (2.5 – 5.0 mg/kg i.p.) of MK801 were not well tolerated, especially not in homozygous mutants, hippocampal SDs were still observed, albeit without subsequent SD appearance in cortex. The abnormal behaviors (loss of posture and immobility) and even early mortality observed in homozygous *Atp1a2*^{T345A} mice following high doses MK801 expand findings of locomotor abnormalities including immobility, ataxia and stereotypic behaviors following high doses systemic administration of MK801 in wildtype mice and rats[62-64] that may warrant some caution when interpreting brain activity, including that of SD following high dosage MK801 under awake conditions. Regardless, our observations with both low and high doses of MK801 suggest reduced sensitivity of homozygous *Atp1a2*^{T345A} mice to NMDAR blockade, at least in the context of spontaneous hippocampal SD initiation. Conversely, the persistent sodium current blocker GS967 did suppress hippocampal SD occurrence, while propagation to cortical regions was not impaired, suggesting that action potential generation is critical for initiation but perhaps not so much for propagation of spontaneous SDs in homozygous *Atp1a2*^{T345A} mice. Our data complement earlier findings from anesthetized rats that showed a small effect of GS967 on increasing the threshold of electrically evoked CSD,[65] suggesting that in the absence of intrinsic hyperexcitability, the role of persistent sodium currents for SD initiation is only modest. Our results may be explained by a (general or transient) increase in brain extracellular K^+ in *Atp1a2*^{T345A} mice, which is expected to decrease the effectiveness of NMDAR antagonists,[30] although this was not demonstrated, while increasing persistent sodium currents.[31] As such, our data suggest that targeting persistent sodium currents, in addition to NMDAR modulation, may be a promising treatment strategy in FHM2, likely depending on the mutation, and which may also be applicable to other SD-related diseases.

Acknowledgements

This work was supported by the Dutch National Epilepsy Foundation (2017-10 to and A.M.J.M.v.d.M., the European Innovation Council EIC Pathfinder Programme Project MICROVASC (no 101070917 to A.M.J.M.v.d.M.), European Union Joint Programme – Neurodegenerative Disease Research project REBALANCE (no 10510062210003 to E.A.T and A.M.J.M.v.d.M.) and the Medical Delta program "Medical NeuroDelta: Ambulant Neuromonitoring for Prevention and Treatment of Brain Disease" (to A.M.J.M.v.d.M.). We thank Praxis Precision Medicines for providing PRAX-330-modified chow and Kris Kahlig for input on the related experiments.

REFERENCES

1. Somjen, G.G., Mechanisms of spreading depression and hypoxic spreading depression-like depolarization. *Physiol Rev*, 2001. 81(3): p. 1065-96.
2. Lauritzen, M., et al., Clinical relevance of cortical spreading depression in neurological disorders: migraine, malignant stroke, subarachnoid and intracranial hemorrhage, and traumatic brain injury. *J Cereb Blood Flow Metab*, 2011. 31(1): p. 17-35.
3. De Fusco, M., et al., Haploinsufficiency of ATP1A2 encoding the Na+/K+ pump alpha2 subunit associated with familial hemiplegic migraine type 2. *Nat Genet*, 2003. 33(2): p. 192-6.
4. Moseley, A.E., et al., The Na,K-ATPase alpha 2 isoform is expressed in neurons, and its absence disrupts neuronal activity in newborn mice. *J Biol Chem*, 2003. 278(7): p. 5317-24.
5. Leo, L., et al., Increased susceptibility to cortical spreading depression in the mouse model of familial hemiplegic migraine type 2. *PLoS Genet*, 2011. 7(6): p. e1002129.
6. Kros, L., K. Lykke-Hartmann, and K. Khodakhah, Increased susceptibility to cortical spreading depression and epileptiform activity in a mouse model for FHM2. *Sci Rep*, 2018. 8(1): p. 16959.
7. Capuani, C., et al., Defective glutamate and K+ clearance by cortical astrocytes in familial hemiplegic migraine type 2. *EMBO Mol Med*, 2016. 8(8): p. 967-86.
8. Sugimoto, H., et al., Astrocytes in Atp1a2-deficient heterozygous mice exhibit hyperactivity after induction of cortical spreading depression. *FEBS Open Bio*, 2020. 10(6): p. 1031-1043.
9. Reiffurth, C., et al., Na(+)/K(+)-ATPase alpha isoform deficiency results in distinct spreading depolarization phenotypes. *J Cereb Blood Flow Metab*, 2020. 40(3): p. 622-638.
10. James, P.F., et al., Identification of a specific role for the Na,K-ATPase alpha 2 isoform as a regulator of calcium in the heart. *Mol Cell*, 1999. 3(5): p. 555-63.
11. Chatron, N., et al., A novel lethal recognizable polymicrogyric syndrome caused by ATP1A2 homozygous truncating variants. *Brain*, 2019. 142(11): p. 3367-3374.
12. Monteiro, F.P., et al., Biallelic loss of function variants in ATP1A2 cause hydrops fetalis, microcephaly, arthrogryposis and extensive cortical malformations. *Eur J Med Genet*, 2020. 63(1): p. 103624.
13. Segall, L., et al., Kinetic alterations due to a missense mutation in the Na,K-ATPase alpha2 subunit cause familial hemiplegic migraine type 2. *J Biol Chem*, 2004. 279(42): p. 43692-6.
14. Schack, V.R., R. Holm, and B. Vilsen, Inhibition of phosphorylation of na+,k+-ATPase by mutations causing familial hemiplegic migraine. *J Biol Chem*, 2012. 287(3): p. 2191-202.
15. Weigand, K.M., et al., Biochemical characterization of sporadic/familial hemiplegic migraine mutations. *Biochim Biophys Acta*, 2014. 1838(7): p. 1693-700.
16. Segall, L., et al., Alterations in the alpha2 isoform of Na,K-ATPase associated with familial hemiplegic migraine type 2. *Proc Natl Acad Sci U S A*, 2005. 102(31): p. 11106-11.
17. Tavraz, N.N., et al., Impaired plasma membrane targeting or protein stability by certain ATP1A2 mutations identified in sporadic or familial hemiplegic migraine. *Channels (Austin)*, 2009. 3(2): p. 82-7.
18. Pettitt, S.J., et al., Agouti C57BL/6N embryonic stem cells for mouse genetic resources. *Nat Methods*, 2009. 6(7): p. 493-5.

19. McAfee, S.S., et al., Minimally invasive highly precise monitoring of respiratory rhythm in the mouse using an epithelial temperature probe. *J Neurosci Methods*, 2016. 263: p. 89-94.
20. Jansen, N.A., et al., First FHM3 mouse model shows spontaneous cortical spreading depolarizations. *Ann Clin Transl Neurol*, 2020. 7(1): p. 132-138.
21. Baker, E.M., et al., The novel sodium channel modulator GS-458967 (GS967) is an effective treatment in a mouse model of SCN8A encephalopathy. *Epilepsia*, 2018. 59(6): p. 1166-1176.
22. Jansen, N.A., et al., Impaired theta-gamma Coupling Indicates Inhibitory Dysfunction and Seizure Risk in a Dravet Syndrome Mouse Model. *J Neurosci*, 2021. 41(3): p. 524-537.
23. Bottger, P., et al., Glutamate-system defects behind psychiatric manifestations in a familial hemiplegic migraine type 2 disease-mutation mouse model. *Sci Rep*, 2016. 6: p. 22047.
24. Haglund, M.M., et al., Developmental and regional differences in the localization of Na,K-ATPase activity in the rabbit hippocampus. *Brain Res*, 1985. 343(1): p. 198-203.
25. Haglund, M.M. and P.A. Schwartzkroin, Role of Na-K pump potassium regulation and IPSPs in seizures and spreading depression in immature rabbit hippocampal slices. *J Neurophysiol*, 1990. 63(2): p. 225-39.
26. Marrannes, R., et al., Evidence for a role of the N-methyl-D-aspartate (NMDA) receptor in cortical spreading depression in the rat. *Brain Res*, 1988. 457(2): p. 226-40.
27. Klass, A., R. Sanchez-Porras, and E. Santos, Systematic review of the pharmacological agents that have been tested against spreading depolarizations. *J Cereb Blood Flow Metab*, 2018. 38(7): p. 1149-1179.
28. Dhir, A., C. Lossin, and M.A. Rogawski, Propofol hemisuccinate suppresses cortical spreading depression. *Neurosci Lett*, 2012. 514(1): p. 67-70.
29. Pietrobon, D. and M.A. Moskowitz, Chaos and commotion in the wake of cortical spreading depression and spreading depolarizations. *Nat Rev Neurosci*, 2014. 15(6): p. 379-93.
30. Petzold, G.C., et al., Increased extracellular K+ concentration reduces the efficacy of N-methyl-D-aspartate receptor antagonists to block spreading depression-like depolarizations and spreading ischemia. *Stroke*, 2005. 36(6): p. 1270-7.
31. Somjen, G.G. and M. Muller, Potassium-induced enhancement of persistent inward current in hippocampal neurons in isolation and in tissue slices. *Brain Res*, 2000. 885(1): p. 102-10.
32. Parker, P.D., et al., Non-canonical glutamate signaling in a genetic model of migraine with aura. *Neuron*, 2021. 109(4): p. 611-628 e8.
33. Ikeda, K., et al., Malfunction of respiratory-related neuronal activity in Na+, K+-ATPase alpha2 subunit-deficient mice is attributable to abnormal Cl- homeostasis in brainstem neurons. *J Neurosci*, 2004. 24(47): p. 10693-701.
34. Tang, C., et al., Characteristics of cortical spreading depression and c-Fos expression in transgenic mice having a mutation associated with familial hemiplegic migraine 2. *Cephalalgia*, 2020. 40(11): p. 1177-1190.
35. Loonen, I.C.M., et al., Brainstem spreading depolarization and cortical dynamics during fatal seizures in Cacna1a S218L mice. *Brain*, 2019. 142(2): p. 412-425.
36. Jansen, N.A., et al., Apnea associated with brainstem seizures in Cacna1a (S218L) mice is caused by medullary spreading depolarization. *J Neurosci*, 2019. 39(48): p. 9633-9644.

37. Jansen, N.A., et al., Brainstem depolarization-induced lethal apnea associated with gain-of-function SCN1A(L263V) is prevented by sodium channel blockade. *Proc Natl Acad Sci U S A*, 2024. 121(14): p. e2309000121.
38. Fox, A.W. and R.L. Davis, Migraine chronobiology. Headache, 1998. 38(6): p. 436-41.
39. van Oosterhout, W., et al., Chronotypes and circadian timing in migraine. Cephalalgia, 2018. 38(4): p. 617-625.
40. Alstadhaug, K., R. Salvesen, and S. Bekkelund, 24-hour distribution of migraine attacks. *Headache*, 2008. 48(1): p. 95-100.
41. Kelman, L. and J.C. Rains, Headache and sleep: examination of sleep patterns and complaints in a large clinical sample of migraineurs. *Headache*, 2005. 45(7): p. 904-10.
42. Bojarskaite, L., et al., Astrocytic Ca(2+) signaling is reduced during sleep and is involved in the regulation of slow wave sleep. Nat Commun, 2020. 11(1): p. 3240.
43. Rasmussen, R., et al., Cortex-wide changes in extracellular potassium ions parallel brain state transitions in awake behaving mice. Cell reports, 2019. 28(5): p. 1182-1194. e4.
44. Ding, F., et al., Changes in the composition of brain interstitial ions control the sleep-wake cycle. *Science*, 2016. 352(6285): p. 550-555.
45. Rasmussen, R., M.H. Jensen, and M.L. Heltberg, Chaotic Dynamics Mediate Brain State Transitions, Driven by Changes in Extracellular Ion Concentrations. *Cell Syst*, 2017. 5(6): p. 591-603 e4.
46. Larrosa, B., et al., A role for glutamate and glia in the fast network oscillations preceding spreading depression. *Neuroscience*, 2006. 141(2): p. 1057-1068.
47. Wei, Y., G. Ullah, and S.J. Schiff, Unification of neuronal spikes, seizures, and spreading depression. *J Neurosci*, 2014. 34(35): p. 11733-43.
48. Ayata, C. and M. Lauritzen, Spreading Depression, Spreading Depolarizations, and the Cerebral Vasculature. *Physiol Rev*, 2015. 95(3): p. 953-93.
49. Koroleva, V.I., L.V. Vinogradova, and J. Bures, Reduced incidence of cortical spreading depression in the course of pentylenetetrazol kindling in rats. *Brain Res*, 1993. 608(1): p. 107-14.
50. Rossi, L.F., et al., Focal cortical seizures start as standing waves and propagate respecting homotopic connectivity. *Nat Commun*, 2017. 8(1): p. 217.
51. Choy, M., et al., Repeated hippocampal seizures lead to brain-wide reorganization of circuits and seizure propagation pathways. *Neuron*, 2021.
52. Mei, Y.Y., et al., NMDA receptors sustain but do not initiate neuronal depolarization in spreading depolarization. *Neurobiol Dis*, 2020. 145: p. 105071.
53. Vitale, M., et al., Mechanisms of initiation of cortical spreading depression. *J Headache Pain*, 2023. 24(1): p. 105.
54. Herreras, O., et al., Role of neuronal synchronizing mechanisms in the propagation of spreading depression in the in vivo hippocampus. *J Neurosci*, 1994. 14(11 Pt 2): p. 7087-98.
55. Anderson, T.R. and R.D. Andrew, Spreading depression: imaging and blockade in the rat neocortical brain slice. *J Neurophysiol*, 2002. 88(5): p. 2713-25.

56. Tottene, A., A. Urbani, and D. Pietrobon, Role of different voltage-gated Ca2+ channels in cortical spreading depression: specific requirement of P/Q-type Ca2+ channels. *Channels (Austin)*, 2011. 5(2): p. 110-4.
57. Willette, R.N., P.G. Lysko, and C.F. Sauermelch, A comparison of (+)SK&F 10047 and MK-801 on cortical spreading depression. *Brain Res*, 1994. 648(2): p. 347-51.
58. Lauritzen, M. and A.J. Hansen, The effect of glutamate receptor blockade on anoxic depolarization and cortical spreading depression. *J Cereb Blood Flow Metab*, 1992. 12(2): p. 223-9.
59. Menniti, F.S., et al., CP-101,606, an NR2B subunit selective NMDA receptor antagonist, inhibits NMDA and injury induced c-fos expression and cortical spreading depression in rodents. *Neuropharmacology*, 2000. 39(7): p. 1147-55.
60. Peeters, M., et al., Effects of pan- and subtype-selective N-methyl-D-aspartate receptor antagonists on cortical spreading depression in the rat: therapeutic potential for migraine. *J Pharmacol Exp Ther*, 2007. 321(2): p. 564-72.
61. Masvidal-Codina, E., et al., Characterization of optogenetically-induced cortical spreading depression in awake mice using graphene micro-transistor arrays. *J Neural Eng*, 2021. 18(5).
62. Tricklebank, M.D., et al., The behavioural effects of MK-801: a comparison with antagonists acting non-competitively and competitively at the NMDA receptor. *Eur J Pharmacol*, 1989. 167(1): p. 127-35.
63. Deutsch, S.I., R.B. Rosse, and J. Mastropaolo, Behavioral approaches to the functional assessment of NMDA-mediated neural transmission in intact mice. *Clin Neuropharmacol*, 1997. 20(5): p. 375-84.
64. Wu, J., et al., Bimodal effects of MK-801 on locomotion and stereotypy in C57BL/6 mice. *Psychopharmacology (Berl)*, 2005. 177(3): p. 256-63.
65. Morais, A., et al., Inhibition of persistent sodium current reduces spreading depression-evoked allodynia in a mouse model of migraine with aura. *Pain*, 2023. 164(11): p. 2564-2571.

SUPPLEMENTARY MATERIAL

FIGURE S1. Homozygous *Atp1a2*^{T345A} mice showed a reduced body weight development and normal behavioral activity levels.

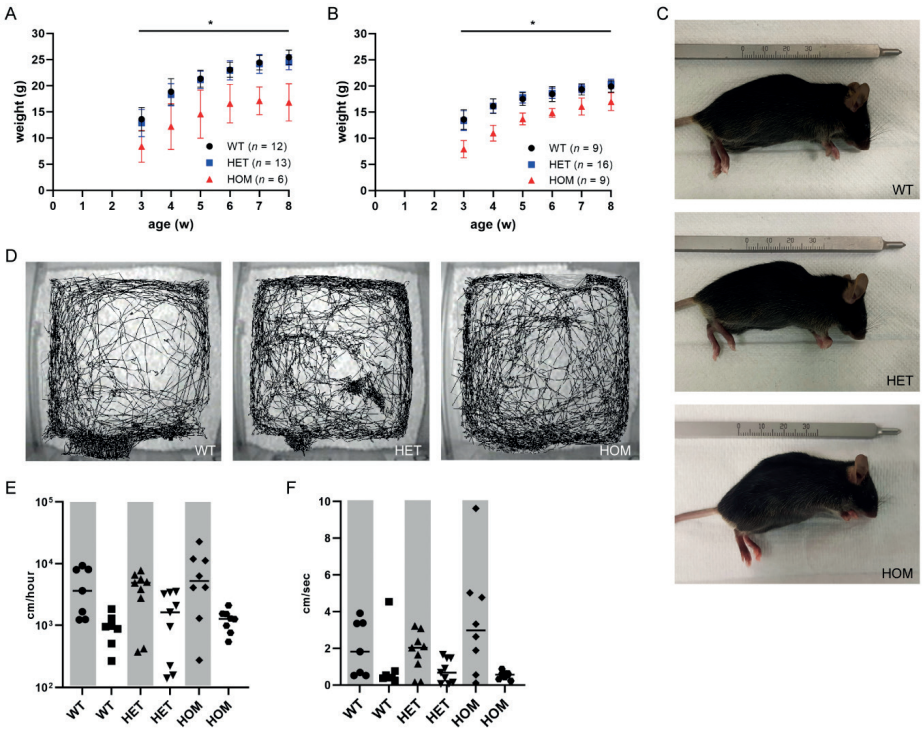

Both male **(A)** and female **(B)** homozygous (HOM), but not heterozygous (HET), *Atp1a2*^{T345A} mice showed reduced body weight (*$p < 0.01$, for WT versus HOM mice) and size (examples in **C**). **(D)** Representative tracking results (45 min, during the dark phase) from a WT, heterozygous and homozygous *Atp1a2*^{T345A} mouse. Total distance moved **(E)** and mean velocity **(F)** did not indicate differences in behavioral activity levels in WT, heterozygous or homozygous *Atp1a2*^{T345A} mice. Analyses from light and the dark periods are indicated by white and gray background, respectively.

FIGURE S2. Example of burst activity preceding SD in a homozygous *Atp1a2*^{T345A} mouse.

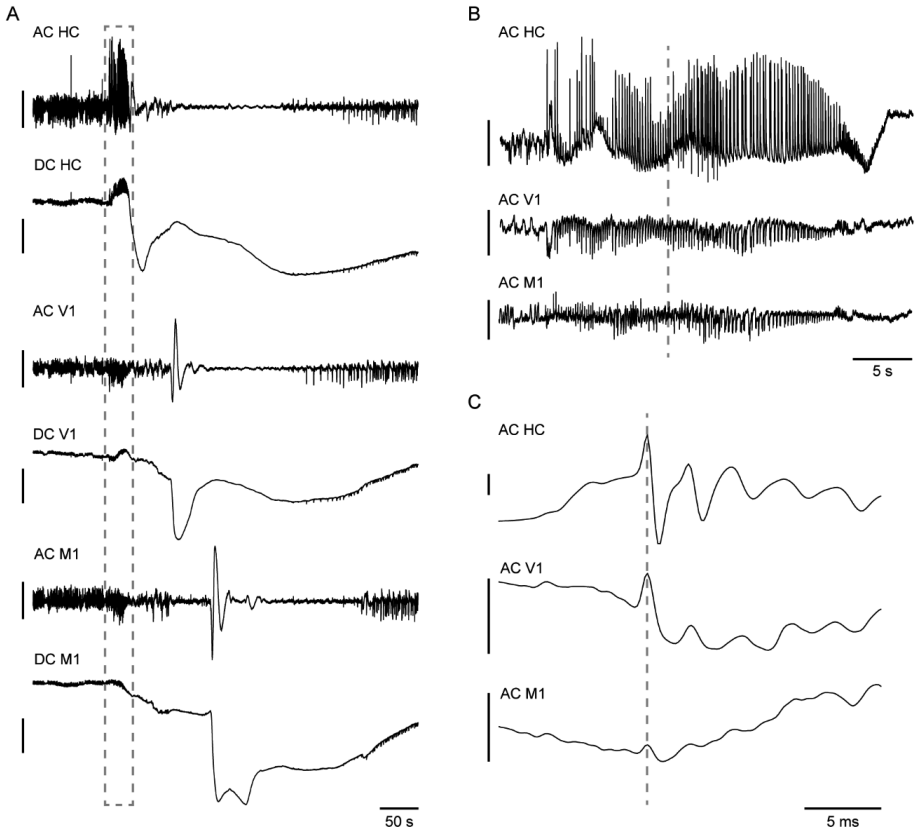

(A) Hippocampal (HC), primary visual cortex (V1) and primary motor cortex (M1) AC and DC LFP recordings during a burst (dashed box, detailed in B) followed by spontaneous SD in a homozygous *Atp1a2*^{T345A} mouse. **(B)** Burst activity amplitude was most pronounced in HC LFP, with high-amplitude spikes (example indicated by dashed line, detailed in **C**) synchronizing with lower amplitude spikes in V1 and M1. Vertical scale bars indicate 2 mV (AC) and 10 mV (DC) for **A** and **B**, and 1 mV for **C**

FIGURE S3. Example of a hippocampal partial oxygen pressure (PO2) recording during spontaneous SD in a homozygous *Atp1a2*^{T345A} mouse.

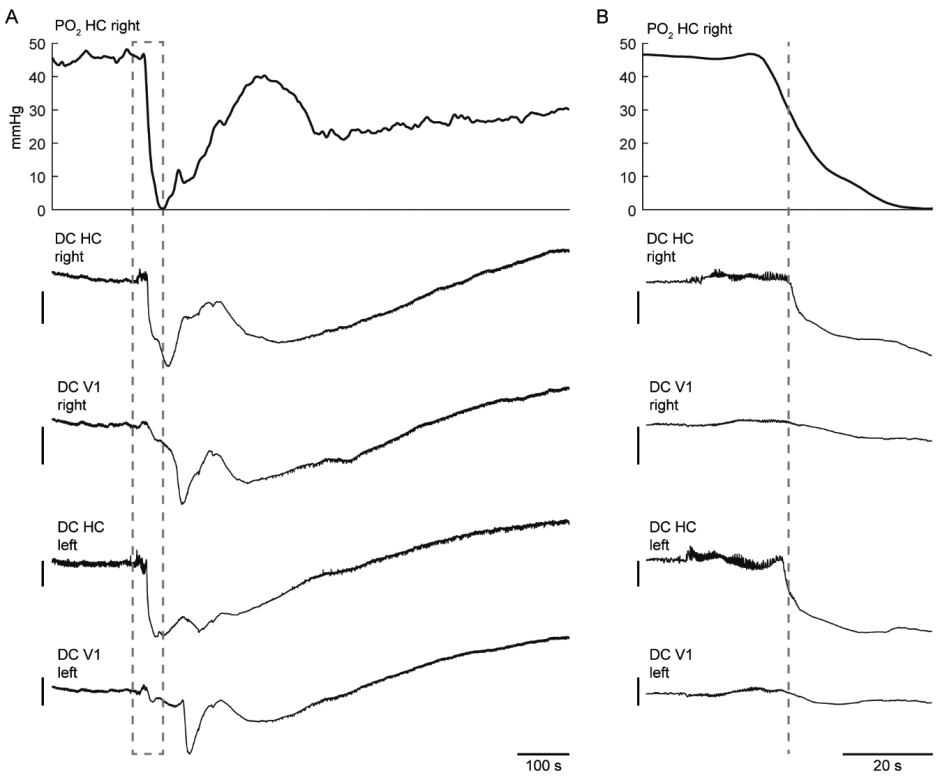

(A) Hippocampal (HC) PO_2 decreased during burst activity (dashed box, detailed in **B**) and the subsequent SD as depicted by the HC DC signal (ipsilateral onset indicated by a dashed line in **B**), preceding SD in the primary visual cortex (V1). Note that HC PO_2 was within normoxic range (>18 mmHg) at the onset of the DC shift. Vertical scale bars indicate 10 mV.

Part II

Mechanisms of sudden death

Chapter 4

Brainstem spreading depolarization and cortical dynamics during fatal seizures in *Cacna1a*^{S218L} mice

Inge C.M. Loonen*
Nico A. Jansen*
Stuart M. Cain*
Maarten Schenke
Rob A. Voskuyl
Andrew C. Yung
Barry Bohnet
Piotr Kozlowski
Roland D. Thijs
Michel D. Ferrari
Terrance P. Snutch
Arn M.J.M. van den Maagdenberg
Else A. Tolner

*These authors contributed equally

Brain 2019;142(2):412-425

ABSTRACT

Sudden unexpected death in epilepsy (SUDEP) is a fatal complication of epilepsy in which brainstem spreading depolarization may play a pivotal role, as suggested by animal studies. Spatiotemporal details of spreading depolarization occurring in relation to fatal seizures have however not been investigated. In addition, little is known about behavioral and neurophysiological features that may discriminate spontaneous fatal from non-fatal seizures. Transgenic mice carrying the missense mutation S218L in the $\alpha 1_A$ subunit of $Ca_V2.1$ (P/Q-type) Ca^{2+} channels exhibit enhanced excitatory neurotransmission and increased susceptibility to spreading depolarization. Homozygous *Cacna1a*^{S218L} mice show spontaneous non-fatal and fatal seizures, occurring throughout life, resulting in a reduced life expectancy. To identify characteristics of fatal and non-fatal spontaneous seizures, we compared behavioral and electrophysiological seizure dynamics in freely behaving homozygous *Cacna1a*^{S218L} mice. To gain insight in the role of brainstem spreading depolarization in SUDEP, we studied the spatiotemporal distribution of spreading depolarization in the context of seizure-related death. Spontaneous and electrically induced seizures were investigated by video-monitoring and electrophysiological recordings in freely behaving *Cacna1a*^{S218L} and wild-type mice. Homozygous *Cacna1a*^{S218L} mice showed multiple spontaneous tonic-clonic seizures and died from SUDEP in adulthood. Death was preceded by a tonic-clonic seizure terminating with hindlimb clonus, with suppression of cortical neuronal activity during and after the seizure. Induced seizures in freely behaving homozygous *Cacna1a*^{S218L} mice were followed by multiple spreading depolarizations and death. In wild-type or heterozygous *Cacna1a*^{S218L} mice, induced seizures and spreading depolarization were never followed by death. To identify temporal and regional features of seizure-induced spreading depolarization related to fatal outcome, diffusion-weighted MRI was performed in anesthetized homozygous *Cacna1a*^{S218L} and wild-type mice. In homozygous *Cacna1a*^{S218L} mice, appearance of seizure-related spreading depolarization in the brainstem correlated with respiratory arrest that was followed by cardiac arrest and death. Recordings in freely behaving homozygous *Cacna1a*^{S218L} mice confirmed brainstem spreading depolarization during spontaneous fatal seizures. These data underscore the value of the homozygous *Cacna1a*^{S218L} mouse model for identifying discriminative features of fatal compared to non-fatal seizures, and support a key role for cortical neuronal suppression and brainstem spreading depolarization in SUDEP pathophysiology.

INTRODUCTION

Sudden unexpected death in epilepsy (SUDEP) is a tragic and poorly understood complication of epilepsy[1] (Nashef et al., 2012), affecting primarily young adults.[2, 3] Rare recordings in SUDEP cases demonstrated post-ictal generalized EEG suppression (PGES) and respiratory depression prior to death.[4, 5] Risk of SUDEP appears higher in those with poorly controlled tonic-clonic seizures,[6, 7] especially during sleep.[5, 8] In addition, mutations in a subset of ion channel genes have been linked to SUDEP risk.[9-11]

Mechanisms of SUDEP are largely unknown. Homozygous $K_V1.1$ knockout, and heterozygous $Na_V1.1$ knockout mice, as well as mice with a R176Q missense mutation in RyR2 have been proposed as SUDEP models as the mutant mice exhibit seizures followed by cardiorespiratory arrest.[12-15] In these models, evoked cortical seizures were associated with respiratory arrest, followed by spreading depolarization (SD) in the dorsal brainstem and death. Seizure-related hypoxia was proposed as a critical trigger of brainstem SD, resulting in loss of brainstem control over respiration inducing further hypoxia and eventually cardiac arrest.[14]

Transgenic mice carrying the familial hemiplegic migraine type 1 S218L gain-of-function missense mutation in the *Cacna1a* gene, which encodes the α1A subunit of voltage-gated $Ca_V2.1$ (P/Q-type) Ca^{2+} channels,[16] exhibit enhanced excitatory neurotransmitter release and increased susceptibility to induced cortical SD.[16-22] SD can propagate to distinct subcortical regions in homozygous *Cacna1a*^{S218L} mice, but is typically constrained to the cortex in wild-type mice.[20, 22] Patients with the *CACNA1A* gain-of-function S218L mutation suffer from hemiplegic migraine that can be associated with seizures and lethality following minor head trauma.[23-25] Homozygous *Cacna1a*^{S218L} mice display spontaneous seizures and fatal events, that can occur throughout life and have been associated to epileptic attacks.[16]

We here compared behavioral and electrophysiological non-fatal and fatal seizure dynamics in *Cacna1a*^{S218L} mice under freely behaving conditions to assess their value as a SUDEP model and investigate SUDEP mechanisms. We employed diffusion-weighted MRI (DW-MRI) to investigate seizure-related propagation of SD to distinct brain regions in anesthetized mice and studied the incidence of brainstem SD during spontaneous seizures in freely behaving homozygous *Cacna1a*^{S218L} mice.

MATERIALS AND METHODS

Animals

Knock-in *Cacna1a*^{S218L} mice harboring the human missense mutation S218L in the mouse *Cacna1a* gene were generated using a gene-targeting approach.[16] Mice (mutant and wild-type littermates), backcrossed to C57BL/6J for at least 10 generations, of 2.5 to 6.5 months were used. Mutant homozygous *Cacna1a*^{S218L} mice were investigated, except for evoked seizure experiments in freely behaving mice, for which both heterozygous and homozygous *Cacna1a*^{S218L} mice were used. Male mice were used, except for behavioral recordings in naive (non-implanted) mice and DW-MRI experiments under anesthesia, for which both male and female mice were used.

Mice were kept under standard housing conditions with a 12-hour light/dark cycle and food and water ad libitum. Mice freely moving during experiments were housed individually. Experimental procedures were carried out during the light period between 10 a.m. and 5 p.m. Experiments were approved by local ethical committees in accordance with recommendations of the European Communities Council Directive (2010/63/EU) (Leiden) or the Canadian Council for Animal Care guidelines (Vancouver). Experiments were carried out in accordance with ARRIVE guidelines. All efforts were made to minimize animal suffering.

Surgery for electrode placement

Cortical EEG electrodes (single or paired 75 µm platinum (Pt)/iridium (Ir), PT6718; Advent Research Materials) were implanted under isoflurane anesthesia (induction 4%; maintenance 1.5% in oxygen-enriched air) at the following coordinates (mm to bregma): 0.5 anterior/2.0 lateral/0.6 depth (left and right sensorimotor cortex (M1/S1); paired Pt/Ir); 3.5 posterior/2.0 lateral/0.5 depth (right visual cortex (V1); single Pt/Ir); two ball-tip electrodes were placed above the cerebellum and served as reference (Ag) and ground (Ag/AgCl). For cortical stimulation experiments, the left M1/S1 electrodes were implanted at 0.2 mm depth. For ECG recordings, 75 or 150 µm Pt/Ir electrodes were placed subcutaneously over the left latissimus dorsi muscle and the right trapezius and/or latissimus dorsi and tunneled to the skull. For brainstem DC recordings, electrodes were implanted at the following coordinates (mm to bregma): 4.8 posterior/0.8 lateral/3.7 depth (oral pontine reticular nucleus (PnO); single Pt/Ir) and 6.7 posterior/1.3 lateral/3.8 depth (medullary reticular formation (MRF); single Pt/Ir). Electrodes were connected to a 7-channel pedestal (E363/0 socket contacts and MS373 pedestal, Plastics One) and secured to the skull using dental cement (DiaDent Europe). Carprofen (5 mg/kg, s.c.) and Temgesic (0.1 mg/kg, s.c.; only in homozygous *Cacna*^{1aS218L} mice) were administered for post-operative pain relief.

Electrophysiological recordings in freely behaving mice

Wild-type and heterozygous *Cacna1a*^{S218L} mice were allowed to recover for 1 week following surgery (except for a subset of heterozygous *Cacna1a*^{S218L} mice that were studied on the day of surgery). Homozygous Cacna1aS218L mice were given a shorter recovery period of 1 h to minimize

chances of missing fatal seizures, which mostly occurred within 5 days after surgery (see Fig. 1A). Recordings in freely behaving mice were performed as described previously.[26] Electrophysiological signals were 3X pre-amplified and fed into separate direct current (DC) potential (500 Hz low-pass; 10X gain) and alternating current (AC) potential (0.05-500 Hz; 800X gain for electrocorticogram (ECoG); 400X gain for ECG; 200X gain for stimulation experiments) amplifiers. Signals were digitized (Power 1401 and Spike2 software, CED) at 1,000 Hz (DC-potential) or 5,000 Hz (ECoG and ECG). Differential signals from paired cortical electrodes were used to detect multi-unit activity (MUA; 500-5,000 Hz; 12,000-36,000X amplification; 25,000 Hz sampling rate). Video recordings were made using a CCD camera (acA1300-60gmNIR, 30 frames/s, Basler). Locomotor activity was recorded using a custom-built passive infrared motion detection sensor.

Analysis of electrophysiological data

Electrophysiological data were analyzed offline using Spike2 software and custom-written MATLAB scripts (The Mathworks). AC-signals were inspected for electrographic seizures, defined as rhythmic discharges (spikes, sharp waves and/or slow waves) with a duration of > 5 s. For peri-ictal power analyses, AC-signals were artifact-rejected, digitally low-pass filtered (Chebyshev IIR 8th order filter) and down-sampled to 500 Hz. Next, a Fast Fourier Transform was performed using a Hamming window of 4 s. Total power was calculated for different spectral bands: delta (1-5 Hz), theta (5-10 Hz), alpha (10-15 Hz), beta (15-30 Hz), gamma (30-45 Hz) and total (1-100 Hz). SDs (in cortex or brainstem) were detected by the presence of a transient negative DC shift with amplitudes > 5 mV on at least 2 recording locations within 60 s from one another. Terminal depolarization was identified by a prolonged DC-shift without recovery in all channels.

Wave marks were identified from MUA recordings in Spike2 using a detection window of 1 ms to extract the population firing rate. Thresholds were set offline above noise level, defined as overall activity during a 1-min period after the terminal depolarization. Consistency of the MUA signal over the recording period was verified for all recordings by comparison of average firing rates across vigilance states. For comparison across animals, ECoG and MUA data were normalized by the respective activity in a 5-min baseline period of continuous non-rapid eye movement (non-REM) sleep. For ECG analyses, R-peak detection was performed in MATLAB.

Electrically induced seizures in freely behaving mice

In the majority of homozygous *Cacna1a*^{S218L} mice (8/11), seizures were induced on the day of surgery, except for a small separate group of mutant mice (n = 3), in which seizures were induced 2 weeks after surgery (by comparing both groups of homozygous mutants it was assessed whether immediate effects of local tissue damage due to the surgical procedure confounded seizure outcome). In the majority of heterozygous *Cacna1a*^{S218L} mice (7/9) and all wild-type mice (n = 7), seizures were induced 2 weeks after surgery, except for a small separate group of heterozygous *Cacna1a*^{S218L} mice (n = 2) that were stimulated on the day of surgery (for comparison of seizure outcome between heterozygous and homozygous *Cacna1a*^{S218L} mice stimulated on the day of surgery).

Electrical stimulation (15-s train consisting of 1-ms bipolar pulses at a frequency of 8 Hz at incrementally increasing current steps (0.25-4 mA) from a constant-current stimulus isolator (A395, WPI)) was administered every 5 min to determine the threshold for afterdischarges (> 5 s) and/or cortical SD recorded in contralateral M1/S1. For experiments performed 2 weeks after surgery, threshold stimulation was repeated the next day for five times with 20-min intervals. If afterdischarges and/or cortical SDs lasted more than 10 min, no subsequent stimuli were administered. For experiments performed on the day of surgery, stimulation sessions were combined on the first day due to high mortality.

Behavioral analysis

Video recordings of the 24 h preceding a fatal seizure were inspected for seizure-related behavior. Single seizures or seizure clusters lasting more than 30 min were regarded as status epilepticus, which qualifies as an exclusion criterion for SUDEP[1] and were therefore excluded from further analysis. Seizure severity was determined using the Racine-scale[27] with slight adaptation whereby the most severe stage 5 also included jumping circling and wild-running behavior. Subconvulsive stage 1/2 seizures were sporadically observed during video analysis but were not considered for further analysis due to low detection sensitivity and absence of ECoG changes. Convulsive stage 3/4 seizures could reliably be detected from video analysis, and showed similar but milder changes of ECoG as observed for stage 5 seizures. Specific behavioral components during the fatal and last non-fatal seizure occurring at least 1 h before the fatal seizure, were analyzed using software for quantitative behavioral assessment (Observer XT, Noldus Information Technology). Vigilance state was determined by inspection of V1 power spectra and behavioral activity, assessed from video and movement sensor, and categorized as (1) awake (high theta and low delta ECoG activity, during behavioral activity), (2) non-REM sleep (high delta activity, no movements) and (3) REM sleep (high theta and low delta activity following a period of non-REM sleep, no movements).

Naive mice were continuously videotaped. Recordings were assessed for spontaneous seizures in the 24 h preceding a fatal seizure and analyzed as described above.

DW-MRI during induced seizures in anesthetized mice

SD is accompanied by an influx of water to the intracellular compartment of brain cells that causes a decrease in MRI apparent diffusion coefficient.[28] Here, a recently developed DW-MRI protocol that allows SD visualization with high time-resolution[22] was combined with ECoG recordings and cortical electrical stimulation. Animals were anesthetized using isoflurane (2-5% in 100% oxygen) during surgical preparation and once implanted transferred to dexmedetomidine/fentanyl/midazolam and spontaneous breathing of normal air for at least 25 min prior to DW-MRI. Carbon fiber electrodes (WPI) were used, given their compatibility with MRI: two in left M1/S1 for stimulation, one in right M1/S1 for ECoG, and one as reference electrode in the cerebellum (coordinates as described above). MRI experiments were performed on a 7 Tesla animal scanner (Bruker). A quadrature radiofrequency coil with 70-mm inner diameter volume was used for

pulse transmission and the MRI signal was received with a 14-mm diameter actively decoupled surface coil. The mouse was laid supine in the MRI cradle with electrodes fed through the center of the radiofrequency coil. Stimulation electrodes were connected to a constant current unit and stimulator (Grass Technologies) outside the scanner. ECoG electrodes were connected to a W2100 amplifier/receiver outside the scanner (Multichannel Systems) and data was acquired at 0.1-1,000 Hz. Respiratory rate, heart rate and body temperature were monitored during scanning with a Model 1025 Control/Gating system (SA Instruments). DW-MRI was acquired using DW spin-echo planar imaging (EPI) with a b-value of 1800 s/mm^2 (echo time/repetition time = 29/2000 ms, 4 shots, field of view = 2x2 cm, matrix size = 64x64, slice thickness = 1.25 mm, 8 interleaved slices) resulting in an 8-s time resolution.

Electrical stimulation was performed as described above until afterdischarges and/or cortical SDs were observed during 15-min DW-MRI scans. Stimulation was applied at 1, 6 and 11 min with increasing stimulation intensity. If afterdischarges were not observed, a second scan with higher intensity stimulations was performed, and similarly for a third scan, if required (scan set 1 [0.25, 0.5, 1], scan set 2 [2, 4, 8], scan set 3 [10, 15, 20] mA). If the animal survived the threshold voltage, stimulation was reapplied at 20-min intervals for 1 h. Seizures were identified by motion artifacts resulting from clonus during DW-MRI acquisition and epileptiform spiking (2-10 Hz) in the ECoG. DW-MRI data were post-processed in MATLAB and ImageJ software (National Institutes of Health) to mask non-brain structures, apply color maps and measure voxel intensity in defined brain regions.[22] Identification of DW-MRI SD events was defined by an increase in signal intensity exceeding 2X the standard deviation of baseline DW-MRI intensity, sustained for a minimum of 24 s in a single region of interest and visually demonstrating a propagating wave pattern into adjacent structures.

Histology

Following experiments, surviving animals were euthanized by CO_2 and transcardially perfused (0.1 M phosphate-buffered saline followed by 4% paraformaldehyde (PFA) in 0.1 M phosphate buffer). Brains were removed, post-fixed in 4% PFA for 2.5 h at room temperature and sucrose-processed. For mice that died during experiments, brains were post-fixed in 4% PFA for 24 h at 4°C. Brains were sagittally sectioned on a sliding microtome (Leica) and sections (40 µm) were Nissl stained to verify electrode locations.

Statistical Analysis

Data visualization and statistical testing were performed using MATLAB and Graphpad Prism (GraphPad). Unless indicated otherwise, data were presented as mean ± SEM and analyzed using 2-tailed paired or unpaired *t*-tests, Mann-Whitney U test, or repeated measures one-way or two-way ANOVA, where appropriate. A P-value < 0.05 was considered significant.

RESULTS

Homozygous *Cacna1a*^{S218L} mice exhibit hallmark features of SUDEP

We first analyzed the occurrence of spontaneous death in homozygous *Cacna1a*^{S218L} mice (n = 27; all males, age 2.5-5.5 months) with implanted electrodes. Twelve mice died within the 1-h recovery period following surgery, i.e. before the start of electrophysiological recordings. Video-analysis (when available) confirmed death following seizure activity. Of the mice that survived the immediate post-surgical period (n = 15), fatal seizures were observed immediately preceding definitive behavioral arrest and death (n = 13; Fig. 1A). One animal survived the 2-week recording period, and one died following status epilepticus (and was excluded from further analysis).

Chronic electrode implantation may influence seizure characteristics by causing brain damage thus fatal seizure behavior was also studied in non-implanted animals. Among naive (non-implanted) homozygous *Cacna1a*^{S218L} mice with fatal events (n = 11 in 6 males and 5 females); in 8 mice seizure behavior was observed immediately preceding definitive behavioral arrest, similar to the fatal seizure phenotype in implanted mice. In the remaining mice (n = 3), seizure-related behavior was followed by a prolonged period (3-22 h) of immobility before death. In both groups implanted and naive mice, the duration of fatal seizure behavior immediately prior to cessation of motor activity was comparable (Fig. 1B). Most seizures (12/13 in implanted and 7/11 in naive mice) were graded stage 5.[27]

Video inspection of fatal seizures in implanted mice revealed respiratory movements indicative of gasps (between 2 and 5) following behavioral stage 5 seizure activity and preceding terminal depolarization (in 6/12 mice with sufficient quality of video recordings). Concomitant recording of cortical neuronal multi-unit activity (MUA), ECoG (DC- and AC-coupled), and behavior revealed suppression of cortical neuronal activity starting during seizure behavior and continuing up to the terminal depolarization (Fig. 2A). Ictal asystole could be excluded as cause of death in a separate group of mice (n = 5) with cortical and thoracic leads. Electrical cardiac activity was evident minutes after the terminal depolarization (Fig. 2B), with electrocardiographic arrest 315-810 s after terminal depolarization. Periods of ictal bradycardia and atrioventricular block were observed during seizure behavior for all fatal cases, but ventricular fibrillation did not occur until minutes after terminal depolarization.

FIGURE 1. Survival of implanted homozygous *Cacna1a*^{S218L} mice and fatal seizure duration in implanted and naive mice.

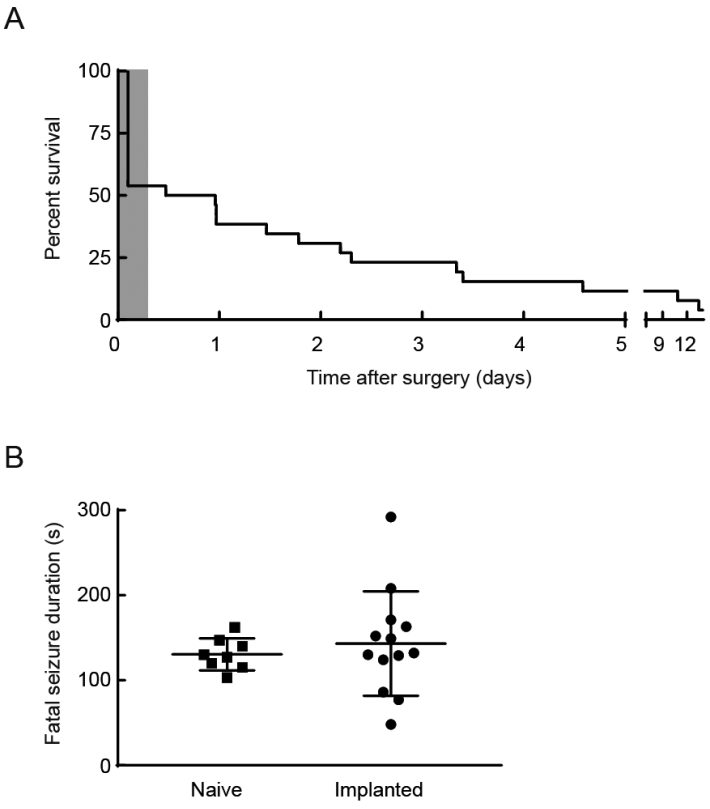

(A) Survival plot of 26 implanted homozygous *Cacna1a*^{S218L} mice showing that the majority of mice died within 1 week after surgery. Note that approximately half (n = 12) died during recovery from surgery (shaded gray), approximately half of the mice (n = 12) died. In the remaining mice (n = 14) that were monitored in the EEG set-up for 2 weeks, fatal seizures occurred in all, except one that survived the recording period. Except for one survivor, all monitored cases (n = 13) showed a fatal seizure preceding death. NB: One case additional mouse died following status epilepticus and was excluded because of death following status epilepticus from further analysis and (not included in the plot). **(B)** Duration of spontaneous fatal seizure behavior was not different for naive and implanted mice (p = 0.50; data shown as mean ± SD).

FIGURE 2. Electrophysiological recordings during spontaneous fatal seizures in homozygous *Cacna1a*^{S218L} mice.

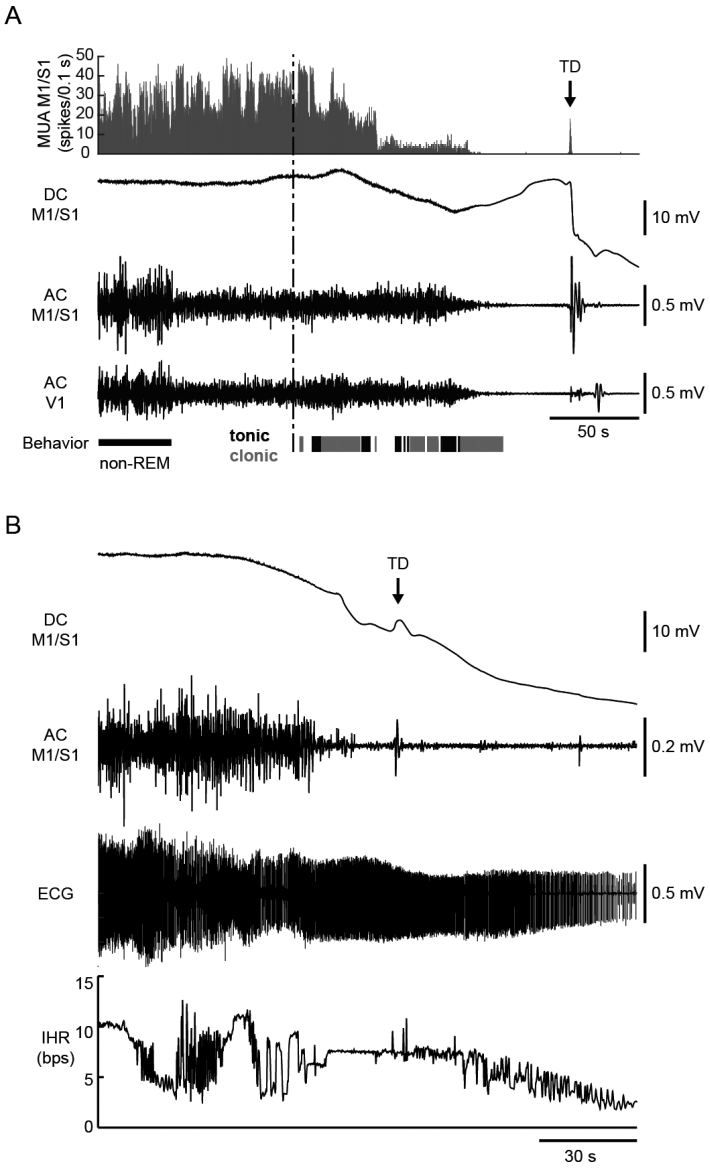

(A) Example of cortical MUA and ECoG (DC and AC) recordings during a fatal seizure (behavioral onset indicated by the vertical dashed line). MUA (histogram) decreased during seizure behavior (clonic behavior in gray, tonic behavior in black). MUA and AC ECoG were attenuated in the minute preceding the terminal depolarization (TD; indicated by an arrow). Note that the pre-ictal transition of AC ECoG amplitude parallels vigilance state (non-REM sleep followed by wakefulness). **(B)** ECG recordings during a fatal seizure in another mouse showing cardiac electrical activity following TD. Electrocardiographic arrest (not shown) occurred 7 min after the TD. The onset of seizure-related behavior preceded the plotted time series. AC = alternating current; Bps = beats per second; DC = direct current; IHR = instantaneous heart rate; REM = rapid eye movement.

Non-fatal and fatal seizures in homozygous *Cacna1a*^{S218L} mice show subtle behavioral differences

To identify discriminative features of fatal seizures, behavioral characteristics were compared between non-fatal and fatal seizures in the 24-h period preceding death in implanted homozygous *Cacna1a*^{S218L} mice. Fatal seizures were typically preceded by multiple behavioral non-fatal seizures (range 1-22/mouse; median 12), of which 41% were classified as stage 3/4 (n = 49 in 9 mice), and 59% as stage 5 (n = 71 in 11 mice). To allow for comparison of non-fatal and fatal seizures independent of seizure severity, only stage 5 seizures were included for further analysis. Non-fatal seizure incidence rates were variable in different animals but seizure frequency did not differ between 0-12 h vs 12-14 h preceding the fatal seizure (p = 0.36; Fig. 3A). Non-fatal seizure duration (averaged per animal) was comparable to fatal seizure duration (191 ± 30 and 131 ± 14 s, respectively; p = 0.37).

Both fatal and non-fatal stage 5 seizures were associated with generalized tonic and clonic behavior and loss of balance, and a subset with circling, jumping and/or wild-running. To detect subtle behavioral differences between the fatal and the last non-fatal seizure (occurring at least 1 h before the fatal seizure), the timing and duration of tonic, clonic, and other seizure behaviors was analyzed in implanted mice (n = 11; Fig. 3B). An increase in clonic behavior was observed in the second half of the fatal seizure. Indeed, closer inspection revealed that all fatal seizures ended with myoclonic jerks of fore- and hindlimbs, gradually decreasing in frequency over a period of 12-36 s. Forelimb clonus always ceased 5-30 s before termination of hindlimb clonus. Non-fatal seizures (n = 11) ended with various seizure-related behaviors (alternating tonic-clonic activity of all limbs (n = 4); exclusive forelimb clonus (n = 4); forelimb and hindlimb clonus (n = 3)). This characteristic pattern of fatal seizure termination, ending with a hindlimb clonus, was also present in naive (non-implanted) *Cacna1a*^{S218L} mice.

The majority of reported human SUDEP events occur at night [5, 8] thus nocturnal patterns in seizure incidence and vigilance state were determined in implanted mice in the 10 min preceding seizures. Stage 5 non-fatal and fatal seizures were equally distributed over the light, dark, and dusk/dawn (transition) phases (Fig. 3C) (non-fatal: 49%, 44% and 7%, respectively; fatal: 50%, 42% and 8%, respectively; p = 0.91). Animals were more often asleep prior to fatal seizures, compared to the last non-fatal seizure, although this difference did not reach statistical significance.

FIGURE 3. Frequency of spontaneous non-fatal and fatal seizures (stage 5) and (pre-)ictal behavior in implanted homozygous *Cacna1a*^{S218L} mice.

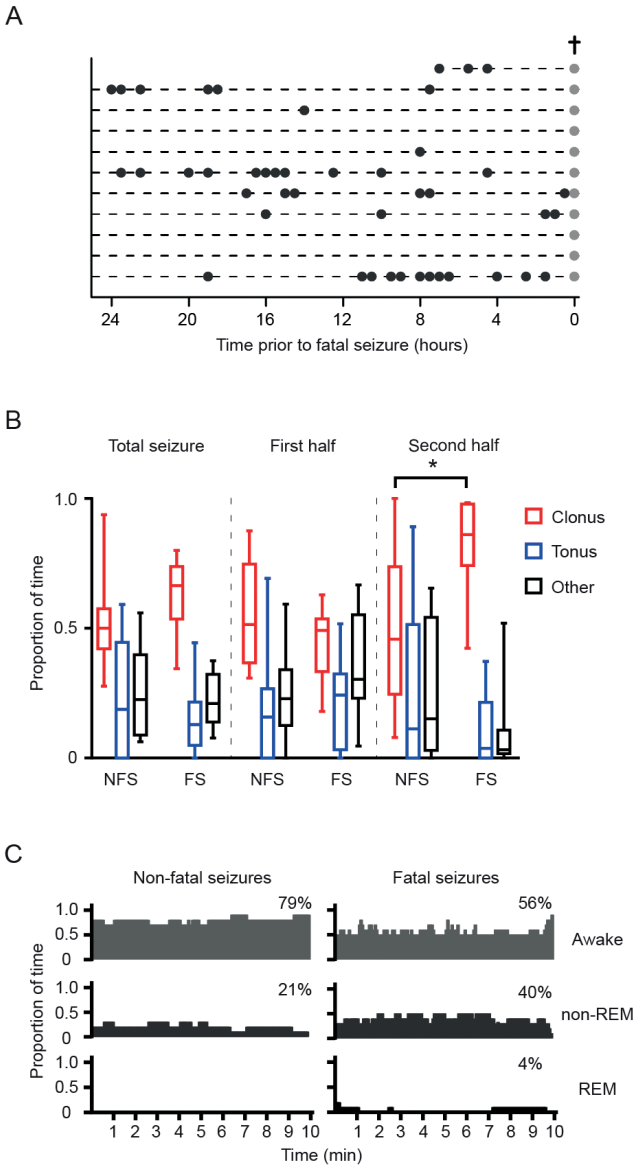

(A) The distribution of non-fatal seizures (black dots) in implanted mice was random over the 24 h preceding the fatal seizure (gray dots; cross). **(B)** Fatal seizures were associated with a proportional increase of clonic behavior during the second half of the seizure at the cost of tonic and other behaviors, when compared to non-fatal seizures ($n = 11$ per group; *$p = 0.001$). **(C)** Vigilance state preceding non-fatal and fatal seizures (percentages indicate fraction of total time) was not significantly different ($p > 0.99$). NFS = non-fatal seizures; FS = fatal seizures; REM = rapid eye movement.

Fatal seizures are associated with specific ECoG dynamics and (post-) ictal neuronal suppression

In implanted homozygous *Cacna1a*^{S218L} mice, rhythmic high-amplitude cortical epileptiform events were never observed during spontaneous non-fatal or fatal seizures (stage 5) but only occurred during status epilepticus (1 non-fatal and 1 fatal). Rather, seizures were associated with reduced ECoG amplitude followed by a period of rhythmic theta band activity (Fig. 4B) and medium-amplitude spikes during pronounced clonic behavior, which often coincided with cortical neuronal suppression (Fig. 4C). Group analysis of (pre)ictal ECoG dynamics confirmed attenuation of total ECoG power, which, for fatal seizures, resulted in complete ECoG suppression during and following the behavioral seizure and never recovered (Fig. 4D). For non-fatal seizures, such suppression of ECoG power was rarely observed (3/54 seizures; example in Supplementary Fig. 1). A decrease in normalized ECoG delta band activity was observed during the first minute of seizure-related behavior for all seizures (Fig. 4E), whereas normalized theta band power was significantly higher during the first minute for fatal compared to non-fatal seizures (Fig. 4F).

Cortical neuronal activity was increased in the seconds to minutes preceding the behavioral onset of the fatal seizure, although not significantly different from non-fatal seizures (Fig. 4G(i) and H). Notably, only during fatal seizures, neuronal activity was significantly attenuated during the last 120 s of seizure-related behavior (Fig 4G(ii) and H). This pattern was followed by low to absent neuronal activity during the post-ictal phase.

Induced seizures in homozygous *Cacna1a*^{S218L} mice are associated with multiple cortical SDs and death

Seizures, induced by stimulation of the sensorimotor cortex, were compared between freely behaving homozygous *Cacna1a*^{S218L} mice (stimulated on the day of surgery (n = 8) or 2 weeks after surgery (n = 3)), heterozygous *Cacna1a*^{S218L} mice (stimulated on the day of surgery (n = 2) or 2 weeks after surgery (n = 7)), and wild-type mice (stimulated 2 weeks after surgery (n = 7)).

Cortical stimulation resulted in severe seizures in all homozygous *Cacna1a*^{S218L} mice (starting immediately to 15.5 min after stimulation) that were fatal in 7 mice. Six mice died following single or multiple stage 5 seizures 2-73 min after stimulation (median 5 min); one mouse died following status epilepticus. Cortical stimulation never resulted in fatal seizures in heterozygous *Cacna1a*^{S218L} mice or wild-type mice. Epileptiform afterdischarges were observed in all heterozygous *Cacna1a*^{S218L} mice and wild-type mice (examples in Fig. 5A and B), but only in 2 out of 11 homozygous *Cacna1a*^{S218L} mice.

Afterdischarges were followed by a single cortical SD, recorded contralateral to the stimulation electrode, in all but one heterozygous *Cacna1a*^{S218L} mice whereas no cortical SDs were observed in wild-type mice (examples in Fig. 5A and B). Severe seizure behavior in homozygous *Cacna1a*^{S218L} mice was, however, associated with multiple cortical SDs (n = 2-38 waves, median 21, in 9/11 mice; example in Fig. 5C). These findings indicate that fatal seizure outcome in homozygous *Cacna1a*^{S218L} mice may relate to an enhanced propensity to seizure-associated SD.

FIGURE 4A-4C. Different ECoG and cortical multi-unit activity during spontaneous non-fatal and fatal seizures in homozygous *Cacna1a*^{S218L} mice.

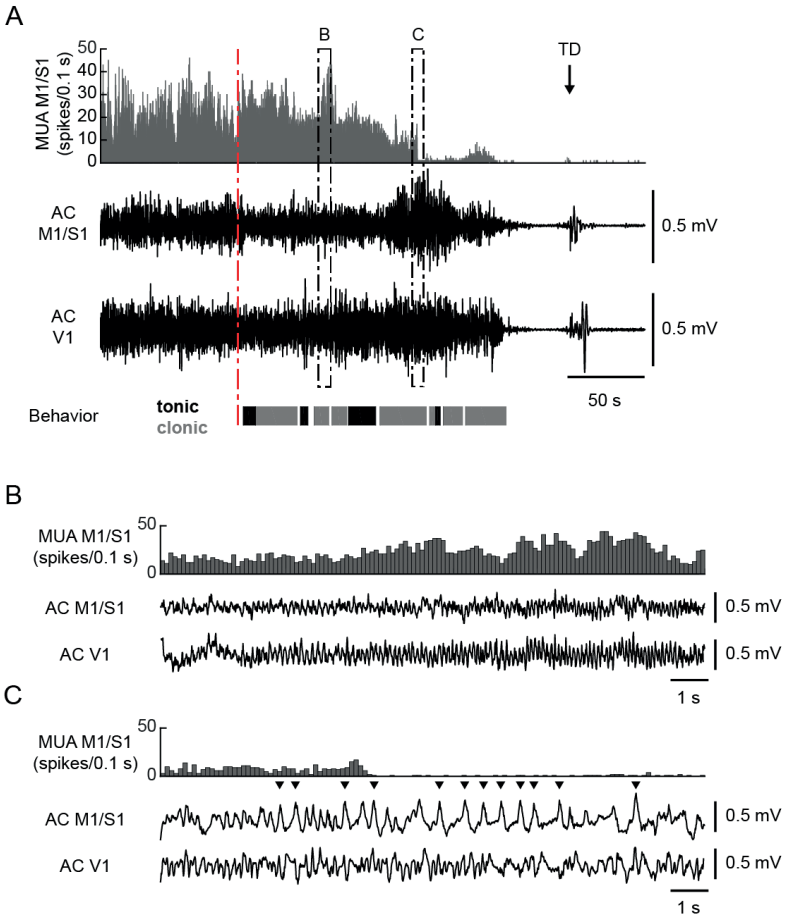

(A) Example cortical MUA and AC ECoG recordings of a fatal seizure (behavioral onset indicated by a red dashed line; clonic behavior is shown in gray, tonic behavior in black; terminal depolarization (TD) indicated by an arrow). Details of ictal AC ECoG and MUA indicated by dashed boxes are shown in panels B and C. **(B)** Detailed inspection of the AC ECoG reveals oscillatory activity corresponding to theta band frequencies and **(C)** spike-wave complexes (indicated by arrowheads) not exceeding normal AC ECoG amplitude, that coincide with loss of cortical MUA.

FIGURE 4D-4H. Different ECoG and cortical multi-unit activity during spontaneous non-fatal and fatal seizures in homozygous *Cacna1a*^{S218L} mice.

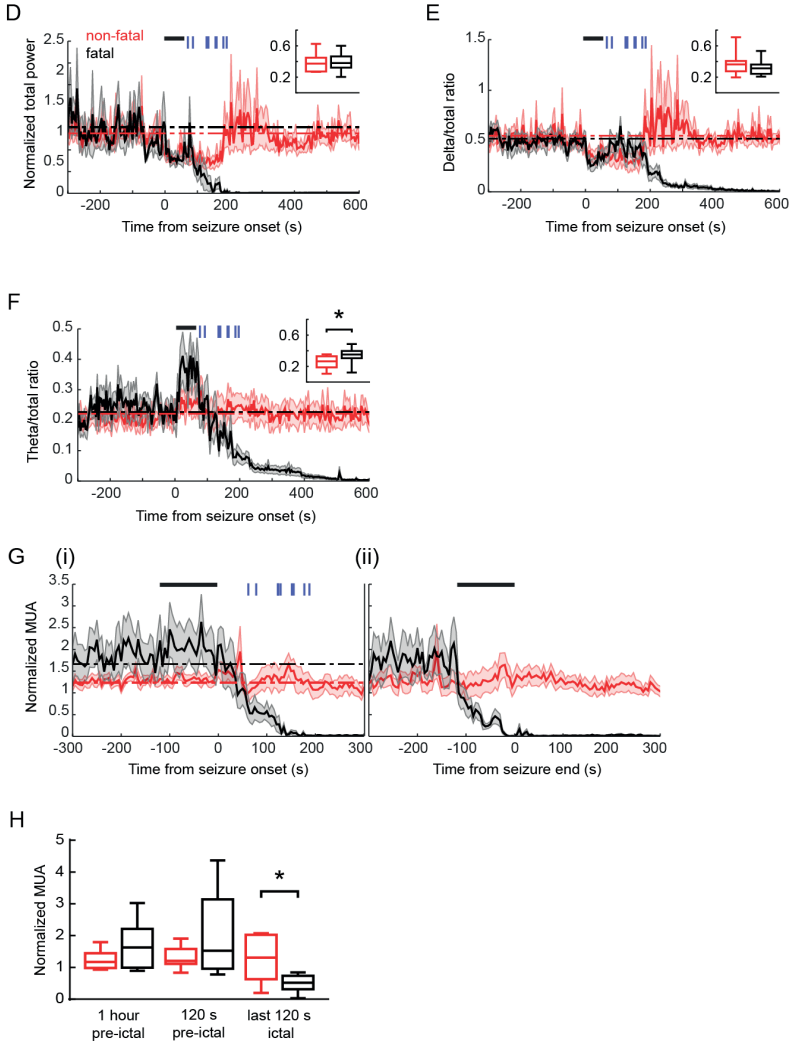

(D, E, F) Spectral analyses of primary sensorimotor (M1/S1) AC ECoG during non-fatal (red) and fatal (black) stage 5 seizures ($n = 9$) for total power **(D)**, delta/total ratio **(E)** and theta/total ratio **(F)**. Power during the first 60 s of all seizures (indicated by black bars) was compared with baseline power (1 h pre-ictal; baseline power levels for non-fatal/fatal seizures are indicated by red/black dashed lines). In addition, non-fatal and fatal seizures were compared over the same ictal period (insets; data is shown as mean ± SD). Normalized total power and delta/total power ratio were attenuated (D and E; $p = 0.001$ and $p = 0.010$ for non-fatal and fatal seizures, respectively). Theta/total ratio was increased only for fatal seizures, compared to both baseline and non-fatal seizures (F; $p < 0.001$ and $^*p = 0.003$, respectively). For all fatal seizures, cessation of seizure-related behavior is indicated by vertical blue bars. **(G, H)** Normalized cortical MUA dynamics in relation to onset **(G(i))** and end **(G(ii))** of seizure-related behavior. Black bars indicate 120-s time windows used for comparison of non-fatal and fatal seizures in (H). MUA decreased during fatal seizures **(G)** and was significantly reduced when compared to non-fatal seizures during the last 120 s of seizure-related behavior (**H**; $^*p = 0.018$). AC = alternating current.

FIGURE 5. Multiple cortical spreading depolarizations associated with induced seizures followed by death in homozygous *Cacna1a*^{S218L} mice.

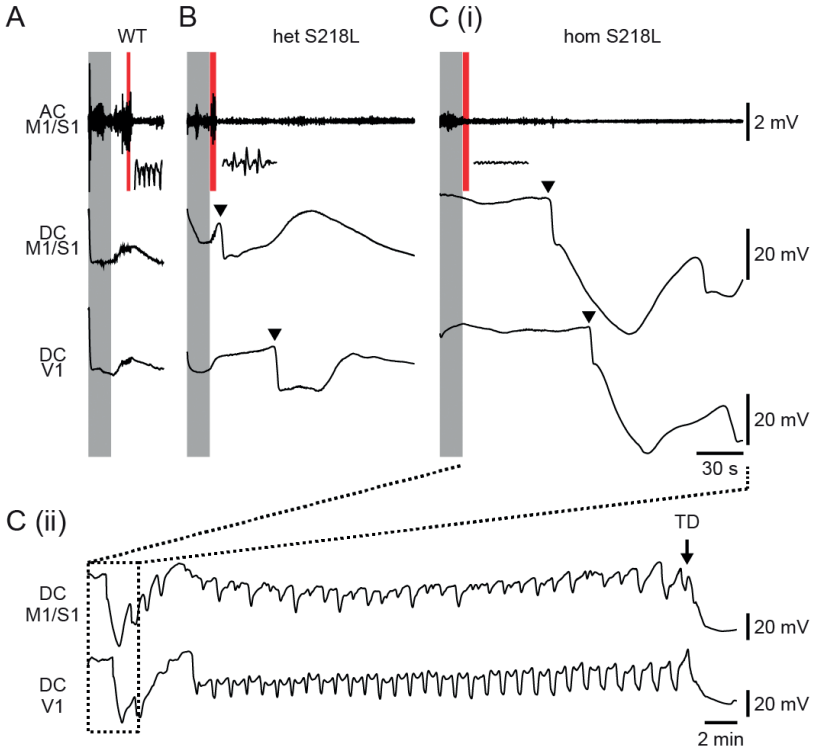

Representative ECoG (AC and DC) recordings showing that stimulation (shaded gray) was followed by afterdischarges in all wild-type (WT) mice (7/7; example in **(A)**) as indicated by insets (corresponding to the shaded red time windows) and heterozygous *Cacna1a*^{S218L} (het S218L) mice (9/9; example in **(B)**), while only in a minority of homozygous *Cacna1a*^{S218L} (hom S218L) mice (2/11; example in **(C(i)B)**, as indicated by insets (corresponding to the shaded red time windows). Cortical SD (indicated by arrowheads in example traces) was observed directly following afterdischarges in all but one heterozygous *Cacna1a*^{S218L} mice. In the homozygous *Cacna1a*^{S218L} mice multiple cortical SDs occurred, followed by a terminal depolarization **(C(ii)B(ii)**; TD; indicated by an arrow). Fatal outcome was observed in 7 out of 11 homozygous *Cacna1a*^{S218L} mice but none of the wild-type and heterozygous *Cacna1a*^{S218L} mice. AC = alternating current; DC = direct current.

Induced fatal seizures in homozygous *Cacna1a*^{S218L} mice are associated with brainstem SD

DW-MRI was used to assess the spatiotemporal propagation of SDs in response to cortically induced seizures in anesthetized homozygous *Cacna1a*^{S218L} (n = 7) and wild-type (n = 3) mice. SD occurrence, visualized by MRI-diffusional changes associated with SD-related cell swelling, was confirmed by simultaneous (ipsilateral) cortical DC recording (Supplementary Fig. 2). Stimulation resulted in epileptiform afterdischarges (2-10 Hz), concurrent with DW-MRI movement artifacts directly following stimulation. In wild-type mice stimulation resulted only in non-fatal seizures (n = 10), while in homozygous *Cacna1a*^{S218L} mice both non-fatal seizures (n = 15) and fatal seizures (n = 4) were observed.

DW-MRI data (from the hemisphere ipsilateral to the stimulation site) showed cortical SD with all fatal (4/4) and most non-fatal seizures (13/15) in homozygous *Cacna1a*^{S218L} mice and with most non-fatal seizures (7/10) in wild-type mice. Cortical SDs were first observed in the dorsal sensorimotor cortex and propagated to the visual cortex with different timing delays between genotypes (in s): wild-type: 43 ± 6; *Cacna1a*^{S218L} non-fatal: 26 ± 3; *Cacna1a*^{S218L} fatal: 20 ± 2 (wild-type vs *Cacna1a*^{S218L} non-fatal: p = 0.016; wild-type vs *Cacna1a*^{S218L} fatal: p = 0.018; *Cacna1a*^{S218L} non-fatal vs *Cacna1a*^{S218L} fatal: p = 0.72). For fatal seizures, cortical SDs were followed by SDs in subcortical structures including striatum (14 ± 13 s, indicating the time delay following SD in the sensorimotor cortex), hippocampus (16 ± 1 s), superior and inferior colliculus (24 ± 5 s) and brainstem (31 ± 4 s) (Fig. 6A, B and E). Within the brainstem, SD in the medulla was detected after SD appearance in the pons (3/4 fatal seizures; delay of 1-3 scan repetitions; 8-24 s). In one animal medullary and pontine SD were detected at the same time point. For non-fatal seizures in homozygous *Cacna1a*^{S218L} mice, cortical SDs were followed by SDs in striatum (n = 8; 59 ± 11 s), hippocampus (n = 6; 46 ± 10 s), and colliculi (n = 5; 45 ± 13 s), but never in the brainstem (Figs. 6C and E). In all but one wild-type mice, SD was not observed in subcortical structures (Fig. 6D). Cortical SD occurrence in the contralateral cortex was only rarely observed in the DW-MRI experiments following non-fatal seizures (2/10) in wild-type mice, in line with ECoG from freely behaving wild-type mice in which contralateral cortical SD was not observed following stimulation. In summary, subcortical SD propagation is more extensive in homozygous *Cacna1a*^{S218L} mice with brainstem SD only observed during fatal seizures.

Respiratory rate and heart rate, monitored during evoked seizure experiments, were increased after non-fatal seizures in homozygous *Cacna1a*^{S218L} and wild-type mice (Fig. 7). Both parameters returned to baseline within 1 minute in wild-type mice, whereas in homozygous *Cacna1a*^{S218L} mice respiratory rate fluctuated for an extended period of time (2-3 min) before returning to baseline. In fatal seizures, respiratory slowing was followed by respiratory arrest that preceded cardiac arrest. Respiratory arrest occurred near-concurrently with the observation of SD in the brainstem (example in Fig. 7A), either shortly before (12 and 5 s) or after (11 or 33 s) brainstem SD (recognizing that the time resolution of DW-MRI was limited to 8 s).

FIGURE 6A-6D. DW-MRI visualization of spreading depolarization following induced seizures in anesthetized homozygous *Cacna1a*^{S218L} mice.

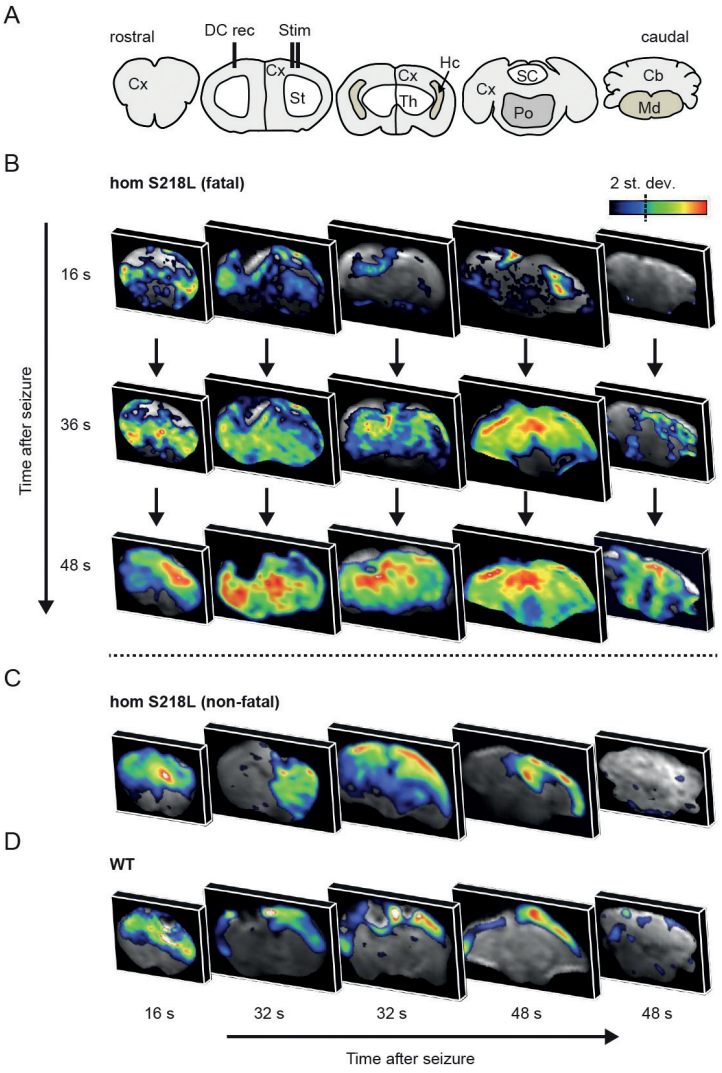

(A) Coronal brain maps corresponding to DW-MRI images in **(B)**, **(C)**, and **(D)**. **(B)** Representative DW-MRI data following an induced fatal and **(C)** non-fatal seizure in a homozygous *Cacna1a*^{S218L} (hom S218L) mouse, and **(D)** a non-fatal seizure in a wild-type (WT) mouse. Data are shown for a single representative time point in each slice, capturing a snapshot of spreading depolarization (SD). Note that in (B) all coronal maps are shown at 3 time points to demonstrate spatiotemporal propagation of SD, whereas in **(C)** and **(D)** different sections at 3 time points are depicted to show the limited subcortical spread of SD in non-fatal seizures.

FIGURE 6E. DW-MRI visualization of spreading depolarization following induced seizures in anesthetized homozygous *Cacna1a*^{S218L} mice.

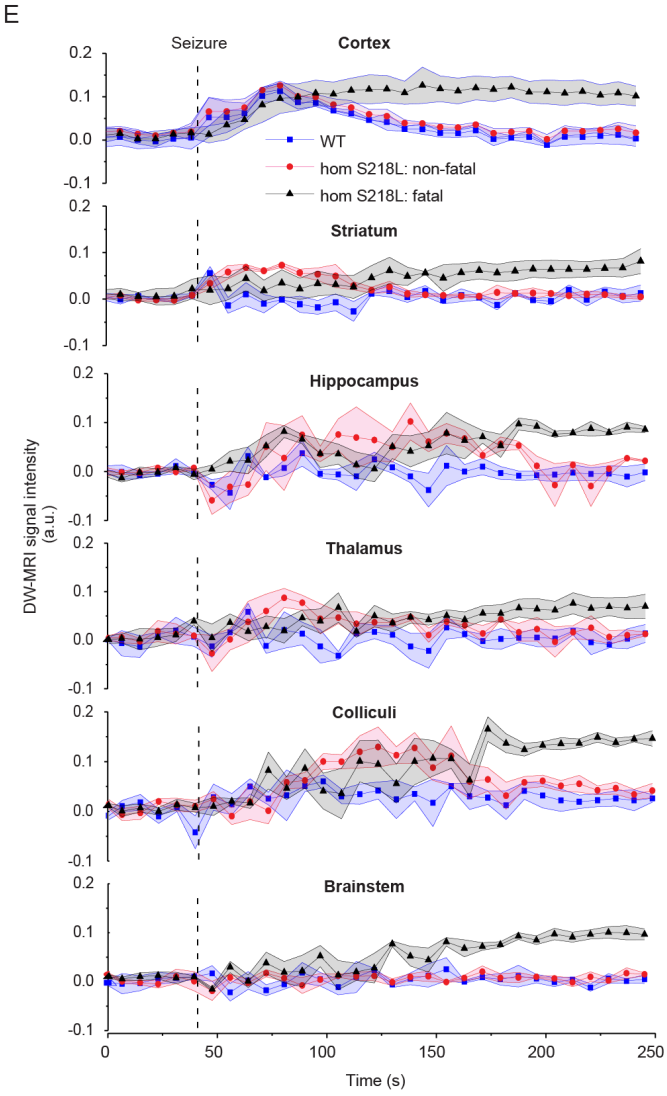

(E) Time course data of wild-type mice (n = 3; 7 SDs) and *Cacna1a*^{S218L} mice (n = 7; 13 non-fatal SDs; 4 fatal SDs) in relation to seizure onset (dashed line) are shown for distinct brain regions obtained from DW-MRI data. In *Cacna1a*^{S218L} mice, SD appeared in the brainstem only during fatal seizures and was constrained to striatum, amygdala, hippocampus and colliculi during non-fatal seizures. Cortical SD occurred in all wild-type and *Cacna1a*^{S218L} mice. A.u. = arbitrary units; Cb = cerebellum; Cx = cortex; DC = direct current; Hc = hippocampus; Md = medulla oblongata; Po = pons; SC = superior colliculus; St = striatum; Th = thalamus.

FIGURE 7. Physiological function following induced seizures during DW-MRI in anesthetized homozygous *Cacna1a*^{S218L} mice.

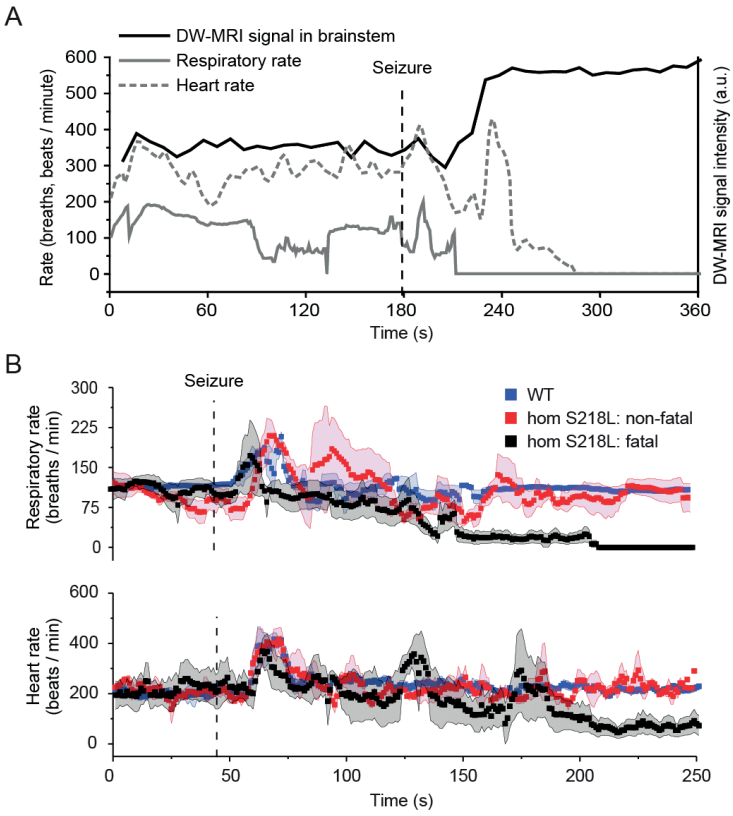

(A) Representative example from a single animal of respiratory rate, heart rate and SD aligned temporally in relation to seizure onset (dashed line). **(B)** Physiological parameters (aligned with SD dynamics shown in Fig. 6E) from homozygous *Cacna1a*^{S218L} (hom S218L) mice, following non-fatal (n = 10) and fatal seizures (n = 4), and wild-type (WT) mice, following non-fatal seizures (n = 15). Simultaneous respiratory (upper trace) and heart rate (lower trace) data acquired during seizures from the same animals showing that, for fatal seizures, respiratory rate decreased until complete arrest and preceded cardiac arrest. A.u. = arbitrary units. Data shown as mean ± SD.

As the amygdala has been implicated in seizure-related respiratory arrest,[29] one could argue that respiratory arrest might be caused by SD occurring in the amygdala. Although SD in the amygdala was observed following cortical SD in *Cacna1a*^{S218L} mice (n = 13) and in wild-type mice (n = 2), this did not coincide with profound respiratory changes (Supplementary Fig. 3).

Brainstem SD occurs during spontaneous fatal seizures in homozygous *Cacna1a*^{S218L} mice

To study the incidence of brainstem SD during spontaneous seizures in homozygous *Cacna1a*^{S218L} mice, brainstem DC ECoG recordings from the pons (PnO) and medulla (MRF) were combined with V1 ECoG and ECG in freely behaving mice. Three mice had a fatal seizure (duration 185-270 s) - after a recording period of 1-3.5 days - that was always associated with brainstem SD. Brainstem SD had an onset during seizure behavior (24-60 s preceding seizure termination) and was followed by ECoG suppression, bradycardia and a cortical terminal depolarization (example in Fig. 8). Gasping was absent during fatal seizures. A delay in MRF SD was observed in 2 mice (9 and 23 s after PnO SD), whereas in 1 mouse SD occurred simultaneously in PnO and MRF. Brainstem SD was not observed during non-fatal seizures (n = 8) or during interictal recordings preceding the fatal seizure.

FIGURE 8. Brainstem DC recordings during a spontaneous fatal seizure in a homozygous *Cacna1a*^{S218L} mouse.

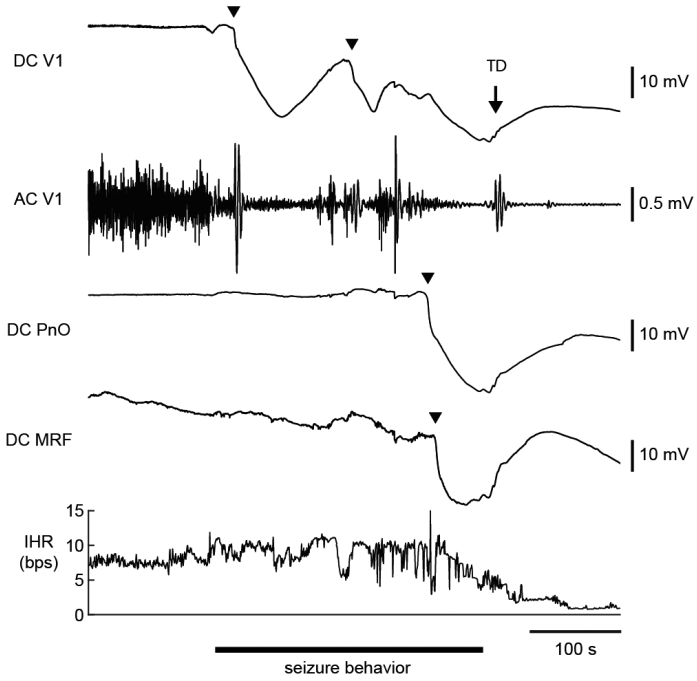

Example of an SD (indicated by arrowheads) that occurred during seizure behavior in the oral pontine reticular nucleus (PnO) and subsequently in the medullary reticular formation (MRF), followed by visual cortex (V1) AC ECoG suppression, bradycardia and cortical terminal depolarization (TD; indicated by an arrow). Note that ictal V1 AC ECoG amplitude was greatly reduced following cortical SD. AC = alternating current; bps = beats per second; DC = direct current; IHR = instantaneous heart rate.

DISCUSSION

Here we describe features that discriminate spontaneous and induced fatal seizures from non-fatal events in homozygous *Cacna1a*^{S218L} mice. Characteristics specific to fatal seizures included: i) an increase in clonic activity during later phases of the seizure, ii) early (ictal) and post-ictal suppression of cortical neuronal activity, iii) subcortical SD spread following induced seizures culminating in brainstem SD with respiratory arrest, and eventually cardiac arrest, and iv) brainstem SD during spontaneous seizures preceding complete ECoG suppression and cardiac arrest.

DW-MRI revealed that cortically-induced non-fatal seizures were associated with SD that remained predominantly restricted to the ipsilateral cortex in wild-type mice, but invaded subcortical structures in *Cacna1a*^{S218L} mice. This is in agreement with previous findings in homozygous *Cacna1a*^{S218L} mice wherein induced cortical SD was followed by striatal and hippocampal[22] and, occasionally, thalamic invasion.[20] Simultaneous cortical DC recordings in a subset of DW-MRI experiments confirm that measured changes in signal intensity indeed result from cortical SD events.

The results from both induced and spontaneous seizures in *Cacna1a*^{S218L} mice indicate that only fatal seizures were associated with brainstem SD, observed in the pons and medulla. This coincided with a decrease in respiratory activity during fatal seizures, suggesting that brainstem SD induces apnea. Although we were unable to measure ictal respiratory activity systematically in freely behaving mice, few post-ictal respiratory gasps were observed in half of the mice whereas in the other half no respiratory activity was observed, indicating limited autoresuscitation. This supports the hypothesis that seizure-induced SD causes death by suppression of brainstem respiratory control. Indeed, in animals with confirmed brainstem SD during the fatal seizure no gasps were observed. Our data contrast with previous studies, where apnea clearly *preceded* brainstem SD, and hypoxia was proposed as a trigger for brainstem SD.[14, 15] Differences in timing between respiratory changes and SD might be explained by methodology, since previous studies relied on electrodes inserted in the dorsocaudal medulla only.[14, 15] Future studies should indicate whether brainstem SD indeed precedes and causes respiratory arrest.

Head trauma due to electrode implantation is likely to have influenced the features of spontaneous fatal seizures in recorded homozygous *Cacna1a*^{S218L} mice. Whereas surgery contributed to seizure frequency and caused a reduction of life span in homozygous *Cacna1a*^{S218L} mice, spontaneous seizure behavior was similar in naive and implanted animals. In addition, cortical stimulation experiments on the day of surgery and after a 2-week recovery period both resulted in fatal seizures in the majority of homozygous *Cacna1a*^{S218L} mice, indicating that acute post-surgery complications are not key contributors to fatal seizure outcome in our model.

All fatal seizures and only a minority of non-fatal seizures in freely behaving *Cacna1a*^{S218L} mice were associated with a late ictal and post-ictal cortical suppression pattern that resembles PGES, a consistent observation in clinical SUDEP recordings.[4, 5] Global[30] and/or local[31] hypoxia could underlie the suppression of cortical neuronal activity. Indeed, in fatal seizures in a mouse

model of Dravet syndrome, an epileptic encephalopathy associated with high SUDEP risk,[11] apnea preceded PGES.[32] Periods of apnea and bradycardia followed by a terminal apnea and asystole have been reported in human SUDEP cases.[5] Our ECG recordings during spontaneous and induced fatal seizures showed intermittent bradycardia. This may indicate autonomic disturbances due to brainstem hyperexcitability, SD, and/or direct effects of intermittent hypoxia on cardiac function and warrants further investigation.

In anesthetized mice in the DW-MRI study fatal outcome occurred within minutes following stimulation whereas in freely behaving mice the delay showed high variation with particularly long delays in some animals. This discrepancy may be explained by consequences of anesthesia, resulting in a reduced respiratory drive in anesthetized animals[33] and possible transient hypoxia that can affect seizure and SD threshold.[34] In freely behaving mice, occurrence of cortical SD following induced seizures will limit spread of seizure activity. With an expected lower cortical SD susceptibility under anesthesia,[35] electrical seizure induction during the DW-MRI experiments may have involved a more extensive seizure network including brainstem areas. Since brainstem SD precedes cortical SD during severe hypoxia,[36] mild hypoxic conditions in anesthetized mice may have increased SD risk in brainstem areas. The short delay between SDs in cortical and subcortical structures in the DW-MRI study would be in line with a contribution of local hyperexcitability, as recent evidence has shown that brainstem epileptiform activity can occur concurrently with fatal seizures.[37] Future studies of fatal seizures in this and other SUDEP mouse models are required to confirm the path of SD propagation from subcortical structures to the brainstem, as suggested by our DW-MRI studies in anesthetized *Cacna1a*^{S218L} mice.

We present *Cacna1a*^{S218L} mice as a relevant and validated model for SUDEP since: (i) homozygous *Cacna1a*^{S218L} mice displayed both non-fatal and fatal seizures, allowing for identification of SUDEP-related seizure dynamics of potential clinical value for anticipating and preventing SUDEP; (ii) mice displayed fatal seizures at various ages reflecting clinical reports of SUDEP incidence rates.[2, 3] A fatal seizure outcome did not occur in heterozygous *Cacna1a*^{S218L} or wild-type mice. Electrographically, cortical epileptiform activity was limited to incidental low-amplitude spikes during myoclonic behavior. This contrasts the pronounced epileptiform activity seen in e.g. $K_V1.1$ and $Na_V1.1$ SUDEP mouse models.[12, 38] However, human semiological, EEG and ECoG data indicate heterogeneity of SUDEP phenomena that involve absence of epileptiform activity and include observations suggesting brainstem involvement.[2, 6, 39] Multiple mechanisms may therefore contribute to SUDEP, and it is conceivable that mechanisms may differ between patients. Clinical reports of monitored SUDEP cases indicated that most fatal events are preceded by tonic-clonic seizures, while in a minority there is no preceding seizure.[5, 40, 41] For those cases in which death was not preceded by epileptiform activity, a brainstem mechanism seems plausible.[40, 41] Practical constraints limit electrography of brainstem areas in human epilepsy. Nevertheless, increased blood flow in the cerebellum, thalamus, and midbrain observed during and following seizure spread in patients with epilepsy supports brainstem involvement in tonic-clonic seizures.[42] Clinical observations also support a link between SUDEP risk and brainstem involvement. Convulsive seizures with tonic

arm extension, thought to coincide with spread of activity to the brainstem, were found to be strongly associated with PGES[30] that is associated with increased SUDEP risk.

Stage 5 seizures generally showed attenuation of the ECoG, with a relative dominance of theta band activity during fatal seizures. ECoG attenuation during seizures has also been reported for idiopathic generalized epilepsy during the tonic phase.[43] The seizure-related behavior in *Cacna1a*^{S218L} mice appears similar to that described for audiogenic seizures in Genetic Epilepsy-Prone Rats (GEPRs), in which ECoG attenuation was observed during tonic hindlimb extension.[44, 45] Behavioral similarities include wild-running, jumping, tonic, and clonic behaviors, which for GEPR models have been linked to involvement of the brainstem reticular formation.[46] Brainstem networks are sufficient for the expression of running and tonic seizure components, whereas generalized clonic seizures require forebrain circuitry.[47, 48] The observed behavioral and ECoG characteristics in *Cacna1a*^{S218L} mice thereby support an important role for the brainstem in the seizure mechanism. We hypothesize that an intricate balance exists between epileptiform activity and SD in *Cacna1a*^{S218L} mice, as indicated by the frequent absence of afterdischarges following cortical stimulation, that may differ for different brain regions and induce seizure activity in brainstem networks while suppressing forebrain seizure activity. Fatal seizures in *Cacna1a*^{S218L} mice specifically terminated with clonic behavior. As brainstem seizure activity may suppress clonic seizure behavior related to the forebrain,[49] the clonic behavior during the second part of fatal seizures in *Cacna1a*^{S218L} mice may result from suppression of brainstem networks by SD. To the best of our knowledge, extensive semiological descriptions of fatal seizures in SUDEP cases that include detailed EEG analyses and timings of tonic and clonic activity are lacking. It therefore remains to be determined whether early cortical neuronal suppression, theta band activity and clonic activity are specific for spontaneous fatal seizures in the *Cacna1a*^{S218L} model or represent a hallmark of SUDEP.

In conclusion, *Cacna1a*^{S218L} mice appear a valid model to study SUDEP mechanisms. Behavioral, neurophysiological and imaging data revealed characteristics specific to fatal seizures, implicating a role for cortical neuronal suppression and brainstem SD in SUDEP pathophysiology. This adds to the fundamental understanding of the processes that underlie seizure termination and risk for SUDEP, and may aid identification of predictive SUDEP biomarkers.

Acknowledgements

The authors thank Mr. Ludo Broos and Dr. Thijs Houben for assistance with histology and electrophysiology.

REFERENCES

1. Nashef, L., et al., Unifying the definitions of sudden unexpected death in epilepsy. *Epilepsia*, 2012. 53(2): p. 227-33.
2. Massey, C.A., et al., Mechanisms of sudden unexpected death in epilepsy: the pathway to prevention. *Nat Rev Neurol*, 2014. 10(5): p. 271-82.
3. Harden, C., et al., Practice guideline summary: Sudden unexpected death in epilepsy incidence rates and risk factors: Report of the Guideline Development, Dissemination, and Implementation Subcommittee of the American Academy of Neurology and the American Epilepsy Society. *Neurology*, 2017. 88(17): p. 1674-1680.
4. Lhatoo, S.D., et al., An electroclinical case-control study of sudden unexpected death in epilepsy. *Ann Neurol*, 2010. 68(6): p. 787-96.
5. Ryvlin, P., et al., Incidence and mechanisms of cardiorespiratory arrests in epilepsy monitoring units (MORTEMUS): a retrospective study. *Lancet Neurol*, 2013. 12(10): p. 966-77.
6. Surges, R., et al., Sudden unexpected death in epilepsy: risk factors and potential pathomechanisms. *Nat Rev Neurol*, 2009. 5(9): p. 492-504.
7. Hesdorffer, D.C., et al., Combined analysis of risk factors for SUDEP. *Epilepsia*, 2011. 52(6): p. 1150-9.
8. Lamberts, R.J., et al., Sudden unexpected death in epilepsy: people with nocturnal seizures may be at highest risk. *Epilepsia*, 2012. 53(2): p. 253-7.
9. Goldman, A.M., et al., Arrhythmia in heart and brain: KCNQ1 mutations link epilepsy and sudden unexplained death. *Sci Transl Med*, 2009. 1(2): p. 2ra6.
10. Bagnall, R.D., et al., Exome-based analysis of cardiac arrhythmia, respiratory control, and epilepsy genes in sudden unexpected death in epilepsy. *Ann Neurol*, 2016. 79(4): p. 522-34.
11. Shmuely, S., et al., Mortality in Dravet syndrome: A review. *Epilepsy Behav*, 2016. 64(Pt A): p. 69-74.
12. Glasscock, E., et al., Kv1.1 potassium channel deficiency reveals brain-driven cardiac dysfunction as a candidate mechanism for sudden unexplained death in epilepsy. *J Neurosci*, 2010. 30(15): p. 5167-75.
13. Moore, B.M., et al., The Kv1.1 null mouse, a model of sudden unexpected death in epilepsy (SUDEP). *Epilepsia*, 2014. 55(11): p. 1808-16.
14. Aiba, I. and J.L. Noebels, Spreading depolarization in the brainstem mediates sudden cardiorespiratory arrest in mouse SUDEP models. *Sci Transl Med*, 2015. 7(282): p. 282ra46.
15. Aiba, I., X.H. Wehrens, and J.L. Noebels, Leaky RyR2 channels unleash a brainstem spreading depolarization mechanism of sudden cardiac death. *Proc Natl Acad Sci U S A*, 2016. 113(33): p. E4895-903.
16. van den Maagdenberg, A.M., et al., High cortical spreading depression susceptibility and migraine-associated symptoms in Ca(v)2.1 S218L mice. *Ann Neurol*, 2010. 67(1): p. 85-98.
17. van den Maagdenberg, A.M., et al., A Cacna1a knockin migraine mouse model with increased susceptibility to cortical spreading depression. *Neuron*, 2004. 41(5): p. 701-10.
18. Eikermann-Haerter, K., et al., Androgenic suppression of spreading depression in familial hemiplegic migraine type 1 mutant mice. *Ann Neurol*, 2009. 66(4): p. 564-8.

19. Tottene, A., et al., Enhanced excitatory transmission at cortical synapses as the basis for facilitated spreading depression in Ca(v)2.1 knockin migraine mice. *Neuron*, 2009. 61(5): p. 762-73.
20. Eikermann-Haerter, K., et al., Enhanced subcortical spreading depression in familial hemiplegic migraine type 1 mutant mice. *J Neurosci*, 2011. 31(15): p. 5755-63.
21. Vecchia, D., et al., Abnormal cortical synaptic transmission in CaV2.1 knockin mice with the S218L missense mutation which causes a severe familial hemiplegic migraine syndrome in humans. *Front Cell Neurosci*, 2015. 9: p. 8.
22. Cain, S.M., et al., In vivo imaging reveals that pregabalin inhibits cortical spreading depression and propagation to subcortical brain structures. *Proc Natl Acad Sci U S A*, 2017. 114(9): p. 2401-2406.
23. Ophoff, R.A., et al., Familial hemiplegic migraine and episodic ataxia type-2 are caused by mutations in the Ca2+ channel gene CACNL1A4. *Cell*, 1996. 87(3): p. 543-52.
24. Kors, E.E., et al., Delayed cerebral edema and fatal coma after minor head trauma: role of the CACNA1A calcium channel subunit gene and relationship with familial hemiplegic migraine. *Ann Neurol*, 2001. 49(6): p. 753-60.
25. Stam, A.H., et al., Early seizures and cerebral oedema after trivial head trauma associated with the CACNA1A S218L mutation. *J Neurol Neurosurg Psychiatry*, 2009. 80(10): p. 1125-9.
26. Houben, T., et al., Optogenetic induction of cortical spreading depression in anesthetized and freely behaving mice. *J Cereb Blood Flow Metab*, 2017. 37(5): p. 1641-1655.
27. Racine, R.J., Modification of seizure activity by electrical stimulation. II. Motor seizure. *Electroencephalogr Clin Neurophysiol*, 1972. 32(3): p. 281-94.
28. de Crespigny, A., et al., Magnetic resonance imaging assessment of cerebral hemodynamics during spreading depression in rats. *J Cereb Blood Flow Metab*, 1998. 18(9): p. 1008-17.
29. Dlouhy, B.J., et al., Breathing Inhibited When Seizures Spread to the Amygdala and upon Amygdala Stimulation. *J Neurosci*, 2015. 35(28): p. 10281-9.
30. Alexandre, V., et al., Risk factors of postictal generalized EEG suppression in generalized convulsive seizures. *Neurology*, 2015. 85(18): p. 1598-603.
31. Farrell, J.S., et al., Postictal behavioural impairments are due to a severe prolonged hypoperfusion/hypoxia event that is COX-2 dependent. *Elife*, 2016. 5.
32. Kim, Y., et al., Severe peri-ictal respiratory dysfunction is common in Dravet syndrome. *J Clin Invest*, 2018. 128(3): p. 1141-1153.
33. Tremoleda, J.L., A. Kerton, and W. Gsell, Anaesthesia and physiological monitoring during in vivo imaging of laboratory rodents: considerations on experimental outcomes and animal welfare. *EJNMMI Res*, 2012. 2(1): p. 44.
34. Wei, Y., G. Ullah, and S.J. Schiff, Unification of neuronal spikes, seizures, and spreading depression. *J Neurosci*, 2014. 34(35): p. 11733-43.
35. Kudo, C., et al., Anesthetic effects on susceptibility to cortical spreading depression. *Neuropharmacology*, 2013. 67: p. 32-6.
36. Richter, F., et al., The relationship between sudden severe hypoxia and ischemia-associated spreading depolarization in adult rat brainstem in vivo. *Exp Neurol*, 2010. 224(1): p. 146-54.

37. Salam, M.T., et al., Mortality with brainstem seizures from focal 4-aminopyridine-induced recurrent hippocampal seizures. *Epilepsia*, 2017. 58(9): p. 1637-1644.
38. Kalume, F., et al., Sudden unexpected death in a mouse model of Dravet syndrome. *J Clin Invest*, 2013. 123(4): p. 1798-808.
39. Devinsky, O., et al., Sudden unexpected death in epilepsy: epidemiology, mechanisms, and prevention. *Lancet Neurol*, 2016. 15(10): p. 1075-88.
40. Lhatoo, S.D., et al., Nonseizure SUDEP: Sudden unexpected death in epilepsy without preceding epileptic seizures. *Epilepsia*, 2016. 57(7): p. 1161-8.
41. Devinsky, O., et al., Sudden unexpected death in epilepsy in patients treated with brain-responsive neurostimulation. *Epilepsia*, 2018. 59(3): p. 555-561.
42. Blumenfeld, H., et al., Cortical and subcortical networks in human secondarily generalized tonic-clonic seizures. *Brain*, 2009. 132(Pt 4): p. 999-1012.
43. Seneviratne, U., M. Cook, and W. D'Souza, The electroencephalogram of idiopathic generalized epilepsy. *Epilepsia*, 2012. 53(2): p. 234-48.
44. Naritoku, D.K., et al., Repetition of audiogenic seizures in genetically epilepsy-prone rats induces cortical epileptiform activity and additional seizure behaviors. *Exp Neurol*, 1992. 115(3): p. 317-24.
45. Jobe, P.C., et al., The genetically epilepsy-prone rat (GEPR). *Ital J Neurol Sci*, 1995. 16(1-2): p. 91-9.
46. Faingold, C.L., Brainstem Networks: Reticulo-Cortical Synchronization in Generalized Convulsive Seizures, in Jasper's Basic Mechanisms of the Epilepsies, J.L. Noebels, et al., *Editors*. 2012: Bethesda (MD).
47. Kreindler, A., et al., Electro-clinical features of convulsions induced by stimulation of brain stem. *J Neurophysiol*, 1958. 21(5): p. 430-6.
48. Browning, R.A. and D.K. Nelson, Modification of electroshock and pentylenetetrazol seizure patterns in rats after precollicular transections. *Exp Neurol*, 1986. 93(3): p. 546-56.
49. Merrill, M.A., et al., Brainstem seizure severity regulates forebrain seizure expression in the audiogenic kindling model. *Epilepsia*, 2005. 46(9): p. 1380-8.

SUPPLEMENTARY MATERIAL

FIGURE S1. Example of a non-fatal seizure associated with MUA and ECoG suppression in a freely behaving homozygous *Cacna1a*^{S218L} mouse.

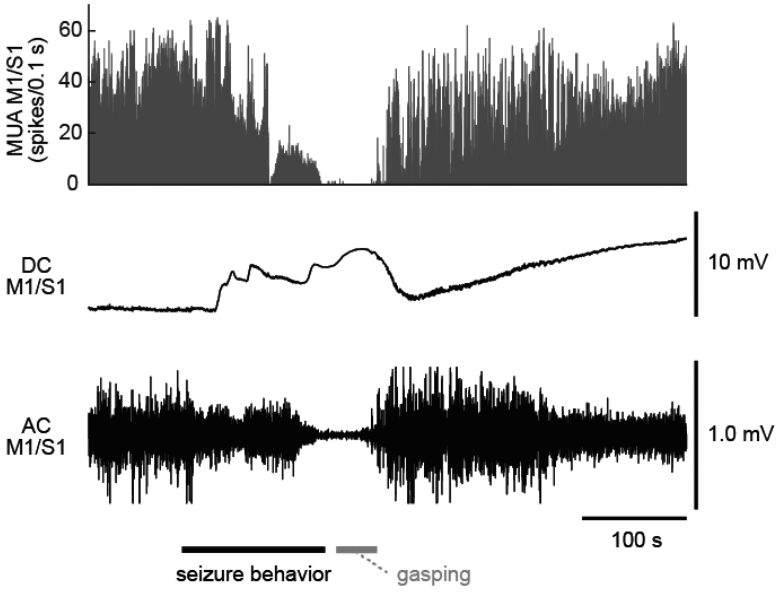

Late ictal and post-ictal suppression of cortical multi-unit activity (MUA) and ECoG lasted approximately 1 min. Local DC recording confirmed that suppression was not due to cortical spreading depolarization (SD), showing only movement-related DC-shifts during seizure behavior. Video recordings showed gasping behavior during recovery of MUA and ECoG activity, indicating successful autoresuscitation.

FIGURE S2. Cortical SD correlates with increased cortical DW-MRI signal intensity.

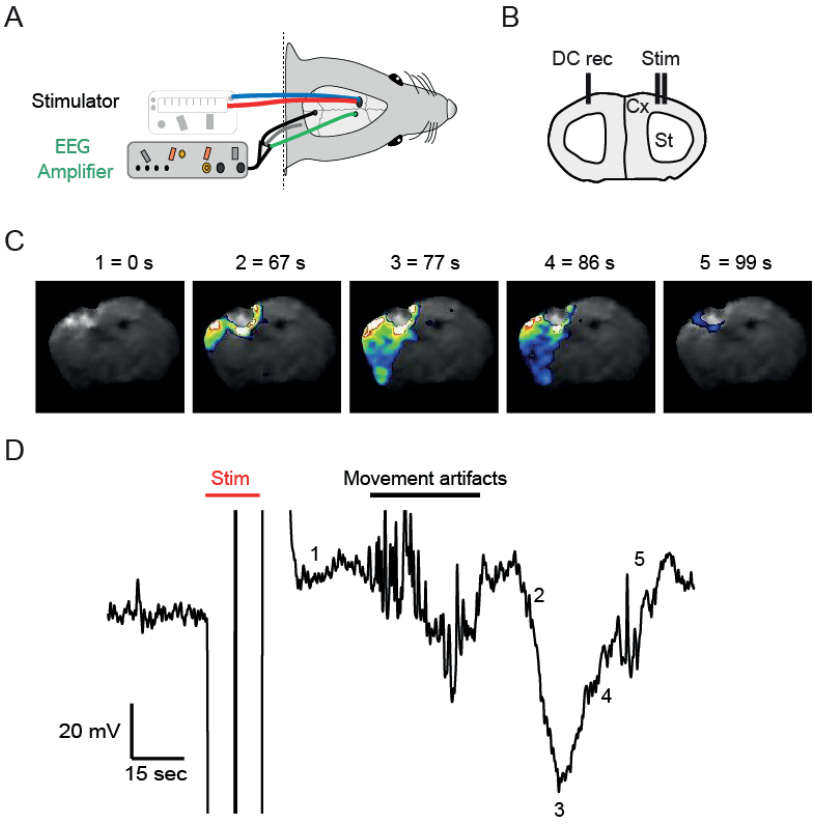

(A,B) Schematics showing placement of ECoG and stimulation electrodes in the contralateral cortex during simultaneous DW-MRI acquisition. **(C)** DW-MRI data showing spread of a single SD event, as measured by increased cell swelling, following seizure induction by electrical stimulation (Stim) of the cortex. Numbers denote the timing of the SD event as measured by DW-MRI relative to **(D)** the same SD event measured by ECoG. Note seizure-related movement artifacts prior to the cortical SD event. Cx = cortex; St = striatum.

FIGURE S3. Amygdala SD does not induce respiratory changes.

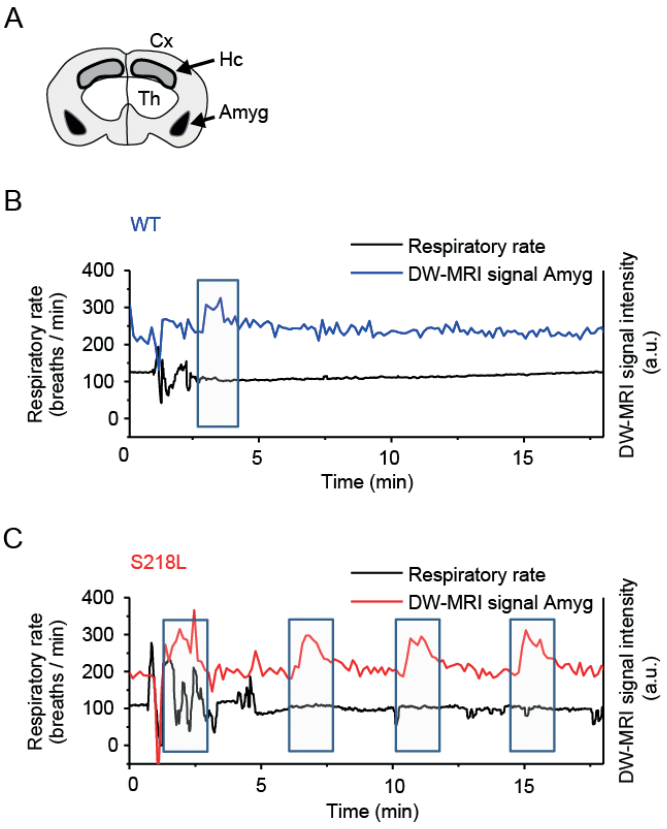

(A) Schematic map of coronal brain slice containing amygdala. **(B,C)** Representative traces of amygdala SD overlaid with respiratory rate for wild-type (WT) **(B)** and homozygous *Cacna1a*^{S218L} (S218L) **(C)** mice. SD events are outlined in blue rectangles. Note that for both the WT (panel B) and *Cacna1a*^{S218L} animal (panel C) SD is observed in the amygdala without any corresponding effect on respiration. A.u. = arbitrary units. Amyg = amygdala; Cx = cortex; Hc = hippocampus; Th = thalamus.

Chapter 5

Apnea associated with brainstem seizures in *Cacna1a*^{S218L} mice is caused by medullary spreading depolarization

Nico A. Jansen
Maarten Schenke
Rob A. Voskuyl
Roland D. Thijs
Arn M.J.M. van den Maagdenberg
Else A. Tolner

J Neurosci 2019;39(48):9633-9644

ABSTRACT

Seizure-related apnea is common and can be lethal. Its mechanisms however remain unclear and preventive strategies are lacking. We postulate that brainstem spreading depolarization (SD), previously associated with lethal seizures in animal models, initiates apnea upon invasion of brainstem respiratory centers. To study this, we assessed effects of brainstem seizures on brainstem function and respiration in male and female mice carrying a homozygous S218L missense mutation that leads to gain-of-function of voltage-gated $Ca_V2.1$ Ca^{2+} channels and high risk for fatal seizures. Recordings of brainstem DC potential and neuronal activity, cardiorespiratory activity and local tissue oxygen were performed in freely behaving animals. Brainstem SD occurred during all spontaneous fatal seizures and, unexpectedly, during a subset of non-fatal seizures. Seizure-related SDs in the ventrolateral medulla correlated with respiratory suppression. Seizures induced by stimulation of the inferior colliculus could evoke SD that spread in a rostro-caudal direction, preceding local tissue hypoxia and apnea, indicating that invasion of SD into medullary respiratory centers initiated apnea and hypoxia rather than *vice versa*. Fatal outcome was prevented by timely resuscitation. Moreover, NMDA receptor antagonists MK-801 and memantine prevented seizure-related SD and apnea, which supports brainstem SD as a prerequisite for brainstem seizure-related apnea in this animal model and has translational value for developing strategies that prevent fatal ictal apnea.

INTRODUCTION

Seizure-related apnea occurs commonly in patients with epilepsy and can result in severe hypoxemia.[1-3] If prolonged, apnea may be fatal, as such apnea preceded cardiac arrest in rarely monitored cases of 'sudden unexpected death in epilepsy' (SUDEP),[4] a fatal complication of epilepsy affecting patients of all ages.[5-7] Seizure-related apnea, however, has a benign outcome in the large majority of cases, yet given its presumed role in SUDEP there is an urgent need to understand mechanisms of potentially lethal respiratory suppression. Neuropathological and structural neuroimaging changes[8-10] in brainstem regions of SUDEP cases suggest seizure-related brainstem dysfunction as a possible critical factor leading to fatal apnea.

In recent years, brainstem spreading depolarization (SD) has been linked to SUDEP based on studies in various transgenic mouse models. A negative DC-potential shift in the dorsal brainstem was observed indicating brainstem SD.[11, 12] In these studies, SD appeared to follow upon severe respiratory compromise, thereby providing an explanation for the absence of autoresuscitation following apnea.[11] Brainstem SD was also demonstrated for cortically induced and spontaneous fatal seizures in mice harboring the homozygous S218L gain-of-function missense mutation in the *Cacna1a* gene that encodes the α_{1A} subunit of voltage-gated $Ca_V2.1$ Ca^{2+} channels.[13] The absence of cortical seizure activity in this model suggests an important role for brainstem circuitry in the genesis of seizures. However, it remains an enigma whether changes in breathing rhythm result in hypoxia and trigger brainstem SD, or *vice versa*, which is key when considering strategies for (preventative) interventions of seizure-related apnea.

Breathing rhythm is generated by the ventral respiratory column, located in the ventrolateral medulla (VLM).[14, 15] The preBötzinger complex (preBötC), a sub-region of the VLM, specifically generates the inspiratory phase that is crucial for respiratory function.[15-18] Rapid suppression of glutamatergic preBötC neurons induces fatal apnea.[19] We postulate that seizure-induced brainstem SD can evoke apnea due to prolonged neuronal suppression in the VLM. To test this, we studied brainstem neuronal activity and cardiorespiratory function during spontaneous seizures and seizures induced by stimulation of the inferior colliculus in freely behaving homozygous *Cacna1a*^{S218L} mice. Reversibility of brainstem SD was evaluated by mechanical ventilation during apnea. Since brainstem SD commonly preceded apnea and local hypoxia, we also tested whether increasing the SD threshold by NMDA antagonism could prevent lethality.

MATERIALS AND METHODS

Animals

Missense mutation S218L was introduced in the mouse *Cacna1a* gene, generating *Cacna1a*^{S218L} mice, using a gene-targeting approach.[20] Mice were backcrossed to C57BL/6J for at least 10 generations and both male and female mice, age 3 to 6 months, were used in experiments. Standard housing conditions and a 12-h light/dark cycle with food and water available *ad libitum* were applied. Experiments were approved by local and national ethical committees in accordance with recommendations of the European Communities Council Directive (2010/63/EU) and carried out in accordance with ARRIVE guidelines.

Surgery for recordings of spontaneous seizures

Cacna1a^{S218L} mice (15 males and 17 females) were implanted with either 7 (n = 11) or 16 (n = 21) electrodes (single or paired 75 µm platinum/iridium, PT6718; Advent Research Materials) under isoflurane anesthesia (induction 4%; maintenance 1.5%). Electrode configurations were as follows (coordinates relative to bregma; in mm anterior, lateral and ventral, respectively): for 7-channel recordings (E363/0 socket contacts and MS373 pedestal; Plastics One), electrodes were implanted in right primary visual cortex (V1; -3.5/2.0/0.5; unipolar) and oral pontine reticular nucleus (PnO; -4.8/0.8/3.7; uni- or bipolar) and VLM (-6.7/1.3/4.1; uni- or bipolar); for 16-channel recordings (#0489 pin receptacles and #831 18-pin pedestal; Mill-Max), unipolar electrodes were implanted in right V1 and bilaterally in primary motor cortex (+1.5/1.8/0.6), hippocampus (-2.2/2.0/1.3) and amygdala (-1.7/2.9/4.0), with bipolar electrodes in right inferior colliculus (IC; -5.0/1.0/0.6), PnO and VLM. Electrodes inserted bilaterally above the cerebellum served as reference and ground. For ECG, electrodes were placed in the flank. For respiratory recordings (n = 13), a thermistor probe (MEAS-G22K7MCD419, Measurement Specialties) was inserted above the epithelium of the anterior nasal cavity as described previously.[21] The pedestal was secured to the skull using dental cement (DiaDent Europe). In a subset of animals (n = 14), cerebral blood flow (CBF) was measured using an optic fiber (200 µm, CFM12L02; Thorlabs, Newton, NJ) placed on the dura overlaying V1. Postoperative analgesia was supplied with carprofen and buprenorphine (5 mg/kg and 0.1 mg/kg respectively, s.c.). Electrode configurations were first tested in wildtype mice for a 2-week period.

Surgery for recordings of induced seizures

For IC stimulation in homozygous *Cacna1a*^{S218L} and wildtype animals, bipolar electrodes were randomly implanted in the left or right IC. Two electrode configurations were used, with i) bipolar electrodes bilaterally in VLM, or ii) electrodes implanted unilaterally in VLM (bipolar) and the rostral and caudal parvicellular reticular nucleus (unipolar; PCRt-r, -5.5/1.4/3.6; PCRt-c, -6.1/1.3/4.0) to create an array of brainstem electrodes ipsilateral to the stimulated IC. An unipolar electrode in right V1 and a nasal thermistor were implanted as described above. Two to 4 days after surgery, a 50-Hz train of 1-ms bipolar pulses was delivered through the IC electrode for 2

s. Threshold for seizure-related behavior, which consistently commenced with wild running, was determined for a range of intensities of [30 50 100 200 500] μA with 10 min between subsequent pulse trains. The threshold current was delivered twice daily for 3 days, but limited to one stimulation in case of a generalized tonic-clonic seizure. In a separate group of *Cacna1a*^{S218L} mice, local oxygen partial pressure (pO_2) was measured using a technique involving oxygen quenching of fluorescence generated in a platinum-based dye in the tip of an optic fiber (Oxylite; Oxford Optronics). This allows for absolute measurements of pO_2 without consuming oxygen.[22] Probes (230 μm), pre-calibrated by the manufacturer and indicated with a T90 response time (i.e. time to reach 90% of the actual pO_2 change) of less than 20 s, were inserted rostral of the VLM electrode (-6.2/1.3/3.8), replacing the PCRt-c electrode. To study the locality of changes in pO_2, a subset of mice was implanted with a second oxygen probe in V1, anterior to the V1 electrode (-3.0/2.0/0.5).

Surgery for recordings of cortically induced SD

For cortical SD induction, a subset of homozygous *Cacna1a*^{S218L} mice was implanted with a bipolar electrode in V1 and unipolar electrodes in the primary somatosensory cortex (S1; -0.5/2.0/0.5) and M1. Directly adjacent to the S1 electrode, an oxygen probe was implanted. Cathodal stimulation (100 μA for 1 s) was administered once daily for 1 or 2 days and reliably resulted in cortical SD.

Mechanical ventilation and pharmacology

Postictal respiratory support (150 breaths/min for 20 – 50 s, 250 μL per breath) was administered via the nostrils by a polyethylene tube connected to a mechanical ventilator (Mini-Vent; Harvard Apparatus). In a sham group, the same procedure was performed with the ventilator switched off.

To test the effects of NMDA receptor antagonists on seizure behavior and outcome, mice that showed brainstem SD in response to initial IC stimulation were used. Vehicle, MK-801 (1 mg/kg BW) or memantine hydrochloride (10 mg/kg BW; both from Sigma-Aldrich) were injected i.p. 30 min prior to IC stimulation by an experimenter blinded to the treatment.

Histology

Surviving animals were euthanized by CO_2. Electrolytic lesions were made at the tip of brain electrodes (10-μA anodal current) in all animals to enable confirmation of electrode positions. After transcardial perfusion (for euthanized animals), brains were post-fixed in 4% paraformaldehyde for 2.5 h at room temperature, or for 24 h at 4°C (for spontaneously deceased animals), and sucrose-processed. Coronal brain sections (40 μm) were made using a sliding microtome (Leica) and Nissl-stained to confirm electrode positions.

Data acquisition and analyses

Immediately following surgery, animals were connected to a commutator (ACO32 for 16-channel recordings; Tucker-Davis Technologies; a custom-made system was used for 7-channel recordings). Data were amplified and digitized as described previously.[23] Recordings of pO_2 were acquired at 1 Hz.

SD was defined as a transient negative DC-shift with amplitude >5 mV measured with a delay at 2 recording locations, or limited to one location if accompanied by depression of local multi-unit activity (MUA). Video-EEG recordings during these events and the 24 h preceding the fatal seizure were analyzed for seizures, which were scored using the Racine-scale.[24] In retrospect, all fatal seizures were of stage 5 and hence stage 5 non-fatal seizures were used for comparative analyses. Single seizures or seizure clusters lasting more than 30 min were regarded as status epilepticus[25] and, as a SUDEP exclusion criterion,[26] excluded from further analyses.

Electrophysiological data were analyzed using custom-written MATLAB (MathWorks) scripts. For ECoG power analyses, AC-signals were artifact-rejected, digitally low-pass filtered (Chebyshev IIR 8th order filter) and down-sampled to 500 Hz. Total ECoG power (1-100 Hz) was calculated using a Fast Fourier Transform. For MUA, the root mean square was computed over 10 or 100 ms. Peak detection was used to determine instantaneous heart rate and respiratory rate from ECG and thermistor recordings respectively. For heart rate variability (HRV) analyses, standard deviation of all normal ECG R-R intervals (SDNN) was calculated.[27] Pre- and postictal parameters were calculated over 5-min periods. Longer-term heart rhythm changes were not analyzed, as HRV is profoundly increased during the first week following surgery.[27] Peri-ictal CBF, MUA and ECoG power were normalized by activity levels during a 1-min period 5 min pre-ictal. For ECoG and CBF analyses, seizures associated with cortical SD were excluded due to local SD-related suppression.

Experimental design and statistical analysis

In total, data from 104 mice were included: recordings from spontaneous seizures were obtained from 32 homozygous *Cacna1a*^{S218L} mice, while seizures were induced in 68 mice (3 wildtype and 65 homozygous *Cacna1a*^{S218L} mice), including 12 mice for mechanical ventilation and 31 mice for pharmacological experiments. A maximum of 3 seizures were induced in untreated animals, while 1 seizure was induced for experiments involving respiratory or pharmacological intervention. Cortical SD induction was performed in 4 homozygous *Cacna1a*^{S218L} mice.

Statistical testing was performed using MATLAB or GraphPad Prism (GraphPad Software). Data are represented as mean ± SEM in text and time series graphs, total range for box-and-whisker graphs and mean ± S.D. for graphs showing individual data points. Data are compared using 2-tailed paired or unpaired Student's *t*-tests, or one-way ANOVA with Dunnett's post-hoc test for multiple comparisons, unless indicated otherwise. $p < 0.05$ was considered significant.

RESULTS

Brainstem SD occurs during seizures in freely behaving *Cacna1a*^{S218L} mice

Over a 2-week recording period, 63% (20/32) of implanted *Cacna1a*^{S218L} mice died after a mean survival period of 2.7 ± 0.5 days (range: 8 h – 9 days). High mortality in the days following surgery in this model was earlier described to be seizure-related.[13] Indeed, mice died following a Racine stage 5 seizure (n = 15; 8 males and 7 females) or status epilepticus (n = 5; 2 males and 3 females). All fatal seizures were accompanied by SDs in brainstem areas including the PnO (11/11 recordings) and VLM (13/13 recordings; Fig. 1A-D) and occasionally IC (3/7 recordings). In contrast, SDs were observed in forebrain areas (neocortex, hippocampus and amygdala) in only 7/15 fatal seizures and during status epilepticus (5/5). All brainstem SDs occurred during seizure behavior, with behavioral arrest starting 84 ± 17 s (range: 15 – 160) after onset of VLM SD and 67 ± 18 s (range: 4 – 142) after PnO SD.

To assess whether brainstem SD was unique for fatal events, we inspected recordings of the 24 h preceding the fatal events. Out of 64 non-fatal stage 5 seizures (n = 12/15 animals [range: 1 – 12 per animal]), 19% were accompanied by brainstem SD (n = 12 in 7 animals; Fig. 1E). The duration of seizures accompanied by brainstem SD was similar to that of seizures without brainstem SD and fatal seizures (185 ± 24, 170 ± 23 and 194 ± 25 s, respectively; p = 0.525; ANOVA). Brainstem SD was never observed during seizures of lower Racine stage or during interictal periods.

Prolonged SD in the ventrolateral medulla is associated with lethal outcome

In all fatal and in most (10/12) non-fatal seizures, parallel DC recordings in the PnO and VLM demonstrated SD in both brainstem areas. During 2 non-fatal seizures, only PnO SD occurred, suggesting that during non-fatal seizures SD in the brainstem remains more local than for fatal seizures. Delay between SD onset in PnO and VLM did not indicate evidence for a consistent spreading pattern during non-fatal or fatal seizures: delay was variable and SD could be first detected in either of the 2 areas (Fig. 2A), indicating that the origin of SD may vary for spontaneous seizures. Duration of VLM SD, as measured from SD onset to partial (20%) recovery of DC-potential, was longer for fatal compared to non-fatal seizures (Fig. 2B).

FIGURE 1. Brainstem spreading depolarization (SD) and cardiorespiratory dysfunction during a spontaneous fatal and non-fatal seizure in a *Cacna1a*^{S218L} mutant.

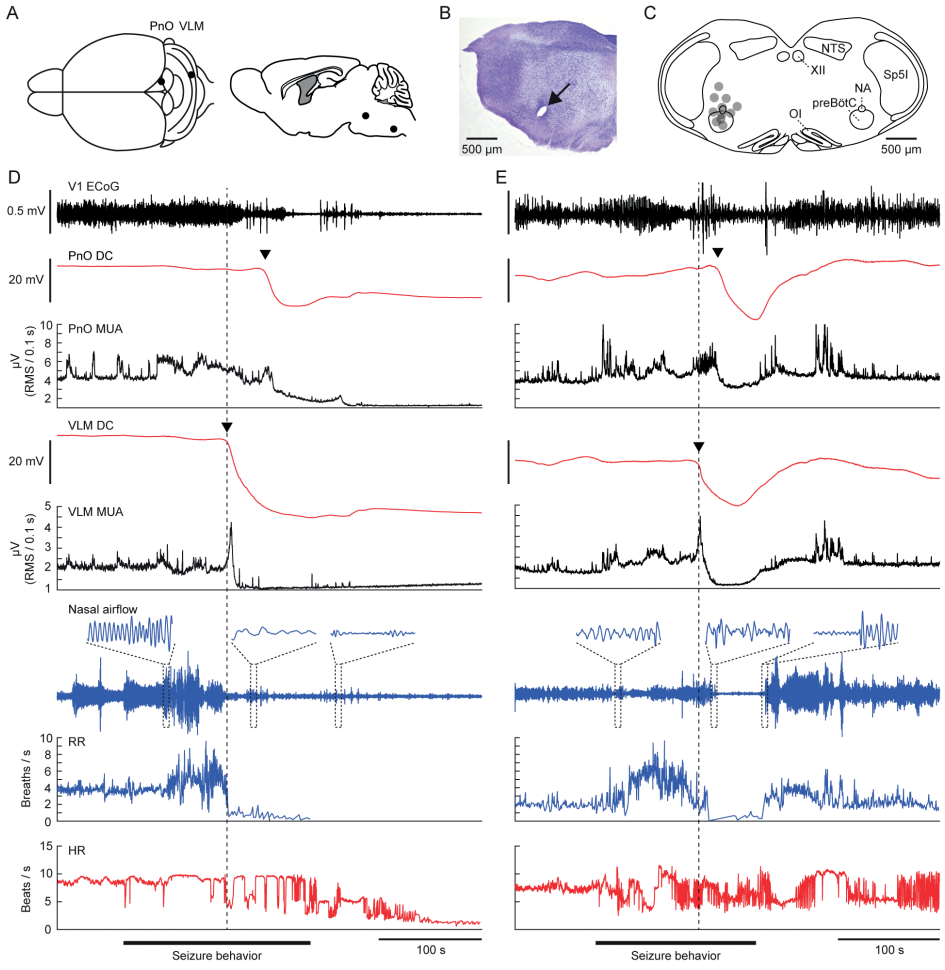

(A) Top and sagittal view of experimental approach for chronic brainstem recordings. **(B)** Nissl staining showing a lesion marking the electrode tip in the ventrolateral medulla (VLM; arrow). **(C)** Schematic of VLM electrode positions (grey dots) in 11 *Cacna1a*^{S218L} mice that died following a spontaneous fatal seizure with VLM SD (NA = nucleus accumbens; NTS = nucleus tractus solitarius; OI = oliva inferior; preBötC = pre-Bötzinger complex; Sp5I = spinal trigeminal nucleus pars interpolaris; XII = nucleus hypoglossus). **(D)** Example of a fatal seizure showing brainstem SD, evidenced by a DC shift (arrowheads), in the oral pontine reticular nucleus (PnO) and VLM. Note that the SDs occurred during seizure behavior, and were associated with a transient increase in multi-unit activity (MUA) followed by suppression (ECoG = electrocorticogram; HR = heart rate; RR = respiratory rate; RMS = root mean square; V1 = primary visual cortex). **(E)** Example of a non-fatal seizure that was associated with brainstem SD, after which DC-potential and MUA spontaneously recovered. Note that in both fatal and non-fatal examples, respiratory activity decreased shortly after onset of VLM SD (indicated by dashed line).

FIGURE 2. Prolonged medullary neuronal depression following fatal spreading depolarization (SD) in *Cacna1a*^{S218L} mice.

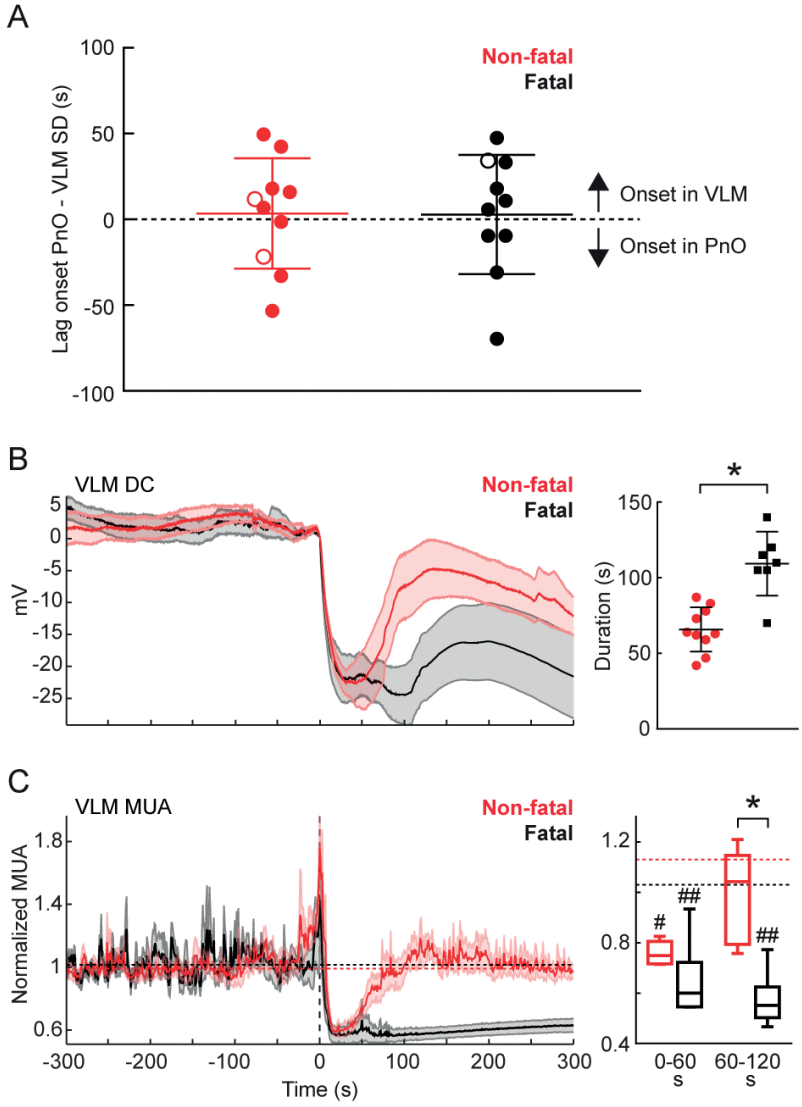

(A) Brainstem SD was observed first in either the ventrolateral medulla (VLM) (positive values) or in the oral pontine reticular nucleus (PnO) (negative values) during non-fatal ($n = 10$) and fatal ($n = 10$) seizures. This variability was observed between animals and within animals, as illustrated by the data points from a single animal with a fatal and 2 non-fatal seizures associated with brainstem SD (open symbols). **(B)** Averaged DC-recordings in VLM showing SD (left; onset at time = 0 s), indicating earlier recovery for non-fatal ($n = 10$) compared to fatal ($n = 10$) seizures (right; 66 ± 15 s *versus* 109 ± 21 s, $t(15) = 5.03$, $^{*}p = 0.0001$, unpaired *t*-test). Note that DC-recordings from three fatal seizures were excluded due to absence of (partial) recovery. **(C)** For fatal *versus* non-fatal seizures, VLM multi-unit activity (MUA) was reduced after SD onset in both groups (right; $n = 5$ and $n = 6$; baseline indicated by dashed lines; $^{\#}p = 0.009$, $^{\#\#}p = 0.0003$ and $^{\#\#}p = 0.0004$ respectively, ANOVA with Dunnett's test), but then recovered only in non-fatal cases ($t(9) = 4.62$, $^{*}p = 0.001$, unpaired *t*-test).

Seizures with brainstem SD confer decreased survival and are followed by ECoG suppression and increased heart rate variability

The time towards a fatal seizure was decreased following non-fatal seizures accompanied by brainstem SD when compared to other stage 5 seizures (4.6 ± 1.1 and 6.3 ± 1.3 h, respectively; t(11) = 2.55, p = 0.031, paired t-test). Behaviorally, the majority of non-fatal seizures with brainstem SD terminated with a hindlimb clonus (10/12; all in seizures with VLM SD), a finding previously reported for fatal seizures in *Cacna1a*^{S218L} mice.[13] Onset of hindlimb clonus and VLM SD were closely aligned (Fig. 3A). Pairwise comparisons of pre- and postictal parameters of stage 5 seizures with and without brainstem SD revealed that V1 ECoG was suppressed during the postictal period specifically for seizures with brainstem SD, whereas no differences in cortical CBF was observed (Fig. 3B). Postictal heart rate variability (HRV) was increased for seizures with brainstem SD, while heart rate remained constant (Table 1). In addition, skipped heart beats occurred more often in the postictal period for seizures with brainstem SD (example in Fig. 3C,D) when compared to seizures without brainstem SD (Table 1).

Seizure-related bradypnea correlates with SD in the ventrolateral medulla

Respiratory activity was recorded in a subset of mice with a spontaneous fatal seizure (n = 6). In 4 mice, 8 non-fatal seizures with brainstem SD occurred: 2 with SD restricted to the PnO and 6 with SD occurring in both PnO and VLM. All seizures with SD in the VLM were associated with bradypnea (defined as <60 breaths/min), in contrast to the cases with SD limited to PnO (example in Fig. 4). Dynamics of VLM SD more closely paralleled changes in respiratory rate when compared to PnO SD (Fig. 5A,B). In a case with strong coupling of oscillatory VLM MUA and breathing rhythm, VLM SD induced immediate cessation of this oscillatory pattern coinciding with bradypnea onset (Fig. 5C). In contrast to the profound respiratory effects, prolonged bradycardia was not observed for non-fatal seizures with VLM SD, while occurring after about one minute following fatal apnea for fatal seizures (Fig. 5D,E).

TABLE 1. Postictal changes in heart rhythm after brainstem spreading depolarization (SD).

n		Heart rate (beats/s)		Heart rate variability (SDNN [ms])		Skipped heart beats (total count)	
Mice	**Seizures**	**Pre-ictal**	**Postictal**	**Pre-ictal**	**Postictal**	**Pre-ictal**	**Postictal**
Seizures with brainstem SD							
6	9	8.12 ± 0.53	7.39 ± 0.34	22.8 ± 4.8	45.1 ± 7.0*	6.50 ± 4.13	65.5 ± 28.5**
Seizures without brainstem SD							
6	9	8.37 ± 0.33	8.44 ± 0.49	20.2 ± 4.4	22.0 ± 3.6	6.61 ± 2.72	6.13 ± 2.80

*p = 0.016, **p = 0.008 for pre-ictal *versus* post-ictal via Wilcoxon test.
SDNN = standard deviation of all normal ECG R-R intervals

FIGURE 3. Seizure behavior and postictal dynamics indicate brainstem spreading depolarization (SD) during non-fatal seizures in *Cacna1a*^{S218L} mice.

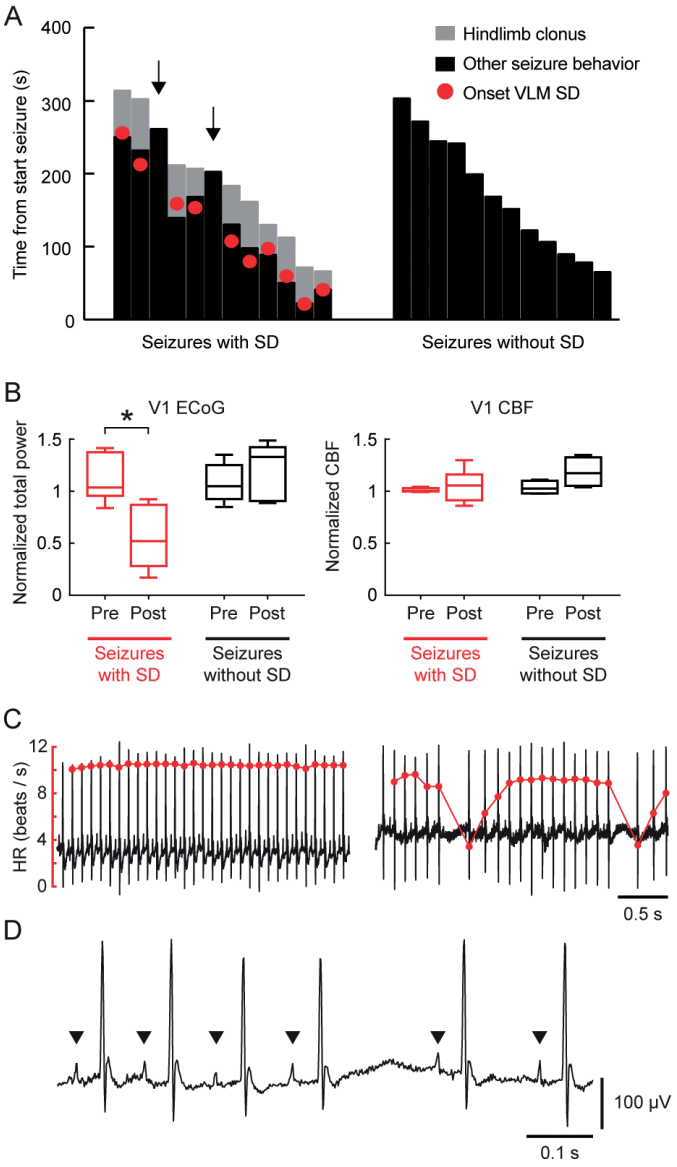

(A) Duration of hindlimb clonus and other seizure behavior for seizures with and without brainstem SD, indicated from onset of seizure behavior (at time = 0 s). Hindlimb clonus only occurred during seizures with SD in ventrolateral medulla (VLM), and started closely to SD onset. Note that hindlimb clonus did not occur during seizures without brainstem SD and seizures with SD restricted to the oral pontine reticular nucleus (PnO; $n = 2$; arrows). **(B)** Electrocorticogram (ECoG) power was significantly suppressed during the postictal period for seizures with brainstem SD ($t(7) = 5.74$, $^*p = 0.001$, paired *t*-test), whereas no difference was present for seizures without brainstem SD. Cortical blood flow (CBF) was not significantly different (V1 = primary visual cortex). **(C)** Examples of ECG signal (black) and heart rate (HR; red) during a pre-ictal (left) and postictal (right) period of a non-fatal seizure with brainstem SD, showing bradyarrhythmias. **(D)** Example of postictal ECG signal showing P-waves (indicated by arrowheads) and their absence during a prolonged R-R pause.

FIGURE 4. Isolated spreading depolarization (SD) in the rostral brainstem during a spontaneous non-fatal seizure.

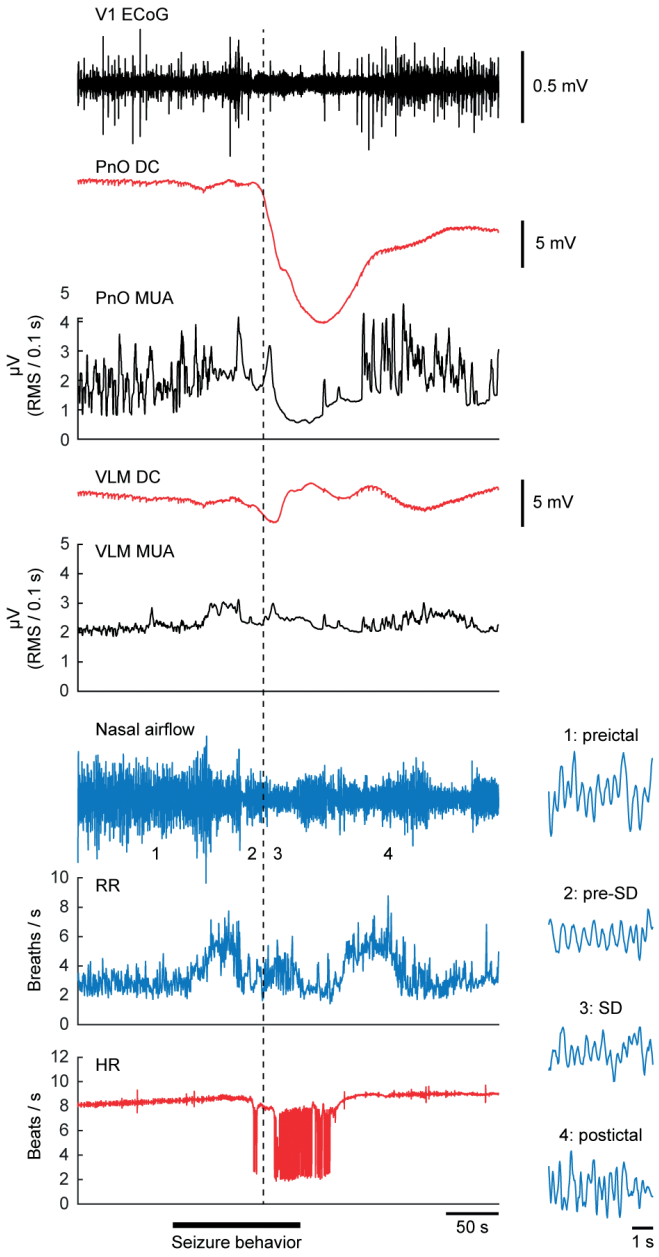

Example of a non-fatal seizure with SD (dashed line) in the oral pontine reticular nucleus (PnO) without evidence of ipsilateral SD in the ventrolateral medulla (VLM). Note that no bradypnea occurred, whereas bradyarrhythmias were observed during and following PnO SD. Insets show details of nasal airflow at time points 1 – 4, indicating no disruption of breathing.

FIGURE 5. Spreading depolarization (SD) in the ventrolateral medulla (VLM) is strongly correlated with seizure-related respiratory suppression in *Cacna1a*^{S218L} mice.

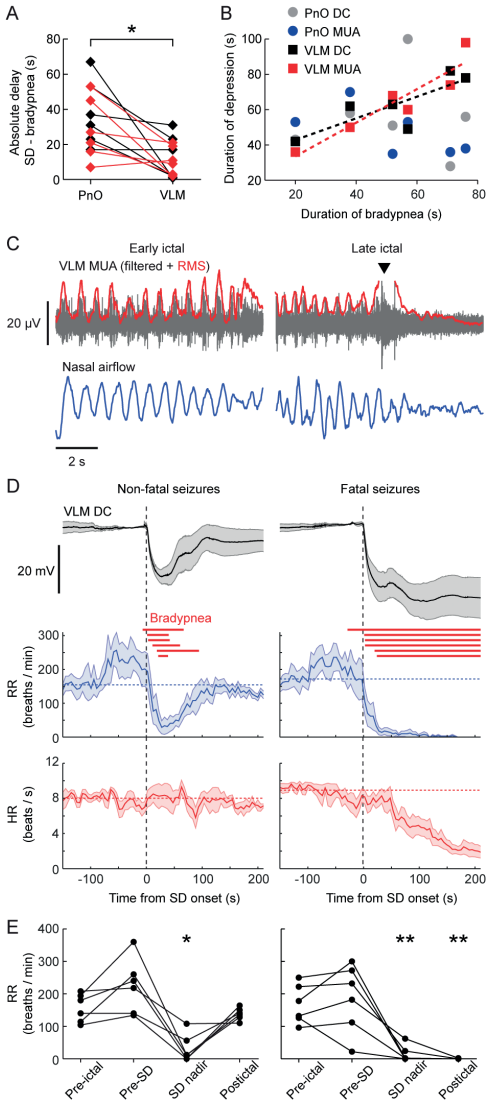

(A) Absolute time delay between onset of bradypnea and SD in the oral pontine reticular nucleus (PnO) and VLM for non-fatal (in red; $n = 6$) and fatal (in black; $n = 6$) seizures, showing that VLM SD occurred significantly closer to onset of bradypnea ($t(11) = 3.64$, $^*p = 0.004$, paired t-test). **(B)** Duration of brainstem DC and multi-unit activity (MUA) depression plotted against duration of bradypnea. Significant correlation was observed only for VLM DC and MUA (dashed lines; $R^2 = 0.671$, $p = 0.046$ and $R^2 = 0.873$, $p = 0.006$, respectively, linear regression). **(C)** Disruption of phase-coupled MUA in the ventrolateral medulla and breathing during a fatal seizure. In this example, VLM MUA was phase-coupled with nasal airflow. Local MUA (RMS = root mean square) peaked during onset of VLM SD (arrowhead), followed by suppression which coincided with cessation of breathing activity. **(D)** VLM DC-potential, RR and HR synchronized at onset of non-fatal (left) and fatal (right) VLM SD (at time = 0 s). Red lines indicate bradypnea duration for single cases. Horizontal dashed lines indicate respiratory rate (RR) and heart rate (HR) during a 60-second pre-ictal period. **(E)** RR was significantly suppressed during SD nadir, but only for fatal seizures suppression continued into the postictal period (30 s after behavioral arrest; $^*p = 0.002$, $^{**}p < 0.001$, ANOVA with Dunnett's test).

FIGURE 6. Stimulation of the inferior colliculus (IC) induces early ipsilateral brainstem spreading depolarization (SD) that propagates from rostral to caudal in *Cacna1a*^{S218L} mice.

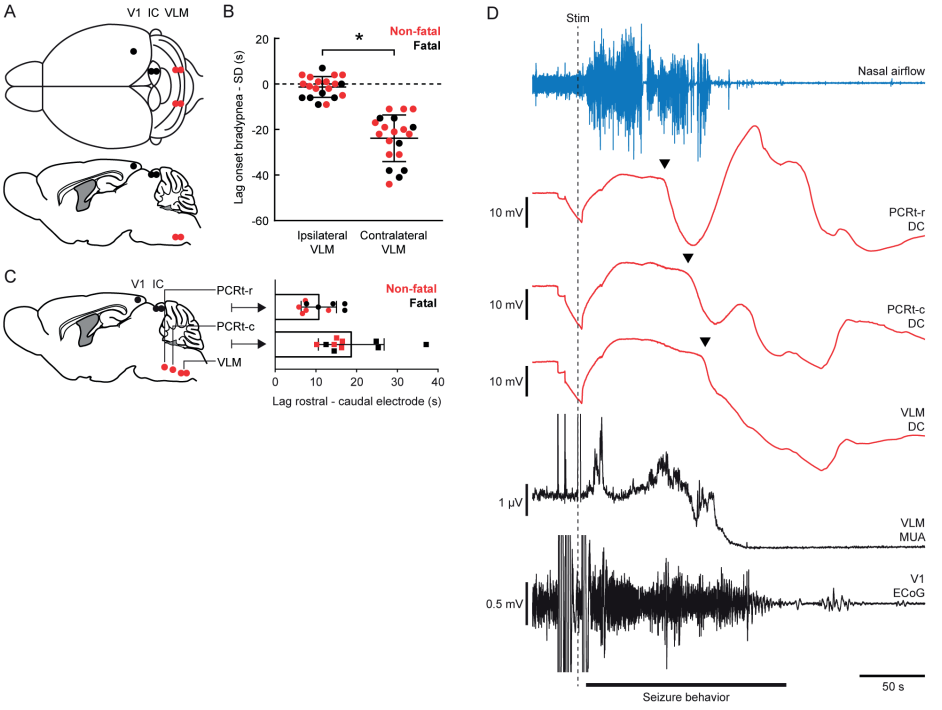

(A) Top and sagittal view of experimental approach for IC stimulation in freely behaving mice (V1 = primary visual cortex; VLM = ventrolateral medulla). **(B)** Time lag in onset of bradypnea (dotted line) and SD in VLM for non-fatal (red) and fatal (black) seizures. Negative values indicate bradypnea preceding SD. Ipsilateral VLM SD always preceded contralateral SD ($t(19) = 9.08$, $^*p < 0.0001$, paired *t*-test), irrespective of laterality ($n = 11$ for left IC, $n = 9$ for right IC). **(C)** Brainstem array recordings showed SD propagation from the parvocellular reticular nucleus (PCRt) to VLM for all seizures induced by IC stimulation. Time lag between SDs was shorter for the rostral (PCRt-r *versus* PCRt-c) when compared to the caudal (PCRt-c *versus* VLM) electrodes ($t(9) = 2.75$, $p = 0.023$, paired *t*-test). **(D)** Example recording of a fatal seizure following IC stimulation (dashed line) indicating sequential SDs (arrowheads) in the rostral (top) to caudal (bottom) brainstem electrodes (ECoG = electrocorticogram; MUA = multi-unit activity).

Inferior colliculus stimulation induces brainstem seizures and SD invasion of the ventrolateral medulla coinciding with bradypnea onset

Seizure behavior and absence of cortical epileptiform activity in *Cacna1a*^{S218L} mice suggest an important role for brainstem networks.[13] We therefore tested whether stimulation of the IC, a component of the brainstem seizure network,[28, 29] could evoke similar seizure behavior but in a more predictable manner than seen with spontaneous brainstem seizures. Unilateral electrical IC stimulation (Fig. 6A) induced a short-lasting running fit (1 – 3 s) in wildtype mice ($n = 3$), whereas all *Cacna1a*^{S218L} mice ($n = 12$) showed a stage 5 seizure already during threshold testing. Thresholds for running fits and/or behavioral seizure activity were lower in *Cacna1a*^{S218L} than wildtype mice

(52 μA [range 30 – 100 μA] *versus* 267 μA [range 100 – 500] respectively; $p = 0.005$, Mann-Whitney test). In total, 27 seizures were induced in *Cacna1a*^{S218L} mice, of which 20 were non-fatal and 7 fatal. Stimulation resulted in stage 5 seizures that were of comparable duration as spontaneous seizures (133 ± 11, 162 ± 6 and 135 ± 3 s for non-fatal seizures without and with brainstem SD and fatal seizures, respectively), and never associated with cortical SD or epileptiform events.

Bilateral VLM recordings in *Cacna1a*^{S218L} mice revealed SD during all 7 fatal and 13/ 20 non-fatal seizures, with a delay of 106 ± 3 and 104 ± 7 s after stimulation, respectively ($t(19) = 0.33$, $p = 0.763$, unpaired *t*-test). SD never occurred in wildtype mice. Notably, we observed VLM SD first at the site ipsilateral to stimulation, coinciding with bradypnea onset (Fig. 6B), although breathing slowed down already seconds preceding VLM SD. The consistent SD delay between left and right VLM following stimulation contrasts the inconsistent delay between PnO and VLM SD during spontaneous seizures, possibly reflecting lack of a local seizure focus for spontaneous events. Hence, we examined the possibility of spread in a separate group of *Cacna1a*^{S218L} mice with electrodes in the VLM and the rostral and caudal parvocellular reticular nucleus (PCRt-r and PCRt-c, respectively) (Fig. 6C). In all animals stimulated ($n = 8$; 10 seizures with brainstem SD, of which 5 were fatal), we observed SD first in PCRt-r, followed by PCRt-c and VLM (Fig. 6C,D). This indicates that SD spread following IC stimulation is predictable, but variable during spontaneous seizures, in *Cacna1a*^{S218L} mice.

Medullary SD is followed by local hypoxia

Ongoing breathing activity does not rule out impaired oxygenation, which can induce brainstem SD.[30] We therefore determined *in situ* brainstem pO_2 immediately rostral to the VLM electrode ($n = 6$ animals; Fig. 7A,B). Following IC stimulation, 7/12 seizures were associated with SD in PCRt-r and VLM, of which 4 were fatal. Baseline pO_2 in the rostral VLM was 34.2 ± 3.1 mmHg and remained within the normoxic range of 20 – 40 mmHg during non-fatal seizures without brainstem SD (Fig. 7D). During seizures with brainstem SD, however, severe local hypoxia (pO_2 <10 mmHg) occurred that extended into the postictal period for both non-fatal and fatal seizures (pO_2 nadir: 1.8 ± 0.9 mmHg and 0 ± 0 mmHg, respectively; Fig. 7E,F). Hypoxia lasted 34 – 74 s for non-fatal cases ($n = 3$) and was followed by a period of hyperoxia (Fig. 7G). No pO_2 recovery occurred in fatal cases (Fig. 7H). SD in PCRt-r always preceded severe local hypoxia by 29 ± 3.1 s, whereas VLM SD preceded hypoxia in the majority of seizures (5/7; Fig. 7I), by 5.4 ± 3.2 s.

FIGURE 7. Seizure-induced brainstem spreading depolarization (SD) precedes local severe hypoxia in *Cacna1a*^{S218L} mice.

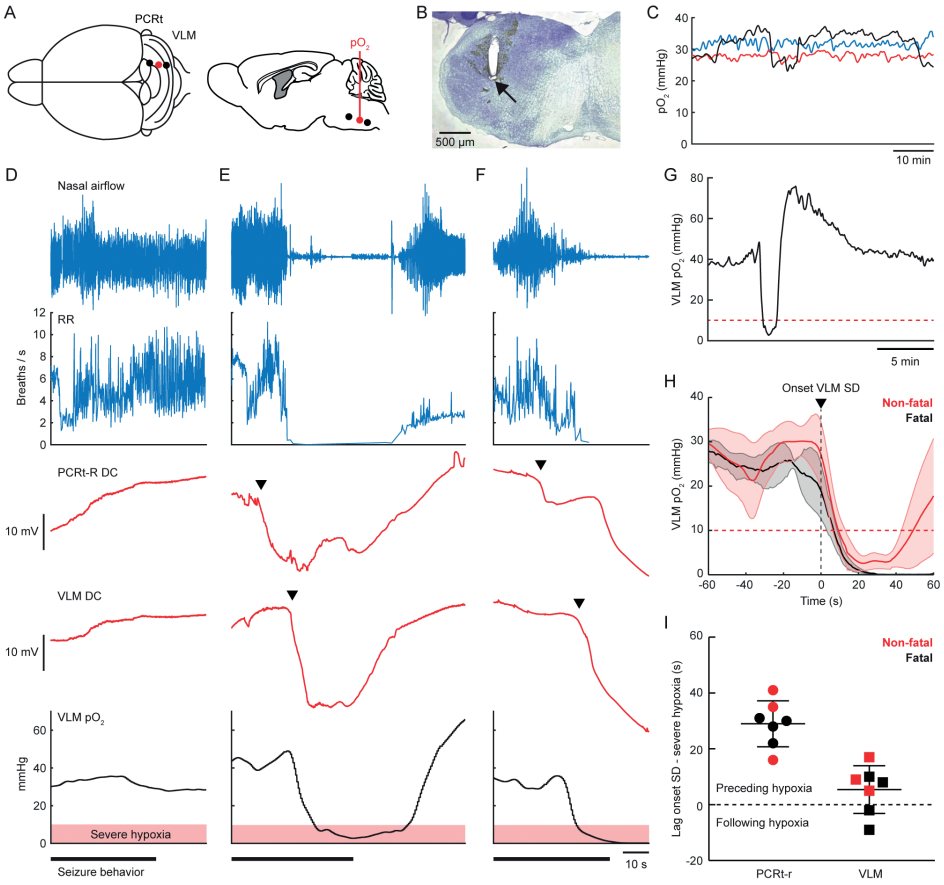

(A) Top and sagittal view of experimental approach for parallel brainstem pO_2 (red) and DC-recordings (PCRt = parvocellular reticular nucleus; VLM = ventrolateral medulla). **(B)** Nissl staining showing the track of an oxygen-sensing probe close to the VLM. **(C)** Example interictal VLM pO_2 recordings for 3 *Cacna1a*^{S218L} mice, which remained within the normoxic range of 20 – 40 mmHg. **(D-F)** Example recordings during termination of IC-induced seizures, including a non-fatal seizure not showing sudden changes in brainstem DC-potential **(D)** and a non-fatal **(E)** and fatal seizure **(F)** during which brainstem SD (arrowheads) occurred. Recordings of local VLM pO_2 (bottom) indicate severe hypoxia (pO_2 <10 mmHg; shaded red) during brainstem SD. **(G)** Expanded timescale of pO_2 measurements during the non-fatal seizure presented in (E), showing rebound hyperoxia for minutes following initial severe hypoxia (red dotted line). **(H)** Average pO_2 during VLM SD (onset at time = 0 s; n = 3 non-fatal and n = 4 fatal seizures). Recovery from severe hypoxia (red dotted line) occurred only for non-fatal seizures. **(I)** Time lag between onset of SD in PCRt-r and VLM and severe hypoxia. All PCRt-r SDs and the majority of VLM SDs preceded hypoxia.

To confirm that the early hypoxia observed in the brainstem was a local effect, we measured pO_2 simultaneously in both V1 cortex and VLM in a subset of animals. Baseline cortical pO_2 was similar to baseline pO_2 levels observed in VLM (32.3 ± 2.5 mmHg). During fatal seizures (n = 5) severe hypoxia in VLM occurred in close association with VLM SD and preceded severe cortical hypoxia

by 25 – 38 s (example in Fig. 8A). In a separate group of *Cacna1a*^{S218L} mice (n = 4), cortical pO_2 dynamics during electrically induced cortical SD (Fig. 8B) confirmed that the pO_2 monitoring system was capable of detecting shifts in pO_2 coinciding with SD, with severe hypoxia detected after 7 – 16 s. Furthermore, pO_2 decreases where more abrupt during induced cortical SDs and SDs in the VLM associated with evoked fatal seizures, when compared to cortical recordings during fatal seizures not associated with cortical SD (Fig. 8C). Finally, cortical DC shifts did occur >60 s after a fatal seizure and long after severe hypoxia had commenced, indicative of anoxic depolarization (AD; Fig. 8D). These data indicate that the pO_2 dynamics measured in the brainstem reflect pO_2 changes induced by local SD, which are distinct from pO_2 dynamics preceding AD.

FIGURE 8. Oxygen dynamics in the ventrolateral medulla indicate that hypoxia is induced by brainstem spreading depolarization (SD) in *Cacna1a*^{S218L} mice.

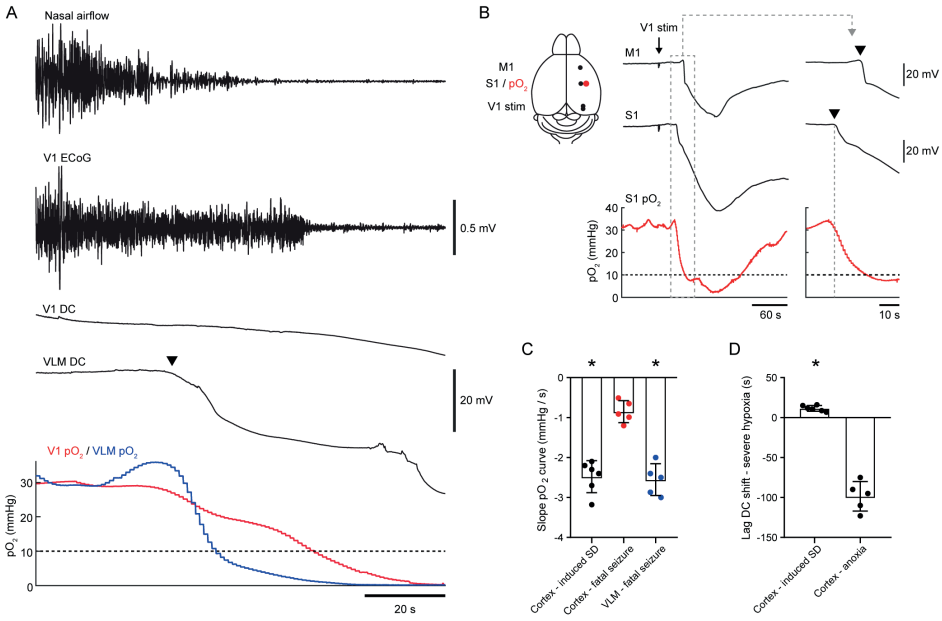

(A) Example of a fatal seizure with parallel pO_2 measurements in the ventrolateral medulla (VLM, blue) and primary visual cortex (V1, red). In this example, severe hypoxia (dashed line) in the VLM preceded cortical hypoxia by 25 s. **(B)** Schematic (left) showing experimental approach for cortical stimulation in freely behaving mice (M1 = primary motor cortex; S1 = primary somatosensory cortex). Cathodal stimulation in the primary visual cortex (V1 stim) resulted in a sequential DC shift in S1 and M1. SD in S1 coincided with a drop in pO_2 (right; arrowheads indicate SD onset), followed by severe hypoxia (10 mmHg, dashed horizontal line) 15 s after SD onset in this example. **(C)** Maximum pO_2 slope measured in 5-s bins indicating a more abrupt decrease in pO_2 for DC shifts during cortically induced SD (black; 6 SDs in n = 4 mice, 1 – 2 SDs per mouse) and VLM SD (blue), when compared to cortical pO_2 during fatal seizures (red; $t(9) = 7.69$ and $t(8) = 7.88$ respectively, $^*p < 0.0001$, unpaired t-tests). **(D)** For cortical recordings, severe hypoxia occurred closer to DC shifts associated with cortically induced SD when compared to DC shifts associated with anoxia following fatal seizures ($t(9) = 14.4$, $^*p < 0.0001$, unpaired t-test).

Fatality following brainstem SD can be prevented by timely respiratory resuscitation

In previous experiments, MUA recovery following VLM SD was observed after 26 ± 8 s (range 15 – 54) and 44 ± 5 s (range: 29 – 62) for spontaneous and induced non-fatal seizures, respectively. We therefore considered VLM SD without MUA recovery within 60 s fatal, and initiated mechanical ventilation >60 s after SD onset. This led to successful resuscitation in 7/9 animals (65 – 79 s for successful attempts; 70 and 76 s for non-successful attempts). During resuscitation, DC-potential recovery in the VLM was observed, that always preceded the first gasp (Fig. 9A). Bradypnea duration in the 7 resuscitated animals was 132 ± 10 s (range: 104 – 180), significantly longer than in animals with spontaneous recovery (n = 12; 75 ± 5 s [range: 75 – 102]; t(17) = 6.21, p <0.0001, unpaired t-test). Breathing did not recover in animals receiving sham ventilation (n = 3; 61, 72 and 80 s after SD onset) or mechanical ventilation initiated >80 s after bradypnea onset (n = 3; 81, 91 and 102 s after SD onset).

Finally, 3 mice implanted with a brainstem oxygen-sensing probe were mechanically ventilated at 62 – 65 s following VLM SD onset. In all animals, an increase in heart rate, recovery of VLM DC-potential and spontaneous breathing activity preceded recovery from severe hypoxia (example in Fig. 9B). In compliance with respiratory data, hypoxic burden, measured by the area below 10 mmHg,[31] was greater in resuscitated animals than in animals with spontaneous recovery (752 – 1580 mmHg*s and 151 – 523 mmHg*s, respectively; both n = 3).

FIGURE 9A. Respiratory resuscitation following spreading depolarization (SD) in ventrolateral medulla (VLM) prevents fatal outcome in *Cacna1a*^{S218L} mice.

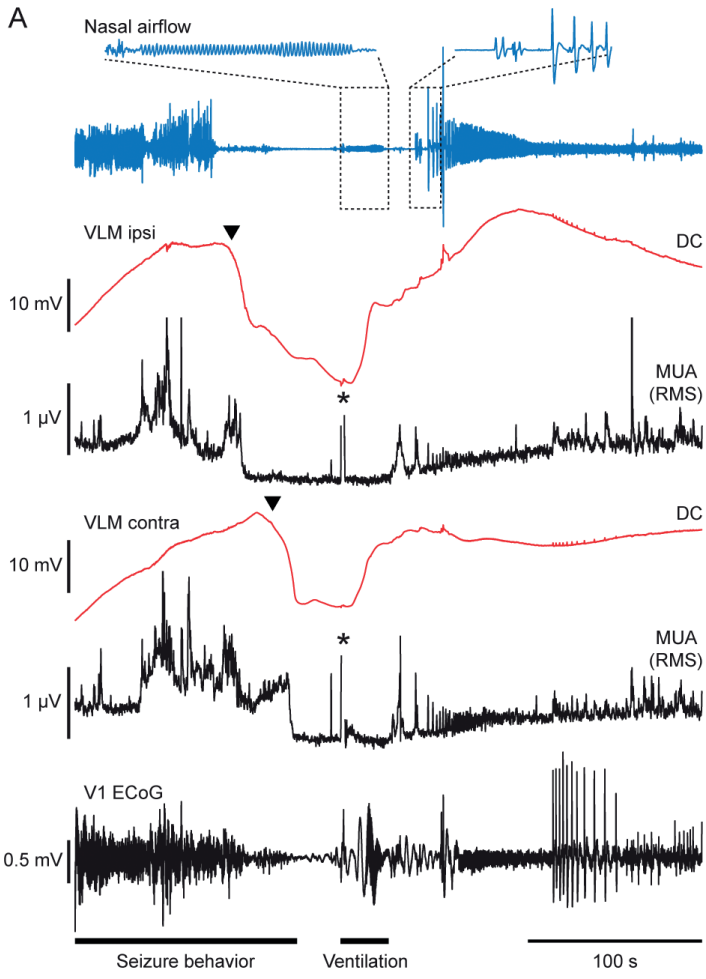

(**A**) Example of a successful resuscitation attempt after bilateral VLM SD (arrowheads) following inferior colliculus (IC) stimulation. Mechanical ventilation was commenced 70 s after VLM SD onset in this case, in absence of spontaneous DC and multi-unit activity (MUA) recovery. Effective delivery of air was confirmed by a regular oscillatory nasal airflow signal (inset top left), and was always accompanied by early recovery of VLM DC-potential, followed by MUA recovery. Respiratory activity invariably resumed with gasping (inset top right). Asterices denote artifacts due to positioning of the animal for mechanical ventilation (RMS = root mean square; V1 ECoG = electrocorticogram in primary visual cortex).

FIGURE 9B. Respiratory resuscitation following spreading depolarization (SD) in ventrolateral medulla (VLM) prevents fatal outcome in *Cacna1a*^{S218L} mice.

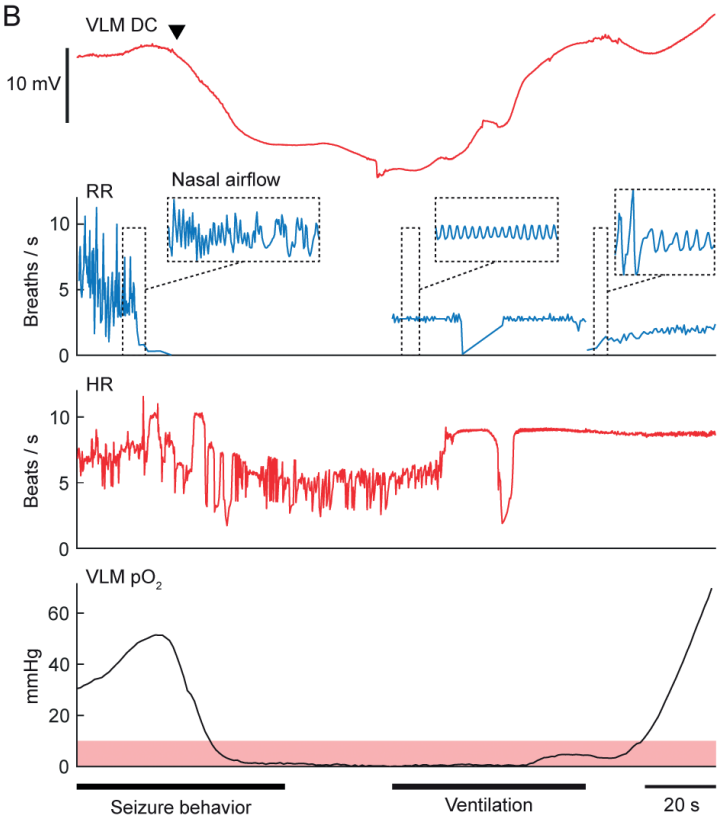

(B) Example of heart rate (HR) and local pO_2 changes during mechanical ventilation after VLM SD (arrowhead), showing that recovery of HR and VLM DC precedes recovery of local pO_2. Note that effective ventilation was unintendedly interrupted in this case, as indicated by the transient drop in respiratory rate (RR). Severe hypoxia (pO_2 <10 mmHg) is indicated in shaded red.

NMDA receptor antagonists prevent seizure-induced brainstem SD and fatality

In vitro and *in vivo* studies showed that blockade of NMDA receptors by MK-801 inhibits locally induced brainstem SD.[11, 32] We tested whether seizure-induced brainstem SD and respiratory compromise can be prevented by treatment with MK-801 (1 mg/kg) preceding IC stimulation. Irrespective of treatment, all animals showed a stage 5 seizure. However, MK-801 prevented brainstem SD, bradypnea and fatal outcome (Fig. 10A,B). Upon recovery of seizures, however, mice demonstrated loss of postural control and hyperactive limb movements for up to 2 h following MK-801 injection. We therefore also tested the effects of memantine, a clinically well-tolerated

NMDA receptor antagonist.[33, 34] Memantine (10 mg/kg) prevented mortality and, in all but 1 mouse, brainstem SD and bradypnea (Fig. 10A,B) and did not result in overt peri-ictal behavioral changes. Absence of hindlimb clonus, that specifically occurred during termination of spontaneous and induced seizures displaying VLM SD, accounted for a shorter seizure duration for memantine-treated, but not MK-801-treated, mice (Fig. 10C).

FIGURE 10. NMDA receptor antagonists prevent seizure-induced medullary spreading depolarization (SD), respiratory suppression and fatal outcome in *Cacna1a*^{S218L} mice.

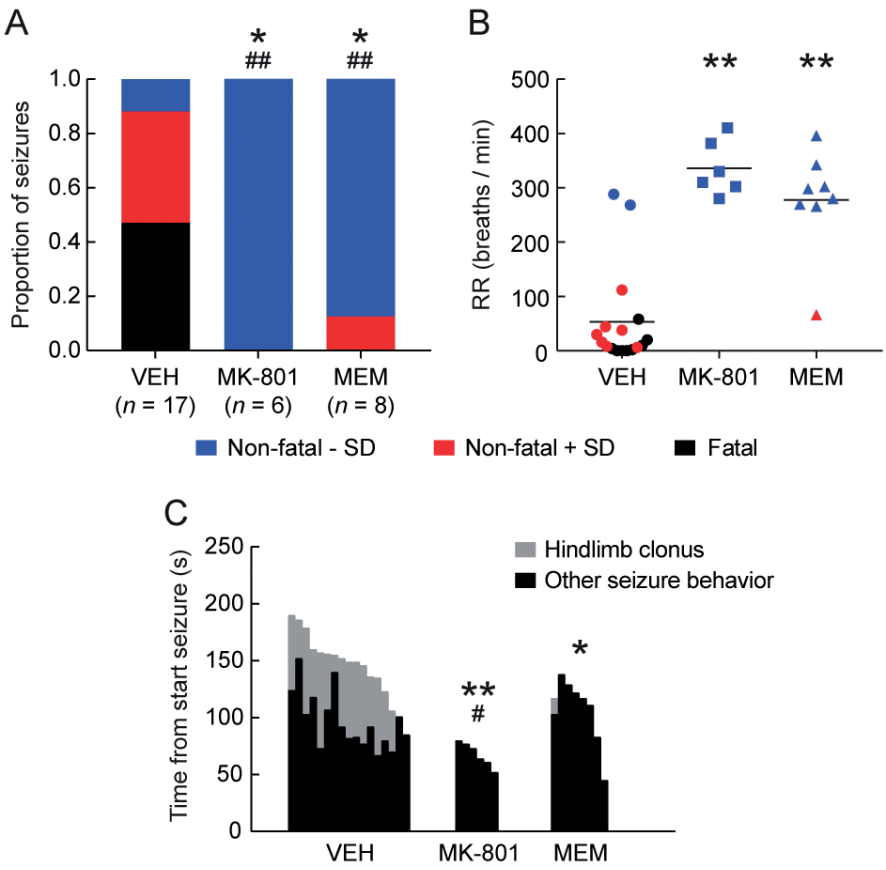

Cacna1a^{S218L} mice received acute intraperitoneal treatment with vehicle (VEH), MK-801 (1 mg/kg), or memantine (MEM, 10 mg/kg) 30 min prior to an inferior colliculus stimulation-induced seizure. **(A)** Proportion of seizures with fatal or non-fatal outcome, with or without SD in the ventrolateral medulla (VLM). Note that all fatal seizures were associated with VLM SD. Animals pretreated with MK-801 or MEM had seizures that were significantly less likely fatal (*p <0.05, χ^2 test) and less likely associated with VLM SD (##p <0.001, χ^2 test). **(B)** Mean respiratory rate (RR) during the last minute of seizure behavior, indicating respiratory suppression during seizures with VLM SD (red and black). RR was significantly greater for animals pretreated with MK-801 or MEM (**p <0.0001, ANOVA with Dunnett's test). **(C)** Seizures were significantly shorter for animals pretreated with MK-801 or MEM (**p = 0.001 and *p = 0.013, respectively, ANOVA with Dunnett's test). When excluding hindlimb clonus (grey), MK-801 pretreatment resulted in shorter seizures while MEM did not (#p = 0.045 and p = 0.755, respectively, ANOVA with Dunnett's test). Hindlimb clonus only occurred for seizures associated with VLM SD (VEH: n = 15; MEM: n = 1).

DISCUSSION

Here we show that spreading depolarization (SD) causes respiratory compromise and apnea upon invasion of the brainstem ventrolateral medulla (VLM) during spontaneous and induced seizures in *Cacna1a*^{S218L} mice. Incidence, onset and recovery of SD in the VLM was strongly related to apnea and SD was not caused by local hypoxia but instead *initiated* such hypoxia. We confirmed that putative fatal SD and subsequent hypoxia were reversible by resuscitation. Furthermore, prevention of SD initiation by NMDA receptor antagonists confirmed that SD is a prerequisite for seizure-related apnea in this animal model.

Cacna1a^{S218L} mice have been proposed as a SUDEP model as homozygotes present spontaneous non-fatal and fatal tonic-clonic seizures at different ages.[13] Here we show that prolonged seizure-related apnea frequently occurs in this genetic mouse model. Data from rare monitored SUDEP cases indicate that apnea precedes cardiac arrest.[4] In patients with implanted electrodes aberrant activity in the amygdala, either caused by a seizure or electrical stimulation, was associated with apnea.[35] Although this revealed a potential mechanism of seizure-related apnea, breathing resumed before seizure termination, suggesting that other or additional mechanisms are involved in SUDEP as apnea in the postictal period appears dangerous.[3, 4]

In the present study, recording electrodes were located in or near the ventral respiratory column, at the level of the pre-Bötzinger Complex (preBötC). PreBötC neurons are essential for breathing rhythm[15] and the respiratory response to hypoxia.[16, 17] Rapid suppression of glutamatergic preBötC neurons induces lethal apnea,[19] whereas unilateral stimulation of inhibitory preBötC populations is sufficient to induce apnea during the stimulation period.[36] Our data indicate that neuronal suppression in the VLM following SD induces apnea, and subsequently hypoxia: i) VLM SD occurred specifically during seizures with bradypnea, ii) bradypnea did not occur during seizures with SD limited to the rostral brainstem (PnO), iii) the timing of bradypnea correlated well with neuronal suppression in the VLM, but not with neuronal suppression in the PnO, and iv) brainstem hypoxia occurred in association with brainstem SD and preceded cortical hypoxia. Variations in onset of VLM SD relative to bradypnea may be explained by small deviations in electrode position (~200 μm), as SD propagation is known to be especially slow in brainstem areas.[32]

Our findings corroborate previous studies that reported brainstem SD in different SUDEP animal models.[11-13] Based on DC-potential recordings in the dorsal medulla, it was proposed that brainstem SD occurred in the postictal period, secondary to ictal hypoxia as fatal apnea was already present upon detection of brainstem SD.[11, 12] Whereas this provides a rationale for the absence of successful autoresuscitation efforts during fatal seizures in SUDEP mouse models,[13, 37] it does not explain the onset of apnea. In the present study, brainstem SD preceded apnea, which may be explained by the different location of the brainstem recording electrode. Previously, this electrode was positioned in the dorsocaudal medulla that is primarily involved in cardiovascular function,[11, 12] while we placed the electrode in the ventrolateral medulla that is primarily involved in respiratory

function. As such, VLM SD may be the underlying mechanism for both the onset of apnea and the absence of autoresuscitation efforts.

Our data indicate that hypoxia is a consequence, rather than a cause, of seizure-related brainstem SD: i) SD was detected rostral and immediately caudal from the brainstem oxygen probe at respectively ~30 s and ~5 s preceding local hypoxia, whereas we found that AD occurred after >60 s following severe hypoxia, in line with a previous study showing AD in the hyperexcitable brainstem after ~60 s,[30] ii) pO_2 decreases were more abrupt in brainstem than in cortex in the absence of cortical SD, but similar to pO_2 decreases after cortical SD, which may be explained by increased local metabolic demand during SD[38] and iii) NMDA antagonists prevented seizure-induced brainstem SD, as shown for locally induced SD,[11, 32] but do not delay cortical AD.[39] Together, this indicates that brainstem hyperexcitability rather than hypoxia initiates seizure-related brainstem SD.

Differences in seizure networks between SUDEP animal models may be crucial in determining the events leading to death. The seizure phenotype in *Cacna1a*^{S218L} mice suggests an important role for brainstem networks,[13] confirmed here by the similar seizure phenotype following IC stimulation. Surgery reduced survival which may be due to an increased risk of SD following tissue trauma, although implanted animals show similar seizures as naïve animals.[13] Seizures associated with cortical epileptiform activity were prolonged (lasting >30 min), whereas we observed forebrain SDs only during half of the fatal seizures, supporting the premise that increased brainstem network excitability is necessary and sufficient for the (lethal) seizures observed in *Cacna1a*^{S218L} mice. Although brainstem networks have not been extensively studied for seizures in other models, decreased thresholds for SD implying hyperexcitable brainstem networks were found in multiple SUDEP animal models.[11, 12] Endogenous brainstem activity was sufficient for hyperthermia- and kainate-induced convulsive seizures in infant rats after precollicular transection.[40] Furthermore, in a mouse model of acquired temporal lobe epilepsy, increased excitability was found in the nucleus tractus solitarius.[41] These preclinical studies implicate brainstem hyperexcitability in SUDEP pathophysiology. However, to generalize our findings, studies in other models are needed that investigate VLM SD in relation to respiratory suppression and hypoxia.

Longer VLM SD duration for fatal seizures was associated with prolonged suppression of local neuronal activity and breathing. Resuscitation resulted in sequential recovery of heart rate, VLM DC-potential, VLM neuronal activity and breathing activity. Interestingly, VLM DC-potential always recovered before VLM pO_2, suggesting that perfusion pressure rather than tissue oxygenation is crucial for initial recovery of brainstem SD, as reported previously for cortical SD.[42] Resuscitation was initiated in a time-window that indicated fatal outcome. Earlier studies initiated resuscitation after a few seconds of apnea[37, 43] or directly after seizure induction.[44] Our data extend these findings and suggest that ventilatory support is sufficient to recover brainstem control of respiratory function during prolonged apnea.

Only non-fatal seizures with VLM SD were associated with apnea. We are unaware of descriptions of prolonged apnea during and following non-fatal seizures in other animal models,

although in clinical epilepsy hypoxemia is common.[2] Other than respiratory effects, non-fatal seizures with brainstem SD could be discriminated from other non-fatal seizures by postictal ECoG suppression and increased HRV. As non-fatal seizures with brainstem SD were associated with a shorter time towards a fatal seizure, these postictal dynamics may be of clinical interest. Increases in pre- and interictal HRV were found in a patient one day prior to a cluster of seizures leading to SUDEP.[45] These and other potential biomarkers, including post-convulsive central apnea[3] and imaging data implicating atrophy in the mesencephalon and medulla oblongata,[8, 9] may improve SUDEP risk assessment.

Our data showed that hindlimb clonus was specific for seizures with VLM SD and displayed strong overlap in timing with SD. This suggests that hindlimb clonus can be the result of SD-induced motor system activation, for example via reticulospinal pathways.[46] In SUDEP cases, apnea and asystole appear to occur postictally.[4] The obvious difference in brainstem dimensions in humans *versus* mice and the slow propagation of SD complicates translation of the observed motor effects to patients. SD-induced behavior and cardiorespiratory collapse may thus have different temporal sequences across species.

Treatment with NMDA receptor antagonists MK-801 or memantine did not affect seizure stage, yet total seizure duration was significantly decreased. Although this decrease was largely attributed to the absence of SD-induced hindlimb clonus, duration *per se* may be a poor predictor of seizure outcome. Indeed, we found no differences in duration of spontaneous seizures with and without brainstem SD in *Cacna1a*^{S218L} mice. Clinical data in fact indicate the contrary, as postictal central apnea is more common for shorter seizures.[3] Activation of NMDA receptors by glutamate following postsynaptic depolarization is importantly implicated in SD.[47] Treatment with MK-801 or memantine largely abolished VLM SD and the associated apnea, thereby preventing fatal outcome. These findings suggest the potential of an NMDA receptor antagonist as preventative treatment option in individuals with a high SUDEP risk. Importantly, clinical evidence for seizure-related brainstem SD is crucial before considering such an approach.

REFERENCES

1. Nashef, L., et al., Apnoea and bradycardia during epileptic seizures: relation to sudden death in epilepsy. *J Neurol Neurosurg Psychiatry*, 1996. 60(3): p. 297-300.
2. Bruno, E., et al., Ictal hypoxemia: A systematic review and meta-analysis. *Seizure*, 2018. 63: p. 7-13.
3. Vilella, L., et al., Postconvulsive central apnea as a biomarker for sudden unexpected death in epilepsy (SUDEP). *Neurology*, 2019. 92(3): p. e171-e182.
4. Ryvlin, P., et al., Incidence and mechanisms of cardiorespiratory arrests in epilepsy monitoring units (MORTEMUS): a retrospective study. *Lancet Neurol*, 2013. 12(10): p. 966-77.
5. Massey, C.A., et al., Mechanisms of sudden unexpected death in epilepsy: the pathway to prevention. *Nat Rev Neurol*, 2014. 10(5): p. 271-82.
6. Devinsky, O., et al., Sudden unexpected death in epilepsy: epidemiology, mechanisms, and prevention. *Lancet Neurol*, 2016. 15(10): p. 1075-88.
7. Harden, C., et al., Practice guideline summary: Sudden unexpected death in epilepsy incidence rates and risk factors: Report of the Guideline Development, Dissemination, and Implementation Subcommittee of the American Academy of Neurology and the American Epilepsy Society. *Neurology*, 2017. 88(17): p. 1674-1680.
8. Mueller, S.G., L.M. Bateman, and K.D. Laxer, Evidence for brainstem network disruption in temporal lobe epilepsy and sudden unexplained death in epilepsy. *Neuroimage Clin*, 2014. 5: p. 208-16.
9. Mueller, S.G., et al., Brainstem network disruption: A pathway to sudden unexplained death in epilepsy? *Hum Brain Mapp*, 2018. 39(12): p. 4820-4830.
10. Patodia, S., et al., The ventrolateral medulla and medullary raphe in sudden unexpected death in epilepsy. *Brain*, 2018. 141(6): p. 1719-1733.
11. Aiba, I. and J.L. Noebels, Spreading depolarization in the brainstem mediates sudden cardiorespiratory arrest in mouse SUDEP models. *Sci Transl Med*, 2015. **7**(282): p. 282ra46.
12. Aiba, I., X.H. Wehrens, and J.L. Noebels, Leaky RyR2 channels unleash a brainstem spreading depolarization mechanism of sudden cardiac death. *Proc Natl Acad Sci U S A*, 2016. 113(33): p. E4895-903.
13. Loonen, I.C.M., et al., Brainstem spreading depolarization and cortical dynamics during fatal seizures in Cacna1a S218L mice. *Brain*, 2019. 142(2): p. 412-425.
14. Smith, J.C., et al., Brainstem respiratory networks: building blocks and microcircuits. *Trends Neurosci*, 2013. 36(3): p. 152-62.
15. Del Negro, C.A., G.D. Funk, and J.L. Feldman, Breathing matters. *Nat Rev Neurosci*, 2018. 19(6): p. 351-367.
16. Gray, P.A., et al., Normal breathing requires preBotzinger complex neurokinin-1 receptor-expressing neurons. *Nat Neurosci*, 2001. 4(9): p. 927-30.
17. McKay, L.C., W.A. Janczewski, and J.L. Feldman, Sleep-disordered breathing after targeted ablation of preBotzinger complex neurons. *Nat Neurosci*, 2005. 8(9): p. 1142-4.
18. Feldman, J.L. and C.A. Del Negro, Looking for inspiration: new perspectives on respiratory rhythm. *Nat Rev Neurosci,* 2006. 7(3): p. 232-42.

19. Tan, W., et al., Silencing preBotzinger complex somatostatin-expressing neurons induces persistent apnea in awake rat. *Nat Neurosci*, 2008. 11(5): p. 538-40.
20. van den Maagdenberg, A.M., et al., High cortical spreading depression susceptibility and migraine-associated symptoms in Ca(v)2.1 S218L mice. *Ann Neurol*, 2010. 67(1): p. 85-98.
21. McAfee, S.S., et al., Minimally invasive highly precise monitoring of respiratory rhythm in the mouse using an epithelial temperature probe. *J Neurosci Methods*, 2016. 263: p. 89-94.
22. Griffiths, J.R. and S.P. Robinson, The OxyLite: a fibre-optic oxygen sensor. *Br J Radiol*, 1999. 72(859): p. 627-30.
23. Houben, T., et al., Optogenetic induction of cortical spreading depression in anesthetized and freely behaving mice. *J Cereb Blood Flow Metab*, 2017. 37(5): p. 1641-1655.
24. Racine, R.J., Modification of seizure activity by electrical stimulation. II. Motor seizure. *Electroencephalogr Clin Neurophysiol*, 1972. 32(3): p. 281-94.
25. Trinka, E., et al., A definition and classification of status epilepticus--Report of the ILAE Task Force on Classification of Status Epilepticus. *Epilepsia*, 2015. 56(10): p. 1515-23.
26. Nashef, L., et al., Unifying the definitions of sudden unexpected death in epilepsy. *Epilepsia*, 2012. 53(2): p. 227-33.
27. Thireau, J., et al., Heart rate variability in mice: a theoretical and practical guide. *Exp Physiol*, 2008. 93(1): p. 83-94.
28. McCown, T.J., et al., Electrically elicited seizures from the inferior colliculus: a potential site for the genesis of epilepsy? *Exp Neurol*, 1984. 86(3): p. 527-42.
29. Faingold, C.L., Brainstem Networks: Reticulo-Cortical Synchronization in Generalized Convulsive Seizures, in Jasper's Basic Mechanisms of the Epilepsies, J.L. Noebels, et al., *Editors*. 2012: Bethesda (MD).
30. Richter, F., et al., The relationship between sudden severe hypoxia and ischemia-associated spreading depolarization in adult rat brainstem in vivo. *Exp Neurol*, 2010. 224(1): p. 146-54.
31. Farrell, J.S., et al., Postictal behavioural impairments are due to a severe prolonged hypoperfusion/hypoxia event that is COX-2 dependent. *Elife*, 2016. 5.
32. Richter, F., et al., Spreading depression in the brainstem of the adult rat: electrophysiological parameters and influences on regional brainstem blood flow. *J Cereb Blood Flow Metab*, 2008. 28(5): p. 984-94.
33. Bullock, R., Efficacy and safety of memantine in moderate-to-severe Alzheimer disease: the evidence to date. *Alzheimer Dis Assoc Disord*, 2006. 20(1): p. 23-9.
34. Winblad, B., et al., Memantine in moderate to severe Alzheimer's disease: a meta-analysis of randomised clinical trials. *Dement Geriatr Cogn Disord*, 2007. 24(1): p. 20-7.
35. Dlouhy, B.J., et al., Breathing Inhibited When Seizures Spread to the Amygdala and upon Amygdala Stimulation. *J Neurosci*, 2015. 35(28): p. 10281-9.
36. Sherman, D., et al., Optogenetic perturbation of preBotzinger complex inhibitory neurons modulates respiratory pattern. *Nat Neurosci*, 2015. 18(3): p. 408-14.
37. Kim, Y., et al., Severe peri-ictal respiratory dysfunction is common in Dravet syndrome. *J Clin Invest*, 2018. 128(3): p. 1141-1153.

38. Takano, T., et al., Cortical spreading depression causes and coincides with tissue hypoxia. *Nat Neurosci*, 2007. 10(6): p. 754-62.
39. Lauritzen, M. and A.J. Hansen, The effect of glutamate receptor blockade on anoxic depolarization and cortical spreading depression. *J Cereb Blood Flow Metab*, 1992. 12(2): p. 223-9.
40. Pospelov, A.S., et al., Forebrain-independent generation of hyperthermic convulsions in infant rats. *Epilepsia*, 2016. 57(1): p. e1-6.
41. Derera, I.D., B.P. Delisle, and B.N. Smith, Functional Neuroplasticity in the Nucleus Tractus Solitarius and Increased Risk of Sudden Death in Mice with Acquired Temporal Lobe Epilepsy. *eNeuro*, 2017. 4(5).
42. Sukhotinsky, I., et al., Perfusion pressure-dependent recovery of cortical spreading depression is independent of tissue oxygenation over a wide physiologic range. *J Cereb Blood Flow Metab*, 2010. 30(6): p. 1168-77.
43. Faingold, C.L., M. Randall, and S. Tupal, DBA/1 mice exhibit chronic susceptibility to audiogenic seizures followed by sudden death associated with respiratory arrest. *Epilepsy Behav*, 2010. 17(4): p. 436-40.
44. Buchanan, G.F., et al., Serotonin neurones have anti-convulsant effects and reduce seizure-induced mortality. *J Physiol*, 2014. 592(19): p. 4395-410.
45. Jeppesen, J., et al., Heart rate variability analysis indicates preictal parasympathetic overdrive preceding seizure-induced cardiac dysrhythmias leading to sudden unexpected death in a patient with epilepsy. *Epilepsia*, 2014. 55(7): p. e67-71.
46. Hirsch, E., et al., Generalized seizures: from clinical phenomenology to underlying systems and networks. 2006: John Libbey Eurotext.
47. Dreier, J.P., The role of spreading depression, spreading depolarization and spreading ischemia in neurological disease. *Nat Med*, 2011. 17(4): p. 439-47.

Chapter 6

Brainstem depolarization –induced lethal apnea associated with gain-of-function *SCN1A*^{L263V} is prevented by sodium channel blockade

Nico A. Jansen
Sandrine Cestèle
Silvia Sanchez Marco
Maarten Schenke
Kirsty Stewart
Jayesh Patel
Else A. Tolner
Andreas Brunklaus
Massimo Mantegazza
Arn M.J.M. van den Maagdenberg

Proc Natl Acad Sci U S A 2024;121(14):e2309000121

ABSTRACT

Apneic events are frightening but largely benign events that often occur in infants. Here we report apparent life-threatening apneic events in an infant with the homozygous *SCN1A*^{L263V} missense mutation, which causes familial hemiplegic migraine type 3 (FHM3) in heterozygous family members, in the absence of epilepsy. Observations consistent with the events in the infant were made in an *Scn1a*^{L263V} knock-in mouse model, in which apnea was preceded by a large brainstem DC-shift, indicative of profound brainstem depolarization. The L263V mutation caused gain of $Na_V1.1$ function effects in transfected HEK293 cells. Sodium channel blockade mitigated the gain-of-function characteristics, rescued lethal apnea in *Scn1a*^{L263V} mice, and decreased the frequency of severe apneic events in the patient. Hence, this study shows that *SCN1A*^{L263V} can cause life-threatening apneic events, which in a mouse model were caused by profound brainstem depolarization. In addition to being potentially relevant to sudden infant death syndrome (SIDS) pathophysiology, these data indicate that sodium channel blockers may be considered as therapeutic for apneic events in patients with these and other gain-of-function *SCN1A* mutations.

INTRODUCTION

Breath-holding spells are apneic events that are common in infants, often occur following emotional provocation, and can lead to loss of consciousness in severe cases.[1] Despite the often frightening appearance these events are considered benign. Prolonged apnea requiring resuscitation is rare, and other abnormalities have been suggested to contribute to apnea in these cases.[1] It is unclear to what extent there is a correlation between these apneic events and sudden infant death syndrome (SIDS).[2, 3] Although genetic factors that predispose to breath-holding spells largely remain to be identified, genetic variants have been associated with SIDS and other sudden death phenotypes together referred to as sudden unexpected death in pediatrics (SUDP), including sudden unexplained death in childhood (SUDC) and sudden unexpected death in epilepsy (SUDEP). Of these, variants in genes encoding voltage-gated sodium channels seem relatively abundant,[4] including variants in *SCN1A*.[4-8]

Here, we report a clinical case of unusually severe apneic events that resulted in apparent life-threatening events. Family history and genetic analyses revealed the presence of hemiplegic migraine caused by a heterozygous *SCN1A*^{L263V} missense mutation in family members, consistent with a diagnosis of familial hemiplegic migraine type 3 (FHM3), and homozygosity of the mutation in the reported case. The *SCN1A* gene encodes the α1 subunit of voltage-gated $Na_V1.1$ sodium channels and FHM3 mutations cause a gain of sodium channel function observed in heterologous expression systems[9, 10] and in an *Scn1a*^{L1649Q} knock-in FHM3 mouse model.[11] Apneic events are not typically associated with FHM, except for anecdotal reports of unexplained respiratory arrest[12] or apnea following general anesthesia[13] but these studies did not investigate the genetic cause underlying these phenotypes. Notably, typical FHM3 phenotypes are milder and mostly involve pure hemiplegic migraine attacks.[14, 15]

In this study, we investigated *Scn1a*^{L263V} knock-in mice, modelling the mutation found in the clinical case. *Scn1a*^{L263V} mice died prematurely due to spontaneous sudden apnea preceded by a large brainstem DC-shift, indicative of profound brainstem depolarization, involving the ventrolateral medulla, a brainstem region vital for generating breathing rhythm,[16, 17] in the absence of epileptiform activity. The mutation resulted in gain-of-function effects on sodium currents in transfected HEK293 cells, which could be mitigated by sodium channel blockers. Similarly, sodium channel blockade prevented apnea in *Scn1a*^{L263V} mice and reduced the frequency of severe apneic events in the clinical case. Thus, *SCN1A*^{L263V} can cause life-threatening apneic events and sodium channel blockers may be considered as therapeutic for patients with these or other gain-of-function *SCN1A* mutations at risk of sudden death.

RESULTS

Severe apneic events in a homozygous *SCN1A*^{L263V} patient in a familial hemiplegic migraine type 3 family

The clinical case (proband; III-1; Fig. 1B) experienced at 2 months of age an apparent life-threatening event. She became distressed and started crying while lying in her cradle during which she became unresponsive, hypotonic, apneic and pale with progressive cyanosis for 5 minutes, requiring physical stimulation to recover. Another apparent life-threatening event occurred at 9 months of age that appeared initiated by agitation. Workup in the hospital at the time did not reveal cardiac abnormalities, and the mother (II-4) was instructed on how to use a manual resuscitator. Between 9-17 months of age, the child experienced approximately 40 apneic events (interpreted as breath-holding spells by the clinicians) that appeared provoked by agitation (crying), during which she became stiff for 2-3 s, then floppy and unresponsive. The mother performed manual resuscitation during the majority of events, and the child regained consciousness within 30-60 s. Obstetric history included maternal gestational diabetes with unremarkable delivery. The child showed normal development until the age of 17 months, although mild speech delay was noticed. At 17 months of age she presented to the emergency department. Previously at home, she became agitated and suddenly stopped breathing after which she lost responsiveness. Cardiopulmonary resuscitation was initiated by the mother and continued by paramedics 6 minutes after the incident; 15 minutes after the incident cardiac output resumed. At the ICU, neuroprotective measures including morphine and midazolam sedation were initiated. During the pediatric ICU stay, hypotension developed that required inotropic support, remaining further uncomplicated. After 72 hours, the child was extubated. MRI showed findings consistent with hypoxic-ischemic brain injury in the basal ganglia (Fig. 1C). There were no abnormalities in other brain regions, including the hippocampi or brainstem. EEG showed high-voltage irregular activity with no epileptiform features. During admission, the patient underwent long-term video EEG recording. The resting record showed no epileptiform abnormality or evidence of subclinical seizures. Two typical events were recorded, one of which requiring resuscitation. The electrographic correlates were widespread rhythmic slow waves of increasing amplitude leading to a period of attenuation and quick return to baseline activity. There was relative bradycardia during the episodes. The sequence of EEG changes was consistent with a physiological response to cerebral hypoxia and the events were in keeping with breath-holding spells without epileptiform features. Similarly, previous wake and sleep EEG recordings at age 2 months following an acute life-threatening episode, and at 7 months showed no epileptiform discharges. ECG and echocardiograms during admissions were normal, however, they did not capture any apneic events. The loop recorder showed sinus rhythm and sinus bradycardia with some possible junctional rhythm (probably during apneic events) with some frequent atrial ectopics.

Family history was negative for breath-holding spells. A sibling (III-2) passed away at 2 years of age from an undetermined cause. She had a history of febrile tonic-clonic seizures associated

with an infectious illness on each occasion. Autopsy revealed severe laryngotracheobronchitis. Several family members were diagnosed with hemiplegic migraine (Fig. 1A and B). The mother of the proband (II-4) was diagnosed with hemiplegic migraine, following several dozen attacks of migraine with auras that included unilateral motor weakness, confusion, and word finding difficulties. The mother's half-sister (II-1), half-brother (II-2) and father (I-2) also had hemiplegic migraine, presenting with similar symptoms. The proband's half-sister (III-3) has presented similar symptoms and she is pending clinical assessment. None of the family members affected by hemiplegic migraine had a history of seizures. Genetic analyses on DNA samples from the proband's maternal side of the family revealed a heterozygous missense mutation in exon 6 of the *SCN1A* gene replacing a leucine for a valine residue at position 263 of the $Na_V1.1$ α1 subunit (Fig. 1A). The mutation co-segregated with all family members with hemiplegic migraine. The heterozygous *SCN1A*^{L263V} mutation was also found in the proband's half-sister (III-3). Most notably, a homozygous *SCN1A*^{L263V} mutation was found in the proband. True homozygosity of the *SCN1A*^{L263V} allele was confirmed by intragenic markers rs994399 (T-allele), rs1542484 (C-allele), rs7580482 (G-allele), rs6432860 (C-allele) and rs2298771 (A-allele) and dosage analysis by multiplex ligation-dependent probe amplification across the *SCN1A* gene. The proband had a gene panel of 1117 epilepsy and arrhythmia genes performed (including *SCN2A*, *SCN3A*, *SCN5A*, *SCN8A* and *MECP2*), which was negative apart from *SCN1A*.

Treatment with levetiracetam (40 mg/kg/day) was initiated in the proband during the pediatric ICU stay, which appeared to have no effect on apneic events (Fig. 1D). Considering the presence of an *SCN1A*^{L263V} mutation, which previously was shown to exert gain-of-function effects in transfected HEK293 cells,[9] treatment with the sodium channel blocker carbamazepine (CBZ; 10 mg/kg/day) was initiated. This was followed by a marked decrease in severity of apneic events (Fig. 1D).

FIGURE 1A-1B. A patient with homozygosity for the *SCN1A*^{L263V} mutation in a familial hemiplegic migraine type 3 family.

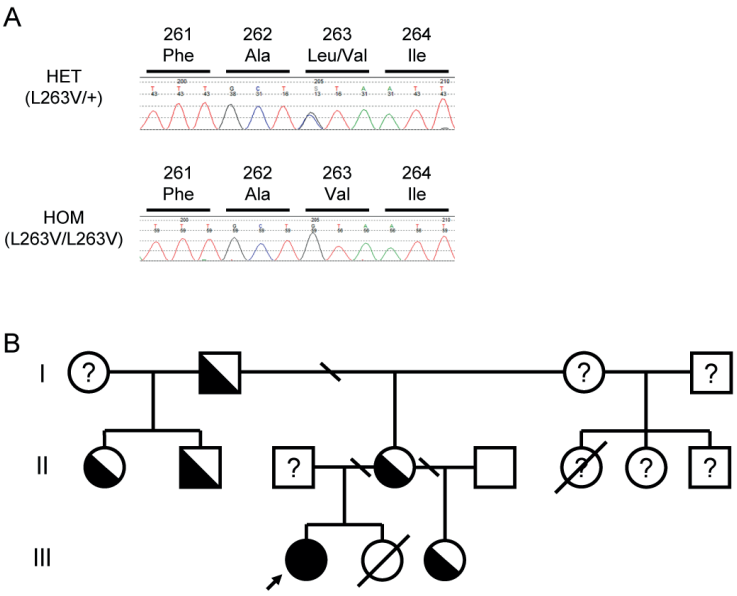

(A) Electropherograms showing single or double copy of the C→G nucleotide change in codon 263 of exon 6 of the *SCN1A* gene, respectively in heterozygous and homozygous carriers. **(B)** Pedigree of the patient's family, showing heterozygous (half-filled) and homozygous (proband (indicated by the arrow); filled) carriers of the *SCN1A*^{L263V} mutation, as well as wild-type (empty) and non-tested (question mark) family members.

FIGURE 1C-1D. A patient with homozygosity for the *SCN1A*^{L263V} mutation in a familial hemiplegic migraine type 3 family.

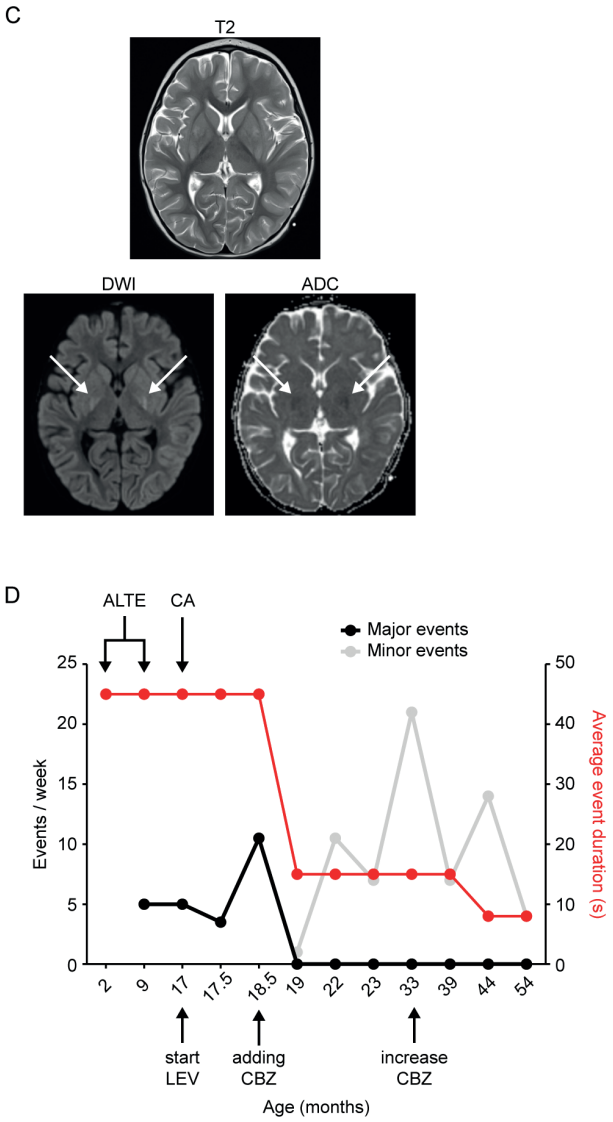

(C) Axial brain 3T MR images obtained from the proband at 17 months following an episode of severe apnea and cardiac arrest requiring cardiopulmonary resuscitation, showing T2-weighted hyperintensity of the basal ganglia bilaterally (top) with areas of restricted diffusion (bottom, arrows), consistent with hypoxic-ischemic brain injury. **(D)** Frequency (black and grey) and duration (red) of apneic events in the proband, with particularly severe events indicated by arrows at the top (ALTE=apparent life-threatening event; CA=cardiac arrest). Note that event duration was not affected by levetiracetam (LEV; 40 mg/kg/day), but decreased following addition of carbamazepine (CBZ; 10 mg/kg/day). Although an increase in minor events (lasting 5-10 s) was observed (grey line), this may reflect an increased awareness of the caregiver and/or physician for such events, which was nevertheless followed by an increase in CBZ dosage to 17 mg/kg/day at 33 months.

Sudden death in *Scn1a*^{L263V} mice is preceded by apnea and a brainstem DC-shift

To investigate the potential mechanism of apneic events in the proband, we studied heterozygous and homozygous mice with the same L263V missense mutation, introduced in the orthologous *Scn1a* gene using a CRISPR/Cas9 strategy.[18] Heterozygous *Scn1a*^{L263V} mice show decreased survival with peak mortality in postnatal weeks 3-4, without overt behavioral abnormalities other than sudden short-lasting behavior in the seconds preceding fatality.[18] We implanted 23 heterozygous *Scn1a*^{L263V} mice to record brain and (cardio)respiratory activity starting from postnatal day 20-21. During 2-week video-EEG recordings, 22 mice died after 104±21 (range 14-332) hours. None of the animals showed cortical epileptiform activity (example in Movie S1). Recordings of cortical and hippocampal activity in a separate group of 8 *Scn1a*^{L263V} mice (total 926 (range 12-264) hours recording time) showed no seizures, spike-and-wave discharges or interictal spikes (examples in SI Appendix, Fig. S1). In the mice that survived > 24 hours after surgery (n=19/22 mice), fatal events more often occurred during the dark phase (6:30 PM-6:30 AM; 15/19 mice, P=0.001, Fisher's test). All mice were awake before the fatal event commenced, as evidenced by video recordings and vigilance state assessment from EEG data. In the majority of mice (n=16/22) behavior lasted only 1-2 s comprising sudden change of posture with (subtle) hindlimb extension (example in Movie S2). In the remaining 6 mice, this was preceded by wild running lasting 7±1.4 (range 2-12) s. Early mortality in homozygous *Scn1a*^{L263V} mice (n=8; postnatal age 16.9±0.3 (range 15-18) days) precluded EEG recordings, due to insufficient recovery from surgery to allow for chronic invasive recordings. However, video recordings from homozygous *Scn1a*^{L263V} mice (n=6) that did not undergo surgery showed behaviors including hindlimb extension (n=6) and wild running (n=3) during fatal events which lasted 1-12 s, similar to what was observed in heterozygous operated mice. When compared to wild-type (WT) mice, heterozygous or homozygous *Scn1a*^{L263V} mice did not show abnormalities in baseline behavior or body weight (6.2±0.3, 5.9±0.3 and 6.5±0.2 g at P14, respectively; n=6 per group; P=0.26, ANOVA).

In 6 heterozygous *Scn1a*^{L263V} mice, recordings of respiratory activity, ECG and EEG revealed a stereotypical pattern involving sudden apnea coinciding with transient bradycardia, followed by EEG suppression (example in Fig. 2). In an FHM1 mouse model, seizure-related apnea was caused by brainstem medullary spreading depolarization.[19] To study whether a similar mechanism may occur here, we implanted heterozygous *Scn1a*^{L263V} mice (n=17) with an electrode in the ventrolateral medulla. In all animals that died during the 2-week recording period (n=16, of which 13 with respiratory and 6 with ECG recordings), a DC-shift occurred during abnormal behavior associated with the fatal event (example in Movie S3) that was immediately followed by apnea and (transient) bradycardia (Fig. 3A and B), preceding EEG suppression, cortical anoxic depolarization (AD) and cardiac arrest (Fig. 3C). Respiratory and ECG recordings showed no abnormalities preceding this event. These findings indicate that *Scn1a*^{L263V} mice show brainstem depolarization-associated apnea resulting in sudden death.

FIGURE 2. Example of brain and cardiorespiratory recordings during spontaneous sudden death in a heterozygous *Scn1a*^{L263V} mouse.

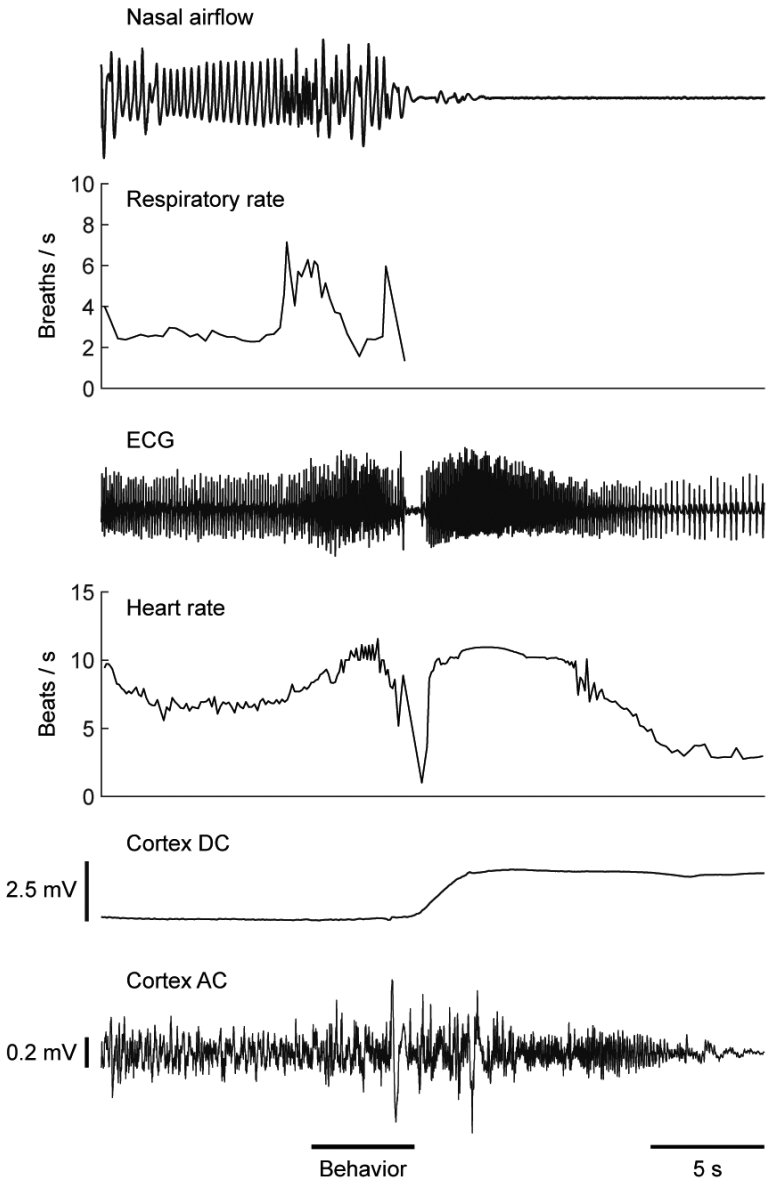

Note that the sudden onset of apnea coincided with transient bradycardia, and preceded suppression of electrocorticogram activity (cortex AC).

FIGURE 3A. Lethal sudden apnea in heterozygous *Scn1a*^{L263V} mice is preceded by a DC-shift in the medulla.

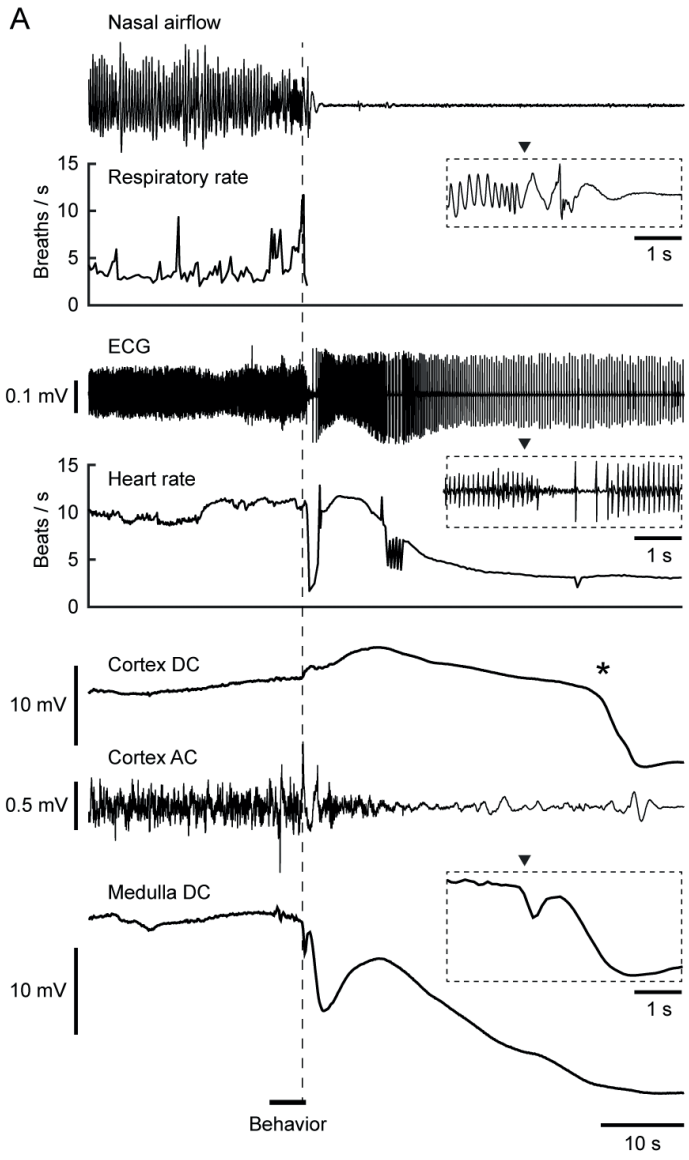

(A) Spontaneous sudden apnea and bradycardia follow soon after onset of a DC-shift in the ventrolateral medulla (dashed line, corresponding to arrowheads in insets) in an *Scn1a*^{L263V} mouse.

FIGURE 3B-3C. Lethal sudden apnea in heterozygous *Scn1a*^{L263V} mice is preceded by a DC-shift in the medulla.

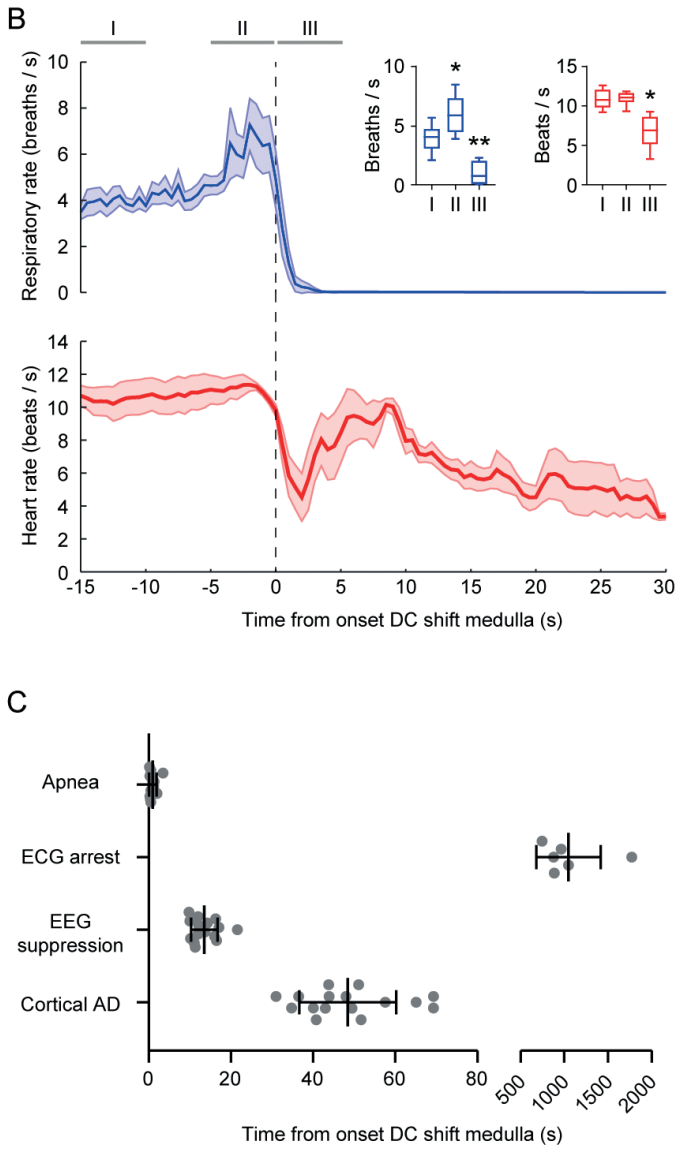

(B) Similar dynamics were observed in recordings from all *Scn1a*^{L263V} mice (n=13 with respiratory recordings, n=6 with ECG), here aligned at onset of the medullary DC-shift (dashed line). When compared to baseline (I), respiratory rate was significantly increased prior to the DC-shift (II), while both respiratory and heart rate were decreased immediately after the DC-shift (III; *P<0.05, **P<0.005, repeated measures ANOVA with Dunnett's test). **(C)** Timing of arrest of brain and cardiorespiratory activity with respect to the medullary DC-shift. A consistent sequence of apnea, EEG suppression, cortical anoxic depolarization (AD) and cardiac arrest was observed in all animals.

A profound brainstem depolarization precedes local and cortical hypoxia in *Scn1a*^{L263V} mice

The brainstem DC-shift suggests that a profound depolarization underlies apnea in *Scn1a*^{L263V} mice. Depolarizations such as those occurring in spreading depolarization (SD) are known to propagate through contiguous grey matter with a speed of several millimeters per minute, and this speed appears lower in brainstem regions.[20] The sudden nature of the events observed in *Scn1a*^{L263V} mice indicates that depolarizations occur either in a limited region crucial for cardiorespiratory functioning, are multifocal and/or propagate at atypically high velocities. To investigate this, we implanted *Scn1a*^{L263V} mice with (bipolar) electrodes in the pons (n=5), and/or contralateral medulla (n=6), in addition to the ventrolateral medulla. Of note, DC-shifts initiated within 2 s from one another and were associated with a transient increase in local multi-unit activity (MUA; Fig. 4A and 5A), which closely paralleled respiratory failure (Fig. 5B). Delay between DC-shifts was greater for ipsi- versus contralateral medulla than for (ipsilateral) pons versus medulla (1.05±0.26 and 0.18±0.08 s, respectively; $t_{(5.9)}$=3.14, P=0.02, Welch's t-test). This yielded estimated propagation velocities of 1.5-14.4 (median 1.9) mm/s and 2.2-20.2 (median 7.8) mm/s between electrodes in medulla-medulla and pons-medulla, respectively. Brainstem DC-shifts had a characteristic shape consisting of an initial steep depolarizing phase with an amplitude of 6.7±0.7 (range 4.9-15.5) mV, followed by plateauing and finally a more persistent potential drop.

Hypoxia can induce SD at multiple foci, [21] which, in the absence of detailed spatial information, complicates the interpretation of DC-shift propagation patterns. Although the sudden onset of apnea during/after the DC-shift suggests that global hypoxia does not precede the DC-shift, local hypoxia may be present. Therefore, we performed simultaneous tissue partial oxygen pressure (PO_2) recordings in the medulla and cortex (n=4) while freely behaving *Scn1a*^{L263V} mice were electrically stimulated in the inferior colliculus (20-100 μA, 50 Hz, 1-ms bipolar pulses for 2 s) – a paradigm that induced brainstem SD in an FHM1 mouse model.[19] Here, all 4 *Scn1a*^{L263V} mice showed fatal apnea 29±9 (range 1-52) s after stimulating with the minimal current intensity eliciting behavior which commenced with a startle response (38±13 μA), which was in all animals followed by running (lasting 1-14 s), immobility and hindlimb extension. Similar to spontaneous events, apnea was preceded by DC-shifts in the brainstem (Fig. 4B). In WT littermates (n=5), stimulation of the inferior colliculus induced a similar startle response followed by running behavior (lasting 1-8 s), but no hindlimb extension, apnea or death, despite increasing current intensities to twice the minimum required to elicit behavior. Tissue PO_2 recordings in *Scn1a*^{L263V} mice indicated normoxia at apnea onset in the medulla and cortex (39.1±5.1 and 29.1±2 mmHg, respectively), but PO_2 dropped to hypoxic levels (<10 mmHg) soon after onset of apnea, which invariably occurred earlier in medulla compared to cortex (Fig. 4C and D). In all cases, medullary hypoxia followed the medullary DC-shift (by 9.6±1.6 (range 6.5-14) s), while cortical hypoxia preceded the cortical DC-shift (by 18±5.3 (range 9-33) s).

To establish whether respiratory support can re-establish cardiorespiratory and brain activity in *Scn1a*^{L263V} mice stimulated in the inferior colliculus, mechanical ventilation was initiated within

60 s after apnea (n=13). Respiratory resuscitation was successful in 8/13 mice, and more often so if initiated early after apnea onset (Fig. 4D). Recovery of autonomous breathing was always preceded by recovery of brainstem DC-potential (example in SI Appendix, Fig. S2). Sham resuscitation (with the ventilator switched off) initiated <30 s after apnea onset (n=4) was never successful.

FIGURE 4. Sudden apnea in heterozygous *Scn1a*^{L263V} mice is induced by a profound brainstem depolarization.

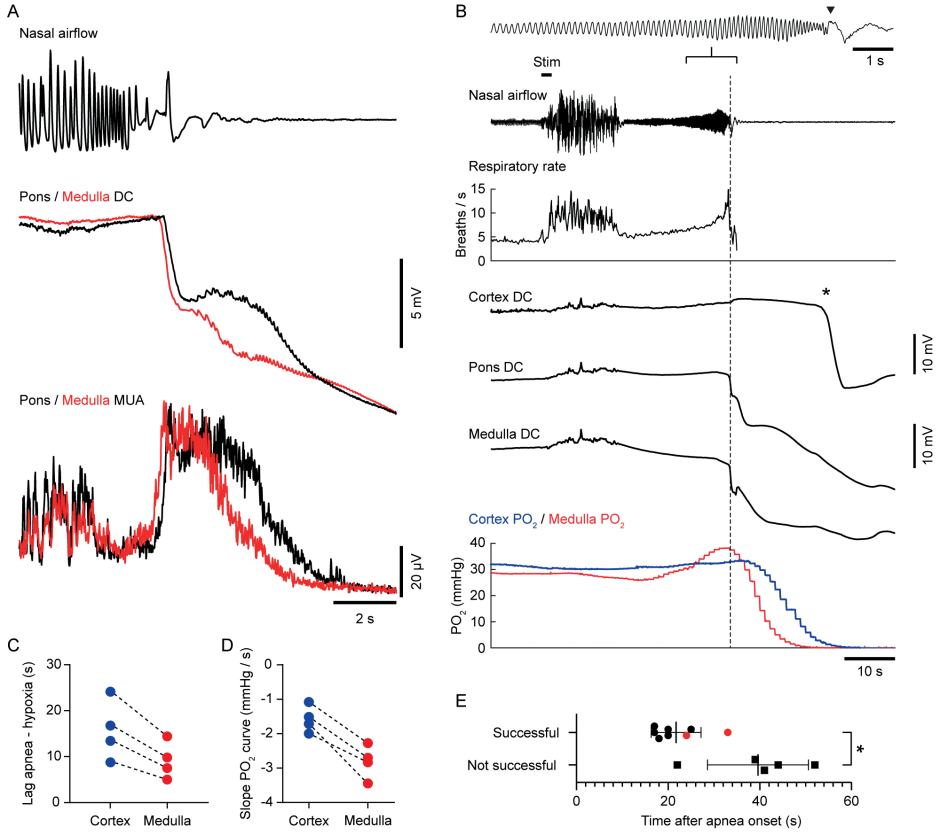

(A) Example of spontaneous and near-simultaneous depolarizations in the pons and medulla of an *Scn1a*^{L263V} mouse. **(B)** Brainstem DC-shifts (onset indicated by dashed line, arrowhead in the inset) following stimulation of the inferior colliculus (Stim) preceded medullary and cortical local PO_2 drops. Note that, on the other hand, the cortical DC-shift followed cortical hypoxia, indicative of an anoxic depolarization (asterisk). **(C)** Following stimulation of the inferior colliculus, medullary hypoxia (PO_2<10 mmHg) consistently preceded cortical hypoxia. **(D)** Local PO_2 consistently decreased faster in the medulla when compared to the cortex. **(E)** Lethality following stimulation of the inferior colliculus could be prevented by timely respiratory resuscitation (*P=0.010; Mann-Whitney test). Resuscitation was also successful during witnessed spontaneous events in two *Scn1a*^{L263V} mice (red).

FIGURE 5. Profound brainstem depolarization in heterozygous *Scn1a*^{L263V} mice preceding spontaneous fatal apnea.

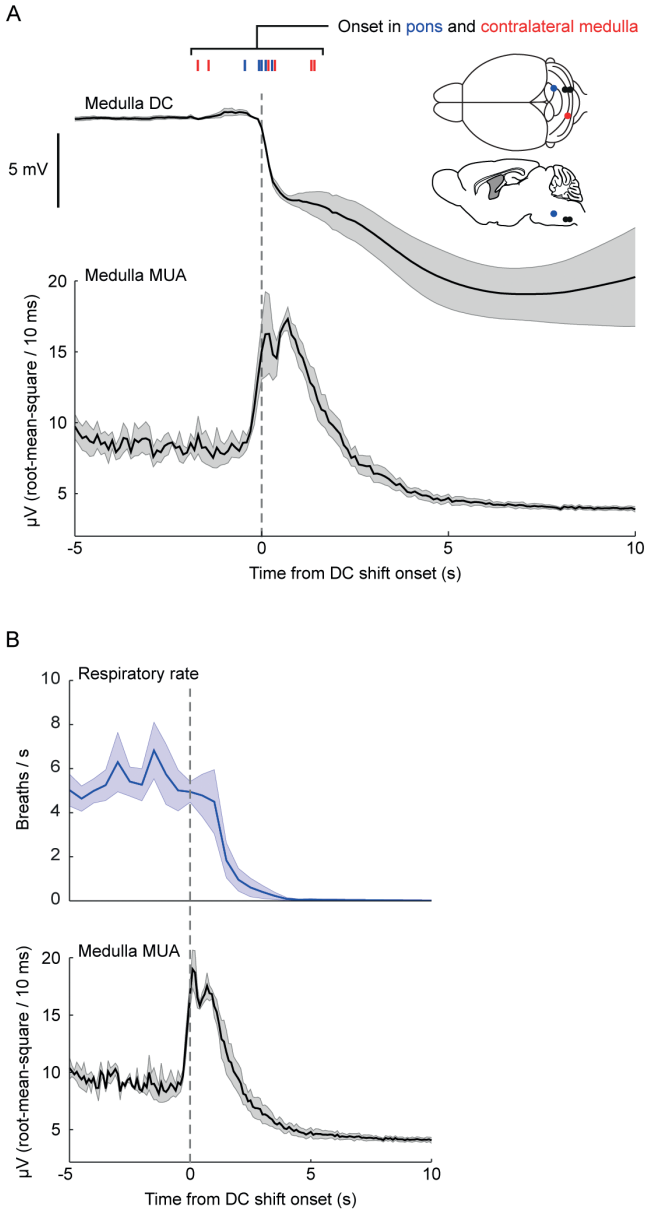

(A) Average DC-signal in the brainstem ventrolateral medulla synchronized at onset of the DC-shift (dashed line at time=0 s). Timing of DC-shift onset in the pons (*n*=5, blue) and contralateral medulla (*n*=6, red) is indicated at the top. Note that an increase in medullary MUA accompanies the negative DC-shift, and is suppressed following the event. **(B)** Average respiratory rate and medullary MUA in *Scn1a*^{L263V} mice (*n*=5) at the time of the medullary DC-shift (dashed line). Note that average MUA is slightly different since only animals with high-quality respiratory recordings are included.

SCN1A^{L263V} causes gain-of-function effects that are reversed by sodium channel blockade

The amelioration of apneic events in our clinical case by CBZ, and the improved breeding of *Scn1a*^{L263V} mice when administered GS967,[18] which promotes use-dependent blockade of sodium channels,[22-24] suggest that sodium channel blockade reduces the abnormalities of the mutant L263V $Na_V1.1$ channels. To test this, we expressed $hNa_V1.1$ in transfected tsA-201 cells and recorded whole-cell sodium currents, comparing the WT and the L263V mutant in the absence or presence of 5 μM GS967 or 15 μM CBZ. The concentration of CBZ used is that found in the cerebrospinal fluid of epileptic patients at standard dosage.[25] There are no data about dosage of GS967 in humans, but previous *in vitro* investigations used it in the micro-molar range.[26, 27] Applying depolarizing steps from a holding potential of -100 mV, we observed robust sodium currents in all groups (Fig. 6A). L263V did not induce a significant modification of maximal current density or voltage-dependence of activation in comparison with WT, whereas both GS967 and CBZ induced a reduction in the former (Fig. 6B). Voltage-dependence of fast inactivation showed a large positive shift induced by the L263V mutation, which was rescued by GS967, but not by CBZ (Fig. 6C). Recovery from fast inactivation was accelerated by L263V (Fig. 6D). GS967 but not CBZ induced a large delay in the recovery that precluded the generation of current in the 20-ms window tested. Current decay, which is induced by inactivation from the open state, was slowed down by L263V (Fig. 6E-G). GS967 completely rescued this effect, whereas CBZ did not. An increase of persistent sodium current (I_{NaP}) for the L263V mutant was not observed (Fig. 6E-G). L263V showed a net decrease of use dependence compared to WT, which was reversed by GS967 but not by CBZ (Fig. 6H-I). Since $Na_v1.1$ is particularly important in fast-spiking GABAergic neurons,[10] we applied as a voltage command its discharge, showing increased action currents in L263V (Fig. 6J-M). GS967 induced a reduction for all the action currents in the discharge, while CBZ induced a smaller reduction in particular during the progression of the discharge.

Overall, the L263V mutant shows a gain of function similar to those previously reported,[9] although we did not observe an increase in I_{NaP}. The limited effect on I_{NaP} is a specific feature of L263V compared to other FHM3 mutants.[14, 27] Sodium channel blockers could revert the effects of the mutation, with GS967 being more effective than CBZ.

FIGURE 6A-6G. Functional modifications induced by L263V on hNa$_v$1.1 and effects of sodium channel blockers GS967 and CBZ.

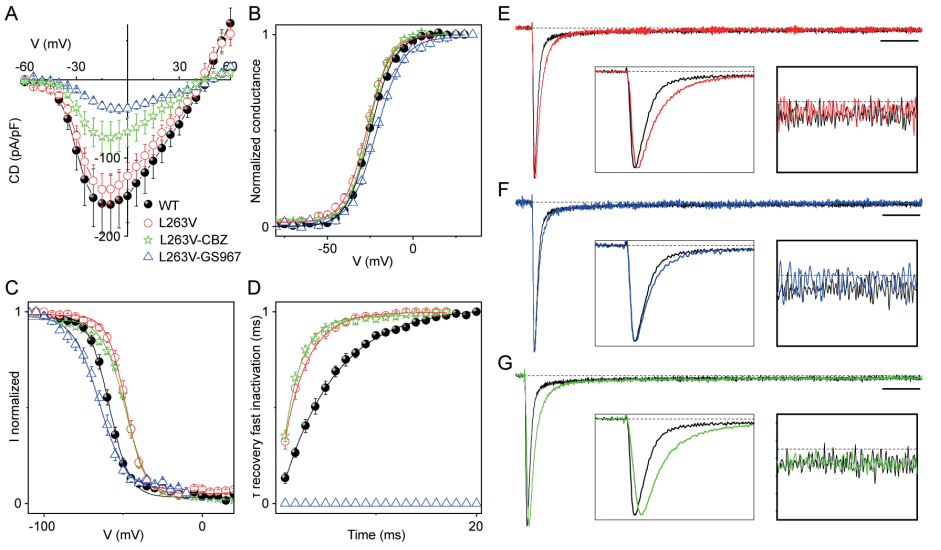

(A) Current density-voltage plots for tsA-201 cells transfected with hNa$_v$1.1-WT (black), hNa$_v$1.1-L263V (red), hNa$_v$1.1-L263V recorded in the presence of 15 μM of CBZ (green) and hNa$_v$1.1-L263V recorded in the presence of 5 μM GS967 (blue). **(B)** Mean voltage-dependence of activation, lines are Boltzmann fits. GS967 induced a 6.1-mV positive shift of the L263V curve (P=0.002), mainly caused by the decrease of the steepness of the curve (20% increase of L263V slope factor, k_d, P=0.007). No statistically significant difference was present between the activation curves of WT, L263V and L263V-CBZ. **(C)** Mean voltage-dependence of fast inactivation, lines are Boltzmann fits. **(D)** Recovery of fast inactivation at -80 mV. (E-G) Comparison of average normalized currents elicited by depolarizing steps to -10 mV for hNav1.1-WT and hNa$_v$1.1-L263V **(E)**, hNa$_v$1.1 and hNa$_v$1.1-L263V-GS967 **(F)**; hNa$_v$1.1 and hNa$_v$1.1-L263V-CBZ **(G)**; calibration bar 5 ms. The left insets show the first 6 ms of the current traces to compare the current decay, the right insets show the traces between 73.5 – 78.5 ms to compare INa_p. (H-I) Use-dependence (current normalized to the first stimulus in the train) induced by trains of 2-ms depolarizing steps to 0 mV from the holding potential of -70 mV at a frequency of 10 Hz

FIGURE 6H-6M. Functional modifications induced by L263V on hNa$_v$1.1 and effects of sodium channel blockers GS967 and CBZ.

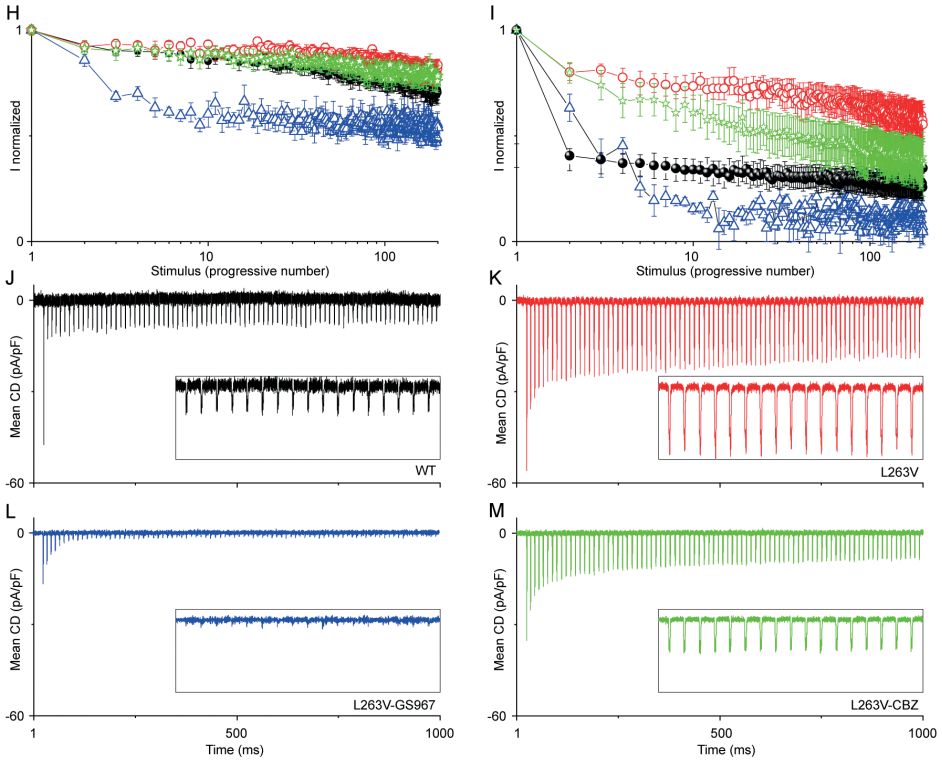

(H) and 100 Hz **(I)** for hNa$_v$1.1-WT, hNa$_v$1.1-L263V, hNa$_v$1.1-L263V-GS967 and hNa$_v$1.1-L263V-CBZ. **(J-M)** Action Na$^+$ currents expressed as mean current density recorded using as voltage stimulus the action potential discharge of a GABAergic fast spiking neuron for hNa$_v$1.1-WT **(J)**, hNa$_v$1.1-L263V **(K)**, hNa$_v$1.1-L263V-GS967 **(L)** and hNa$_v$1.1-L263V-CBZ **(M)**. Data points are displayed as mean ± SEM. See SI Appendix Fig. S3, S4 and Table S1 for statistical comparisons.

Sodium channel blockers prevent brainstem depolarization and apnea in *Scn1a*^{L263V} mice

To test whether sodium channel blockade prevents brainstem DC-shifts, apnea and death *in vivo* in *Scn1a*^{L263V} mice, we evaluated the effects of GS967-compounded chow (8 mg/kg chow). Mice receiving the GS967-compounded chow showed improved survival, while the sudden death phenotype resumed in the days after switching back to normal chow (Fig. 7A). Following stimulation of the inferior colliculus in *Scn1a*^{L263V} mice that received GS967-compounded chow (96±25 μA, compared to 45±7 μA with normal chow; P=0.08, Mann-Whitney test), running behavior was rarely followed by a brainstem DC-shift, apnea or death (Fig. 7B), even when stimulated at more than twice the threshold current. Acute intraperitoneal treatment with GS967

or CBZ prior to stimulation of the inferior colliculus rescued the sudden death phenotype (Fig. 7C). However, pretreatment with MK-801, a potent NMDA receptor antagonist that effectively prevents SD in the preconditioned rat brainstem[20] and in FHM1 mice after stimulation of the inferior colliculus,[19] was ineffective at blocking brainstem DC-shifts, apnea or death in *Scn1a*^{L263V} mice (Fig. 7C). Together, these data indicate that sodium channel blockade impedes lethal apnea in *Scn1a*^{L263V} mice by preventing brainstem DC-shifts.

FIGURE 7. Sodium channel blockers prevent lethal apnea in heterozygous *Scn1a*^{L263V} mice.

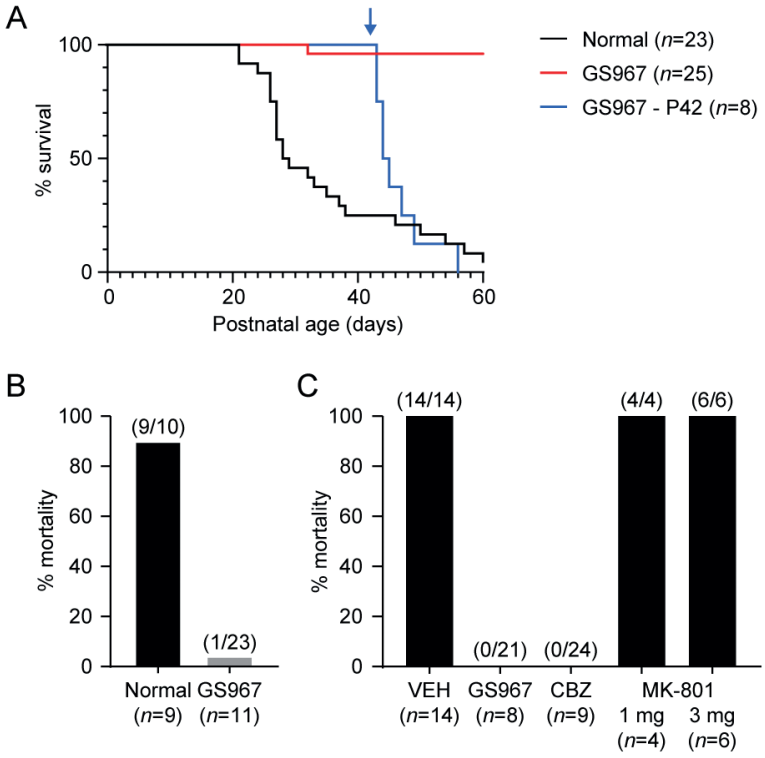

(A) Survival of *Scn1a*^{L263V} mice is improved by chow compounded by GS967 (8 mg/kg chow; red; $P<0.0001$, Mantel-Cox test). In a separate group, withdrawal from GS967 at P42 (blue, arrow) reinstated the sudden death phenotype. **(B)** Stimulation of the inferior colliculus was less likely fatal in mice maintained on GS967-compounded, when compared to normal, chow ($P<0.0001$, Fisher's exact test). **(C)** Intraperitoneal pretreatment with GS967 or CBZ prevented death following stimulation, when compared to vehicle (VEH; $P<0.0001$, Fisher's exact test), whereas MK-801 did not increase survival at the two doses tested ($P>0.99$, Fisher's exact test).

DISCUSSION

We here report a case of an infant with severe and life threatening apneic events, associated with a homozygous *SCN1A*^{L263V} missense mutation. Heterozygous mutation carriers within the family were affected by hemiplegic migraine, consistent with a diagnosis of FHM3, similar to earlier reports.[28, 29] The respiratory phenotype of the clinical case was essentially replicated in *Scn1a*^{L263V} mice, in which a profound brainstem depolarization preceded apnea onset. Sodium channel blockade rescued L263V-associated gain-of-function properties *in vitro*, prevented fatal apnea *in vivo* and decreased the severity of apneic events in the clinical case. These findings indicate that *SCN1A* gain of function can result in life-threatening sudden apnea induced by brainstem dysfunction.

The proband had prolonged periods of apnea that required (cardio)pulmonary resuscitation, suggesting that autoresuscitation following severe hypoxia failed in this child. Failure of autoresuscitation has been implicated in SIDS pathogenesis.[30] Although SIDS is generally believed to occur in sleeping infants, breath-holding during arousal may be an initiating factor in some SIDS cases.[31] We here propose that sudden profound depolarization of brainstem neurons caused by $Na_V1.1$ gain of function can trigger fatal apnea. Previous studies have implicated brainstem SD in epilepsy-related fatal apnea.[19, 32, 33] Here, however, neither the presented clinical case nor *Scn1a*^{L263V} mice showed evidence of seizure activity in behavior or EEG/LFP recordings. Although *Scn1a*^{L263V} mice showed (typically short-lasting) behaviors that may originate from abnormal activity in brainstem centers[34, 35] – behaviors indeed occurred during locally increased MUA and the subsequent DC-shift – convulsive behaviors including clonic or profound tonic activity were never observed. Running behavior was replicated by stimulation of the inferior colliculus in both WT and *Scn1a*^{L263V} mice, and has previously been ascribed to its role in the initiation of aversive states.[36] Interestingly, a recent study described *SCN1A* gain-of-function carriers that presented with seizure-related apnea.[37] Seizure-related brainstem SD was reported in a transgenic FHM1 mouse model[33] and in an *Scn1a* loss-of-function mouse model of Dravet syndrome.[32] In FHM1 mice, SD caused apnea upon propagation to medullary respiratory centers,[19] while SD occurred in the dorsal medulla in Dravet mice.[32] However, NMDA antagonists blocked brainstem SD in previous studies,[19, 20, 32] but did not block brainstem DC-shifts in *Scn1a*^{L263V} mice, suggesting that a different mechanism underlies the profound brainstem depolarization we observed in *Scn1a*^{L263V} mice.

High extracellular potassium renders NMDA antagonists ineffective against SD.[38] Studies have shown that $Na_V1.1$ gain of function leading to hyperexcitability of GABAergic interneurons can facilitate SD initiation because of extracellular potassium build up induced by neuronal spiking,[39, 40] which was confirmed in another FHM3 mouse model in which homozygous *Scn1a*^{L1649Q} knock-in resulted in premature death.[11] A potassium transient may be also caused by $GABA_A$ receptor-mediated redistribution of chloride and bicarbonate and subsequent homeostatic processes.[41, 42] Notably, immaturity of the glial syncytium mediating potassium spatial buffering may increase the susceptibility of the immature brainstem to SD.[43] Indeed, DC-shifts evoked in the

immature rat brainstem are not sensitive to NMDA blockade.[44] Thus, although direct evidence for brainstem DC-shifts in infants may prove difficult to obtain, observations of the clinical phenotype and the presence of DC-shifts in *Scn1a*^{L263V} mice suggest that such profound depolarization should be considered in sudden death pathogenesis.

In addition to insensitivity to NMDA blockade, the delay between brainstem DC-shifts was <2 s in *Scn1a*^{L263V} mice, yielding estimated very high propagation velocities with a median of 1.9 and 7.8 mm/s, between electrodes in medulla-medulla and pons-medulla, respectively. This is in contrast to SD that is characterized by a slower continual spread of a DC-shift at a velocity of a few millimeters per *minute,*[45] suggesting that the present events spread much faster and/or occur at multiple brainstem sites simultaneously. Although hypoxia can cause multifocal SD, which was recently proposed as a mechanism of death in a kainic acid SUDEP mouse model,[46] the PO_2 measurements here indicate that hypoxia is a consequence rather than a cause of the brainstem DC-shift in *Scn1a*^{L263V} mice. In hyperexcitable rat brainstem preparations, DC-shifts propagated at high velocities (up to 30 times faster than SD), roughly similar to observations in *Scn1a*^{L263V} mice, and were also associated with neuronal silencing and prevented by sodium channel blockade.[47] Although the DC-shifts in *Scn1a*^{L263V} mice were invariably fatal and thus showed a persistently negative potential, the initial steep depolarizing phase was of a similar moderate amplitude (a mean of 6.7 mV here, compared to approximately 7-8 mV in previous studies[47]). It was proposed that the high propagation velocities may be facilitated by gap junctions perhaps by allowing fast-propagating Ca^{2+} waves, as earlier reported in the hippocampus.[48, 49] Nevertheless, DC-shifts in *Scn1a*^{L263V} mice show similarities to these fast-spreading events including a characteristic steep negative DC-shift associated with a burst of neuronal activity followed by neuronal silence. Thus, these events may belong to what can be described as the "SD continuum".[50] Estimated propagation velocities in *Scn1a*^{L263V} mice exceeding those earlier published may be explained by focal initiation of the DC-shift in an area between the recording electrodes, or by multifocal initiation that may result from widespread brainstem hyperexcitability due to a high expression of $Na_V1.1$ in brainstem regions.[51, 52]

SCN1A genetic variants have been reported in SIDS cases[5] and sudden unexpected death in pediatrics (SUDP).[4, 53] Seemingly, the gain-of-function effects we report here for *SCN1A*^{L263V} are at odds with loss-of-function effects found with SIDS-associated *SCN1A* mutations.[5] Yet, fatal brainstem SD was first described in a mouse model with a loss-of-function *Scn1a* mutation.[32] Also, *SCN1A* variants associated with SIDS/SUDP are missense and might, instead, show gain of function in a neuronal environment upon rescue of folding/trafficking defects, as it has been reported for some FHM3 mutants.[10, 54] Thus, in addition to *SCN1A*^{L263V}, the risk of brainstem depolarization-induced apnea is likely increased in other *SCN1A* variants. This may explain earlier counterintuitive findings of reduced lethality, despite unchanged or even increased seizure activity, following treatment with sodium channel blockers in epileptic *Scn1a* knockout mice.[55] Similarly, GS967 improved survival in *Scn1a* knockout mice, although this effect could be in part caused

by downregulation of expression of $Na_V1.6$ channels.[22] Brainstem depolarization may thus be a mechanism of sudden death in different *SCN1A* variants.

We report sudden death in both heterozygous and homozygous *Scn1a*^{L263V} mice, whereas severe apneic events were only reported in the homozygous *SCN1A*^{L263V} clinical case. Patients with a heterozygous *SCN1A*^{L263V} mutation in this family, as well as in other families already reported, presented with a phenotype typical of FHM3, not including respiratory dysfunctions, seizures, coma or death related to migraine attacks such as observed in other FHM subtypes.[14] This indicates that the brainstem phenotype of *Scn1a*^{L263V} mice is more severe than in patients, which may be related to interspecies differences in brainstem cytoarchitecture,[56] pattern of $Na_V1.1$ expression, and/or potassium buffering capacity. Alternatively, phenotype severity may be explained by differences in the dimensions of the brainstem and its white matter structures, which effectively interrupt SD propagation.[45] The observational and pharmacological data presented here suggest that brainstem depolarization as observed in our mouse model triggered apneic events in the clinical case. Interspecies differences deserve further attention in future studies to understand the potential risk of profound brainstem depolarizations in other patients.

METHODS

Animals

Scn1a^{L263V} mice were generated by CRIPR/Cas9-mediated homologous recombination as described previously.[18] Mice were maintained on a C57BL/6J background. To improve breeding, heterozygous *Scn1a*^{L263V} male mice used for breeding were maintained on chow containing GS967 (8 mg/kg chow; Research Diets), which was estimated to result in a dosage of 1.5 mg/kg a day.[26] To prevent exposure to GS967 in offspring, male heterozygous *Scn1a*^{L263V} mice received normal chow during the mating period. To generate homozygous *Scn1a*^{L263V} mice, heterozygous male and female *Scn1a*^{L263V} mice continuously received GS967 in food pellets. For behavioral and survival analysis of homozygous *Scn1a*^{L263V} offspring, video recordings from pairs of P14 mice fed with normal chow were obtained, and compared with mice receiving GS967-compounded chow. Approval for experiments was obtained from local and national ethical committees that conformed to the European Communities Council Directive (2010/63/EU). Experiments were carried out in accordance with ARRIVE guidelines.

Surgery

Mice were implanted with platinum/iridium electrodes (75 µm, PT6718, Advent Research Materials) at P19-23 in different configurations: (i) primary visual cortex (-3.5/2.0/0.5; mm relative to bregma, i.e. anterior, lateral and ventral, respectively) and primary motor cortex (+1.5/1.8/0.5), (ii) primary visual and motor cortex, and dorsal (-2.2/2.0/1.3) and ventral (-3.2/3.0/3.5) hippocampus, (iii)

primary visual cortex and brainstem ventrolateral medulla (-6.5/1.3/4.1), and (iv) primary visual cortex, brainstem caudal pontine reticular nucleus (-5.5/1.3/3.9) and ventrolateral medulla. To record MUA, a bipolar electrode was inserted at this location. A reference and ground electrode were placed above the cerebellum. In all mice, a thermistor probe (MEAS-G22K7MCD419, Measurement Specialties) was placed above the nasal epithelium to detect in- and expiration.[57] Two electrodes were inserted in the right and left flank to obtain ECG in a subset of mice. Electrodes were connected to a 7-channel pedestal (MS373; Plastics One), compounded by individual pins (#0489 pin receptacles, Mill-Max), if needed, and secured to the skull using dental cement (DiaDent Europe). Measurements of tissue PO_2 were obtained using a fluorescence-based technique that does not consume oxygen.[58] Probes (230 µm) were inserted in the vicinity of electrodes in the visual cortex (-3.0/2.0/0.5) and ventrolateral medulla (-6.2/1.3/3.8).

In vivo oxygen measurements, pharmacology and resuscitation

For stimulation, a bipolar pulse train (50 Hz, 1-ms pulses) was delivered through a bipolar electrode implanted in the inferior colliculus (-5.0/1.0/0.6) at least 2 days after surgery in WT and heterozygous *Scn1a*^{L263V} mice. Current intensity was increased in steps (20, 50, 100, 200, 500 µA) until running behavior occurred. In case of survival, the current was increased by one step until 3 suprathreshold stimulations were administered. For oxygen measurements, PO_2 was sampled at 1 Hz, starting at least 30 min prior to stimulation.

Respiratory resuscitation (200 breaths/min for 20-120 s, 200 µl/breath) was attempted by positioning a tube connected to a mechanical ventilator (Mini-Vent, Harvard Apparatus) over the nostrils of the animal 17-52 s after apnea onset. As a sham procedure, the ventilator was switched off.

Heterozygous *Scn1a*^{L263V} mice received normal or GS967-compounded chow (8 mg/kg chow) for 2 days prior to stimulation of the inferior colliculus. To test the effect of acute treatment on survival, treatment-naïve mice received an intraperitoneal injection of vehicle, GS967 (1 mg/kg; Cayman Chemical) or CBZ (20 mg/kg; Sigma-Aldrich) 1 h prior to stimulation, or vehicle or MK-801 (1 or 3 mg/kg; Sigma-Aldrich) 30 min prior to stimulation. All injections were performed by an experimenter blinded to the treatment.

Histology

Surviving mice were killed by CO_2 and transcardially perfused. Brains were collected (due to tissue degradation not for all mice that died spontaneously) and postfixed in 4% paraformaldehyde for 2.5 h at 21°C, or for 24 h at 4°C (following spontaneous death), and sucrose-processed. Coronal brain sections (40 µm) were obtained using a sliding microtome (Leica) and Nissl-stained to confirm electrode positions.

Data acquisition and analyses of *in vivo* data

Continuous video-EEG recordings were acquired in a shielded Faraday cage for 2 weeks, or until death of the animal. Both DC- and AC-signals were obtained from brain electrodes, as described previously.[19] MUA was obtained by using the differential signal of bipolar electrodes, and the root-mean-square was calculated over 10-ms bins. Data were analyzed using custom-written MATLAB (MathWorks) scripts. Peak detection was used to calculate instantaneous respiratory and heart rate, and the time of the last peak was used to define onset of apnea and ECG arrest, respectively. EEG suppression was defined as <10% of baseline total EEG power (calculated for 1-100 Hz using a fast Fourier transform).

Plasmids, mutagenesis, cell culture and transfections

For cell transfection, site-directed mutagenesis was achieved by using the shorter splice variant isoform (-11 aa) of the human $Na_V1.1$ a1 channel subunit (GenBank database accession no. NM_006920.4), the predominant $Na_V1.1$ variant expressed in brain also used in earlier studies.[10, 59, 60] The $Na_V1.1$ cDNA was subcloned into the pCDM8 plasmid vector to minimize rearrangements. The L263V mutation was introduced with the Quick Change Lightning Kit (Stratagene), obtaining the mutant $hNa_V1.1$-L263V.

The cell line tsA-201 (Sigma-Aldrich 96121229) was maintained and transiently transfected with $CaPO_4$ as previously reported.[60] Cells were co-transfected with the pCDM8-$hNa_v1.1$ vector and a reporter vector expressing Yellow Fluorescent Protein (pEYFP-N1; Clontech) in order to identify the transfected cells for electrophysiological recordings.

Electrophysiological recordings from transfected cells

Sodium currents were recorded using the whole-cell configuration of the patch-clamp technique as previously reported.[10, 59, 60] Recording solutions (in mM): external solution 150 NaCl, 1 $MgCl_2$, 1.5 $CaCl_2$ and 10 HEPES (pH 7.4 with NaOH); internal pipette solution 105 CsF, 35 NaCl, 10 EGTA, 10 HEPES and (pH 7.4 with CsOH). Voltage dependence of activation was studied applying test pulses of 100-ms from -110 to +60 mV from a holding potential at -120 mV. Voltage dependence of inactivation was studied with a 100-ms prepulse at different potentials followed by a test pulse at -10 mV. Conductance-voltage curves were derived from current-voltage (I-V) curves according to $G=I/(V-V_r)$, where I is peak current, V is test voltage, and V_r is the apparent observed reversal potential for tsA-201. The voltage dependence of activation and the voltage dependence of inactivation were fit to Boltzmann relationships in the form $y=1/(1+\exp((V_{½}-V)/k)$, where y is normalized G_{Na} or I_{Na}, $V_{½}$ is the voltage of half-maximal activation (V_a) or inactivation (V_h) and k is a slope factor; for the inactivation curve we included a baseline. Recovery from fast inactivation was studied using a test pulse at 0 mV followed by a repolarization at -80 mV of different duration and another test pulse. I_{NaP} was quantified as the current during 40-50 ms of the voltage step, expressed as % of maximal transient current (I_{NaT}). Use dependence was evaluated with trains of 200 2-ms-long depolarizing steps to 0 mV from a holding potential of -70 mV at 10 and 100 Hz (leak was subtracted off-line

with a P/3 paradigm). Action potential clamp recordings were performed using as voltage stimulus a discharge recorded from a GABAergic fast-spiking basked cell injecting a 1-s depolarizing current step[39]; the instantaneous firing frequency of the discharge was 82-106 Hz. Recordings were not corrected for junction potentials. GS967 or CBZ were added 15-45 min prior to recordings. Cells were maintained at the holding potential of -100 mV for 5 min prior to recordings.

Statistics

Statistical testing was performed in MATLAB (MathWorks), Graphpad Prism (GraphPad Software) or Origin2021 (Originlab). Data are reported as mean ± SEM, individual data points with mean ± SEM, mean ± standard deviation or box-and-whisker graphs (total range). For *in vivo* data, depending on distribution normality assessed by the Kolmogorov-Smirnov test, the Welch *t*-test or Mann-Whitney test was used for single comparisons. For multiple comparisons, ANOVA or repeated measures ANOVA with Dunnett's test was used. For data obtained in transfected cells, the Kolmogorov-Smirnov test and Levene's test were used prior to comparisons performed with one way ANOVA and Tukey's test. $P < 0.05$ was considered significant.

Acknowledgments

We thank S. van Heiningen for assistance with mouse breeding.

REFERENCES

1. F. J. DiMario, Jr., Breath-holding spells in childhood. *Am J Dis Child* 146, 125-131 (1992).
2. A. Kahn *et al.*, Sleep and cardiorespiratory characteristics of infant victims of sudden death: a prospective case-control study. *Sleep* 15, 287-292 (1992).
3. B. T. Thach, Potential Central Nervous System Involvement in Sudden Unexpected Infant Deaths and the Sudden Infant Death Syndrome. *Compr Physiol* 5, 1061-1068 (2015).
4. H. Y. Koh *et al.*, Genetic Determinants of Sudden Unexpected Death in Pediatrics. *Genet Med* 24, 839-850 (2022).
5. C. A. Brownstein *et al.*, SCN1A variants associated with sudden infant death syndrome. *Epilepsia* 59, e56-e62 (2018).
6. M. Halvorsen *et al.*, Mosaic mutations in early-onset genetic diseases. *Genet Med* 18, 746-749 (2016).
7. R. D. Bagnall *et al.*, Exome-based analysis of cardiac arrhythmia, respiratory control, and epilepsy genes in sudden unexpected death in epilepsy. *Ann Neurol* 79, 522-534 (2016).
8. A. E. Baruteau, D. J. Tester, J. D. Kapplinger, M. J. Ackerman, E. R. Behr, Sudden infant death syndrome and inherited cardiac conditions. *Nat Rev Cardiol* 14, 715-726 (2017).
9. K. M. Kahlig *et al.*, Divergent sodium channel defects in familial hemiplegic migraine. *Proc Natl Acad Sci U S A* 105, 9799-9804 (2008).
10. S. Cestele, E. Schiavon, R. Rusconi, S. Franceschetti, M. Mantegazza, Nonfunctional NaV1.1 familial hemiplegic migraine mutant transformed into gain of function by partial rescue of folding defects. *Proc Natl Acad Sci U S A* 110, 17546-17551 (2013).
11. E. Auffenberg *et al.*, Hyperexcitable interneurons trigger cortical spreading depression in a Scn1a migraine-model. *J Clin Invest* (2021).
12. P. Neligan, D. G. Harriman, J. Pearce, Respiratory arrest in familial hemiplegic migraine: a clinical and neuropathological study. *Br Med J* 2, 732-734 (1977).
13. J. Willson, S. Kapur, Apnoeic spells following general anaesthesia in a patient with familial hemiplegic migraine. *Anaesthesia* 62, 956-958 (2007).
14. M. Mantegazza, S. Cestele, Pathophysiological mechanisms of migraine and epilepsy: Similarities and differences. *Neurosci Lett* 667, 92-102 (2018).
15. M. D. Ferrari, R. R. Klever, G. M. Terwindt, C. Ayata, A. M. van den Maagdenberg, Migraine pathophysiology: lessons from mouse models and human genetics. *Lancet Neurol* 14, 65-80 (2015).
16. J. C. Smith, H. H. Ellenberger, K. Ballanyi, D. W. Richter, J. L. Feldman, Pre-Bötzinger complex: a brainstem region that may generate respiratory rhythm in mammals. *Science* 254, 726-729 (1991).
17. C. A. Del Negro, G. D. Funk, J. L. Feldman, Breathing matters. *Nat Rev Neurosci* 19, 351-367 (2018).
18. N. A. Jansen *et al.*, First FHM3 mouse model shows spontaneous cortical spreading depolarizations. *Ann Clin Transl Neurol* 7, 132-138 (2020).
19. N. A. Jansen *et al.*, Apnea associated with brainstem seizures in Cacna1a (S218L) mice is caused by medullary spreading depolarization. *J Neurosci* 39, 9633-9644 (2019).

20. F. Richter, R. Bauer, A. Lehmenkuhler, H. G. Schaible, Spreading depression in the brainstem of the adult rat: electrophysiological parameters and influences on regional brainstem blood flow. *J Cereb Blood Flow Metab* 28, 984-994 (2008).
21. C. R. Jarvis, T. R. Anderson, R. D. Andrew, Anoxic depolarization mediates acute damage independent of glutamate in neocortical brain slices. *Cereb Cortex* 11, 249-259 (2001).
22. L. L. Anderson, N. A. Hawkins, C. H. Thompson, J. A. Kearney, A. L. George, Jr., Unexpected Efficacy of a Novel Sodium Channel Modulator in Dravet Syndrome. *Sci Rep* 7, 1682 (2017).
23. F. Potet, C. G. Vanoye, A. L. George, Jr., Use-Dependent Block of Human Cardiac Sodium Channels by GS967. *Mol Pharmacol* 90, 52-60 (2016).
24. L. Belardinelli *et al.*, A novel, potent, and selective inhibitor of cardiac late sodium current suppresses experimental arrhythmias. *J Pharmacol Exp Ther* 344, 23-32 (2013).
25. S. I. Johannessen, R. E. Strandjord, Concentration of carbamazepine (Tegretol) in serum and in cerebrospinal fluid in patients with epilepsy. *Epilepsia* 14, 373-379 (1973).
26. L. L. Anderson *et al.*, Antiepileptic activity of preferential inhibitors of persistent sodium current. *Epilepsia* 55, 1274-1283 (2014).
27. R. Barbieri, S. Bertelli, M. Pusch, P. Gavazzo, Late sodium current blocker GS967 inhibits persistent currents induced by familial hemiplegic migraine type 3 mutations of the SCN1A gene. *J Headache Pain* 20, 107 (2019).
28. M. J. Castro *et al.*, First mutation in the voltage-gated Nav1.1 subunit gene SCN1A with co-occurring familial hemiplegic migraine and epilepsy. *Cephalalgia* 29, 308-313 (2009).
29. J. Barros *et al.*, Familial hemiplegic migraine due to L263V SCN1A mutation: discordance for epilepsy between two kindreds from Douro Valley. *Cephalalgia* 34, 1015-1020 (2014).
30. H. C. Kinney, B. T. Thach, The sudden infant death syndrome. *N Engl J Med* 361, 795-805 (2009).
31. B. Thach, Tragic and sudden death. Potential and proven mechanisms causing sudden infant death syndrome. *EMBO Rep* 9, 114-118 (2008).
32. I. Aiba, J. L. Noebels, Spreading depolarization in the brainstem mediates sudden cardiorespiratory arrest in mouse SUDEP models. *Sci Transl Med* 7, 282ra246 (2015).
33. I. C. M. Loonen *et al.*, Brainstem spreading depolarization and cortical dynamics during fatal seizures in Cacna1a S218L mice. *Brain* 142, 412-425 (2019).
34. A. Kreindler, E. Zuckermann, M. Steriade, D. Chimion, Electro-clinical features of convulsions induced by stimulation of brain stem. *J Neurophysiol* 21, 430-436 (1958).
35. T. J. McCown, R. S. Greenwood, G. D. Frye, G. R. Breese, Electrically elicited seizures from the inferior colliculus: a potential site for the genesis of epilepsy? *Exp Neurol* 86, 527-542 (1984).
36. J. E. Pandossio, M. L. Brandao, Defensive reactions are counteracted by midazolam and muscimol and elicited by activation of glutamate receptors in the inferior colliculus of rats. *Psychopharmacology (Berl)* 142, 360-368 (1999).
37. A. Brunklaus *et al.*, The gain of function SCN1A disorder spectrum: novel epilepsy phenotypes and therapeutic implications. *Brain* 145, 3816-3831 (2022).

38. G. C. Petzold *et al.*, Increased extracellular K+ concentration reduces the efficacy of N-methyl-D-aspartate receptor antagonists to block spreading depression-like depolarizations and spreading ischemia. *Stroke* 36, 1270-1277 (2005).
39. O. Chever *et al.*, Initiation of migraine-related cortical spreading depolarization by hyperactivity of GABAergic neurons and NaV1.1 channels. *J Clin Invest* 131 (2021).
40. L. Lemaire *et al.*, Modeling NaV1.1/SCN1A sodium channel mutations in a microcircuit with realistic ion concentration dynamics suggests differential GABAergic mechanisms leading to hyperexcitability in epilepsy and hemiplegic migraine. *PLoS Comput Biol* 17, e1009239 (2021).
41. K. Kaila, K. Lamsa, S. Smirnov, T. Taira, J. Voipio, Long-lasting GABA-mediated depolarization evoked by high-frequency stimulation in pyramidal neurons of rat hippocampal slice is attributable to a network-driven, bicarbonate-dependent K+ transient. *J Neurosci* 17, 7662-7672 (1997).
42. T. Viitanen, E. Ruusuvuori, K. Kaila, J. Voipio, The K+-Cl cotransporter KCC2 promotes GABAergic excitation in the mature rat hippocampus. *J Physiol* 588, 1527-1540 (2010).
43. F. J. Binmoller, C. M. Muller, Postnatal development of dye-coupling among astrocytes in rat visual cortex. *Glia* 6, 127-137 (1992).
44. F. Richter, S. Rupprecht, A. Lehmenkuhler, H. G. Schaible, Spreading depression can be elicited in brain stem of immature but not adult rats. *J Neurophysiol* 90, 2163-2170 (2003).
45. G. G. Somjen, Mechanisms of spreading depression and hypoxic spreading depression-like depolarization. *Physiol Rev* 81, 1065-1096 (2001).
46. A. G. George *et al.*, Sudden unexpected death in epilepsy is prevented by blocking postictal hypoxia. *Neuropharmacology* 231, 109513 (2023).
47. F. Richter, R. Bauer, A. Ebersberger, A. Lehmenkuhler, H. G. Schaible, Enhanced neuronal excitability in adult rat brainstem causes widespread repetitive brainstem depolarizations with cardiovascular consequences. *J Cereb Blood Flow Metab* 32, 1535-1545 (2012).
48. O. Herreras, C. Largo, J. M. Ibarz, G. G. Somjen, R. Martin del Rio, Role of neuronal synchronizing mechanisms in the propagation of spreading depression in the in vivo hippocampus. *J Neurosci* 14, 7087-7098 (1994).
49. P. E. Kunkler, R. P. Kraig, Calcium waves precede electrophysiological changes of spreading depression in hippocampal organ cultures. *J Neurosci* 18, 3416-3425 (1998).
50. J. P. Dreier, C. Reiffurth, The stroke-migraine depolarization continuum. *Neuron* 86, 902-922 (2015).
51. I. Ogiwara *et al.*, Nav1.1 localizes to axons of parvalbumin-positive inhibitory interneurons: a circuit basis for epileptic seizures in mice carrying an Scn1a gene mutation. *J Neurosci* 27, 5903-5914 (2007).
52. T. Furuyama, Y. Morita, S. Inagaki, H. Takagi, Distribution of I, II and III subtypes of voltage-sensitive Na+ channel mRNA in the rat brain. *Brain Res Mol Brain Res* 17, 169-173 (1993).
53. A. M. Rochtus *et al.*, The role of sodium channels in sudden unexpected death in pediatrics. *Mol Genet Genomic Med* 10.1002/mgg3.1309, e1309 (2020).
54. S. Dhifallah *et al.*, Gain of Function for the SCN1A/hNav1.1-L1670W Mutation Responsible for Familial Hemiplegic Migraine. *Front Mol Neurosci* 11, 232 (2018).

55. N. A. Hawkins *et al.*, Screening of conventional anticonvulsants in a genetic mouse model of epilepsy. *Ann Clin Transl Neurol* 4, 326-339 (2017).
56. S. Fujita *et al.*, Cytoarchitecture-Dependent Decrease in Propagation Velocity of Cortical Spreading Depression in the Rat Insular Cortex Revealed by Optical Imaging. *Cereb Cortex* 26, 1580-1589 (2016).
57. S. S. McAfee *et al.*, Minimally invasive highly precise monitoring of respiratory rhythm in the mouse using an epithelial temperature probe. *J Neurosci Methods* 263, 89-94 (2016).
58. J. R. Griffiths, S. P. Robinson, The OxyLite: a fibre-optic oxygen sensor. *Br J Radiol* 72, 627-630 (1999).
59. S. Cestele *et al.*, Divergent effects of the T1174S SCN1A mutation associated with seizures and hemiplegic migraine. *Epilepsia* 54, 927-935 (2013).
60. S. Cestele *et al.*, Self-limited hyperexcitability: functional effect of a familial hemiplegic migraine mutation of the Nav1.1 (SCN1A) Na+ channel. *J.Neurosci.* 28, 7273-7283 (2008).
61. M. Mantegazza *et al.*, Identification of an Nav1.1 sodium channel (SCN1A) loss-of-function mutation associated with familial simple febrile seizures. *Proc Natl Acad Sci U S A* 102, 18177-18182 (2005).

SUPPLEMENTARY MATERIAL

FIGURE S1. Representative examples of hippocampal and cortical activity in a heterozygous *Scn1a*^{L263V} mouse.

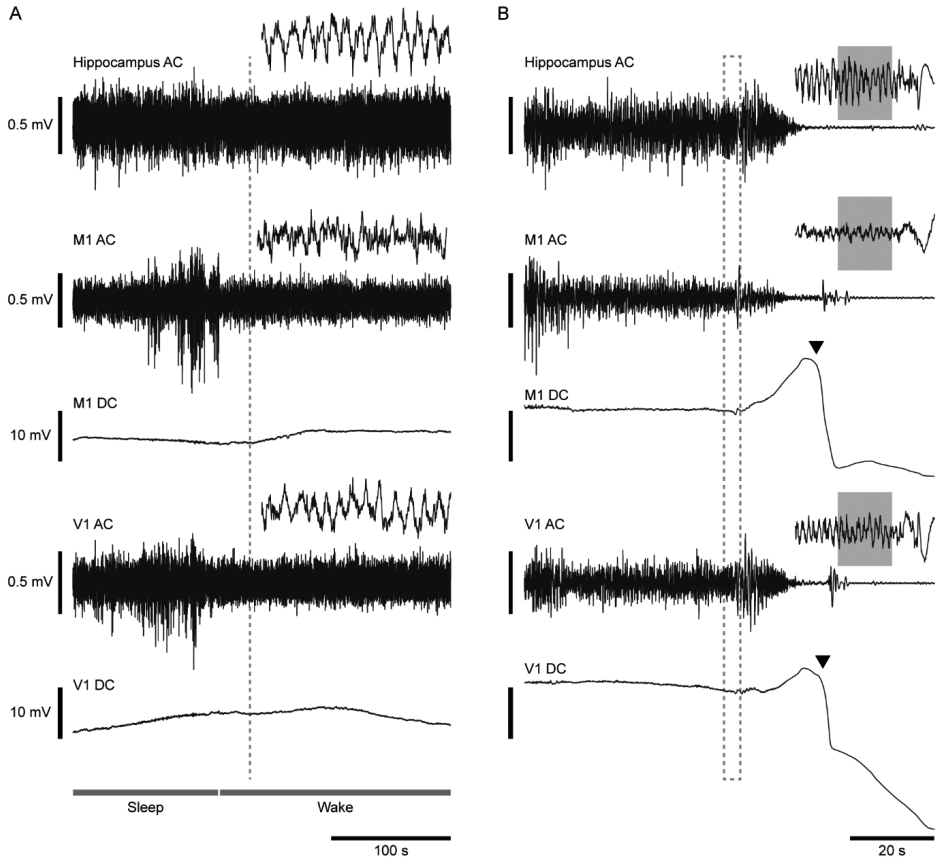

(A) Baseline recordings during sleep and wakefulness. Insets (corresponding with the dashed line, detailing 2 s of local field potential) show characteristic theta wave activity in hippocampus and V1 during movement. Note the moderate-amplitude activity in M1 and V1 during sleep, corresponding with slow waves. No epileptiform activity was noted. **(B)** Recordings during the fatal event showed no epileptiform activity. Insets (corresponding with the dashed box, detailing 4 s of local field potential) show activity during abnormal behavior comprising of change of posture and hindlimb extension (shaded gray).

FIGURE S2. Example of successful respiratory resuscitation of a heterozygous *Scn1a*^{L263V} mouse.

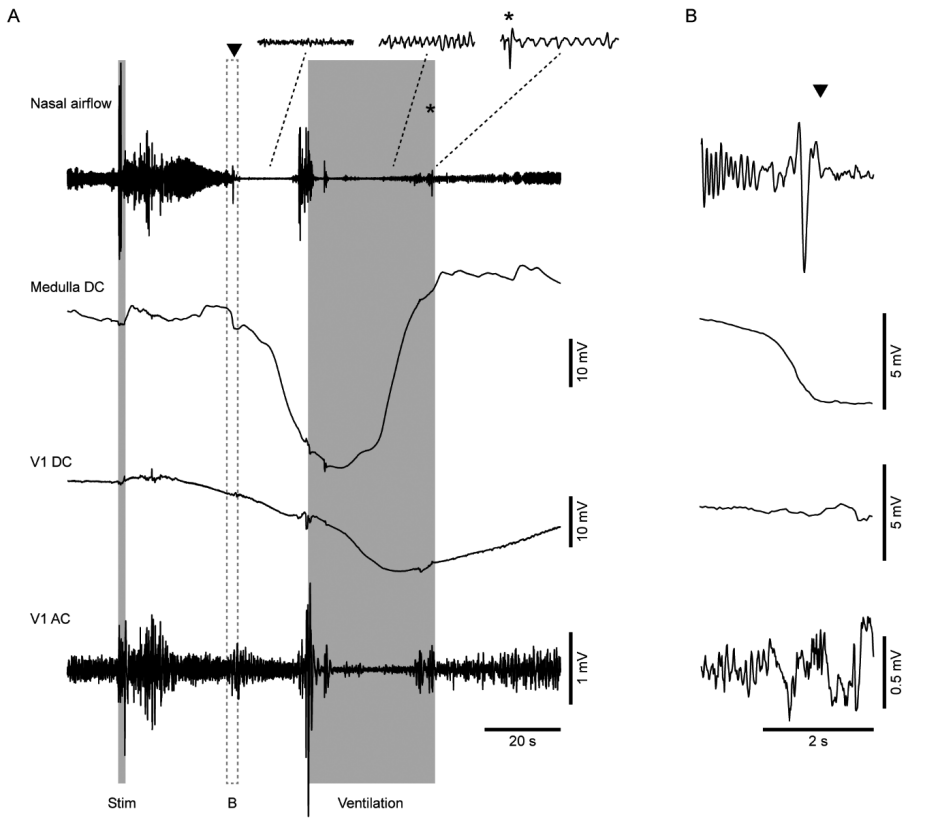

(A) Stimulation of the inferior colliculus (Stim) resulted in a medullary DC-shift followed by apnea (arrowhead; detailed in **B**). During mechanical ventilation (Ventilation), medullary DC-potential recovered prior to the first gasp (asterisk), which was followed by regular breathing. Note that high-amplitude artefacts occurred during stimulation, as well as during positioning the animal immediately prior to mechanical ventilation.

FIGURE S3. Statistical comparisons for functional modifications induced by L263V and effects of 5 µM GS967 and 15 µM CBZ: activation and inactivation properties.

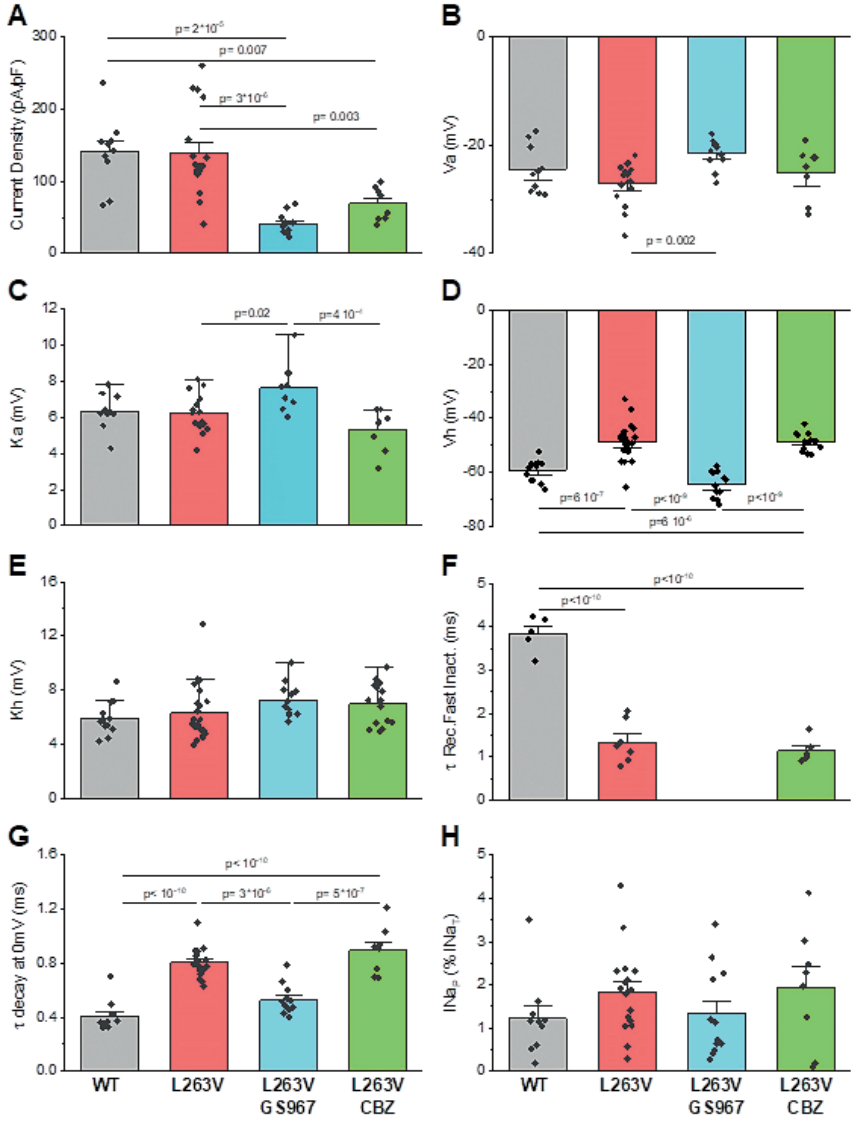

(A) Comparison of maximal current density. **(B)** Comparison of the voltage of half activation (Va) obtained by fits of Boltzmann relationships to the experimental data. **(C)** Comparison of the slope factor of voltage-dependence of activation curves (k_a) obtained by Boltzmann fits of the experimental data. **(D)** Comparison of the voltage of half fast inactivation (Va) obtained by Boltzmann fits of the experimental data. **(E)** Comparison of the slope factor of voltage-dependence of fast inactivation curves (k_h) obtained by Boltzmann fits to the experimental data. **(F)** Comparison of the time constant of recovery from fast inactivation obtained by fits of single exponential relationships to the experimental data. **(G)** Comparison of the time constant of the decay of the current at -10 mV obtained by fits of single exponential relationships to the experimental data. **(H)** Comparison of the maximal INaP. Statistical comparisons have been performed with one way ANOVA followed by Tukey post-hoc test, statistical significant differences ($P < 0.05$) are indicated by solid lines. The bars indicate mean values ± SEM (see also Table S1).

FIGURE S4. Statistical comparisons for functional modifications induced by L263V and effects of 5 μM GS967 and 15 μM CBZ: use dependence and action currents.

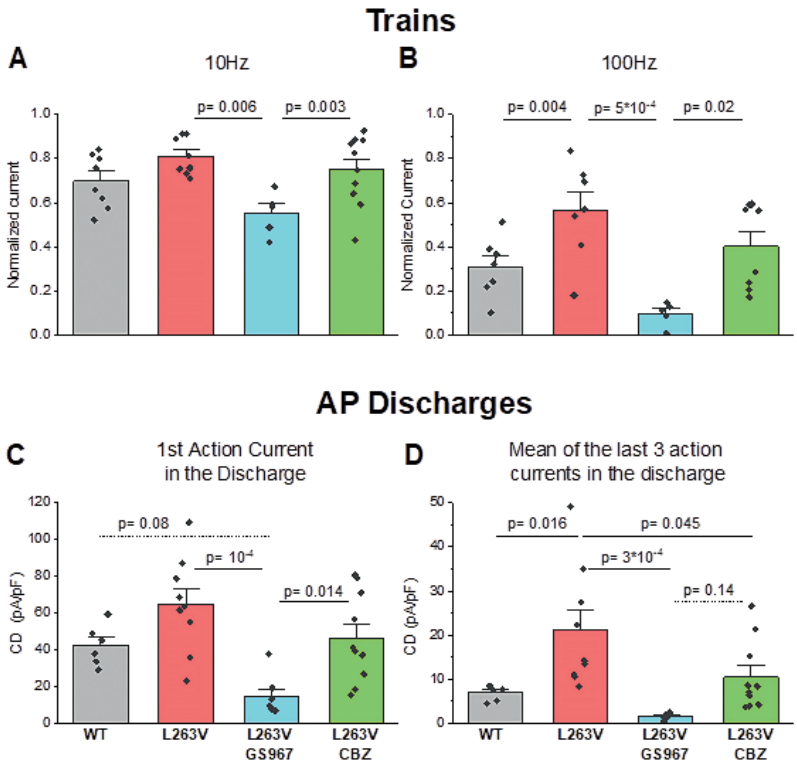

(A) Comparison of use dependence at 10 Hz, evaluating the residual current at the end of a train of 200 2-ms-long depolarizing steps to 0 mV from a holding potential of -70 mV. **(B)** Comparison of use dependence at 100 Hz, evaluating the residual current at the end of a 100-Hz train of depolarizations. **(C)** Comparison of the amplitude of the first action current, expressed as current density, elicited using as voltage command the action potential discharge of a fast spiking GABAergic neuron. **(D)** Comparison of the mean amplitude of the last 3 action currents in the discharge, expressed as current density. Statistical comparisons have been performed with one way ANOVA followed by Tukey post-hoc test, statistical significant differences ($P < 0.05$) are indicated by solid lines, trends by dashed lines. The bars indicate mean values ± SEM (see also Table S1).

FIGURE S5. Medullary electrode locations in heterozygous *Scn1a*^{L263V} mice.

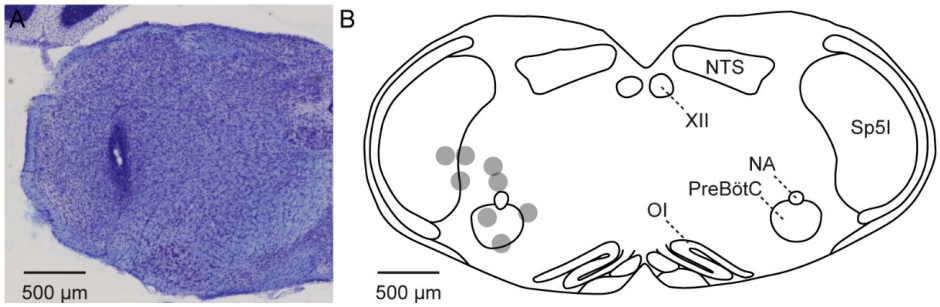

(A) Nissl staining showing an example of an electrode track recovered in an *Scn1a*^{L263V} mouse. **(B)** Schematic of recovered electrode positions (gray dots) in 8 *Scn1a*L263V mice that showed brainstem depolarization and apnea that resulted in death, or that were successfully resuscitated and transcardially perfused. PreBötC, pre-Bötzinger complex; NA, nucleus accumbens; NTS, nucleus tractus solitarius; OI, oliva inferior; Sp5I, spinal trigeminal nucleus pars interpolaris; XII, nucleus hypoglossus.

TABLE S1. Functional properties of sodium currents recorded from tsA-201 cells transfected with hNa$_v$1.1-WT, hNa$_v$1.1-L263V, hNa$_v$1.1-L263V in the presence of 5 µM GS967 and hNa$_v$1.1-L263V in the presence of 15 µM carbamazepine (CBZ). See Figs. S3 and S4 for statistical comparisons.

	WT	L263V	L263V-GS967	L263V-CBZ
Current Density (pA/pF)	140.9 ± 15.2 (*n* = 10)	139.8 ± 14.6 (*n* = 17)	41.0 ± 4.1 (*n* = 12)	69.1 ± 8.2 (*n* = 8)
Va (mV)	-24.5 ± 1.4 (*n* = 10)	-27.1 ± 1.0 (*n* = 17)	-21.4 ± 2.7 (*n* = 12)	-25.0 ± 1.7 (*n* = 8)
Ka (mV)	6.4 ± 0.3	6.3 ± 0.3	7.6 ± 0.4	5.3 ± 0.4
Vh (mV)	-59.2 ± 1.1 (*n* = 13)	-48.6 ± 1.3 (*n* = 24)	64.4 ± 1.4 (*n* = 12)	48.8 ± 0.8 (*n* = 15)
Kh (mV)	5.9 ± 0.3	6.3 ± 0.4	7.3 ± 0.4	7.0 ± 0.4
τ Recovery from Fast Inactivation at -80mV (ms)	3.8 ± 0.2 (*n* = 5)	1.3 ± 0.2 (*n* = 7)	- (*n* = 6)	1.1 ± 0.1 (*n* = 6)
τ Current Decay at 0mV (ms)	0.41 ± 0.04 (*n* = 10)	0.80 ± 0.03 (*n* = 17)	0.53 ± 0.03 (*n* = 12)	0.89 ± 0.06 (*n* = 8)
INa_{PMax} (% INa_{TMax})	1.2 ± 0.3 (*n* = 10)	1.8 ± 0.2 (*n* = 17)	1.3 ± 0.3 (*n* = 12)	1.9 ± 0.5 (*n* = 8)
Use dependence at 10 Hz (fraction of the initial current)	0.70 ± 0.04 (*n* = 8)	0.81 ± 0.03 (*n* = 8)	0.55 ± 0.04 (*n* = 5)	0.75 ± 0.05 (*n* = 10)
Use dependence at 100 Hz (fraction of the initial current)	0.31 ± 0.05 (*n* = 7)	0.56 ± 0.08 (*n* = 7)	0.09 ± 0.02 (*n* = 5)	0.40 ± 0.07 (*n* = 8)
1st action current in the FS discharge (pA/pF)	42.2 ± 4.5 (*n* = 6)	64.7 ± 8.6 (*n* = 9)	14.9 ± 3.7 (*n* = 8)	46.5 ± 7.7 (*n* = 10)
Average of last 3 action currents in the FS discharge (pA/pF)	6.9 ± 0.7 (*n* = 6)	21.3 ± 4.6 (*n* = 9)	1.6 ± 0.2 (*n* = 8)	10.5 ± 2.5 (*n* = 10)

Movie S1 (separate file). Example of cortical activity during a fatal event in an *Scn1a*^{L263V} mouse. The animal shows a sudden change of posture and subtle hindlimb extension, in total lasting approximately 1-2 s, followed by suppression of cortical activity and finally cortical anoxic depolarization. Note the absence of cortical epileptiform activity.

Movie S2 (separate file). Example of behavior during the fatal event in an *Scn1a*^{L263V} mouse. The animal shows exploratory behavior followed by drinking, during which a sudden change of posture occurs with loss of balance and subtle hindlimb extension.

Movie S3 (separate file). Example of brainstem DC-shift during the fatal event in an *Scn1a*^{L263V} mouse. The animal shows a sudden change of posture that co-occurs with a DC-shift in the medulla, which is repeated in slow-motion at the end.

Part III

Epileptogenesis in Dravet syndrome

Chapter 7

Focal and generalized seizure activity after local hippocampal or cortical ablation of $Na_V1.1$ channels in mice

Nico A. Jansen
Anisa Dehghani
Cor Breukel
Else A. Tolner
Arn M.J.M. van den Maagdenberg

Epilepsia 2020;61(4):e30-e36

SUMMARY

Early onset seizures are a hallmark of Dravet syndrome. Previous studies in rodent models have shown that the epileptic phenotype is caused by loss-of-function of voltage-gated $Na_V1.1$ sodium channels, which are chiefly expressed in GABAergic neurons. Recently, a possibly critical role has been attributed to the hippocampus in the seizure phenotype, as local hippocampal ablation of $Na_V1.1$ channels decreased the threshold for hyperthermia-induced seizures. However, the effect of ablation of $Na_V1.1$ channels restricted to cortical sites has not been tested. We here studied local field potential (LFP) and behavior in mice following local hippocampal and cortical ablation of *Scn1a*, a gene encoding the a1 subunit of $Na_V1.1$ channels, and compared seizure characteristics with those of heterozygous global knockout *Scn1a*$^{-/+}$ mice. We found a high incidence of spontaneous seizures following either local hippocampal or cortical ablation, notably during a transient time window, similar to *Scn1a*$^{-/+}$ mice. Non-convulsive seizure activity in the injected area was common and preceded generalized seizures. Moreover, mice were susceptible to hyperthermia-induced seizures. In conclusion, local ablation of $Na_V1.1$ channels in the hippocampus and cortex results in focal seizure activity that can generalize. These data indicate that spontaneous epileptic activity may initiate in multiple brain regions in Dravet syndrome.

INTRODUCTION

Dravet syndrome is an epilepsy syndrome characterized by early onset seizures, developmental delays, behavioral disorders and severe cognitive deficits.[1,2] In the majority of patients, a *de novo* heterozygous loss-of-function mutation in the *SCN1A* gene is found, encoding the pore-forming α1 subunit of voltage-gated $Na_V1.1$ sodium channels. Symptoms including spontaneous seizures, cognitive deficits, autism-related behavior and premature death are also observed in mice with *Scn1a* loss-of-function.[3-5] In *Scn1a* knockout mice, voltage-dependent sodium currents are reduced in hippocampal GABAergic neurons, whilst being unaffected in hippocampal pyramidal neurons.[3] In hippocampus and cortex, $Na_V1.1$ is mostly expressed in GABAergic neurons[6] and loss of $Na_V1.1$ expression in forebrain inhibitory interneurons is sufficient to reproduce the epileptic phenotype of heterozygous *Scn1a* knockout (*Scn1a*$^{-/+}$) mice.[7]

The role of different brain regions in epilepsy networks in Dravet syndrome, however, remains unclear. The hippocampus has been suggested as a primary driver of epileptiform activity in a mouse model of Dravet syndrome.[8] In addition, Stein et al.[9] recently demonstrated that local ablation of $Na_V1.1$ channels restricted to hippocampus results in an increased sensitivity to thermally evoked seizures. Since patients with *SCN1A* mutations may manifest with focal (cortical) epilepsy,[10,11] the relevance of various brain regions is of interest. We therefore studied the effects of local $Na_V1.1$ ablation in hippocampus and cortex on local field potential (LFP) and behavior, and compared seizure characteristics with those of *Scn1a*$^{-/+}$ mutants.

METHODS

Animals

To enable (local) ablation of $Na_V1.1$ channels in mice, a novel conditional *Scn1a* mouse model was generated. To this end, homologous recombination was used to replace exon 8 of the *Scn1a* gene, by using a targeting vector that contained the same exon but flanked by loxP sites in addition to a neomycin selection cassette flanked by *flippase* recognition target sites, introduced in strain IB10 mouse embryonic stem cells (a subclone of line E14 that is derived from 129/Ola mice). Clones were injected in C57BL/6J blastocysts to generate chimeras, which were then bred with C57BL/6J mice to achieve germline transmission, followed by breeding with a *flippase*-expressing mouse (C57BL/6-Tg(CAG-flpe)36Ito/ItoRbrc, stock # RBRC01834, RIKEN BioResource Center) to delete the neomycin cassette and backcrossing to C57BL/6J mice for at least 5 generations. No alterations in behavior or survival were noted in heterozygous or homozygous floxed (*Scn1a*$^{fl/+}$ or *Scn1a*$^{fl/fl}$, respectively) mice, when compared to wildtype (WT) littermates. To create *Scn1a*$^{-/+}$ mice, *Scn1a*$^{fl/+}$ males were crossed with EIIA-Cre deleter mice (B6.FVB-Tg(EIIa-cre)C5379Lmgd/J, stock # 003724, Jackson Laboratory).[12] Offspring were bred with C57BL/6J mice to achieve germline

transmission. Interbreeding of *Scn1a*$^{-/+}$ mice was used to obtain homozygous (*Scn1a*$^{-/-}$) and heterozygous (*Scn1a*$^{-/+}$) *Scn1a* global knockout mice, as well as WT littermates.

Experiments were approved by local and national ethical committees in accordance with recommendations of the European Communities Council Directive (2010/63/EU) and carried out in accordance with ARRIVE guidelines.

Viral infection and electrode implantation

AAV vectors expressing eGFP-Cre (AAV-GFP-Cre; Addgene viral prep # 105545-AAV8) or eGFP only (AAV-GFP; Addgene viral prep # 105530-AAV8), both gifts from James M. Wilson, were used for viral infection. For ablation of $Na_V1.1$ channels in the hippocampus, AAV-GFP-Cre was bilaterally injected (500 nL per injection, 50 nL/min) in the dorsal (-2.2 AP, ±1.4 ML, -1.7 DV; coordinates in mm relative to bregma) and ventral (-3.0 AP, ±2.9 ML, -2.8 DV) hippocampus of P21 *Scn1a*$^{fl/fl}$ mice, followed by implantation of LFP electrodes (75 µm platinum/iridium, PT6718; Advent Research Materials) at all 4 sites, and in the right occipital cortex (-3.5 AP, 2.4 ML, -0.5 DV). For cortical ablation of $Na_V1.1$ channels, 500 nL of AAV-GFP-Cre was bilaterally injected in the occipital cortex, followed by implantation of LFP electrodes at both sites, as well as bilaterally in the frontal cortex (+1.5 AP, ±1.8 ML, -0.5 DV). Reference and ground electrodes were implanted above the cerebellum. Electrodes were attached to a 7-channel pedestal (MS373 pedestal; Plastics One). For control experiments, P21 *Scn1a*$^{fl/fl}$ littermates received injections of AAV-GFP preceding implantation of the electrodes.

For recordings in *Scn1a*$^{-/+}$ mice, LFP electrodes were implanted at P21 at the same location as for mice receiving hippocampal or cortical injections.

Hyperthermia-induced seizures

In a separate set of *Scn1a*$^{-/+}$ mice and injected *Scn1a*$^{fl/fl}$ mice, the threshold for hyperthermia-induced seizures was tested as described previously,[13] adapted for freely behaving animals as follows: following implantation of electrodes, a thermistor (MEAS-G22K7MCD419, Measurement Specialties) was placed in the peritoneal cavity. In week 4-5 after surgery (i.e. P43-49), a heat lamp was positioned above the mouse during video-EEG recording. Core temperature was gradually increased (0.5 °C every 2 minutes) until a seizure occurred, or 42.0 °C was reached.

Data acquisition and analyses

Naive (i.e. not implanted) *Scn1a*$^{-/+}$ mice were videotaped from P21-49 for detection of spontaneous seizures. For video-EEG recordings, *Scn1a*$^{fl/fl}$ mice were connected to a commutator in a Faraday cage for 24 hours of video-EEG recordings at day 7, 14 and 21 following surgery. For *Scn1a*$^{-/+}$ mice, recordings used for comparison with *Scn1a*$^{fl/fl}$ mice were performed at P25-28 for 24 hours, as spontaneous seizures are prevalent at this developmental window in another Dravet mouse model.[5] LFP signals were pre-amplified (3X), band-pass filtered (0.05-500 Hz), amplified (400X; custom-

built recording hardware) and digitized (Power1401 with Spike2 software; Cambridge Electronic Design) at 5000 Hz.

Electrophysiological recordings were inspected for epileptiform activity. For epileptiform discharges lasting >5 seconds, video recordings were scored using the Racine scale.[12] Stage 4 and 5 seizures were used for comparison of seizure duration and power analyses, and seizure onset was defined as time of onset of motor symptoms, i.e. facial movements and/or forelimb clonus. Total LFP power (1-100 Hz) was calculated by a Fast Fourier Transform and normalized to baseline (60 seconds pre-ictal) using a custom-written MATLAB (Mathworks) script.

Immunohistochemistry

Following euthanization by CO_2 and transcardial perfusion with PBS and 4% PFA, brains were post-fixed, cryoprotected and coronally sectioned (20 µm). Antigen retrieval was done for 10 minutes at 80°C in 10 mM sodium citrate buffer with 0.05% Tween. Sections from *Scn1a*$^{fl/fl}$ mice (P43-49) were blocked with 10% normal goat serum and incubated in rabbit anti-$Na_V1.1$ (1:200; Alomone Labs), followed by incubation in goat anti-rabbit Cy2 or anti-rabbit Cy3 (both 1:200; Jackson Immunoresearch). For *Scn1a*$^{-/+}$ mice (P14 and P21), sections were additionally incubated in mouse anti-GAD67 (1:200; Millipore Sigma), followed by goat anti-mouse Cy3 (1:200; Jackson Immunoresearch). Sections were mounted in glycerol/PBS (1:1) containing 12.5 mg/mL sodium azide and 1 µL/mL Hoechst-33258 and examined using confocal microscopy.

RESULTS

Generation of conditional Scn1afl/fl and global Scn1a knockout mice

Conditional *Scn1a*$^{fl/fl}$ mice were generated using homologous recombination, replacing exon 8 of the *Scn1a* gene by the same exon flanked by loxP sites (Figure S1A,B). Breeding with EIIA-Cre deleter mice resulted in global knockout *Scn1a*$^{-/+}$ and *Scn1a*$^{-/-}$ mice, with absence of $Na_V1.1$ expression in the latter (Figure S1D). Survival of *Scn1a*$^{-/+}$ was decreased and *Scn1a*$^{-/-}$ mice did not survive past P15 (Figure S1E), in line with findings from a similar *Scn1a* knockout model.[3] Generalized seizures were observed in the 4th postnatal week in both naive and implanted *Scn1a*$^{-/+}$ mice (example in Figure S1F). Of the recorded naive *Scn1a*$^{-/+}$ mice (n = 21), 5 died during recording, in all cases immediately following a stage 5 seizure.

Local hippocampal ablation of $Na_V1.1$ results in spontaneous seizures

Hippocampal injection of AAV-GFP-Cre in P21 *Scn1a*$^{fl/fl}$ mice (Figure 1A-C) resulted in reduced $Na_V1.1$ staining in GFP-positive cells, indicating successful ablation of $Na_V1.1$ by AAV-GFP-Cre, while $Na_V1.1$ staining was still present following control AAV-GFP injections (Figure 1D). Spontaneous generalized seizures were recorded in 6 out of 7 mice injected with AAV-GFP-Cre,

compared to 0 out of 6 mice injected with control AAV-GFP ($P = 0.005$, Fisher's exact test). Stage 4/5 seizures: represented 54% (13/24) of seizures, and had an average duration of 29.5 ± 2.2 seconds, which was significantly shorter compared to stage 4/5 seizures in *Scn1a*$^{-/+}$ mice (38.5 ± 6.6 seconds, 16 seizures in 6/15 mice; $P = 0.01$, Mann-Whitney test). All behavioral seizures in *Scn1a*$^{fl/fl}$ mice injected with AAV-GFP-Cre were preceded by high-amplitude epileptiform discharges in the hippocampus, usually first detected in the ventral hippocampus (Figure 1E), while these local discharges were not observed in *Scn1a*$^{-/+}$ mice or *Scn1a*$^{fl/fl}$ mice injected with control AAV-GFP. These localized discharges were also observed in isolation (Figure 1F) at day 14 and 21 after injection. However, generalized seizures were more rare at 21 days after injection (Figure 1G). Similarly, 24-hour recordings in *Scn1a*$^{-/+}$ mice at P36-39 showed a decrease in seizure frequency over time (1 seizure at P36-39 *versus* 16 seizures at P25-28, in 360 hours of recording per age window; n = 15 mice; $P < 0.001$, Fisher's exact test).

Local cortical ablation of $Na_V1.1$ results in spontaneous seizures

To test whether spontaneous seizure activity is specific for ablation of $Na_V1.1$ in hippocampus, we injected AAV-GFP-Cre locally in the occipital cortex of *Scn1a*$^{fl/fl}$ mice (Figure 2A,B; n = 6), yielding reduced $Na_V1.1$ staining in GFP-positive cells (Figure 2C). Local cortical ablation of $Na_V1.1$ resulted in spontaneous generalized seizures in all mice, while no seizures were observed in mice receiving cortical control AAV-GFP (n = 6; $P = 0.002$, Fisher's exact test). Of all spontaneous seizures, 36% (12/33) were classified as stage 4/5 seizures. Seizure duration was significantly shorter when compared to seizures in *Scn1a*$^{-/+}$ mice (27.1 ± 4.1 seconds and 38.5 ± 6.6 seconds, respectively, $P = 0.007$, Mann-Whitney test) but of similar duration as observed after hippocampal ablation of $Na_V1.1$ channels ($P = 0.35$, Mann-Whitney test). Also similar to hippocampal injections, generalized seizures occurred most frequently at day 14 after injection (Figure 2E) and were preceded by local discharges (Figure 2D). Local discharges that did not generalize were also observed (Supplemental Figure S2). Pre-ictal LFP showed increased power in the occipital cortex preceding seizure behavior, which was not observed in the frontal cortex or in *Scn1a*$^{-/+}$ mice (Figure 2F,G). Local seizure activity was not observed following cortical control AAV-GFP injections (n = 6 mice).

Both hippocampal and cortical ablation of $Na_V1.1$ lower the threshold for hyperthermia-induced seizures

An increase in core temperature causes generalized seizures in *Scn1a*$^{-/+}$ mice[13] and in mice with local hippocampal $Na_V1.1$ ablation,[9] reflecting the early febrile seizures often observed in infants with Dravet syndrome.[1,2] We therefore tested whether seizures could also be induced by hyperthermia in our *Scn1a*$^{-/+}$ (n = 7) and AAV-GFP-Cre-injected *Scn1a*$^{fl/fl}$ (hippocampus: n = 4; cortex: n = 5) mice. Both groups showed stage 4/5 seizures at temperatures <42.0 °C, while none of the *Scn1a*$^{fl/fl}$ mice injected with control AAV-GFP (n = 6) developed seizures. *Scn1a*$^{-/+}$ mice showed lower seizure thresholds than AAV-GFP-Cre-injected *Scn1a*$^{fl/fl}$ mice, whereas no differences were noted between *Scn1a*$^{fl/fl}$ mice injected in hippocampus or cortex (Supplemental Figure S3).

FIGURE 1A-1D. Local ablation of $Na_V1.1$ channels in the hippocampus of mice results in spontaneous seizures that are preceded by local discharges.

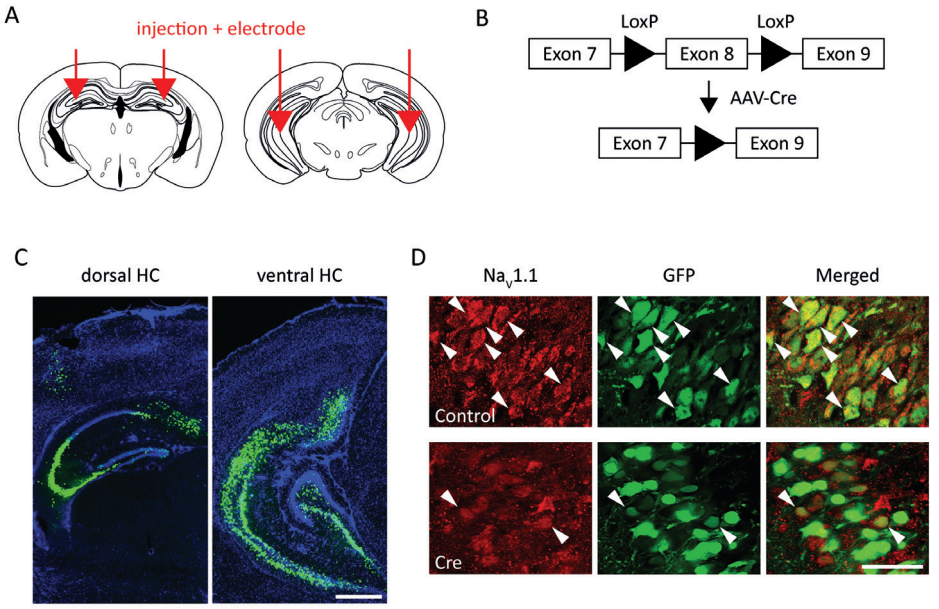

Bilateral AAV-GFP-Cre or control AAV-GFP injections **(A)** in dorsal (left) and ventral (right) hippocampus (HC) were followed by electrode implantation, in P21 mice with loxP-flanked exon 8 of *Scn1a* **(B)**. Hippocampal cells infected by AAV-GFP-Cre, as evidenced by GFP labelling **(C)**, showed reduced $Na_V1.1$ staining **(D,** detail of CA2 region), while cells infected by AAV-GFP did not (double-labelled cells indicated by white arrowheads). Scale bars: 500 µm in C, 50 µm in D.

FIGURE 1E-1G. Local ablation of $Na_V1.1$ channels in the hippocampus of mice results in spontaneous seizures that are preceded by local discharges.

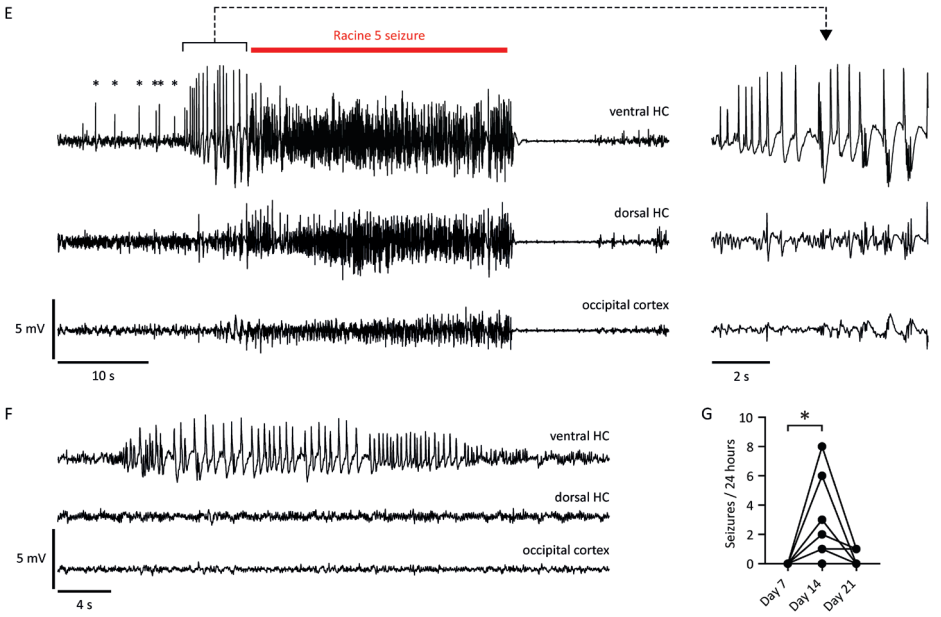

(E) Spontaneous generalized seizure preceded by spikes (asterisks) and discharges (inset) in the ventral HC. **(F)** Local discharge in the ventral HC at day 21 following injection. **(G)** Behavioral seizures occurred frequently at day 14 following injection, but were rare at day 21 (*$P = 0.02$, Friedman test).

FIGURE 2A-2C. Local ablation of $Na_V1.1$ channels in the occipital cortex of mice results in spontaneous seizures that are preceded by local discharges.

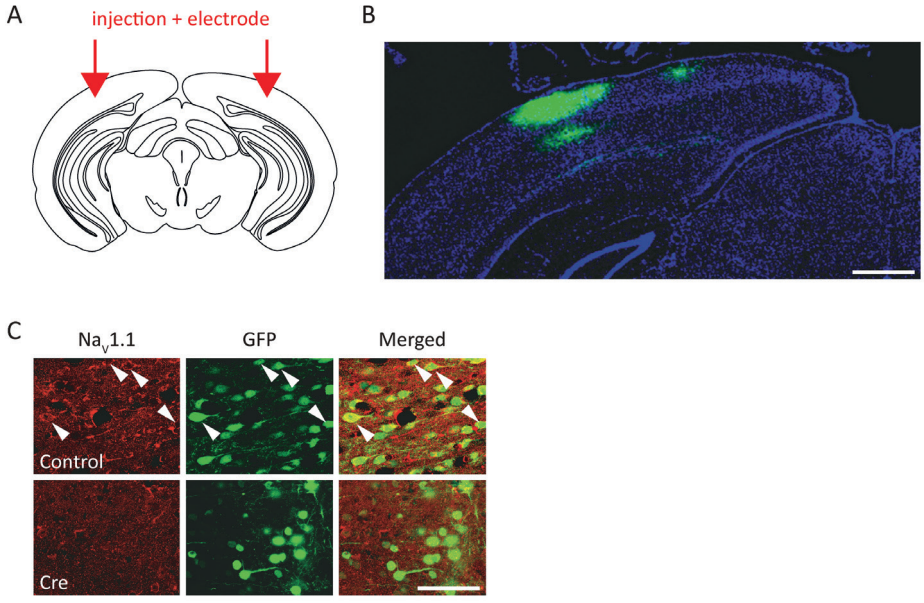

(A) Bilateral AAV-GFP-Cre or control AAV-GFP injections in the occipital cortex, followed by electrode implantation, including in the bilateral frontal cortex, in *Scn1a*$^{fl/fl}$ mice. B,C, AAV-mediated GFP-Cre expression, limited to cortex **(B)**, resulted in reduced $Na_V1.1$ staining (**C**, detail of occipital cortex), while this was not the case for cells infected by AAV-GFP (double-labelled cells indicated by white arrowheads). Scale bars: 500 µm in B, 50 µm in **(C)**.

FIGURE 2D-2G. Local ablation of $Na_V1.1$ channels in the occipital cortex of mice results in spontaneous seizures that are preceded by local discharges.

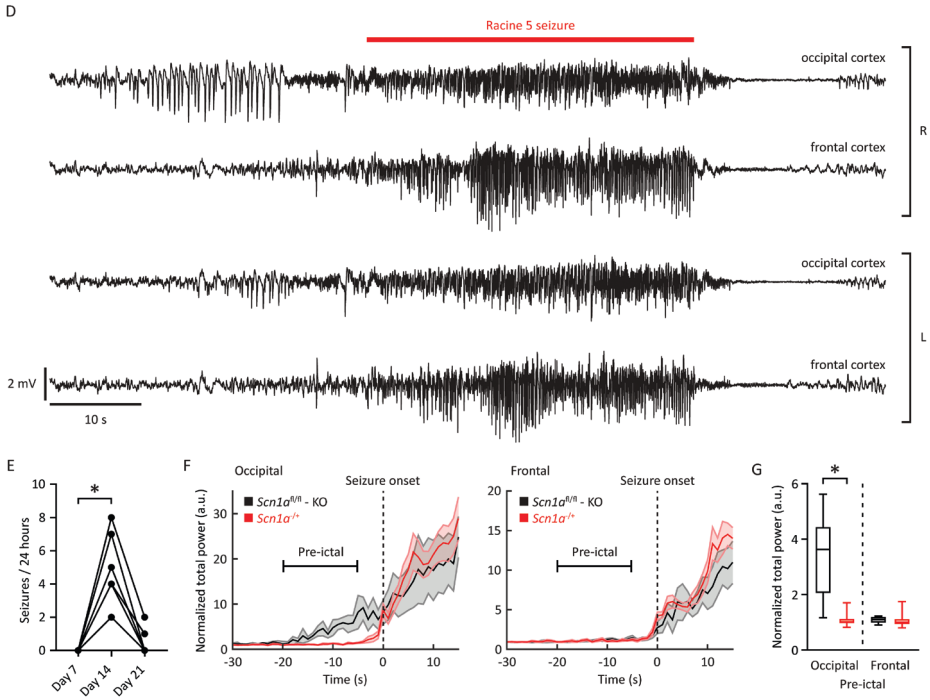

(D), Spontaneous generalized seizure at day 14 following injection, preceded by discharges in the occipital cortex. **(E)**, Behavioral seizures occurred most frequently at day 14 following injection (*P = 0.008, Friedman test). **(F)**, Pre-ictal time series of total LFP power (1-100 Hz) for occipital (left) and frontal (right) cortex in *Scn1a*$^{fl/fl}$ mice injected with AAV-GFP-Cre in occipital cortex (black; n = 12 seizures in 6 mice) and *Scn1a*$^{-/+}$ mice (red; n = 16 seizures in 6 mice; data presented as mean ± SEM). **(G)**, Pre-ictal LFP power was increased in occipital cortex of *Scn1a*$^{fl/fl}$ mice, but not in frontal cortex, or in either of two locations in *Scn1a*$^{-/+}$ mice (*P < 0.001, Mann-Whitney test).

DISCUSSION

Here, we show that local ablation of $Na_V1.1$ channels in hippocampus or cortex is sufficient to induce spontaneous generalized seizures in mice. We found that localized discharges occurred in the infected area, which did not always generalize to distant electrodes.

Of note, recently, Stein et al.[9] did not observe spontaneous seizures following hippocampal $Na_V1.1$ ablation using a similar approach. While differences in mouse strain, AAV serotype and variability in the affected hippocampal area may contribute to this discrepancy, seizure development was not assessed in the 21 days following injection. In their study, mice showed a reduced threshold for thermally induced seizures, measured 21 days after viral infection, similar to our findings. However, in the absence of longitudinal recordings before day 21, spontaneous seizures may have gone undetected, as *Scn1a*$^{-/+}$ mice show spontaneous seizures with a high frequency between P21-28,[5] approximately 10-18 days after $Na_V1.1$ expression is first detected in brain tissue.[6] After this time, seizure frequency is much lower,[5] which we confirmed in our *Scn1a*$^{-/+}$ mice. Onset of spontaneous (fatal) seizures in *Scn1a*$^{-/-}$ mice occurs already before P16.[3] Here, we observed spontaneous seizures 14 days after AAV-GFP-Cre injection in the hippocampus, while seizures were rare at 21 days, supporting a critical time window for spontaneous seizures following loss of *Scn1a* function. In *Scn1a*$^{-/+}$ mice, excitability of cortical GABAergic neurons normalizes to WT levels by P35,[15] which parallels the reduction in seizure frequency. Mechanisms such as upregulation of other voltage-gated sodium channel subtypes may underlie these findings, as suggested previously,[15] and may also cause the eventual decrease in seizure frequency following local ablation of $Na_V1.1$.

Notably, we found that also local cortical $Na_V1.1$ ablation was sufficient to induce spontaneous seizures and reduce the threshold for hyperthermia-evoked seizures. Similar to local hippocampal ablation, generalized seizures were preceded by discharges only observed in the injected area. Pre-ictal LFP amplitude was increased in the occipital cortex, which was not the case for *Scn1a*$^{-/+}$ mice. In patients, *SCN1A* mutations have been implicated in focal epilepsy, which could progress into a phenotype typical of Dravet syndrome.[10,11] Our study is the first to show seizure activity from a cortical focus following localized ablation of $Na_V1.1$, offering a paradigm to study focal seizures and their generalization. In addition, although the hippocampus is likely an important driver of seizures in Dravet syndrome,[8] our data challenge the (curative) potential for future region-specific gene therapy in these patients.

Although *Scn1a*$^{-/+}$ mice showed seizure-related mortality, no mortality was observed in mice in which $Na_V1.1$ was locally ablated in either hippocampus or cortex. This may be explained by a limited duration or severity of seizures following local $Na_V1.1$ ablation, and/or by the absence of $Na_V1.1$ ablation in other brain areas that could be critically involved in seizure-related mortality.

We observed localized seizure activity following local ablation of $Na_V1.1$ channels, but not in heterozygous global knockout *Scn1a*$^{-/+}$ mice. Although non-convulsive seizures have been reported in a mouse model of Dravet syndrome,[16] the activity we observed following local $Na_V1.1$ ablation appears more localized and of higher amplitude. This localized seizure activity may affect behavioral

outcomes such as reported by Stein et al.[9], by disrupting neuronal populations that are not directly affected by $Na_V1.1$ ablation, suggesting that recordings from injected areas are necessary for interpretation of behavioral outcomes.

In conclusion, local ablation of $Na_V1.1$ channels in hippocampus or cortex results in epileptic discharges that may generalize, indicating that localized dysfunction of $Na_V1.1$ channels is sufficient to induce generalized seizures characteristic of Dravet syndrome.

Acknowledgments

We thank Maarten Schenke, Sandra van Heiningen and Margot Linssen for experimental assistance. This work was funded by the Dutch National Epilepsy Foundation (2017-10, A.M.J.M.v.d.M., E.A.T.).

REFERENCES

1. Wolff M, Casse-Perrot C, Dravet C. Severe myoclonic epilepsy of infants (Dravet syndrome): natural history and neuropsychological findings. Epilepsia 2006;47 Suppl 2:45-8.
2. Dravet C. The core Dravet syndrome phenotype. Epilepsia 2011;52 Suppl 2:3-9.
3. Yu FH, Mantegazza M, Westenbroek RE, et al. Reduced sodium current in GABAergic interneurons in a mouse model of severe myoclonic epilepsy in infancy. Nat Neurosci 2006;9:1142-9.
4. Han S, Tai C, Westenbroek RE, et al. Autistic-like behaviour in Scn1a+/- mice and rescue by enhanced GABA-mediated neurotransmission. Nature 2012;489:385-90.
5. Kalume F, Westenbroek RE, Cheah CS, et al. Sudden unexpected death in a mouse model of Dravet syndrome. J Clin Invest 2013;123:1798-808.
6. Ogiwara I, Miyamoto H, Morita N, et al. Nav1.1 localizes to axons of parvalbumin-positive inhibitory interneurons: a circuit basis for epileptic seizures in mice carrying an Scn1a gene mutation. J Neurosci 2007;27:5903-14.
7. Cheah CS, Yu FH, Westenbroek RE, et al. Specific deletion of NaV1.1 sodium channels in inhibitory interneurons causes seizures and premature death in a mouse model of Dravet syndrome. Proc Natl Acad Sci U S A 2012;109:14646-51.
8. Liautard C, Scalmani P, Carriero G, et al. Hippocampal hyperexcitability and specific epileptiform activity in a mouse model of Dravet syndrome. Epilepsia 2013;54:1251-61.
9. Stein RE, Kaplan JS, Li J, Catterall WA. Hippocampal deletion of NaV1.1 channels in mice causes thermal seizures and cognitive deficit characteristic of Dravet Syndrome. Proc Natl Acad Sci U S A 2019;116:16571-6.
10. Harkin LA, McMahon JM, Iona X, et al. The spectrum of SCN1A-related infantile epileptic encephalopathies. Brain 2007;130:843-52.
11. McDonald CL, Saneto RP, Carmant L, Sotero de Menezes MA. Focal Seizures in Patients With SCN1A Mutations. J Child Neurol 2017;32:170-6.
12. Lakso M, Pichel JG, Gorman JR, et al. Efficient in vivo manipulation of mouse genomic sequences at the zygote stage. Proc Natl Acad Sci U S A 1996;93:5860-5.
13. Oakley JC, Kalume F, Yu FH, et al. Temperature- and age-dependent seizures in a mouse model of severe myoclonic epilepsy in infancy. Proc Natl Acad Sci U S A 2009;106: 3994-9.
14. Racine RJ. Modification of seizure activity by electrical stimulation. II. Motor seizure. Electroencephalogr Clin Neurophysiol 1972;32:281-94.
15. Favero M, Sotuyo NP, Lopez E, et al. A Transient Developmental Window of Fast-Spiking Interneuron Dysfunction in a Mouse Model of Dravet Syndrome. J Neurosci 2018;38:7912-27.
16. Ritter-Makinson S, Clemente-Perez A, Higashikubo B, et al. Augmented Reticular Thalamic Bursting and Seizures in Scn1a-Dravet Syndrome. Cell Rep 2019;26:54-64.

SUPPORTING INFORMATION

FIGURE S1. Generation of conditional *Scn1a*$^{fl/fl}$ and global knockout *Scn1a* mice.

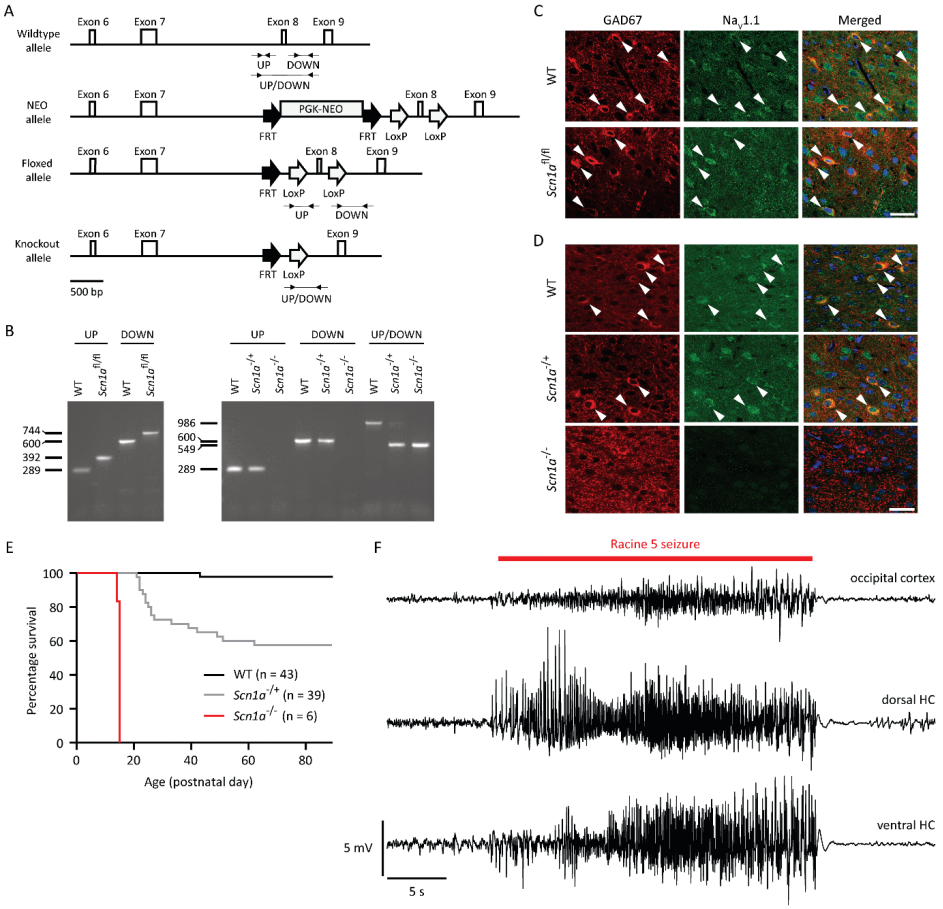

(A), Exon 8 of the *Scn1a* gene was targeted using a vector (details can be obtained upon request) containing the same exon but flanked by LoxP sites and an upstream PGK promotor driven neomycin selection (PGK-NEO) cassette flanked by *flippase* FLP recombinase recognition target (FRT) sites. After breeding with a *flippase*-expressing mouse (C57BL/6-Tg(CAG-flpe)36Ito/ItoRbrc, stock # RBRC01834, RIKEN BioResource Center) and backcrossing with C57BL/6J mice, mice with the floxed allele were obtained. *Scn1a*$^{fl/+}$ mice were then bred with EIIA-Cre deleter mice (B6.FVB-Tg(Ella-cre) C5379Lmgd/J, stock # 003724, Jackson Laboratory), and their offspring were bred with C57BL/6J mice to achieve germline transmission and obtain heterozygous global knockout *Scn1a*$^{-/+}$ mice. **(B),** Polymerase chain reaction (PCR) results from genomic tissue DNA of WT and floxed *Scn1a*$^{fl/fl}$ (*left*) and WT, heterozygous and homozygous knockout *Scn1a* (*right*) mice. The location of the primers used for the UP, DOWN and UP/DOWN PCRs are shown in panel A (primer sequences can be provided upon request). Expected PCR product lengths are indicated to the left of the gel (in bp) for every band. **(C,D,)** Immunofluorescence of $Na_V1.1$ protein in the occipital cortex of P21 WT and *Scn1a*$^{fl/fl}$ mice **(C)** and P14 WT, *Scn1a*$^{-/+}$ and *Scn1a*$^{-/-}$ mice **(D)**, showing considerable overlap of $Na_V1.1$ with GAD67, a marker for GABAergic neurons (double-labelled cells indicated by white arrowheads). No $Na_V1.1$ immunoreactivity was observed in homozygous *Scn1a*$^{-/-}$ mice, indicating absence of $Na_V1.1$ protein expression. Scale bars: 50 µm. **(E)**, Survival curves showing early mortality in *Scn1a*$^{-/+}$ and *Scn1a*$^{-/-}$ mice, when compared to WT mice ($p < 0.001$, Log-rank test). **(F)**, Example of a spontaneous generalized seizure in a P26 *Scn1a*$^{-/+}$ mouse recorded by LFP electrodes in the occipital cortex and hippocampus (HC).

FIGURE S2. Local discharge following ablation of $Na_V1.1$ in the occipital cortex, at day 14 after injection of AAV-GFP-Cre in an *Scn1a*$^{fl/fl}$ mouse. Epileptiform discharges that remained confined to the occipital cortex were not associated with motor symptoms.

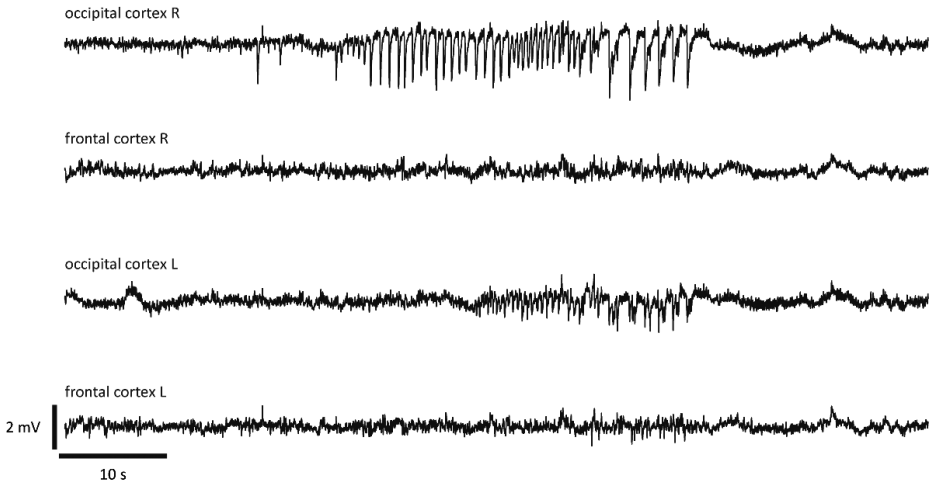

FIGURE S3. Hyperthermia-induced seizures in conditional *Scn1a*$^{fl/fl}$ and heterozygous global knockout *Scn1a*$^{-/+}$ mice.

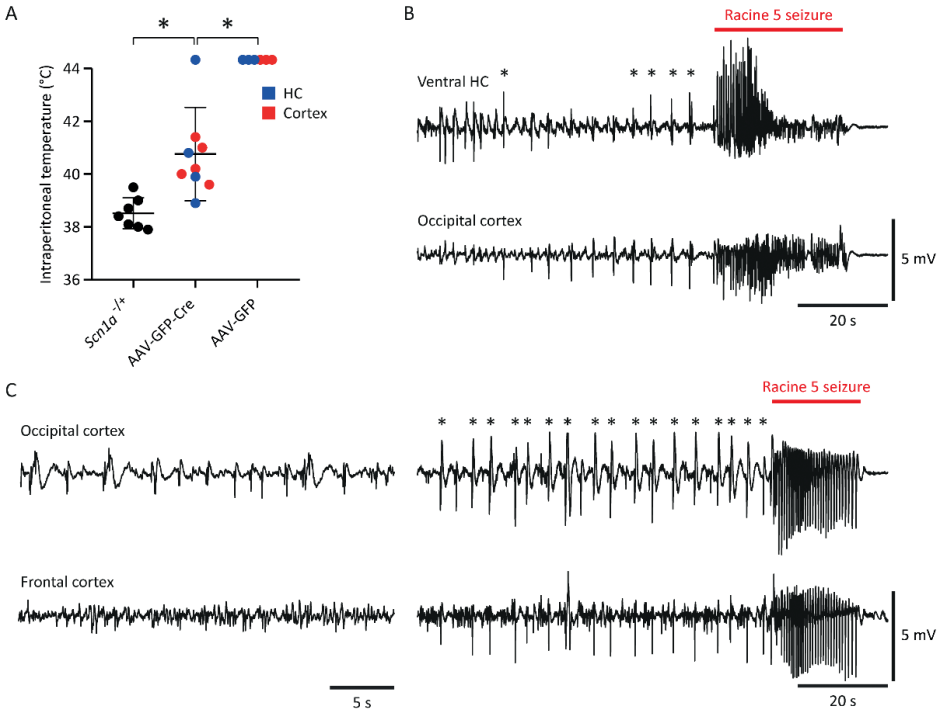

(A), Seizures were observed after increasing core temperature (monitored by an intraperitoneal thermistor) in *Scn1a*$^{-/+}$ mice (7/7) and conditional *Scn1a*$^{fl/fl}$ mice injected with AAV-GFP-Cre (8/9; in cortex (n = 5) or hippocampus (HC; n = 4)), but not in *Scn1a*$^{fl/fl}$ mice injected with control AAV-GFP (0/6; in cortex (n = 3) or hippocampus (n = 3); *P < 0.001, Fisher's exact test). Seizure threshold was lower in *Scn1a*$^{-/+}$ mice, when compared to the AAV-GFP-Cre group, in which no seizures were observed upon temperature rises up to 42 ºC (*P = 0.001, Mann-Whitney test). Seizure threshold was similar for mice injected with AAV-GFP-Cre in cortex or hippocampus (P = 0.90, Mann-Whitney test). Data points outside of y-axis limits indicate animals in which no seizures were observed. **(B,C)** Examples of LFP during hyperthermia-induced seizures in *Scn1a*$^{fl/fl}$ mice injected with AAV-GFP-Cre in hippocampus **(B)** or occipital cortex **(C)**. Asterisks denote myoclonic events. Note that early spikes were most prominent in the injected area (ventral HC in B, occipital cortex in C). LFP traces shown on the left in C were recorded 4 minutes prior to seizure onset.

Chapter 8

Impaired θ-γ coupling indicates inhibitory dysfunction and seizure risk in a Dravet syndrome mouse model

Nico A. Jansen
Carlos Perez
Maarten Schenke
Anouk W. van Beurden
Anisa Dehghani
Rob A. Voskuyl
Roland D. Thijs
Ghanim Ullah
Arn M.J.M. van den Maagdenberg
Else A. Tolner

J Neurosci 2021;41(3):524-537

ABSTRACT

Dravet syndrome (DS) is an epileptic encephalopathy that still lacks biomarkers for epileptogenesis and its treatment. Dysfunction of $Na_V1.1$ sodium channels, which are chiefly expressed in inhibitory interneurons, explains the epileptic phenotype. Understanding the network effects of these cellular deficits may help predict epileptogenesis. Here, we studied theta-gamma coupling as a potential marker for altered inhibitory functioning and epileptogenesis in a DS mouse model. We found that cortical theta-gamma coupling was reduced in both male and female juvenile DS mice and persisted only if spontaneous seizures occurred. Theta-gamma coupling was partly restored by cannabidiol. Locally disrupting $Na_V1.1$ expression in the hippocampus or cortex yielded early attenuation of theta-gamma coupling, which in the hippocampus associated with fast ripples, and which was replicated in a computational model when voltage-gated sodium currents were impaired in basket cells. Our results indicate attenuated theta-gamma coupling as a promising early indicator of inhibitory dysfunction and seizure risk in DS.

INTRODUCTION

Dravet syndrome (DS) is an epileptic encephalopathy characterized by early-onset seizures, followed by severe cognitive and behavioral deficits.[1, 2] The majority of DS cases result from a heterozygous loss-of-function mutation in the *SCN1A* gene, which encodes the pore-forming α1 subunit of voltage-gated sodium channel type 1 ($Na_V1.1$). In mice with a heterozygous knock-out of *Scn1a*, core clinical features of DS including spontaneous seizures,[3] cognitive deficits and autism-related behavior[4] are replicated. Voltage-dependent sodium currents are reduced in GABAergic inhibitory interneurons, whilst unaffected in hippocampal pyramidal neurons of DS mice.[3] In the hippocampus and cortex, $Na_V1.1$ is mostly expressed in interneurons[5] and loss of $Na_V1.1$ function in inhibitory populations is sufficient to reproduce the epileptic phenotype of DS mice.[6] These studies thus implicate loss of inhibitory functioning in DS pathophysiology.

How loss of $Na_V1.1$ function affects network dynamics, however, remains unclear, while such knowledge is crucial to understanding epileptogenesis and cognitive deficits. Although excitability of cortical inhibitory interneurons was decreased in brain slices of DS mice, *in vivo* cortical local field potential (LFP) and spontaneous interneuron firing appeared unaffected.[7] Fast-spiking parvalbumin-positive interneurons, a class of inhibitory interneurons that is affected in DS mice,[7, 8] importantly contribute to LFP gamma oscillations.[9, 10] Parvalbuminergic neurons show a particularly high propensity to fire phase-locked to theta oscillations in the hippocampus[11] and cortex,[12] suggesting a key role of these interneurons in theta-gamma cross-frequency coupling.[9] Coupling of gamma oscillations to theta rhythm is indeed decreased when synaptic inhibition onto parvalbumin-positive neurons is impaired.[13] Recently, local loss of hippocampal $Na_V1.1$ function was shown to impair inhibitory firing and coupling of gamma amplitude to theta phase in rats.[14] How this relates to seizure development, hippocampal and cortical dynamics in DS mice, however, remains to be explored.

Here, we studied spontaneous cortical network dynamics during development in DS mice for early changes in theta or gamma oscillations and their cross-frequency phase-amplitude coupling. By inducing local heterozygous or homozygous knock-out of *Scn1a* in the hippocampus or cortex, we addressed the effect of partial or total ablation of $Na_V1.1$, respectively, within these structures on network dynamics in relation to seizure development. We found that theta-gamma coupling was decreased in DS mice compared to wildtype, which, also upon local ablation of $Na_V1.1$, preceded seizure activity. Decreased theta-gamma coupling persisted only in animals with spontaneous seizures, and associated with hippocampal fast ripples. In a computational hippocampal network model, loss of voltage-gated sodium currents in inhibitory neurons reproduced the main experimental findings, including a pronounced impairment of theta-gamma coupling. These results suggest that theta-gamma coupling may serve as an early indicator of inhibitory dysfunction and seizure risk in DS.

MATERIALS AND METHODS

Animals

Mice with a deletion of exon 8 of the *Scn1a* gene were created as described previously.[15] These global *Scn1a*$^{-/+}$ mice (referred to as "DS mice") were backcrossed to C57BL/6J mice for at least 5 generations. Both male and female DS mice and wildtype (WT) littermates were used for experiments. In the conditional *Scn1a* mouse line, exon 8 of the *Scn1a* gene is flanked by LoxP sites,[15] which allows for region-specific ablation after exposure to Cre recombinase. Heterozygous and homozygous floxed (*Scn1a*$^{fl/+}$ or *Scn1a*$^{fl/fl}$, respectively) mice and WT littermates were used for the viral injection experiments. Animals had free access to food and water and were kept under standard housing conditions (temperature of 22 ± 1.5°C, 12-hour light/dark cycle). All experiments were approved by local and national ethical committees following recommendations of the European Communities Council Directive (2010/63/EU) and carried out in accordance with ARRIVE guidelines.

Surgery and viral infection

For chronic recordings in DS mice and WT littermates, local-field potential (LFP) electrodes (75 µm platinum/iridium; PT6718, Advent Research Materials, Oxford, UK) were implanted at P20-21 under isoflurane anesthesia (induction 4%; maintenance 1.5%). Electrodes were implanted in primary visual cortex (V1; -3.5 anteroposterior [AP], ±2.4 mediolateral [ML], -0.5 dorsoventral [DV]; mm relative to bregma) and primary motor cortex (M1; +1.5 AP, ±1.8 ML, -0.5 DV). A subset of WT and DS mice was implanted with an additional LFP electrode in the right dorsal hippocampus (-2.0 AP, +2.2 ML, -1.4 DV).

To induce local knock-out of *Scn1a*, an AAV vector expressing mCherry-Cre under the EF1α-promotor (viral prep # 55632, a gift from Karl Deisseroth, Addgene, Watertown, MA) was injected in P42-56 *Scn1a*$^{fl/+}$ and *Scn1a*$^{fl/fl}$ mice. Injections (500 nL per injection, 50 nL/min) were made bilaterally in dorsal (-2.0 AP, ±2.2 ML, -1.4 DV) and ventral (-3.0 AP, ±3.1 ML, -2.6 DV) hippocampus, or in V1, followed by implantation of LFP electrodes. For cortically injected animals, LFP electrodes were implanted in V1 and M1. The use of heterozygous and homozygous floxed mice was predicted to result in a partial and total ablation of $Na_V1.1$ following local expression of Cre, respectively. WT littermates that underwent the same procedure served as controls. For cortical injections, in a subset of *Scn1a*$^{fl/+}$ mice, a different AAV vector was used (expressing eGFP-Cre; viral prep #105545, a gift from James M. Wilson, Addgene) to allow comparison with previously published data.[15]

Pharmacology

Cannabidiol (Tocris, Bristol, UK) was dissolved in DMSO, which was diluted in a vehicle solution (5% DMSO: 5% cremophor: 90% saline) immediately prior to injection. P35-36 DS mice received an intraperitoneal (i.p.) injection of cannabidiol (100 mg/kg body weight) or vehicle on two consecutive days between 8-10 A.M., in a randomized fashion and by an experimenter blinded to the treatment.

Immunohistochemistry

After experiments, animals were euthanized by CO_2 and transcardially perfused with phosphate-buffered saline (PBS) and 4% paraformaldehyde. Following removal and post-fixation of brain tissue, coronal sections (20 μm) were prepared. Sections were heated in 10 mmol/L sodium citrate buffer with 0.05% Tween for 10 minutes at 80°C. Subsequently, a blocking solution containing 10% normal goat serum was applied, and sections were incubated in rabbit anti-$Na_V1.1$ (1:200; Alomone Labs, Jerusalem, Israel), followed by incubation in goat anti-rabbit Cy2 (1:200; Jackson Immunoresearch, Cambridgeshire, UK). Mounting was performed in glycerol/PBS (1:1) containing 12.5 mg/mL sodium azide and 1 μL/mL Hoechst-33258. Sections were examined using an epifluorescence or confocal microscope with appropriate filter sets.

Data acquisition and analysis

DS mice and WT littermates were videotaped from P18-19 in a PhenoTyper® home cage (Noldus, Wageningen, the Netherlands) to allow detection of early spontaneous seizures, until the day of surgery at P20-21. Immediately after surgery, both these mice and virally injected mice were connected to a 7-channel commutator in a Faraday cage for continuous recordings of LFP and video. Signals were pre-amplified (3X), filtered (0.05-500 Hz) and amplified (200X and 400X for hippocampal and cortical recordings, respectively) using custom-build hardware, and digitized at 5 kHz (Power 1401 and Spike2 software, CED, Cambridge, UK). All LFP recordings were *post hoc* inspected for epileptiform activity. The Racine scale[16] was used for scoring of behavior from video recordings during discharges that lasted >5 seconds. Seizures that progressed to stage 3-5 were included in analyses, as these seizures could also be reliably detected when only video recordings were available (i.e. for P18-21 mice). For detection of interictal spikes (IIS) following local knock-out of *Scn1a*, local LFP power in the 30-100 Hz range was calculated every 24 hours for 1 hour of non-REM sleep, a vigilance state during which IIS are prevalent in DS mice.[17] Candidate events exceeding a threshold of 3 SDs of signal were visually inspected, and animals were considered showing IIS if >5 IIS were observed during the analyzed 1-hour window on that day. To detect fast ripples, hippocampal LFP recordings were bandpass filtered (infinite impulse response Butterworth filter of 2nd order) between 200-600 Hz and candidate events were detected by thresholding (>10 SDs), which effectively distinguished fast ripples from IIS. Only events that occurred during behavioral immobility – assessed from the reference signal and locomotor activity recorded by an infrared motion detection sensor in the Faraday cage – were visually inspected, as muscle artifacts were often found in the 200-600 Hz frequency range during active wakefulness.

To assess cortical network dynamics during REM sleep and active wakefulness, LFP recorded during the morning (6-12 A.M.) was analyzed, starting at P23, allowing 2-3 days of habituation to the recording setup. Vigilance state was determined per 5-second epoch using V1 LFP, the reference signal and locomotor activity recorded by the infrared motion detection sensor. Epochs during seizures and/or postictal periods (1 hour after the end of a seizure) were excluded from further analyses. REM sleep was defined by a theta (5-10 Hz) to delta (1-4 Hz) power ratio of

>2.5, in the absence of locomotor activity or motion artifacts. Active wakefulness was defined by a theta-delta power ratio of >2 during epochs containing locomotor activity and/or high variance in the reference signal. Epochs were artifact-rejected, low-pass-filtered (Chebyshev IIR eighth-order filter) and down-sampled to 1 kHz. A total of 10 minutes of randomly selected epochs was used for further analyses. Power spectra were computed by applying a Hamming window over each epoch, followed by a fast Fourier transform and averaging of the resulting power spectra. Phase-amplitude coupling was assessed using a measure referred to as the modulation index (MI), calculated as described previously.[18] In short, LFP epochs were bandpass-filtered for phase (3-14 Hz, 2-Hz bandwidths, steps of 1 Hz) and amplitude (40-200 or 40-300 Hz, 4-Hz bandwidths, steps of 2 Hz) frequencies. The Hilbert transform was applied to extract phase and amplitude information. Each phase frequency was binned in 18 bins of 20°, and mean amplitude per amplitude frequency was calculated inside each bin. A distribution was subsequently obtained by normalization of the mean amplitude in each phase bin by the sum over all bins. To compare the resulting phase-amplitude distribution with a uniform distribution, the Kullback-Leibler distance was calculated. The MI was obtained by normalizing this metric to the logarithm of the number of phase bins. For group analyses, theta-gamma coupling was expressed in a single value by averaging over all theta and gamma frequencies, or over specific gamma bands, as indicated. All analyses were performed using custom-written MATLAB (versions used: 2018b and 2019b, MathWorks, Natick, MA) scripts.

Computer modeling

The basic equations for the membrane potential of individual neurons and various ion channels were adopted from.[19] The model network consists of 5 pyramidal cells (EX), 5 oriens-lacunosum moleculare (OLM) interneurons, and 5 fast-spiking basket cell (BC) interneurons, with all-to-all connections. We noticed that increasing the network size did not change the conclusions from the model as long as the synaptic connections were properly scaled (not shown). The equations for individual cells were modified and extended to incorporate the dynamics of various ion species in the intra- and extracellular spaces of the neurons and neurotransmitter homeostasis using a formalism previously developed.[20-22] Full details about the model are given in Figure 10-1. Here, we describe the main equations.

The membrane potential, V_m, of each EX, BC, and OLM neuron in the network is controlled by various Na^+ (I_{Na}), K^+ (I_K), and Cl^- (I_{Cl}) currents, Na^+ and K^+ currents due to the Na^+/K^+-ATPase (I_{pump}), and random inputs from neurons that were not a part of the network, modeled as a Gaussian distribution (I_{stoch}), that is

$$C_m \frac{d V_m^{EX,BC,OLM}}{dt} = I_{Na}^{EX,BC,OLM} + I_K^{EX,BC,OLM} + I_{Cl}^{EX,BC,OLM} + I_{stoch}^{EX,BC,OLM} \quad (1)$$

where C_m is the membrane capacitance and superscripts *EX*, *BC*, and *OLM* correspond to pyramidal, basket cell, and OLM neurons, respectively. Various currents used for the different neuron types are given in the section "Membrane Potential" of Figure 10-1.

To model the dynamics of various ionic species, we considered the extracellular space (ECS) as a separate compartment surrounding each cell. Each neuron exchanged ions with its ECS compartment through active and passive currents, and the Na^+/K^+-ATPase. The ECS compartment can also exchange K^+ with the glial compartment, and perfusion solution (or vasculature in intact brain).[20, 23-25] Including diffusion of ions between the ECS compartments of neighboring neurons did not affect the results, and were therefore ignored.

The change in extracellular K^+ concentration ($[K^+]_o$) is a function of I_K, I_{pump}, uptake by glia surrounding the neuron (I_{glia}), and the diffusion between the neuron and bath perfusate (I_{diff}).

$$\frac{d[K^+]_o}{dt} = -\gamma\beta I_K - 2\gamma\beta I_{pump} + I_{glia} - I_{diff} \qquad (2)$$

Where β is the ratio of intracellular space (ICS) to ECS. $\gamma = A_m^{(n)} \times 10^4/(F \times \omega_i)$ is the conversion factor from current units to flux units. F, $A_m^{(n)}$, and ω_i are the Faraday's constant, surface area of the neuron, and intracellular volume of the neuron, respectively. The factor 2 in front of I_{pump} is due to the fact that the Na^+/K^+ pump extrudes two K^+ in exchange for three Na^+ ions.

The rate of change of intracellular Na^+ concentration ($[Na^+]_i$) is controlled by I_{Na} and I_{pump},[20] that is

$$\frac{d[Na^+]_i}{dt} = -\gamma I_{Na} - 3\gamma I_{pump} \qquad (3)$$

The fluxes used in equations (2) and (3) are listed in section "Ion Concentrations" of Figure 10-1. The concentrations of intracellular K^+ ($[K^+]_i$), intracellular Cl^- ($[Cl^-]_i$), extracellular Na^+ ($[Na^+]_o$), and extracellular Cl^- ($[Cl^-]_o$) are given by conservation laws and are also listed in the same section.

In addition to ion concentration dynamics, our model also incorporates the details of neurotransmitter homeostasis. Glutamate and GABA in the synaptic cleft and ECS are regulated by i) spiking-related release from EX (for glutamate), and BC and OLM (for GABA), ii) uptake by pre- and postsynaptic neurons and glia through glutamate and GABA transporters, iii) diffusion between the cleft and ECS, and iv) the recycling into releasable pools. The model also includes the binding and unbinding of glutamate to NMDA and AMPA receptors, and GABA to $GABA_A$ receptors, and the currents due to these receptors. Details of the equations are given in the section "Neurotransmission" of Figure 10-1.

The LFP is modeled by considering a non-spiking pyramidal neuron in the network as described in.[19] This neuron receives the same synaptic inputs as the active pyramidal neurons in the network, but it does not generate action potentials due to the absence of the main currents responsible for action potential generation. The model LFP thus reflects subthreshold voltage changes in the EX-cell population. Similar to the *in vivo* data analysis, 10 minutes of simulated LFP data were used to obtain power spectra and phase-amplitude coupling metrics, as described earlier.

Experimental design and statistical analysis

Data from 89 mice were included, including 15 WT and 26 DS mice for video-EEG recordings, 9 DS mice for pharmacological experiments, and 13 WT, 14 *Scn1a*$^{fl/+}$ and 12 *Scn1a*$^{fl/fl}$ mice for AAV vector injections. Data are presented as mean ± SEM, unless indicated otherwise. Statistical testing was conducted in MATLAB or GraphPad Prism (GraphPad Software, La Jolla, CA). Based on whether data were paired and their distribution normality, which was assessed by the Anderson-Darling test, data were compared using the Welch's *t*-test, paired *t*-test, Mann-Whitney test or Wilcoxon test for single comparisons. For multiple comparisons, a one or two-way ANOVA with Tukey's test, repeated-measures ANOVA with Dunnett's test or Kruskal-Wallis with Dunn's test was used. Sample sizes were not based on statistical methods, but instead informed by those frequently used in the field. $p < 0.05$ was considered to indicate significance.

RESULTS

Modulation of cortical gamma amplitude by theta phase is attenuated in juvenile DS mice

Cortical LFP and video were recorded in freely behaving *Scn1a*$^{-/+}$ (DS) and wildtype (WT) mice starting from P20-21. Modulation of cortical gamma oscillations by theta rhythm is low during vigilance states lacking prominent theta oscillations, i.e. during quiet wakefulness and non-REM sleep.[26] We therefore limited our analyses to epochs during vigilance states with prominent cortical theta oscillations, i.e. REM sleep (examples in Fig. 1A) and active wakefulness. Average V1 LFP power spectral density for theta (5-10 Hz), low gamma (40-90 Hz) and high gamma (90-160 Hz) frequencies during REM sleep at P23 was similar between genotypes (Fig. 1B,C), although a decrease in theta peak frequency was observed in DS mice (Fig. 1D). Comodulogram analyses of V1 LFP in WT mice showed that theta phase modulated the amplitude of low and high gamma (Fig. 1E). Although this pattern was also present in DS mice, the modulation of gamma power by theta phase was significantly impaired for both frequency ranges (Fig. 1F). The theta phase at which gamma amplitude peaked was similar between genotypes, with high gamma peaking significantly later in the theta cycle than low gamma for both WT and DS mice (Fig. 1G,H). Average REM sleep duration was similar between WT and DS mice (48.9 ± 4.2 s and 46.6 ± 3.0 s, respectively; $t_{(26)} = 0.45$, $p = 0.66$, *t*-test), thereby excluding changes in REM sleep duration as a potential cause for impaired theta-gamma coupling strength.[27] Similar results were obtained from epochs during active wakefulness (Fig. 2), although in both WT and DS mice modulation of high gamma oscillations was largely absent, and modulation of both low and high gamma frequencies was lower when compared to REM sleep (Fig. 2F-I). These data indicate that cortical theta-gamma coupling is attenuated in juvenile DS mice, which cannot be explained by changes in theta or gamma power.

FIGURE 1A-1E. Dravet syndrome (DS) mice display decreased cortical theta-gamma cross-frequency coupling at P23.

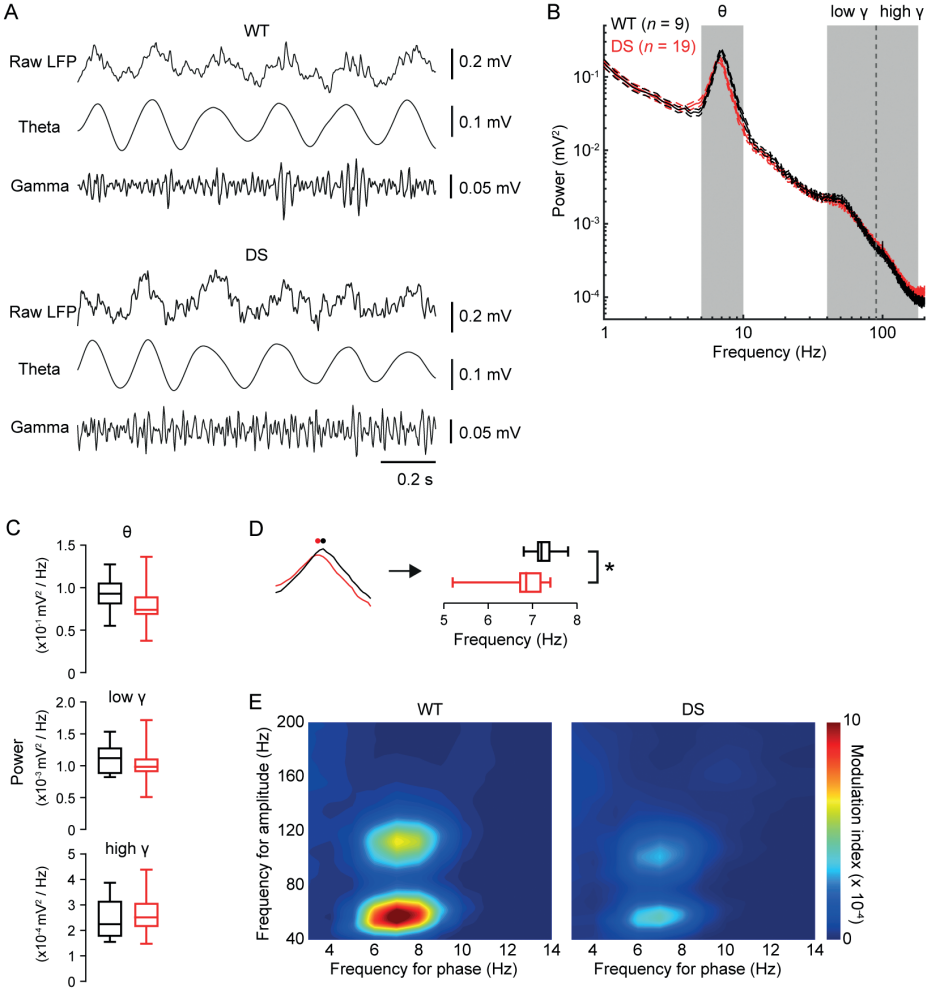

(A) Example traces of raw, theta-filtered (5-10 Hz) and gamma-filtered (40-160 Hz) LFP in the primary visual cortex (V1) during REM sleep in a wildtype (WT) and DS mouse. **(B)** Average V1 LFP power spectra during REM sleep in WT (black) and DS (red) mice. Peak theta frequency was significantly reduced in DS mice (**C**; detail of mean power in theta range, black and red dots indicate average peak theta frequency; $t_{(27)} = 2.5$, $^*p = 0.020$, Welch's *t*-test). **(D)** No significant differences in power were present between genotypes within theta (θ), low (40-90 Hz) or high gamma (γ; 90-160 Hz) frequency ranges. **(E)** Average phase-amplitude comodulograms of V1 during REM sleep in WT ($n = 9$) and DS ($n = 19$) mice at P23

FIGURE 1F-1H. Dravet syndrome (DS) mice display decreased cortical theta-gamma cross-frequency coupling at P23.

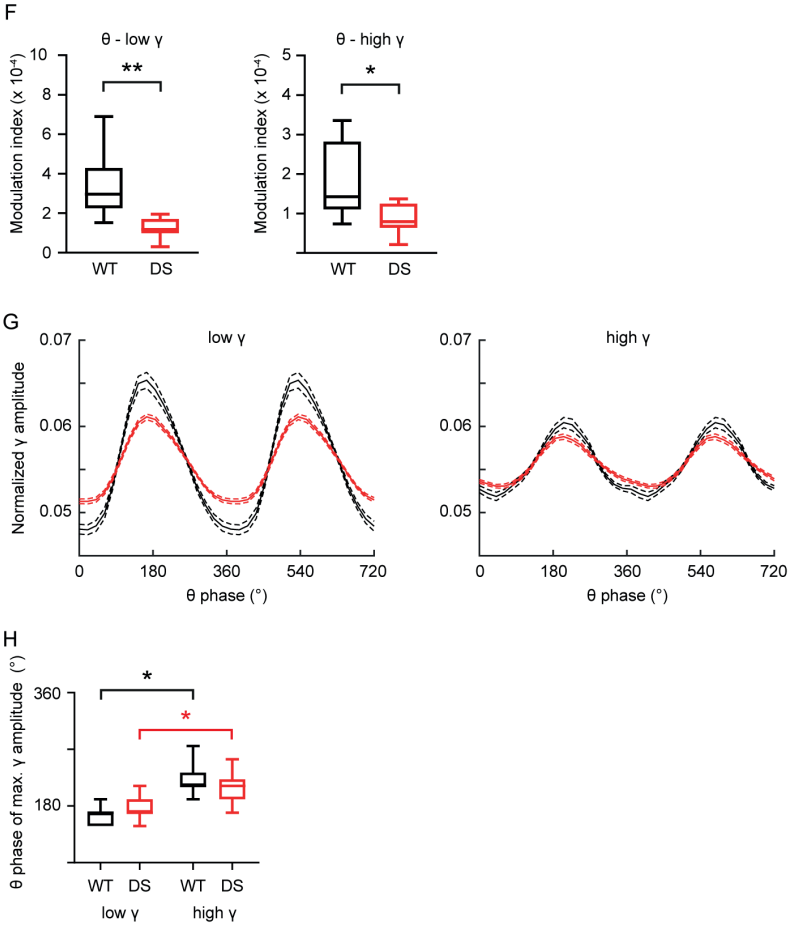

(F) Theta-gamma coupling was significantly reduced in DS mice, for both low and high gamma frequencies ($t_{(8,9)}$ = 3.8 and $t_{(9.2)}$ = 2.9, respectively, *p = 0.019 and **p = 0.004, Welch's t-test). **(G)** Normalized gamma amplitude per 20° phase bin of the theta cycle for V1 during REM sleep. No significant differences were present between WT and DS mice. **(H)** High gamma amplitude peaked significantly later in the theta cycle than low gamma in both genotypes (*p < 0.005, Wilcoxon test).

FIGURE 2. Deficient cortical theta-gamma coupling during active wakefulness in Dravet syndrome (DS) mice.

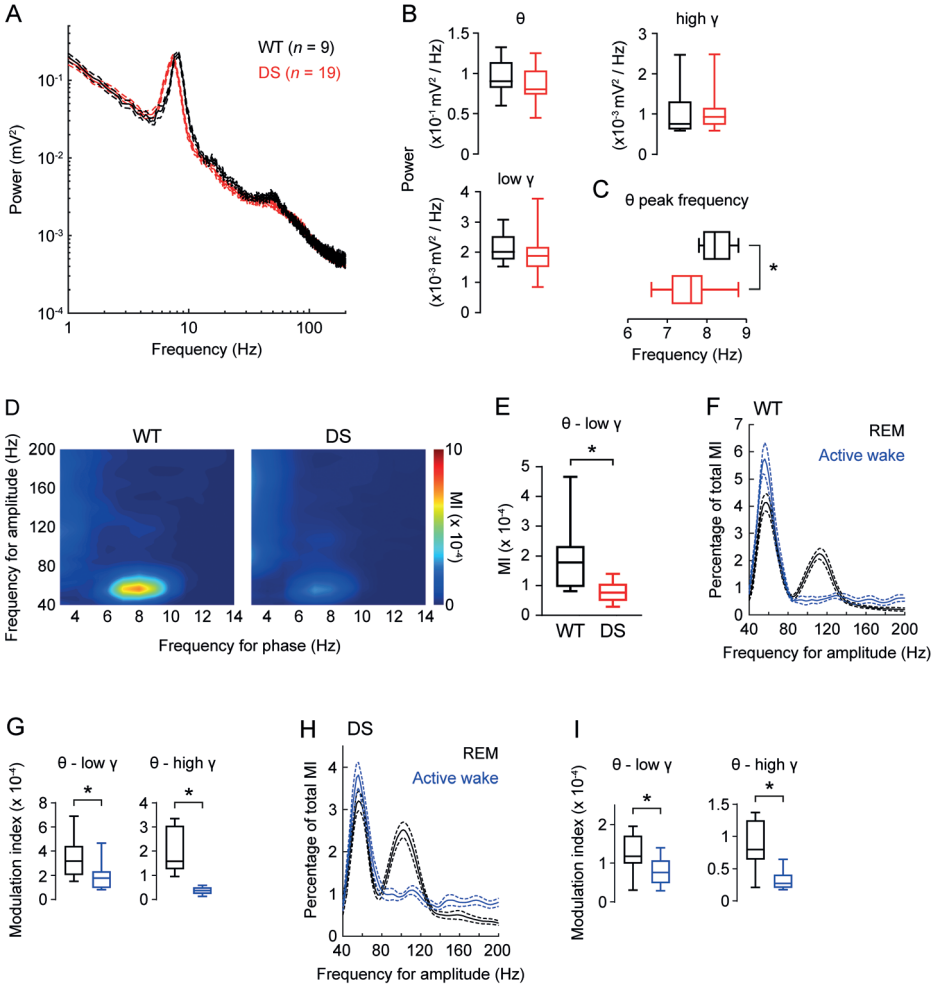

(A) Average primary visual cortex (V1) LFP power spectra during wakefulness in wildtype (WT; black) and DS (red) mice. No significant differences were present between genotypes in power within theta (θ; 5-10 Hz), low gamma (γ; 40-90 Hz) or high gamma (90-160 Hz) frequency ranges **(B)**. **(C)** Peak theta frequency was significantly reduced in DS mice ($t_{(22.7)}$ = 3.5, *p = 0.002, Welch's t-test). **(D)** Average phase-amplitude comodulograms of V1 LFP during active wakefulness in WT (n = 9) and DS (n = 19) mice at P23. **(E)** Theta-low gamma coupling was significantly reduced in DS mice ($t_{(7.9)}$ = 2.7, *p = 0.030, Welch's t-test). For both WT **(F,G)** and DS **(H,I)** mice, theta modulation of gamma amplitude was largely limited to low gamma frequencies during active wakefulness, while modulation of both low and high gamma frequencies was lower when compared to REM sleep.

Impaired theta-gamma coupling in the hippocampus of juvenile DS mice

Previous studies indicate that theta oscillations recorded in the neocortex are volume-conducted currents originating from the hippocampus.[12, 28] The hippocampus, a brain region that importantly contributes to the epileptic phenotype of DS mice,[15, 29, 30] also displays theta-gamma phase-amplitude coupling.[31, 32] To establish whether hippocampal theta-gamma coupling is disturbed in DS mice, we assessed hippocampal LFP in WT (n = 6) and DS (n = 7) mice during REM sleep at P23. Similar to results obtained from V1, theta and gamma power were not significantly different between genotypes (Fig. 3A,B), whereas theta peak frequency was reduced in DS mice (inset Fig. 3A). Variability in gamma power and theta-gamma coupling appeared increased when compared to cortical LFP, which may be explained by slight variations in electrode position within the hippocampus since patterns of theta-gamma coupling are different among hippocampal sublayers.[33] Hippocampal theta-gamma coupling was, however, robustly decreased in DS mice (Fig. 3C,D).

FIGURE 3. Deficient theta-gamma coupling in the hippocampus of Dravet syndrome (DS) mice.

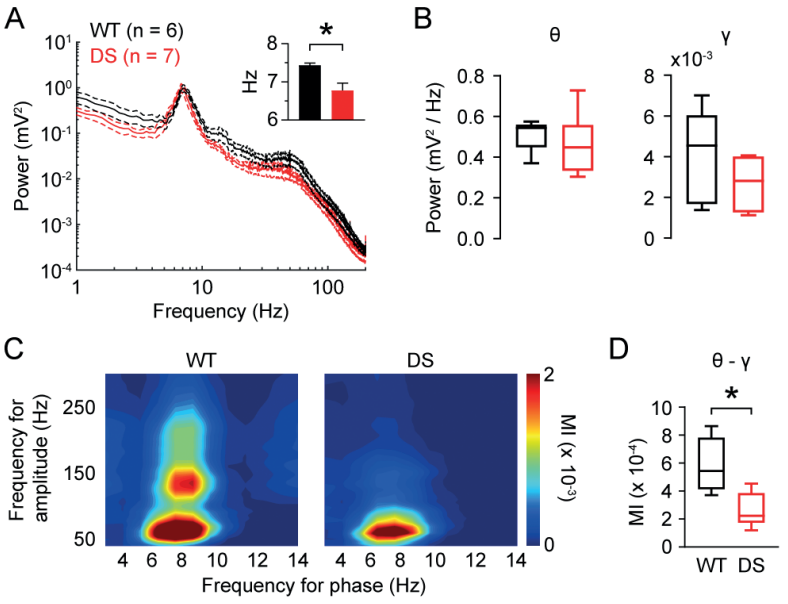

(A) Power spectral density of LFP recorded in the dorsal hippocampus during REM sleep in wildtype (WT; black) and DS (red) mice. Peak theta frequency was significantly reduced in DS mice (inset; $t_{(6.9)}$ = 3.2, *p = 0.011, Welch's t-test). No significant differences were present between genotypes in power within theta (θ; 5-10 Hz) and gamma (γ; 40-300 Hz) frequency ranges **(B)**. **(C)** Average phase-amplitude comodulograms of the same LFP signals. MI, modulation index. **(D)** Theta-gamma coupling was significantly reduced in DS mice ($t_{(8.1)}$ = 3.64, *p = 0.006, Welch t-test).

Cortical theta-gamma coupling normalizes in DS mice without spontaneous seizures

The profound cortical theta-gamma coupling (for both low and high gamma) observed during REM sleep led us to limit subsequent analyses to this vigilance state. First, we assessed whether developmental changes in cortical theta-gamma coupling occurred over the 3-week recording period by analyzing V1 LFP during REM sleep at 2, 7, 14 and 21 days after surgery (i.e. postnatal day 23, 28, 35 and 42; Fig. 4). Theta-gamma coupling increased over this period in both WT and DS mice (Fig. 4A,B). Similar to the observations at P23, DS mice showed decreased theta-gamma coupling when compared to WT mice at P42 (MI values of $5.2 \pm 0.7 \times 10^{-4}$ and $10.4 \pm 1.5 \times 10^{-4}$, respectively; calculated for the total gamma range [40-160 Hz]; $t_{(11)} = 3.2$, $p = 0.009$, Welch's t-test).

The recording period included postnatal week 4, during which spontaneous seizures are most prevalent in DS mice.[34] Accordingly, here, spontaneous seizures in DS mice were most often detected between P21-28 (Fig. 4C). Three DS mice had a fatal seizure (during P24-26), whereas a subset of DS mice (7 out of 19) remained seizure-free over the 3-week recording period. As early seizures, induced by hyperthermia or a chemoconvulsant, were shown to aggravate the epileptic phenotype and cognitive deficits in a knock-in DS mouse model,[35] we assessed whether theta-gamma coupling progressed differently in DS mice that did or did not express seizures during the recording period. Although seizure-free DS mice did show a decrease in cortical theta-gamma coupling for both low and high gamma at baseline (P23), no significant differences were present at P28, P35 and P42 in these mice compared to WT littermates (Fig. 4D). In contrast, theta-gamma coupling was persistently decreased, for both low and high gamma, in DS mice that showed at least one seizure during the 3-week recording period (seizure count per mouse: 5.1 ± 1.5, range 1-19), when compared to WT mice (Fig. 4D).

Decreased progression of cortical theta-gamma coupling in DS mice is improved by cannabidiol

To test whether antiseizure drug treatment could improve attenuated cortical theta-gamma coupling, a separate group of DS mice ($n = 9$) was used to assess the effects of cannabidiol (CBD). CBD decreased seizure frequency in patients with Dravet syndrome,[36] while in DS mice it decreased seizure frequency and severity and increased inhibitory neurotransmission in the hippocampus.[37] Here, in DS mice, the progression of cortical theta-gamma coupling ceased after P35, contrasting the steady progression of theta-gamma coupling observed in WT mice (Fig. 5A,B). DS mice received a single i.p. injection of cannabidiol (CBD; 100 mg/kg) or vehicle at P35 using a randomized crossover design at an interval of 24 hours. Theta-gamma coupling was assessed in V1 LFP during REM sleep up to 5 hours after i.p. injection, during which plasma and brain CBD levels are high in mice.[38] When compared to vehicle, acute treatment of DS mice with CBD resulted in a modest but consistent increase in theta-gamma coupling (Fig. 5C,D).

FIGURE 4. Persistently reduced cortical theta-gamma coupling in Dravet syndrome (DS) mice that show spontaneous seizures.

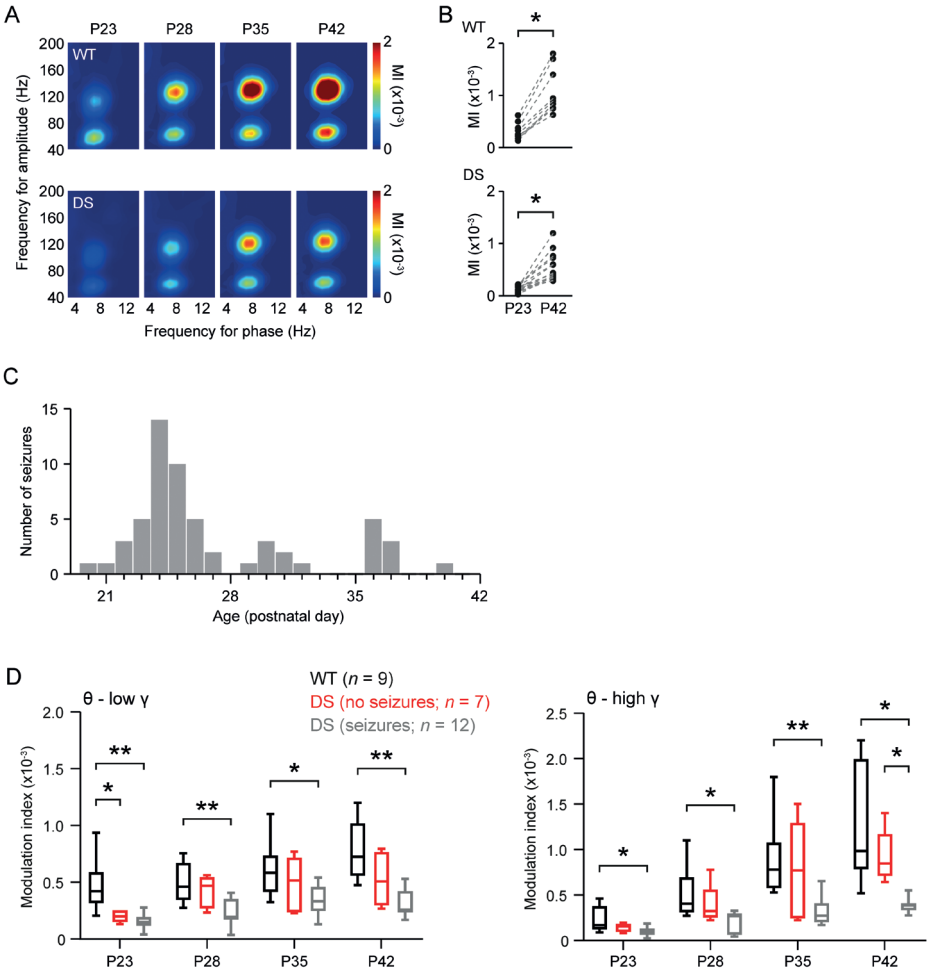

(A) Average phase-amplitude comodulograms of primary visual cortex (V1) showing progression of cortical theta-gamma coupling during postnatal week 4-7. **(B)** Average modulation index (MI), calculated for theta (5-10 Hz) and total gamma (40-160 Hz), was markedly increased in both wildtype (WT) and DS mice at P42, when compared to P23 ($t_{(8)}$ = 7.0 and $t_{(15)}$ = 6.4, respectively, *p < 0.0001, paired t-test). **(C)** Total frequency of spontaneous seizures in DS mice (n = 19). A subset of DS mice (n = 3) died during the recording period, between P24-26. **(D)** Progression of cortical theta-gamma cross-frequency coupling for WT (black) and DS mice with (grey) and without (red) spontaneous seizures over the recording period. Note that at P23 the MI was significantly decreased compared to WT for both groups of DS mice, while at later ages this decrease was maintained only in DS mice with seizures for both low (40-90 Hz) and high (90-160 Hz) gamma ($F_{(2,22)}$ = 9.5, *p < 0.05, **p < 0.005, repeated-measures ANOVA with Tukey's test).

FIGURE 5. Acute treatment with cannabidiol (CBD) improves progression of theta-gamma coupling in Dravet syndrome (DS) mice.

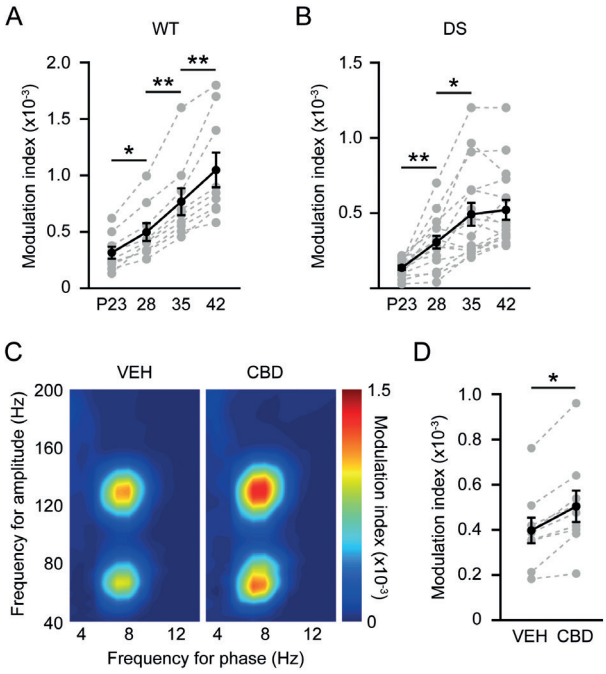

Wildtype (WT) mice showed steady progression of average theta-gamma cross-frequency coupling over time (**A**; calculated for total gamma [40-160 Hz]; $F_{(3,8)} = 15.5$), while for DS mice progression stagnated after P35 (**B**; $F_{(3,15)} = 27.5$, $^{*}p < 0.05$, $^{**}p < 0.005$, repeated-measures ANOVA with Tukey's test). Note that analyses presented in A and B are performed on the same groups as included in Figure 2, excluding DS mice that died during the recording ($n = 3$). **(C)** Average phase-amplitude comodulograms of primary visual cortex (V1) following treatment with vehicle (VEH) or CBD (100 mg/kg) in DS mice between P35-42. **(D)** Average modulation index (MI), calculated for theta (5-10 Hz) and total gamma (40-160 Hz), was significantly increased following treatment with CBD ($t_{(8)} = 5.1$, $^{*}p = 0.0009$, ratio paired *t*-test).

Attenuation of cortical theta-gamma coupling precedes seizures following hippocampal-specific knock-out of *Scn1a*

The early attenuation of cortical theta-gamma coupling that was observed in DS mice at P23 occurred regardless of the epileptic phenotype. Thus, the deficit in cross-frequency coupling may be directly related to the inhibitory dysfunction caused by impaired sodium currents in the DS model.[3] Alternatively, attenuated coupling may result from a secondary effect of inhibitory dysfunction on cortical connectivity during critical period plasticity.[39, 40] We aimed to address this issue by introducing the *Scn1a* defect at adult age, using local brain injections of an AAV vector expressing mCherry-Cre in P42-56 mice in which exon 8 of the *Scn1a* gene is floxed by LoxP sites (in one or both copies of the gene, i.e. $Scn1a^{fl/+}$ or $Scn1a^{fl/fl}$, respectively). This approach additionally allowed assessment of the effects of brain region-specific $Na_V1.1$ dysfunction on theta-gamma coupling.

Hippocampal ablation of $Na_V1.1$ results in an increased susceptibility to seizures.[15, 30] Here, we studied the effect of exposure to Cre recombinase in the dorsal and ventral hippocampus (Fig. 6A) of $Scn1a^{fl/fl}$ mice, resulting in complete $Na_V1.1$ ablation, and $Scn1a^{fl/+}$ mice, to study also partial $Na_V1.1$ ablation (Fig. 6B) which may be more relevant in light of the haploinsufficiency observed in patients and $Scn1a^{-/+}$ DS mice. Within 28 days after injection, all $Scn1a^{fl/fl}$ mice and the majority of $Scn1a^{fl/+}$ mice developed interictal spikes (IIS; n = 6/6 and n = 6/7, respectively; Fig. 6D) and spontaneous seizures (n = 6/6 and n = 5/7, respectively; Fig. 6C,E), whereas neither were observed in WT controls injected with AAV-mCherry-Cre (n = 7). Statistical comparison indicated a significant increase in seizure count for $Scn1a^{fl/fl}$ and $Scn1a^{fl/+}$ mice when compared to controls (18.8 ± 6.8 and 9.4 ± 3.8 seizures, respectively; $H_{(2)} = 11.7$, $p < 0.05$, Kruskal-Wallis with Dunn's test), but seizure count did not differ significantly between the two genotypes ($p = 0.68$). Average onset of IIS was 11.5 days (range 9-14), while the first seizure was observed 13.1 days (range 10-18) after injection. Cortical theta-low gamma coupling was impaired already on day 7 after injection for $Scn1a^{fl/fl}$ mice (Fig. 6F,G). Also, theta-high gamma coupling was impaired at this time in $Scn1a^{fl/fl}$ and $Scn1a^{fl/+}$ mice (Fig. 6F,H). Modulation of both gamma frequency ranges did not recover over subsequent weeks (Fig. 6G,H). Power changes were limited to an increase in gamma power in $Scn1a^{fl/fl}$ mice on day 21 after injection ($1.5 \pm 0.1 \times 10^{-3}$ and $2.2 \pm 0.3 \times 10^{-3}$ mV^2/Hz, on day 2 and 21, respectively; $t_{(6)} = 3.1$, $p = 0.042$, paired t-test). These data indicate that attenuation of cortical theta-gamma coupling precedes IIS and spontaneous seizures following hippocampal deletion of $Na_V1.1$, independent of changes in power spectral density.

FIGURE 6. Chronic seizure activity following hippocampal ablation of $Na_V1.1$ is preceded by decreases in cortical theta-gamma coupling.

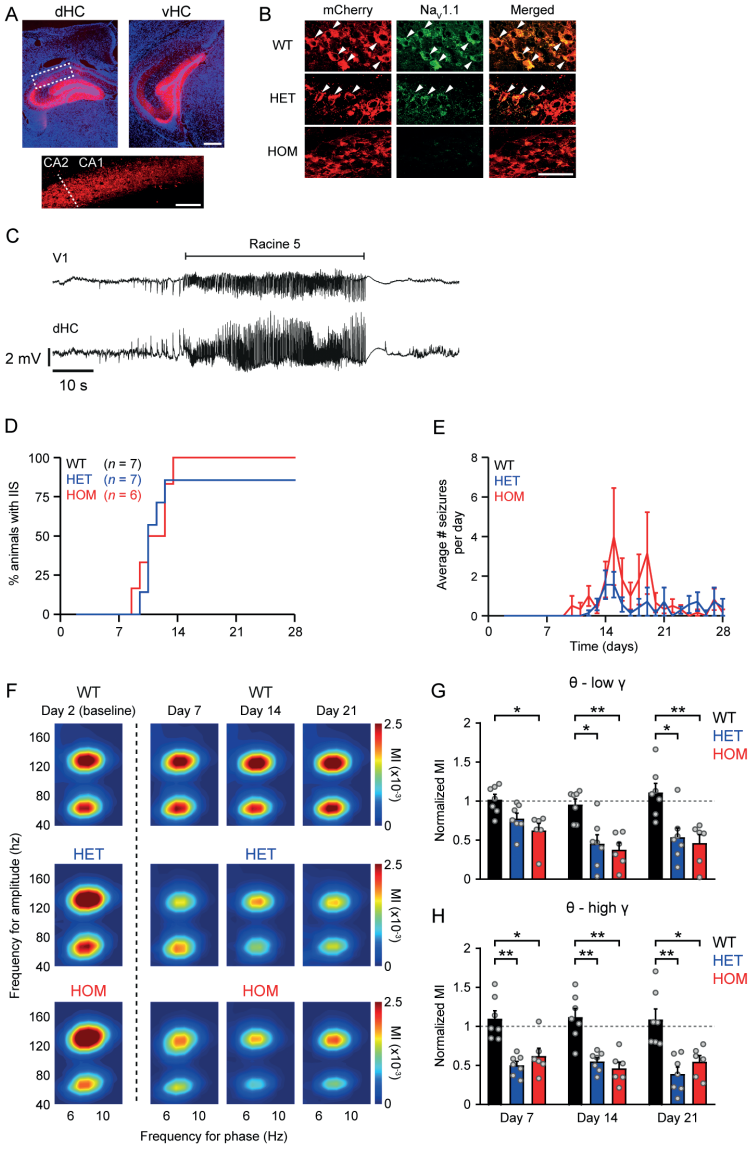

(A) Example of dorsal and ventral hippocampal areas (dHC and vHC, respectively) infected by AAV-mCherry-Cre (red; Hoechst in blue). Scale bar 500 µm. The targeted area included the CA1 and 2 region (boxed area expanded in bottom inset; dashed line indicates border CA1/2; scale bar 200 µm). **(B)** Detail of hippocampal CA1/2 region showing reduced $Na_V1.1$ staining in cells infected by AAV-mCherry-Cre (arrowheads indicate double-labeled cells) in *Scn1a*$^{fl/+}$ (HET) and *Scn1a*$^{fl/fl}$ (HOM) when compared to wildtype (WT). Scale bar 50 µm. **(C)** Spontaneous seizure in a HOM mouse on day 19 after hippocampal AAV-mCherry-Cre (V1 = primary visual cortex). **(D)** Proportion of HET ($n = 7$) and HOM ($n = 6$) mice with interictal spikes (IIS), after hippocampal AAV-mCherry-Cre on day 0. No IIS were observed in WT ($n = 7$). **(E)** Average frequency of spontaneous seizures following AAV-mCherry-Cre. **(F)** Average phase-amplitude comodulograms of V1 at different time points after injection. **(G,H)** Modulation index (MI), normalized to values obtained on day 2, was significantly decreased for both low gamma (γ; 40-90 Hz; G) and high gamma (90-160 Hz; H) frequencies in HET and HOM mice, when compared to WT mice ($F_{(2,17)} = 14.5$ and $F_{(2,17)} = 24.9$, respectively, $^*p < 0.05$, $^{**}p < 0.005$; two-way ANOVA with Tukey's test).

Attenuation of theta-high gamma coupling occurs independently of seizures following cortical-specific knock-out of *Scn1a*

In DS mice, both hippocampal and cortical regions may contribute to seizures,[15] and inhibitory dysfunction has been demonstrated in both structures.[3, 8] We therefore studied the effect of local cortical knock-out of *Scn1a* by injecting AAV-mCherry-Cre in V1 in *Scn1a*$^{fl/+}$ and *Scn1a*$^{fl/fl}$ mice, and WT controls (Fig. 7A,B). Interestingly, all *Scn1a*$^{fl/fl}$ mice developed IIS during the recording period, whereas this was the case for only a subset of *Scn1a*$^{fl/+}$ mice (n = 6/6 and n = 2/7, respectively; Fig. 7D). Spontaneous seizures were observed in a subset of *Scn1a*$^{fl/fl}$ mice (n = 2/6), but never in *Scn1a*$^{fl/+}$ mice (Fig. 7E). Previously, we reported a higher incidence of seizures in *Scn1a*$^{fl/fl}$ mice (n = 6/6) following cortical injections with an AAV vector expressing GFP-Cre under the CMV promotor.[15] As the discrepancy with our current data suggests a greater potency of the latter AAV vector, we tested whether this vector (AAV-GFP-Cre) would result in seizures following cortical injections in 6 *Scn1a*$^{fl/+}$ mice. Again, none of the *Scn1a*$^{fl/+}$ mice developed seizures, indicating that homozygous, but not heterozygous, knock-out of *Scn1a* in V1 predisposes animals to develop spontaneous seizures. Early attenuation of theta-gamma coupling, evident 7 days after injection, was restricted to the high gamma frequency range and persisted in *Scn1a*$^{fl/fl}$ mice but recovered in *Scn1a*$^{fl/+}$ (Fig. 7F-H). Power changes were limited to an increase in gamma power in *Scn1a*$^{fl/+}$ mice on day 21 after injection ($1.8 \pm 0.2 \times 10^{-3}$ and $2.4 \pm 0.2 \times 10^{-3}$ mV^2/Hz, on day 2 and 21, respectively; $t_{(6)} = 12.1$, $p < 0.0001$, paired t-test), while theta peak frequency was decreased in both *Scn1a*$^{fl/+}$ and *Scn1a*$^{fl/fl}$ on day 21 (difference of -0.2 ± 0.1 and -0.4 ± 0.1 Hz, respectively; $t_{(6)} = 2.6$, $p = 0.038$, and $t_{(5)} = 3.9$, $p = 0.012$, paired t-test). These observations suggest that cortical $Na_V1.1$ is required for modulation of high gamma by theta.

Hippocampal fast ripples and attenuated theta-gamma coupling precede epilepsy onset following hippocampal-specific knock-out of *Scn1a*

In addition to cortical LFP, mice that were injected in the hippocampus had local LFP recorded from AAV injection sites. Hippocampal theta-gamma coupling, theta and gamma power, and theta peak frequency decreased over time following injection in both *Scn1a*$^{fl/+}$ and *Scn1a*$^{fl/fl}$ mice (Fig. 8) and comodulograms showed modulation of different gamma frequency ranges, including those above 150 Hz (Fig. 9A). Interestingly, the gamma frequency range that showed the strongest modulation by theta phase decreased over time following local *Scn1a* knock-out (Fig. 8A and Fig. 9A). As such, the decrease in theta-gamma coupling (Fig. 8B) was caused by a strong reduction in theta-modulated high gamma, while low gamma was not significantly affected (Fig. 8C,D).

FIGURE 7. Cortical ablation of $Na_V1.1$ specifically decreases theta-high gamma coupling.

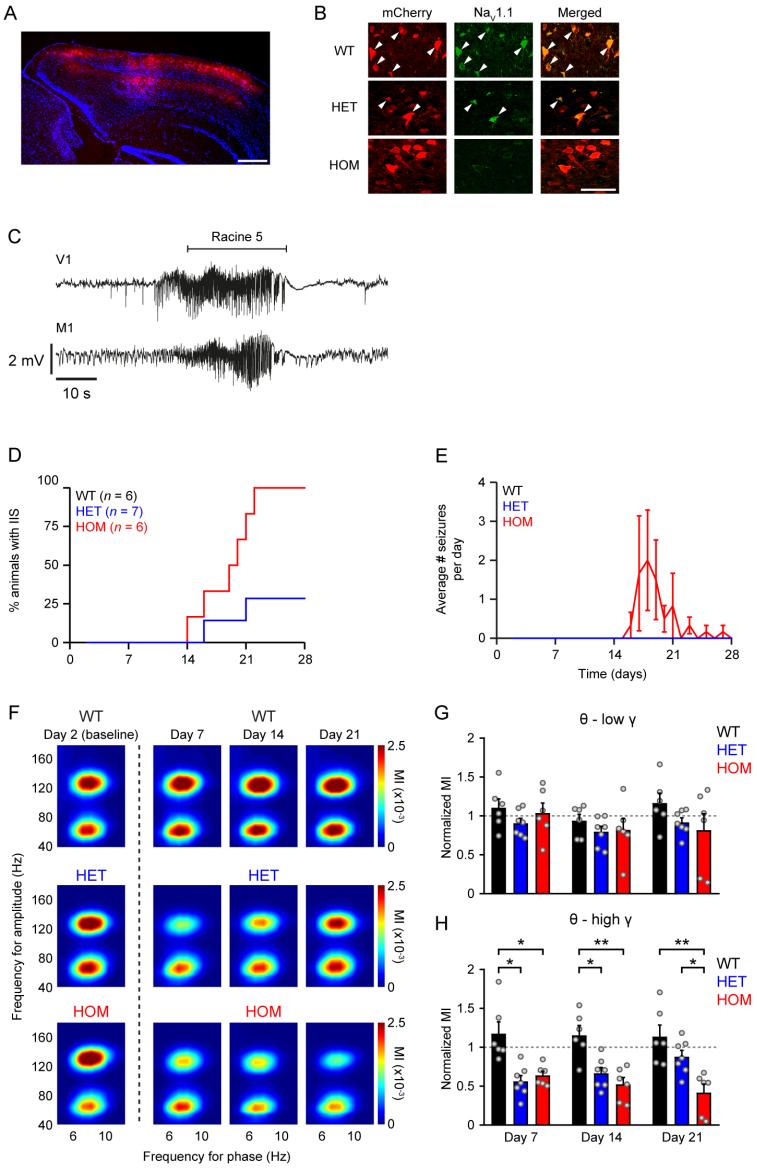

(A) Example of the primary visual cortex (V1) area infected by AAV-mCherry-Cre (red; Hoechst in blue). Scale bar 500 µm. **(B)** Detail of V1 showing reduced $Na_V1.1$ staining in cells infected by AAV-mCherry-Cre (arrowheads indicate double-labeled cells) in *Scn1a*$^{fl/+}$ (HET) and *Scn1a*$^{fl/fl}$ (HOM) when compared to wildtype (WT). Scale bar 50 µm. **(C)** Spontaneous seizure recorded in an *Scn1a*$^{fl/fl}$ mouse on day 18 after cortical AAV-mCherry-Cre (M1 = primary motor cortex). **(D)** Proportion of HET (n = 7) and HOM (n = 6) mice with interictal spikes (IIS), following cortical AAV-mCherry-Cre on day 0. No IIS were observed in WT mice (n = 6). **(E)** Average frequency of spontaneous seizures following injection of AAV-mCherry-Cre. **(F)** Average phase-amplitude comodulograms of V1 at different time points after injection. **(G,H)** Modulation index (MI), normalized to values obtained on day 2, was significantly decreased for high gamma (γ; H), but not low gamma, in HET and HOM mice when compared to WT mice ($F_{(2,16)}$ = 18.5 and $F_{(2,16)}$ = 1.3, respectively, *p < 0.05, **p < 0.005; two-way ANOVA with Tukey's test).

FIGURE 8. Deficient hippocampal theta-gamma coupling and power following local ablation of $Na_V1.1$.

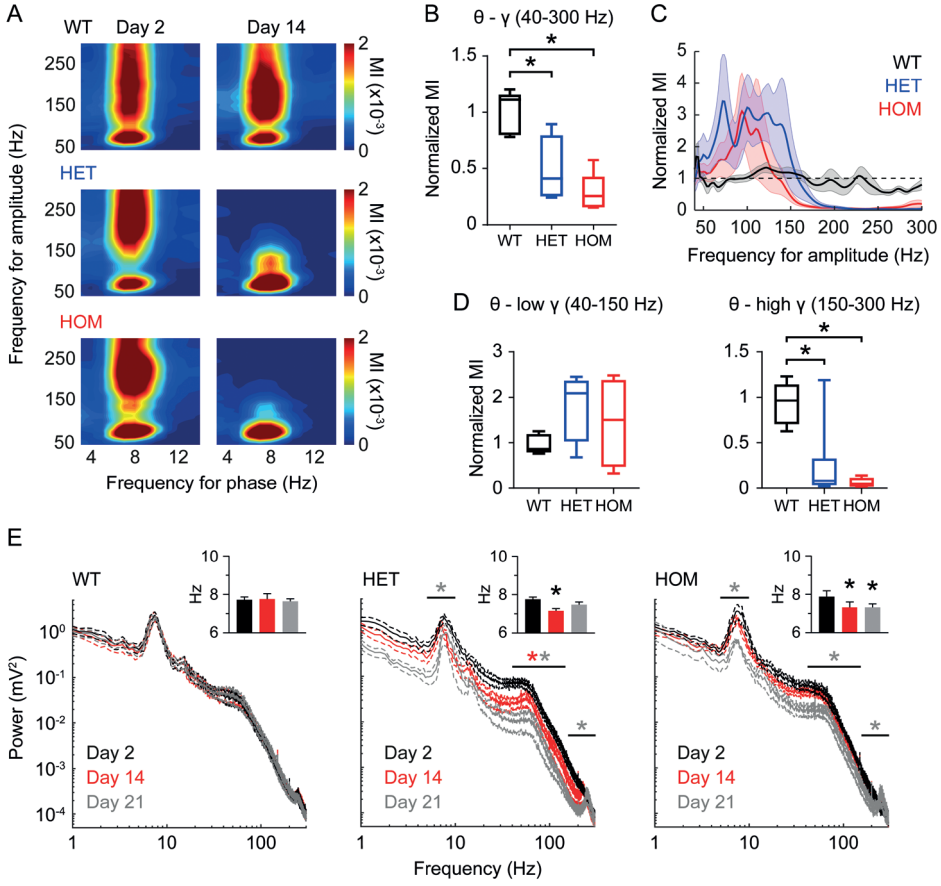

(A) Average phase-amplitude comodulograms of LFP obtained from dorsal hippocampus during day 2 (left) and 14 (right) after hippocampal injection of mCherry-Cre. **(B)** Theta-gamma coupling was reduced in *Scn1a*$^{fl/+}$ and *Scn1a*$^{fl/fl}$ mice on day 14 (total theta-gamma modulation index [MI] normalized to day 2; $F_{(2,17)} = 13.9$, $^*p < 0.01$, one-way ANOVA with Dunnett's test). **(C)** MI normalized per 2-Hz gamma (γ) frequency bin revealed that MI was specifically reduced for gamma frequencies >150 Hz, while showing large variation for the lower gamma range. **(D)** Statistical comparison revealed no difference for theta-modulated low gamma ($F_{(2,17)} = 1.3$, $p = 0.31$), but a significant reduction for high gamma ($F_{(2,17)} = 11.4$, $p = 0.001$) for both *Scn1a*$^{fl/+}$ and *Scn1a*$^{fl/fl}$ mice ($^*p = 0.004$ and $^*p = 0.001$, ANOVA with Dunnett's test). **(E)** Hippocampal LFP power spectral density during REM sleep in wildtype (WT, $n = 7$), *Scn1a*$^{fl/+}$ (HET, $n = 7$) and *Scn1a*$^{fl/fl}$ (HOM, $n = 6$) mice during day 2 (black), 14 (red) and 21 (grey) after hippocampal injection of mCherry-Cre. Power was significantly reduced only in HET and HOM mice. Asterisks of corresponding color indicate significant differences of power in theta (5-10 Hz), low gamma (40-150 Hz) or high gamma (150-300 Hz) on day 2 ($^*p < 0.05$, paired *t*-tests).

Hippocampal fast ripples (250-500 Hz) appear to occur specifically in the seizure onset zone,[41] independent of cell loss associated with hippocampal sclerosis.[42] To study the association between fast ripples and local theta-gamma coupling following hippocampal-specific knock-out of *Scn1a*, we inspected hippocampal LFP recordings for fast ripples over 12 hours preceding the first spontaneous seizure. In 7 out of 13 animals (n = 3 *Scn1a*$^{fl/+}$ and n = 4 *Scn1a*$^{fl/fl}$ mice), we found fast ripples that were superimposed on interictal discharges (Fig. 9B) in either the ventral (n = 4) or dorsal (n = 3) hippocampus. Following exclusion of one animal with bilateral fast ripples, comparison of hippocampal theta-gamma coupling ipsi- and contralateral to the fast ripples revealed a profound reduction in average MI for the ipsilateral electrode (Fig. 9C). The difference between baseline and preictal MI was also significantly greater for the ipsilateral compared to the contralateral electrode ($-7.8 \pm 1.5 \times 10^{-4}$ and $-2.1 \pm 0.6 \times 10^{-4}$, respectively; p = 0.002, Mann-Whitney test). Similarly, the gamma frequency that showed the strongest modulation by theta phase was decreased in the hours preceding seizure activity, specifically for the ipsilateral electrode (Fig. 9D). The drop in gamma frequency between baseline and the preictal period was not significantly different between sides (-79 ± 19 Hz and -36 ± 18 Hz for ipsi- and contralateral, respectively; p = 0.14, Mann-Whitney test). These data confirm theta-gamma coupling as a marker for epileptogenesis in these mice, as its attenuation precedes the first spontaneous seizure in an area corresponding to the seizure onset zone.

FIGURE 9. Theta-gamma coupling is affected more in areas that show fast ripples following hippocampal $Na_V1.1$ ablation.

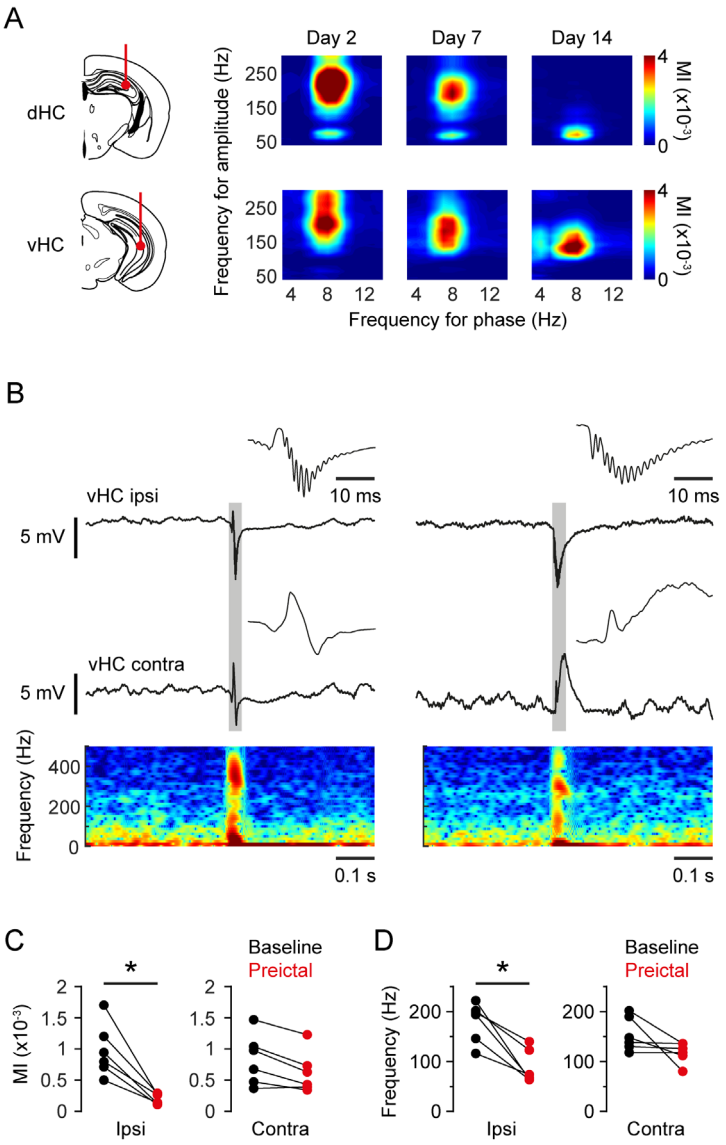

(A) Example phase-amplitude comodulograms of LFP in the dorsal and ventral hippocampus (dHC and vHC, respectively) following hippocampal injection of AAV-mCherry-Cre on day 0 in an *Scn1a*$^{fl/fl}$ mouse. **(B)** Examples of fast ripples observed in the ventral hippocampus of an *Scn1a*$^{fl/fl}$ (left) and *Scn1a*$^{fl/+}$ (right) mouse. Fast ripples (detailed in insets, corresponding to the shaded area) were observed unilaterally (vHC ipsi) and had a high power in the 250-500 Hz range, as shown by the spectrogram of the ipsilateral vHC signal at the bottom. Their onset preceded or coincided with interictal spikes on the contralateral side (vHC contra). **(C)** For hippocampal LFP that contained fast ripples (ipsi), theta-gamma coupling, assessed by the modulation index (MI; averaged for the total gamma frequency range [40-300 Hz]), was significantly decreased in the 12 hours preceding the first seizure (preictal) when compared to day 2 after injection (baseline; $*p = 0.031$, Wilcoxon test). In parallel, the gamma frequency showing peak MI was significantly reduced (**D**; $p = 0.031$, Wilcoxon test). MI changes of contralateral LFP that did not contain fast ripples (contra) did not reach statistical significance.

Impairment of voltage-gated sodium currents in inhibitory neurons attenuates theta-gamma coupling and theta frequency in a computational model

Our *in vivo* experiments indicate that theta-gamma coupling decreases prior to the first spontaneous seizure, suggesting that epilepsy-related remodeling is not responsible for this deficit in network functioning. To test whether decreased theta-gamma coupling may result from loss of voltage-gated sodium currents in inhibitory neurons, we developed a hippocampal network model in which we varied the amount of voltage-gated sodium channel (Na_V) function by decreasing their sodium conductance in modified Hodgkin–Huxley neurons representing fast-spiking basket cell (BC) neurons[43] and oriens-lacunosum moleculare (OLM) neurons.[44] Synaptic connections between BC, OLM and pyramidal (EX) neurons were all-to-all (Fig. 10A) and five neurons of each type were included in the model. LFP generated by the model was dominated by theta oscillations both at baseline (BC: 10 mS/cm^2, OLM: 35 mS/cm^2) and after decreasing sodium conductance in inhibitory neurons (BC: 6 mS/cm^2, OLM: 28 mS/cm^2; Fig. 10B). Theta peak frequency however was shifted to the left in case of impaired Na_V function when compared to baseline, while power in the gamma range was comparable (9.49×10^{-5} and 9.51×10^{-5}, respectively; Fig. 10C). Modulation of gamma by theta was present in both conditions, but reduced in case of impaired Na_V function, which was most evident for gamma oscillations >100 Hz (Fig. 10D). Impairment of inhibitory Na_V function in this computational model thus faithfully replicates both the reduced theta frequency and reduced theta-gamma coupling observed in DS mice.

To delineate the specific roles of the two populations of inhibitory interneurons in this model, we next systematically decreased Na_V function in either BC or OLM neurons. We found that the leftward shift in theta power results from Na_V dysfunction in the OLM population (Fig. 10E). Decreasing Na_V function in BC or OLM neurons had opposite effects on theta-gamma coupling: decreasing Na_V function in BC neurons alone impaired theta-gamma MI, while decreasing Na_V function in OLM neurons increased MI (Fig. 10F). Simultaneous reduction of Na_V function in both BC and OLM neurons resulted in a progressive decrease in theta-gamma MI over the high gamma (100-200 Hz) range, while a slight increase followed by a decrease occurred over the low gamma (40-100 Hz) range. Thus, theta-modulated high gamma is more strongly affected than low gamma in this computational model, which reproduces the *in vivo* results obtained following local *Scn1a* knock-out.

FIGURE 10. Modeling impaired Na_V functioning in inhibitory neurons replicates the attenuated theta-gamma coupling and decreased theta frequency observed after ablation of $Na_V1.1$.

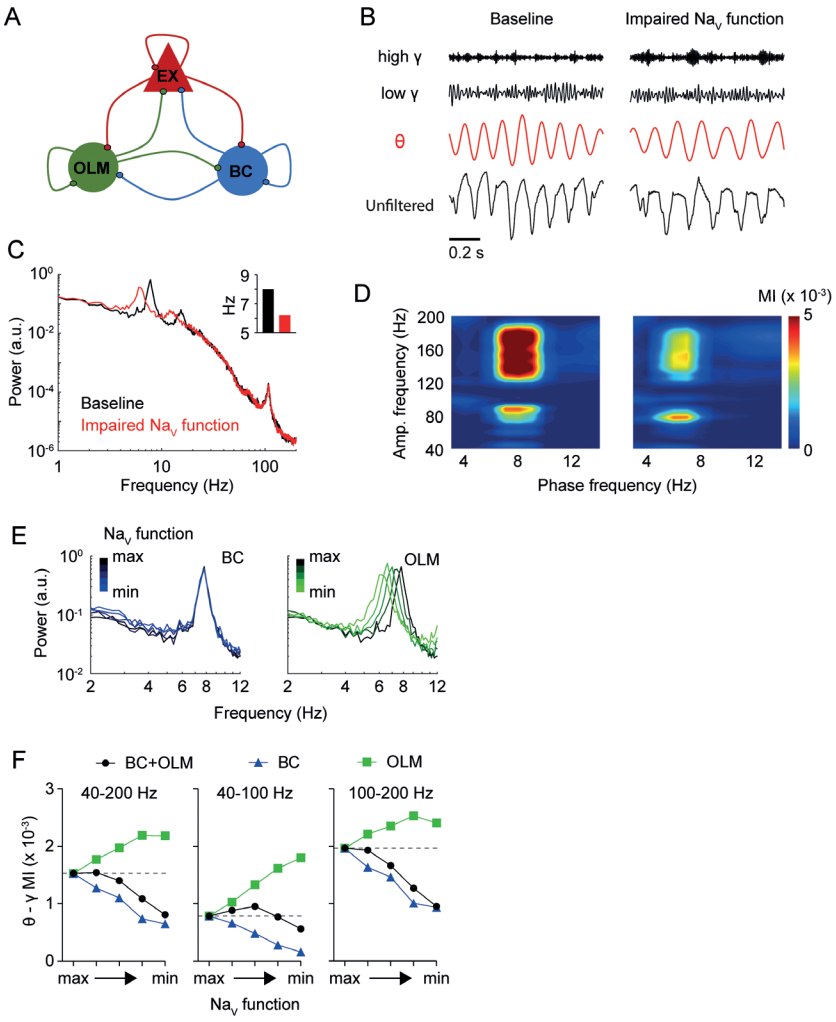

(A) Schematic of the computational network consisting of 5 pyramidal (EX), oriens-lacunosum moleculare (OLM) and fast-spiking basket cell (BC) neurons each with all-to-all connectivity. Full details about the model are provided in Figure 10-1. **(B)** Example traces of raw, theta-filtered (θ; 5-10 Hz), low gamma-filtered (low γ; 40-100 Hz), and high gamma (high γ; 100-200 Hz) filtered local field potential (LFP) from the model with normal (baseline) and impaired Na_V function in both OLM neurons (35 and 28 mS/cm^2, respectively) and BC neurons (10 and 6 mS/cm^2, respectively). **(C)** Average LFP power spectra from the same simulations used in **(B)** with normal (black) or impaired (red) inhibitory Na_V function, showing intact gamma power and a reduced theta peak frequency in the latter (C, inset). **(D)** Phase-amplitude comodulograms of these simulations show impaired theta-modulated gamma. **(E)** Stepwise impairment of Na_V function specifically in BC neurons (blue, left plot) or OLM neurons (green, right plot) resulted in a leftward shift in peak theta frequency for OLM neurons (black: 35 mS/cm^2, bright green: 28 mS/cm^2, steps of 1.75 mS/cm^2), but not for BC neurons (black: 10 mS/cm^2, bright blue: 6 mS/cm^2, steps of 1 mS/cm^2). **(F)** Average theta-gamma modulation index (MI) calculated for total gamma (left), low gamma (center), and high gamma (right) with decreasing levels of Na_V function in BC neurons (blue), OLM neurons (green) and both BC and OLM neurons (black).

DISCUSSION

We here report in juvenile DS mice impaired theta-gamma phase-amplitude coupling, that persisted in mice that developed spontaneous seizures but recovered to WT levels in mice that remained seizure-free. Impaired theta-gamma coupling was improved following acute CBD treatment. Hippocampal or cortical-specific knock-out of *Scn1a* impaired cortical theta-gamma coupling, which preceded spontaneous seizures. Attenuated modulation of high gamma by theta in the hippocampus, which colocalized with fast ripple activity preceding the start of chronic epileptic activity, was reproduced in a computational model in which Na_V dysfunction was selectively introduced in inhibitory neurons. Together, our findings indicate that theta-gamma coupling may serve as an early indicator of inhibitory dysfunction and epileptogenesis in DS.

Dysfunction of inhibitory interneurons has been demonstrated in DS mouse models,[7, 8, 45, 46] and may depend on age window or brain region.[47, 48] Reports on how inhibitory dysfunction affects network dynamics in DS mice appear more ambiguous. For instance, decreased delta power during non-REM sleep was reported in DS mice,[17] but changes in sleep-related delta power were not present in another DS model.[49] Also, interneurons were hypoexcitable, but LFP power was unchanged in DS mice during the pre-epileptic period.[7] Clinically, patients with DS often have a normal background EEG at 1 to 2 years of age, while seizures already manifest at this time.[50, 51] We did not detect differences in theta or gamma power during REM sleep and active wakefulness in DS *versus* WT mice. This contrasts with a previous study reporting decreased theta power during REM sleep in DS mice,[17] which may be explained by differences in mouse strain background and the cortical area studied. Also, we used a strict cutoff in theta/delta ratio to delineate epochs of REM sleep and active wakefulness, which may have rendered our analyses less sensitive to subtle differences in theta power. Nevertheless, our results indicate that theta-gamma coupling is a more sensitive measure of network dysfunction in DS than power spectral density.

Knock-out of *Scn1a* appears to specifically affect inhibitory populations, with reduced sodium currents lowering their excitability,[3, 5, 8, 47] although increased sodium currents have been reported in hippocampal excitatory neurons.[52] Such hyperexcitability of hippocampal excitatory neurons may be attributed to seizure-induced remodeling in DS mice.[35, 53] Importantly, chronic epilepsy may impair theta-gamma coupling, as demonstrated for the hippocampal CA1 region in a rat model of temporal lobe epilepsy.[54] Similarly, impairments in theta-gamma coupling were recently found in the hippocampus of rats following local knock-down of *Scn1a*, whereas no epileptiform activity was observed.[14] Although such activity may not be detected since recordings were performed during wakefulness, when IIS are rare,[17] $Na_V1.1$ dysfunction was induced only in CA1 of the dorsal hippocampus,[14] which may prove insufficient to cause epileptiform activity. In our study, the majority of the hippocampus was targeted, such that subregional effects of $Na_V1.1$ dysfunction cannot be discerned. DS mice and mice with local hippocampal or cortical knock-out of *Scn1a* showed early impairment of theta-gamma coupling before, or in the absence of, chronic epileptic activity. This impairment was transient in seizure-free DS mice, but persisted in mice with

spontaneous seizure activity. Thus, our data indicate that theta-gamma coupling is impaired early in *all* DS mice, but persistence of impaired theta-gamma coupling at later stages is dependent on seizure-induced network remodeling.

Over postnatal weeks 4 to 7, WT and DS mice showed an increase in cortical theta-gamma coupling. In mice, this is a developmental period of high cortical plasticity that starts with maturation of fast-spiking parvalbumin-positive interneurons.[39,40] In seizure-free DS mice, we found that theta-gamma coupling is impaired at P23, but normalized to WT levels at P28-42. This evolution roughly corresponds to developmental data from cortical parvalbumin-positive interneurons that show decreased firing only at P18-21, but not at P35-56, suggesting that their dysfunction contributes to the onset, but not chronification, of epilepsy in DS.[47] Here, local cortical heterozygous knock-out of *Scn1a* resulted in transient attenuation of theta-gamma coupling, which may reflect such temporary inhibitory dysfunction. CBD, which increases inhibitory neurotransmission in DS mice,[37] increased theta-gamma coupling, supporting a link between inhibitory functioning and theta-gamma coupling. Evidence that theta rhythms modulate a greater proportion of inhibitory interneurons when compared to excitatory neurons[11,12] suggests that inhibitory dysfunction particularly impacts theta-gamma coupling. This is further attested by impaired modulation of hippocampal gamma amplitude by theta phase in mice that lacked inhibition onto parvalbumin-positive interneurons, while theta power and peak frequency was reduced.[13] Similarly, we found a reduced theta peak frequency in DS mice, and following local $Na_V1.1$ ablation. Decreased $Na_V1.1$ expression was also observed in a mouse model of Alzheimer's disease, as well as in patients, providing an explanation for dysfunction of parvalbumin-positive interneurons.[55] Since impaired theta-gamma coupling has been demonstrated in Alzheimer's models,[56,57] similar mechanisms may underlie such rhythmopathies in Alzheimer's disease and DS models.

In our computational model, decreases in theta peak frequency could be attributed to Na_V dysfunction in OLM neurons. In animal models of temporal lobe epilepsy, hippocampal theta frequency is decreased[58,59] and degeneration of OLM neurons, resulting in loss of dendritic inhibition, has been observed.[60] Thus, decreased theta frequency appears to be a general feature of the epileptic hippocampus, and dysfunction and/or loss of OLM neurons may underlie this phenomenon. Although (parvalbuminergic) BC neurons appear to maintain their function in the epileptic hippocampus,[60,61] dysfunction of these neurons has been related to impaired theta-gamma coupling,[54] which we confirmed here by modeling BC Na_V dysfunction. Together, our findings suggest that decreased theta frequency and theta-gamma coupling reflect the impaired inhibitory functioning observed in DS mice. Network dynamics underlying cross-frequency coupling, however, are complex, and different factors may affect theta-gamma coupling in other disease models.

We distinguished low and high gamma bands, supported by evidence that mechanisms underlying these oscillations are different.[9] High gamma (above 80-90 Hz) peaks at a different phase of the theta cycle than low gamma,[62] as confirmed by our data, and strongly correlates with neuronal spiking.[63] Local $Na_V1.1$ dysfunction impaired local theta-modulated high, but not low, gamma

oscillations, which was computationally replicated. This suggests that $Na_V1.1$ dysfunction impairs modulation of *local* neuronal firing by theta, as previously shown for CA1 neurons following local $Na_V1.1$ knock-down.[14] The critical role for fast-spiking BC in regulating spike timing by somatic inhibition[40] may explain these early deficits in theta-high gamma coupling.

Increased hippocampal theta-gamma coupling is associated with memory recall in rodents[64] and humans.[65, 66] Memory impairment is frequently observed in patients with temporal lobe epilepsy.[67, 68] Although we did not relate changes in theta-gamma coupling to learning, previous studies indicate that context-dependent and spatial memory are impaired in DS mouse models.[4, 35] Cognitive deficits were only present in adult DS mice that had experienced seizures at juvenile age,[35] which may be related to persistent deficits in theta-gamma coupling that we only observed in adult DS mice with juvenile-onset seizures. The hippocampus appears to critically contribute to spatial memory deficits and the epileptic phenotype in DS mice.[29, 30] Our data suggest that impaired theta-gamma coupling precedes seizures and associates unilaterally with fast ripple activity in the hippocampus, a marker for epileptogenesis.[41] Further studies are required to translate these findings to other epilepsy models. Reductions in theta frequency in such models have been suggested to underlie cognitive deficits in epilepsy,[59, 69] but in our experiments occurred regardless of epileptic activity. Similarly, local knock-down of $Na_V1.1$ in the medial septum, which provides input to the hippocampus, decreased theta frequency and disrupted spatial memory in rats[70] without inducing seizure activity,[71] indicating that regions other than the hippocampus may contribute to impaired spatial memory and theta rhythmogenesis in DS. To recapitulate rhythmopathies in DS, the precision of computational models may therefore be improved by including inputs such as provided by the medial septum.

REFERENCES

1. Wolff, M., C. Casse-Perrot, and C. Dravet, Severe myoclonic epilepsy of infants (Dravet syndrome): natural history and neuropsychological findings. *Epilepsia*, 2006. 47 Suppl 2: p. 45-8.
2. Dravet, C., The core Dravet syndrome phenotype. *Epilepsia*, 2011. 52 Suppl 2: p. 3-9.
3. Yu, F.H., et al., Reduced sodium current in GABAergic interneurons in a mouse model of severe myoclonic epilepsy in infancy. *Nat Neurosci*, 2006. 9(9): p. 1142-9.
4. Han, S., et al., Autistic-like behaviour in Scn1a+/- mice and rescue by enhanced GABA-mediated neurotransmission. *Nature*, 2012. 489(7416): p. 385-90.
5. Ogiwara, I., et al., Nav1.1 localizes to axons of parvalbumin-positive inhibitory interneurons: a circuit basis for epileptic seizures in mice carrying an Scn1a gene mutation. *J Neurosci*, 2007. 27(22): p. 5903-14.
6. Cheah, C.S., et al., Specific deletion of NaV1.1 sodium channels in inhibitory interneurons causes seizures and premature death in a mouse model of Dravet syndrome. *Proc Natl Acad Sci U S A*, 2012. 109(36): p. 14646-51.
7. De Stasi, A.M., et al., Unaltered Network Activity and Interneuronal Firing During Spontaneous Cortical Dynamics In Vivo in a Mouse Model of Severe Myoclonic Epilepsy of Infancy. *Cereb Cortex*, 2016. 26(4): p. 1778-94.
8. Tai, C., et al., Impaired excitability of somatostatin- and parvalbumin-expressing cortical interneurons in a mouse model of Dravet syndrome. *Proc Natl Acad Sci U S A*, 2014. 111(30): p. E3139-48.
9. Buzsaki, G. and X.J. Wang, Mechanisms of gamma oscillations. *Annu Rev Neurosci*, 2012. 35: p. 203-25.
10. Freund, T.F. and I. Katona, Perisomatic inhibition. *Neuron*, 2007. 56(1): p. 33-42.
11. Csicsvari, J., et al., Oscillatory coupling of hippocampal pyramidal cells and interneurons in the behaving *Rat. J Neurosci,* 1999. 19(1): p. 274-87.
12. Sirota, A., et al., Entrainment of neocortical neurons and gamma oscillations by the hippocampal theta rhythm. *Neuron*, 2008. 60(4): p. 683-97.
13. Wulff, P., et al., Hippocampal theta rhythm and its coupling with gamma oscillations require fast inhibition onto parvalbumin-positive interneurons. *Proc Natl Acad Sci U S A*, 2009. 106(9): p. 3561-6.
14. Sakkaki, S., et al., Focal Dorsal Hippocampal Nav1.1 Knock Down Alters Place Cell Temporal Coordination and Spatial Behavior. *Cereb Cortex*, 2020. 30(9): p. 5049-5066.
15. Jansen, N.A., et al., Focal and generalized seizure activity after local hippocampal or cortical ablation of NaV 1.1 channels in mice. *Epilepsia*, 2020. 61(4): p. e30-e36.
16. Racine, R.J., Modification of seizure activity by electrical stimulation. II. Motor seizure. *Electroencephalogr Clin Neurophysiol*, 1972. 32(3): p. 281-94.
17. Kalume, F., et al., Sleep impairment and reduced interneuron excitability in a mouse model of Dravet Syndrome. *Neurobiol Dis*, 2015. 77: p. 141-54.
18. Tort, A.B., et al., Measuring phase-amplitude coupling between neuronal oscillations of different frequencies. *J Neurophysiol*, 2010. 104(2): p. 1195-210.
19. Kopell, N., et al., Gamma and theta rhythms in biophysical models of hippocampal circuits, in *Hippocampal microcircuits*. 2010, Springer. p. 423-457.

20. Cressman, J.R., Jr., et al., The influence of sodium and potassium dynamics on excitability, seizures, and the stability of persistent states: I. Single neuron dynamics. *J Comput Neurosci*, 2009. 26(2): p. 159-70.
21. Hubel, N., et al., The role of glutamate in neuronal ion homeostasis: A case study of spreading depolarization. *PLoS Comput Biol*, 2017. 13(10): p. e1005804.
22. Ullah, G., The role of transporters and synaptic cleft morphology in glutamate and GABA homeostasis and their effect on neuronal function. *BioRxiv*, 2019: p. 670844.
23. Ullah, G. and S.J. Schiff, Assimilating seizure dynamics. *PLoS Comput Biol*, 2010. 6(5): p. e1000776.
24. Ullah, G., et al., The Role of Cell Volume in the Dynamics of Seizure, Spreading Depression, and Anoxic Depolarization. *PLoS Comput Biol*, 2015. 11(8): p. e1004414.
25. Wei, Y., G. Ullah, and S.J. Schiff, Unification of neuronal spikes, seizures, and spreading depression. *J Neurosci*, 2014. 34(35): p. 11733-43.
26. Scheffzuk, C., et al., Selective coupling between theta phase and neocortical fast gamma oscillations during REM-sleep in mice. *PLoS One*, 2011. 6(12): p. e28489.
27. Bandarabadi, M., et al., Dynamic modulation of theta-gamma coupling during rapid eye movement sleep. *Sleep*, 2019. 42(12).
28. Gerbrandt, L.K., et al., Origin of the neocortically monitored theta rhythm in the curarized rat. *Electroencephalogr Clin Neurophysiol*, 1978. 45(4): p. 454-67.
29. Liautard, C., et al., Hippocampal hyperexcitability and specific epileptiform activity in a mouse model of Dravet syndrome. *Epilepsia*, 2013. 54(7): p. 1251-61.
30. Stein, R.E., et al., Hippocampal deletion of NaV1.1 channels in mice causes thermal seizures and cognitive deficit characteristic of Dravet Syndrome. *Proc Natl Acad Sci U S A*, 2019. 116(33): p. 16571-16576.
31. Bragin, A., et al., Gamma (40-100 Hz) oscillation in the hippocampus of the behaving rat. *J Neurosci*, 1995. 15(1 Pt 1): p. 47-60.
32. Buzsaki, G., et al., Hippocampal network patterns of activity in the mouse. *Neuroscience*, 2003. 116(1): p. 201-11.
33. Schomburg, E.W., et al., Theta phase segregation of input-specific gamma patterns in entorhinal-hippocampal networks. *Neuron*, 2014. 84(2): p. 470-85.
34. Kalume, F., et al., Sudden unexpected death in a mouse model of Dravet syndrome. *J Clin Invest*, 2013. 123(4): p. 1798-808.
35. Salgueiro-Pereira, A.R., et al., A two-hit story: Seizures and genetic mutation interaction sets phenotype severity in SCN1A epilepsies. *Neurobiol Dis*, 2019. 125: p. 31-44.
36. Devinsky, O., et al., Trial of Cannabidiol for Drug-Resistant Seizures in the Dravet Syndrome. *N Engl J* Med, 2017. 376(21): p. 2011-2020.
37. Kaplan, J.S., et al., Cannabidiol attenuates seizures and social deficits in a mouse model of Dravet syndrome. *Proc Natl Acad Sci U S A*, 2017. 114(42): p. 11229-11234.
38. Deiana, S., et al., Plasma and brain pharmacokinetic profile of cannabidiol (CBD), cannabidivarine (CBDV), Delta(9)-tetrahydrocannabivarin (THCV) and cannabigerol (CBG) in rats and mice following oral and intraperitoneal administration and CBD action on obsessive-compulsive behaviour. *Psychopharmacology* (Berl), 2012. 219(3): p. 859-73.

39. Takesian, A.E. and T.K. Hensch, Balancing plasticity/stability across brain development. *Prog Brain Res*, 2013. 207: p. 3-34.
40. Cardin, J.A., Inhibitory Interneurons Regulate Temporal Precision and Correlations in Cortical Circuits. *Trends Neurosci*, 2018. 41(10): p. 689-700.
41. Jefferys, J.G., et al., Mechanisms of physiological and epileptic HFO generation. *Prog Neurobiol*, 2012. 98(3): p. 250-64.
42. Jiruska, P., et al., Epileptic high-frequency network activity in a model of non-lesional temporal lobe epilepsy. *Brain*, 2010. 133(Pt 5): p. 1380-90.
43. Wang, X.J. and G. Buzsaki, Gamma oscillation by synaptic inhibition in a hippocampal interneuronal network model. *J Neurosci*, 1996. 16(20): p. 6402-13.
44. Tort, A.B., et al., On the formation of gamma-coherent cell assemblies by oriens lacunosum-moleculare interneurons in the hippocampus. *Proc Natl Acad Sci U S A*, 2007. 104(33): p. 13490-5.
45. Rubinstein, M., et al., Genetic background modulates impaired excitability of inhibitory neurons in a mouse model of Dravet syndrome. *Neurobiol Dis*, 2015. 73: p. 106-17.
46. Goff, K.M. and E.M. Goldberg, Vasoactive intestinal peptide-expressing interneurons are impaired in a mouse model of Dravet syndrome. *Elife*, 2019. 8.
47. Favero, M., et al., A Transient Developmental Window of Fast-Spiking Interneuron Dysfunction in a Mouse Model of Dravet Syndrome. *J Neurosci*, 2018. 38(36): p. 7912-7927.
48. Almog, Y., Brusel, M., Anderson, K., Rubinstein, M., Early hippocampal hyperexcitability followed by disinhibition in a mouse model of Dravet syndrome. *bioRxiv*, 2019(790170).
49. Papale, L.A., et al., Altered sleep regulation in a mouse model of SCN1A-derived genetic epilepsy with febrile seizures plus (GEFS+). *Epilepsia*, 2013. 54(4): p. 625-34.
50. Bureau, M. and B. Dalla Bernardina, Electroencephalographic characteristics of Dravet syndrome. *Epilepsia*, 2011. 52 Suppl 2: p. 13-23.
51. Wirrell, E.C., et al., Optimizing the Diagnosis and Management of Dravet Syndrome: Recommendations From a North American Consensus Panel. *Pediatr Neurol*, 2017. 68: p. 18-34 e3.
52. Mistry, A.M., et al., Strain- and age-dependent hippocampal neuron sodium currents correlate with epilepsy severity in Dravet syndrome mice. *Neurobiol Dis*, 2014. 65: p. 1-11.
53. Dutton, S.B.B., et al., Early-life febrile seizures worsen adult phenotypes in Scn1a mutants. *Exp Neurol*, 2017. 293: p. 159-171.
54. Lopez-Pigozzi, D., et al., Altered Oscillatory Dynamics of CA1 Parvalbumin Basket Cells during Theta-Gamma Rhythmopathies of Temporal Lobe Epilepsy. *eNeuro*, 2016. 3(6).
55. Verret, L., et al., Inhibitory interneuron deficit links altered network activity and cognitive dysfunction in Alzheimer model. *Cell*, 2012. 149(3): p. 708-21.
56. Ittner, A.A., et al., p38 MAP kinase-mediated NMDA receptor-dependent suppression of hippocampal hypersynchronicity in a mouse model of Alzheimer's disease. *Acta Neuropathol Commun*, 2014. 2: p. 149.
57. Zhang, X., et al., Impaired theta-gamma coupling in APP-deficient mice. *Sci Rep*, 2016. 6: p. 21948.
58. Dugladze, T., et al., Impaired hippocampal rhythmogenesis in a mouse model of mesial temporal lobe epilepsy. *Proc Natl Acad Sci U S A*, 2007. 104(44): p. 17530-5.

59. Kilias, A., et al., Theta frequency decreases throughout the hippocampal formation in a focal epilepsy model. *Hippocampus*, 2018. 28(6): p. 375-391.
60. Cossart, R., et al., Dendritic but not somatic GABAergic inhibition is decreased in experimental epilepsy. *Nat Neurosci*, 2001. 4(1): p. 52-62.
61. Wittner, L., et al., Surviving CA1 pyramidal cells receive intact perisomatic inhibitory input in the human epileptic hippocampus. *Brain*, 2005. 128(Pt 1): p. 138-52.
62. Belluscio, M.A., et al., Cross-frequency phase-phase coupling between theta and gamma oscillations in the hippocampus. *J Neurosci*, 2012. 32(2): p. 423-35.
63. Ray, S. and J.H. Maunsell, Different origins of gamma rhythm and high-gamma activity in macaque visual cortex. *PLoS Biol*, 2011. 9(4): p. e1000610.
64. Tort, A.B., et al., Theta-gamma coupling increases during the learning of item-context associations. *Proc Natl Acad Sci U S A*, 2009. 106(49): p. 20942-7.
65. Axmacher, N., et al., Cross-frequency coupling supports multi-item working memory in the human hippocampus. *Proc Natl Acad Sci U S A*, 2010. 107(7): p. 3228-33.
66. Heusser, A.C., et al., Episodic sequence memory is supported by a theta-gamma phase code. *Nat Neurosci*, 2016. 19(10): p. 1374-80.
67. Vlooswijk, M.C., et al., Functional MRI in chronic epilepsy: associations with cognitive impairment. *Lancet Neurol*, 2010. 9(10): p. 1018-27.
68. Helmstaedter, C. and C.E. Elger, Chronic temporal lobe epilepsy: a neurodevelopmental or progressively dementing disease? *Brain*, 2009. 132(Pt 10): p. 2822-30.
69. Shuman, T., B. Amendolara, and P. Golshani, Theta Rhythmopathy as a Cause of Cognitive Disability in TLE. *Epilepsy Curr*, 2017. 17(2): p. 107-111.
70. Bender, A.C., B.W. Luikart, and P.P. Lenck-Santini, Cognitive Deficits Associated with Nav1.1 Alterations: Involvement of Neuronal Firing Dynamics and Oscillations. *PLoS One*, 2016. 11(3): p. e0151538.
71. Bender, A.C., et al., Focal Scn1a knockdown induces cognitive impairment without seizures. *Neurobiol Dis*, 2013. 54: p. 297-307.

SUPPLEMENTARY MATERIAL

Extended data

FIGURE 10 - 1. Currents and fluxes regulating membrane potential, ion concentrations and neurotransmitter homeostasis for the computational neuronal network model.

Chapter 9

General discussion

GENERAL DISCUSSION

The main aim of this work was to establish mouse models of seizures and spreading depolarizations (SDs), in an effort to study their mechanisms and potentially debilitating consequences. To this end various transgenic animal models were generated and characterized in which aberrant neuronal excitability was a common denominator, but each model had otherwise unique features. An important contribution to the field is that all models showed seizures and/or spreading depolarizations in an apparent unprovoked fashion, increasing their clinical significance and allowing the study of initiation mechanisms of these events. These models may thereby prove a valuable tool to understand how excessive neuronal excitability results in episodic disorders as distinctive as epilepsy and migraine, as well as their complications, aiding the development of (preventative) treatment strategies.

In this Chapter, I will summarize, integrate and discuss the main findings from preceding chapters, and finally provide a perspective for future research.

Part I: Spontaneous spreading depolarizations

Cortical SD as first described by Leão[1] is considered the underlying substrate for the migraine aura.[2] This theory has gradually displaced the "vascular theory" of the migraine aura, which posits that the focal (visual) symptoms of the migraine aura are the result of vasoconstriction.[3] The latter theory has failed to explain the highly stereotypical propagating nature of the migraine aura.[4] This is often illustrated by the scintillating scotoma in visual auras, which starts in the center of the visual field and propagates to the periphery over the course of several minutes.[5] Early imaging studies in migraine patients demonstrated a "spreading oligemia" that propagated in a posterior-to-anterior pattern over the cerebral cortex.[6-9] However, it was already early recognized that the timing of this oligemia poorly correlated with the focal symptoms of the migraine aura.[9] Later measurements of cortical magnetic resonance imaging (MRI) blood oxygenation level dependent (BOLD) signal during migraine auras found similar patterns within the visual cortex, which commenced with initial hyperemia of a duration and propagation characteristic of cortical SD, correlating with aura symptoms, and which were later followed by hypoperfusion.[10] Thereby, an SD propagating through the visual cortex is considered the homotopic equivalent of the experience of a scintillating scotoma in the visual field.

Shifting focus to spreading depolarization initiation

Despite progress in our understanding of factors that may evoke SD and facilitate or inhibit their propagation, little is known about the physiology underlying the spontaneous initiation of SDs. Experimental studies have resorted to actively inducing SD, which is convenient, reliable, and replicable. Models allowing the study of unprovoked SD initiation were hitherto lacking, limiting our ability to identify clinically relevant mechanisms of SD initiation. In **Chapters 2 and 3**, we present two novel models of familial hemiplegic migraine (FHM) in which SDs occur

spontaneously. The mouse models harbor fundamentally different pathogenic mutations: the FHM3-related *Scn1a*^{L263V} mutation, expected to result in $Na_V1.1$ gain of function, presumably resulting in interneuron hyperexcitability, and the FHM2-related *Atp1a2*^{T345A} mutation, expected to result in decreased Na^+/K^+-ATPase pump function in glia. Thus, although different proteins expressed in different cell types are involved, these models share a hyperexcitability phenotype that results in spontaneous SDs. In both models, SDs in the cortex propagated in a caudal-to-rostral (i.e. posterior-to-anterior) direction, similar to studies of cerebral blood flow and MRI BOLD signal in patients during migraine attacks described above. Interestingly, we found that the large majority of spontaneous SDs in homozygous *Atp1a2*^{T345A} mice occurred during awakening. Although we cannot at this point rule out that animals are in fact awakening *from* the SD, clinical studies indicate that migraine attacks (with and without aura) have a predilection to occur in the early morning[11, 12] and upon awakening.[13] The question that follows is: what could initiate these SDs?

Previous literature convincingly showed that inhibition of N-methyl-D-aspartate receptors (NMDARs) blocks experimentally induced SD, although uncertainty persists whether this is caused by impairment of SD initiation or propagation, or both.[14] Studies in another FHM2 model harboring the *Atp1a2* W887R missense mutation have suggested impaired glutamate clearance as a primary trigger of SD.[15, 16] Treatment of these FHM2 mice with a compound that was expected to increase glutamate uptake – by inducing upregulation of a glutamate transporter – resulted in an increased threshold for induced SD.[15] Since glutamate would facilitate SD by activation of NMDARs, allowing regenerative influx of K^+ and other cations through their pores,[17] these data support the view that NMDAR activation is crucial for SD initiation. Indeed, MK801, a potent NMDAR antagonist, blocked the spreading depolarization near the site of initial depolarization evoked by high levels of KCl.[18] In contrast, our results in *Atp1a2*^{T345A} mice indicate that MK801 is ineffective at blocking spontaneous hippocampal SD in homozygous *Atp1a2*^{T345A} mice, while SD propagation to the cortex was blocked. Mei et al.[19] similarly found that blockade of NMDAR, by intracellular administration of compounds, did not affect initiation of SD in the hippocampus of wildtype mice. To explain these apparent discrepancies, we have to consider the area studied: we found a hippocampal origin of SD in *Atp1a2*^{T345A} mice, and Mei et al.[19] studied hippocampal slices. Indeed, NMDAR blockade was previously shown not to prevent SD in hippocampal slices, although its timing and waveform were affected.[20] In contrast, Vitale et al.[18] studied cortical slices. SD mechanisms may vary depending on the area studied, as was earlier proposed given the higher dosage of NMDAR antagonists required to block SD in hippocampus *versus* cortex.[14] Regardless, former studies have relied on some form of experimental induction of SD, be it current injection, pinprick or application of KCl to the dura or brain slice. Given the "all-or-none" character of SD – which entails that once started, its amplitude is independent from the trigger[21] – studying the eventual threshold is key to understanding SD initiation. This was indeed also recognized by Vitale et al.,[18] who found a specific level of NMDAR activation to be required for SD initiation. And yet, this is especially discrepant with our data, as we found that spontaneous SDs in homozygous *Atp1a2*^{T345A} mice were in fact more likely to occur *earlier* after MK801 administration (**Chapter**

3). Although we did not investigate why this occurred, NMDAR antagonists may paradoxically increase excitability by preferential inhibition of inhibitory neurons,[22] possibly by higher ambient glutamate in excitatory to inhibitory synapses.[23] In any case, our data argue against a crucial role for glutamate and NMDARs in SD *initiation*, at least in the context of the T345A FHM2 mutation, in contrast to the widely appreciated crucial role for glutamate and NMDARs in SD *duration* and *propagation*.[17] This should compel us to look for potential alternative mechanisms of SD initiation.

Van Harreveld *versus* Grafstein: potassium persists

A crucial role for increases in extracellular K^+ in the initiation and propagation of SD was suggested in an early study by Grafstein.[24] Based on previous research, increases in extracellular K^+ under conditions of increased excitability could be a common trigger for SD in our FHM2 and FHM3 models. In FHM2, the *Atp1a2*^{T345A} mutation results in impaired clearance of extracellular K^+ in transfected cell cultures.[25] In FHM3, since *Scn1a*-encoded $Na_V1.1$ channels are being predominantly expressed in inhibitory interneurons, the gain-of-function effects of the *Scn1a*^{L263V} mutation[26] could result in accumulation of extracellular K^+ due to increased intensity of interneuron firing.[27] Indeed, experimentally induced activation of $Na_V1.1$ channels or hyperactivity of inhibitory interneurons is sufficient to induce cortical SD, even when neurotransmitter release is blocked.[28] Increases in extracellular K^+ can generate a self-sustaining inward current if exceeding K^+ clearance, resulting in SD.[17]

In mice, cortical extracellular K^+ is relatively low during sleep[29] and increases throughout the cortex immediately prior to brain state transitions.[30] Such state-dependent changes in K^+ occurred much faster – within seconds – than changes in other cations such as Ca^{2+}.[29] Following these changes, a relatively stable K^+ concentration was maintained during each brain state.[29] Interestingly, since we found in **Chapter 3** that the majority of spontaneous SDs in homozygous *Atp1a2*^{T345A} mice occurred during awakening, this raises the possibility that "physiological" changes in extracellular K^+ could contribute to SD initiation, especially when increased release (such as in FHM3) or decreased clearance (such as in FHM2) cause extracellular K^+ rises to overshoot its clearance. Hence the question arises: how would such overshoots cause SD?

For SDs to initiate, inward currents are required that inactivate only slowly.[31] Persistent sodium currents have been identified in neurons and are thought to act as amplifiers of synaptic potentials,[32] regulating the excitability of neurons. Although the magnitude of these sodium currents is relatively small during resting conditions, it is greatly enhanced when extracellular K^+ is increased,[31] as well as during hypoxic conditions.[33] This points to the relevance of overshoots in extracellular K^+ for SD initiation. If large enough, such overshoots may render NMDAR antagonists ineffective against SD.[34] Similarly, we found that a potent NMDAR antagonist did not block SD in our FHM2 mouse model (**Chapter 3**), or massive depolarization in our FHM3 mouse model (**Chapter 6**). Instead, the persistent sodium current blocker GS967[35] effectively reduced SD frequency in homozygous FHM2 mice and prevented lethal massive brainstem depolarization in FHM3 mice, indicating

that persistent sodium currents are a promising target for SD prevention when extracellular K^+ overshoots are suspected.

Future research on initiation mechanisms of spreading depolarizations

Recently, increased concentrations of extracellular K^+ were demonstrated during SD in a different transgenic FHM3 mouse model that expresses the L1649Q missense mutation,[36] previously found in a Dutch family with hemiplegic migraine.[37] Similar to our data (**Chapter 2**), these mice showed a decreased threshold for induction of cortical SD (i.e. with electrical stimulation), with no differences in SD propagation velocity when compared to wildtype animals. This suggests a selective effect on SD initiation by increased extracellular concentrations of K^+. However, spontaneous SDs were not demonstrated in this FHM3 model. Indeed, there is currently no direct evidence of a critical role for K^+ overshoots – or any other mechanism – in SD initiation, since there is a paucity of models available to study spontaneous SDs reliably. One study demonstrated spontaneous cortical SDs in a mouse model with a knock-out of *Atp1a2* specifically in astrocytes.[38] It may be argued that such a model is not clinically representative of FHM2 because of the genetic approach used (homozygous knockout of *Atp1a2* limited to astrocytes), or because of the observed premature mortality such as in our models, as has been argued by some.[36] Indeed, in the models presented here, spontaneous (cortical) SDs always occurred in genotypes that were also prone to early mortality (see next paragraph). And yet, these models provide a unique possibility to study SD initiation mechanisms. Most notably, the complete penetrance of the SD phenotype shown for *Atp1a2*^{T345A} mice (**Chapter 3**) should facilitate the study of spontaneous SD. Longitudinal recordings and modulation of local extracellular K^+ [29, 30, 39] in such models would be a promising research strategy to identify alterations in network dynamics that culminate in SD initiation.

Part II: Mechanisms of sudden death

Although we have managed to breed mice with a monogenic mutation causing FHM1, -2 and -3, early mortality occurred in all models. Early mortality is not a typical feature of the clinical FHM phenotype, which may tempt us to perceive this as an oddity resulting from genetic dosage effects in these model organisms. However, in addition to homozygous animals, early mortality was especially striking in heterozygous *Scn1a*^{L263V} FHM3 mice (**Chapters 2 and 6**), which showed ~90% mortality at P60 (compared to ~30% in homozygous *Cacna1a*^{S218L} FHM1 mice[40] and ~40% in homozygous *Atp1a2*^{T345A} FHM2 mice (**Chapter 2**)). In addition, sporadic deaths were noted in heterozygous FHM2 mice to occur spontaneously and over the course of hippocampal kindling (**Chapter 3**). It should be noted that in all models deaths occurred suddenly, i.e. not secondary to impaired mobility or prolonged seizure activity. In fact, behavioral seizure activity was only a consistent phenotypical feature in *Cacna1a*^{S218L} mice. As described in **Chapters 4-6**, sudden deaths in homozygous *Cacna1a*^{S218L} and *Scn1a*^{L263V} mice were mediated by brainstem (spreading) depolarizations.

Brainstem SD in FHM models

Requirements for SDs to occur in brain tissue have been proposed to include tissue homogeneity, high neuronal density and absence of myelinated borders.[41] As such, the brainstem – which constitutes a region with nuclei of relatively low neuronal density and bordered by myelin-rich structures – appears cytoarchitecturally impervious to SD. *In vitro* and *ex vivo* experiments in the rat and mouse brainstem have indeed shown that brainstem regions are highly resistant to K^+-induced SD.[42, 43] However, SD could be induced by K^+ in the rat brainstem, be it after extensive preconditioning in order to create hyperexcitable conditions.[44] It is likely that in our studies, such hyperexcitable conditions are intrinsically met by the pathogenic mutation, rendering the brainstem much more sensitive to SD. For example, the $Na_V1.1$ sodium channel, encoded by the *Scn1a* gene, is abundantly expressed in the pons and medulla (**Figure 1**).[45] *Scn1a*^{L263V} gain-of-function effects may thus disproportionally affect brainstem excitability, culminating in the SD-induced apnea observed in *Scn1a*^{L263V} mice (**Chapter 6**).

FIGURE 1. Expression of NaV1.1 protein as detected by immunohistochemistry in mice pups with WT *Scn1a* (a) and (b) a homozygous R1407X nonsense mutation (RX/RX), resulting in truncated NaV1.1.

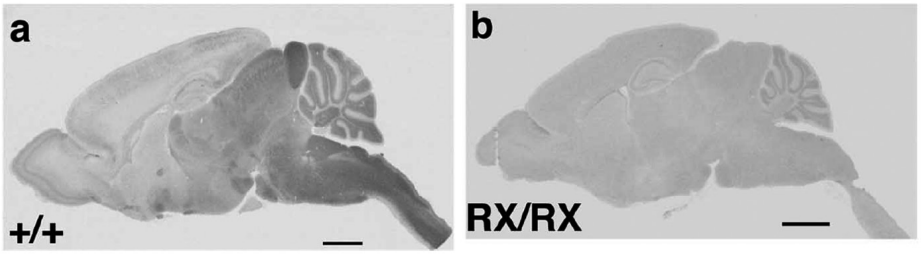

Note the marked differences in expression in the mid- and hindbrain. Scale bars indicating 1 mm. Source: Ogiwara et al. Nav1.1 Localizes to Axons of Parvalbumin-Positive Inhibitory Interneurons: A Circuit Basis for Epileptic Seizures in Mice Carrying an Scn1a Gene Mutation, Journal of Neuroscience 2007;27(22):5903-5914. Image reproduced with permission of the rights holder, Society of Neuroscience.

Despite a common sudden death phenotype, our studies reveal notable differences between the FHM1, -2 and -3 models. First of all, in *Cacna1a*^{S218L} mice all deaths were preceded by seizure behavior (**Chapters 4 and 5**). Second, brainstem SD evidently spread slowly – over the course of tens of seconds – throughout the brainstem. And finally, brainstem SD was not necessarily lethal in these animals, although it always suppressed breathing activity when involving the ventrolateral medulla. In contrast, *Scn1a*^{L263V} mice did not show behavioral or electrophysiological evidence of seizures, and brainstem "SD" in fact showed sub-second delay between brainstem regions, and was lethal in all cases (**Chapter 6**). As such, the expected propagation rate is an order of a magnitude greater in *Scn1a*^{L263V} mice when compared to *Cacna1a*^{S218L} mice, suggesting different mechanisms

of the observed depolarizations. This is further reflected by a different treatment response: whereas the sudden death phenotype in *Cacna1a*^{S218L} mice is completely rescued by NMDAR antagonist MK801 (**Chapter 5**), this drug was ineffective in *Scn1a*^{L263V} mice (**Chapter 6**). In accordance with the reasoning in the first paragraph, these results may be due to a selective effect of MK801 on inhibition of *SD propagation*, as occurring in *Cacna1a*^{S218L} mice, whereas modulation of brainstem depolarization in *Scn1a*^{L263V} mice may in fact require inhibition of *SD initiation*.

FIGURE 2. Location of the pre-Bötzinger complex in humans (A and B) and mice (C and D).

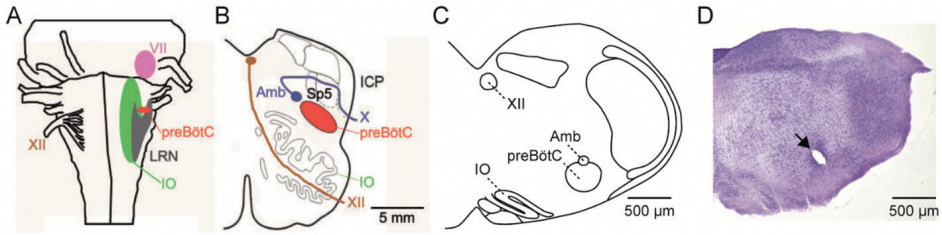

(A) Schematic ventral view of the human brainstem. (B and C) Schematic transversal view of the human (B) and mouse (C) brainstem, at the level of the pre-Bötzinger complex (preBötC). In both species, the pre-Bötzinger complex is located (latero)dorsal from the inferior olive (IO), interpositioned between the facial nucleus (VII) and lateral reticular nucleus (LRN) at the transversal level of the nucleus ambiguus (Amb) and hypoglossus (XII). (D) Lesion (arrow) produced at the electrode tip that recorded SDs in a *Cacna1a*^{S218L} mouse, located in the expected location of the pre-Bötzinger complex (**Chapter 6**). Source: panels A and B are adapted from Schwarzacher et al.,[47] panels C and D are adapted from Jansen et al.[51]

The vital node

Early descriptions by Pierre Flourens, a French physiologist and physician, identified a *noeud vital* – or "vital node" – in the medulla oblongata: a region critical for respiratory pacemaking. Later efforts, most notably a lesioning study,[46] have demonstrated that the *noeud vital* was in fact the pre-Bötzinger complex, a paired nucleus consisting of a few hundred neurons located in the ventrolateral medulla oblongata, which was later also identified in humans.[47] Since animal studies have shown that bilateral,[48, 49] but not unilateral,[50] disruption of the pre-Bötzinger complex results in lethal apnea, the slow propagation of SD would theoretically pose a less severe threat to humans when compared to smaller mammals such as mice: the distance between the bilateral nuclei is roughly a factor 5 – 10 times bigger in humans than in mice (**Figure 2**), with similar differences in nucleus size. Similar cortical SD propagation velocities in humans and smaller mammals[1, 7, 10] would thus predict a sub-minute delay between SDs in the pre-Bötzinger complex of mice, *versus* a delay of several minutes in humans, presuming an SD propagation rate of 2 – 4 mm/min in the brainstem.[44] Such timing differences could be crucial, since duration of non-fatal neuronal suppression by SD was around 1 – 1.5 min in our study in FHM1 mice (**Chapter 5**). These interspecies differences, in addition to cytoarchitectural differences such as increased thickness of myelin-rich borders,

could contribute to a lower risk of SD-induced fatal apnea in humans with similar genetic dosage compared to our model organisms.

Brainstem spreading depolarization: are humans at risk?

And yet, certain conditions may enhance the risk of SD-induced fatal apnea in both mice and humans. Up until now, we have presumed that SD originates from a single source, consecutively spreading through a heterogenous brainstem and impeded by white matter structures. However, SDs can occur in the setting of seizure activity.[52-54] Seizures can spread throughout brain tissue via contiguous grey matter, similar to SDs, clinically referred to as "Jacksonian march".[55] Alternatively, seizures can spread via white matter structures to homotopic regions.[56] As such, brainstem areas may become involved in the seizure network expanding from local[57] or more distant[58] epileptogenic foci, perhaps initiating SDs in multiple brainstem areas. This hypothesis would need verification in different SUDEP models, including larger model organisms.

In our FHM2 and FHM3 mouse models (**Chapters 2, 3 and 6**), sudden death occurred always (in FHM3) or mostly (FHM2) in the absence of electrographic or behavioral seizure activity. In *Scn1a*^{L263V} mice, fatal apnea coincided with profound depolarizations in two (relatively) distant brainstem electrodes, with often sub-second delay between the electrodes (**Chapter 6**). Such propagation velocities are incompatible with unifocal SD, and rather support a preceding synchronizing event. Such "prodromal" events have been demonstrated in the setting of hippocampal SD,[20] presumed to be mediated by gap junctions. Whether such a mechanism could premediate the massive brainstem depolarization observed in *Scn1a*^{L263V} mice remains a topic for future investigation. In any case, *SCN1A* mutations are clinically strongly associated with SUDEP, the leading cause of death in Dravet syndrome,[59] as well as sudden death in infancy (SIDS) and childhood (sudden unexpected death in pediatrics (SUDP)).[60-62] Although these mutations are typically considered to result in loss of function, missense variants may be rescued *in vivo*.[63] In addition, despite the tendency of sodium channel blockers to increase seizure frequency and severity in Dravet syndrome,[64] they effectively *reduced* lethality in *Scn1a* knockout mice.[65] This effective dissociation of seizure incidence and mortality risk was related to a decreased occurrence of tonic seizure behavior (tonic hindlimb extension),[65] which was associated with lethal apnea in another SUDEP mouse model.[66] Thus, our findings in *Scn1a*^{L263V} mice may extend to other *SCN1A* variants – in addition to the clinical homozygous *SCN1A*^{L263V} carrier we presented in **Chapter 6** – supporting a crucial role for brainstem (spreading) depolarization in sudden death.

Future research on mechanisms of sudden death

How then does the "brainstem SD" hypothesis relate to other hypotheses regarding sudden death pathophysiology? Both SUDEP and SIDS are considered to result from "cardiorespiratory dysfunction" and decreased arousal.[67] Slowly, this "cardiorespiratory dysfunction" has been specified as a sequence of respiratory arrest followed by cardiac arrest, most notably motivated by the MORTEMUS study.[68] Of course, cardiac-driven SUDEP/SIDS may occur, but the latter data

suggest that respiratory arrest underlies a majority of cases. This shift in thinking is aptly illustrated by data from animal studies, which demonstrated lethal bradycardia in a Dravet syndrome mouse model,[69] which was later shown to result from peri-ictal apnea.[70] Several mechanisms underlying sudden (peri-ictal) apnea have been proposed, including impaired CO_2-mediated arousal (whether or not related to brainstem serotonergic dysfunction),[67, 71] increased adenosine release,[72] and laryngospasm – either due to increased reflexes[73] or seizure activity in brainstem motor nuclei.[74, 75] In fact, several of these mechanisms may co-occur in SUDEP/SIDS cases. What these hypotheses have in common, however, is that integrity of neuronal activity is the *sine qua non*. The occurrence of brainstem SD under normoxic conditions – as demonstrated in our studies – would thus effectively decrease the relevance of these other hypothetical mechanisms to modulating factors (i.e. affecting SD risk and/or recovery of physiological activity following SD). As such, efforts should be made to investigate the plausibility of brainstem SD in patients at risk of sudden death. To do so, a first step would be to replicate our results in other SUDEP and SIDS animal models. Second, experiments in larger model organisms should be considered to approach the dimensions of the human brainstem. Similar to the postictal changes we observed in heart rate parameters in *Cacna1a*^{S218L} mice (**Chapter 5**), such studies could allow identification of SD-related changes in neurophysiology, behavior and vagal output to establish more readily available SD biomarkers that could facilitate its detection in patients.

Part III: Epileptogenesis in Dravet syndrome

A variant in the *SCN1A* gene is the most frequently encountered cause of monogenic epilepsy.[76] The associated phenotype, however, can range from no/mild epilepsy burden to the epileptic encephalopathy that constitutes Dravet syndrome, characterized by early-onset seizures and severe cognitive and behavioral deficits.[77, 78] In this respect, age of seizure onset was shown to be a better predictor than mutation type,[78] although a recent study showed increased prediction performance when a more elaborate *SCN1A* genetic score was added.[79] These improvements in outcome prediction will improve patient and caregiver counselling, yet improvement in treatment outcomes, including seizure control, will ultimately rely on more than baseline patient characteristics.

Probing for inhibitory dysfunction

Patients with Dravet syndrome will likely benefit from recent clinical treatment advances,[80, 81] as well as promising targeted interventions aimed at enhancing $Na_V1.1$ activity developed in pre-clinical research.[82-85] However, biomarkers for treatment monitoring are currently lacking, although the pathophysiological basis for Dravet syndrome is relatively well-understood. Haploinsufficiency of the *SCN1A* gene, encoding the α1 subunit of $Na_V1.1$ channels, is expected to result in decreased voltage-dependent sodium currents specifically in GABAergic interneurons,[86, 87] evidenced by selective expression of $Na_V1.1$ in inhibitory neurons[45, 88] and reproduction of the epileptic phenotype when *Scn1a* knockout is limited to inhibitory neurons.[89] These findings have helped explain clinical observations of adverse outcome in Dravet syndrome following treatment with lamotrigine, a

sodium channel blocker.[64] Studies have suggested, however, that interneuron impairment is not permanent in Dravet syndrome, as cortical GABAergic neurons show only transient impairment of excitability in *Scn1a*$^{-/+}$ mice,[90] while in the hippocampus only fast-spiking GABAergic neurons remain impaired.[91] Although *homozygous* knockout of *Scn1a* resulted in spontaneous seizures when limited to hippocampus or visual cortex (**Chapter 7**), local *heterozygous* knockout resulted in seizures only for hippocampus and not visual cortex (**Chapter 8**), indicating regional differences in epileptogenesis susceptibility. Since recently developed treatment strategies aim to increase transcriptional[84] or post-transcriptional[82] expression of the healthy *SCN1A* allele, it appears ever more crucial to know when and where to introduce such therapies for the individual patient. A good disease biomarker should ideally reflect both underlying neuronal dynamics, thereby for example preventing efforts to increase *SCN1A* expression in individuals that have $Na_V1.1$ functional dominant negative effects due to a gain of function,[92] as well as the clinical phenotype including seizure burden and cognitive deficits. In **Chapter 8**, we propose local field potential (LFP) theta-gamma phase-amplitude coupling as such a biomarker, by showing that it correlated with the expected transience in cortical inhibitory dysfunction, as well as with expression of seizure activity in mice with local or global *Scn1a* knockout. Further, these changes were shown to be amenable to acute cannabidiol treatment, which improved seizure burden in Dravet syndrome [80] and increased inhibitory functioning in *Scn1a*$^{-/+}$ mice.[93] The pattern of theta-gamma coupling, i.e. coupling of theta to high *versus* low gamma, correlated with the locality of $Na_V1.1$ dysfunction (i.e. neocortex *versus* hippocampus). As such, theta-gamma coupling may aid in determining the strategy, timing and location of treatment in Dravet syndrome.

Future research on theta-gamma coupling

However, challenges await before such a biomarker can be clinically implemented. First, detection of oscillations noninvasively, such as in scalp EEG, is generally limited to frequencies <100 Hz. Second, localization of subcortical activity from scalp EEG is often not considered feasible. Lastly, although neocortical theta-gamma coupling has been demonstrated in human subjects during cognitive processing,[94] it is likely much more abundant in the neocortex of mice due to volume conductance of theta oscillations from hippocampal sources in the latter.[95, 96] Yet, relatively recently have investigators managed to record (biologically relevant) higher frequencies such as high-frequency oscillations,[97, 98] as well as subcortical activity[99-101] from scalp EEG and/or MEG. Since fast-spiking GABAergic interneurons importantly contribute to (high) gamma oscillations[102, 103] and remain impaired in the hippocampus of *Scn1a*$^{-/+}$ mice,[91] such advances may be critical for informative recordings in Dravet syndrome.

The quest for a biomarker of inhibitory dysfunction will not only benefit patients with Dravet syndrome. Impaired hippocampal theta-gamma coupling has been associated with dysfunctional fast-spiking GABAergic interneurons in animal models of temporal lobe epilepsy[104] and Alzheimer's disease.[105-107] Clinically, these disease processes show overlap, as epilepsy and epilepsy-related cognitive decline are associated with amyloid β aggregation[108] – a characteristic

finding in Alzheimer's disease – whereas increased seizure risk[109] as well as subclinical epileptiform activity,[110] which may remain undetected on EEG,[111] are associated with Alzheimer's disease. Similarly, identical treatment strategies aimed at improving inhibitory dysfunction could benefit multiple patient groups, as has been demonstrated for models of Alzheimer's disease and Dravet syndrome.[112] As such, a primary aim should be to establish a clinically reproducible measure of theta-gamma coupling or other markers of dysfunctional network inhibition in order to guide treatment and provide insight in pathophysiological similarities and differences between these neurological disorders.

REFERENCES

1. Leao, A.A., Spreading depression of activity in the cerebral cortex. *Journal of neurophysiology*, 1944. 7(6): p. 359-390.
2. Headache Classification Committee of the International Headache Society (IHS) The International Classification of Headache Disorders, 3rd edition. *Cephalalgia*, 2018. 38(1): p. 1-211.
3. Wolff, H.G., Headache and Other Head Pain. Vol. 2nd Edition. 1963: Oxford University Press, New York.
4. Lauritzen, M., Pathophysiology of the migraine aura. The spreading depression theory. *Brain*, 1994. 117 (Pt 1): p. 199-210.
5. Lashley, K.S., Patterns of cerebral integration indicated by the scotomas of migraine. *Archives of Neurology & Psychiatry*, 1941. 46(2): p. 331-339.
6. Olesen, J., et al., Timing and topography of cerebral blood flow, aura, and headache during migraine attacks. *Ann Neurol*, 1990. 28(6): p. 791-8.
7. Olesen, J., B. Larsen, and M. Lauritzen, Focal hyperemia followed by spreading oligemia and impaired activation of rCBF in classic migraine. *Ann Neurol*, 1981. 9(4): p. 344-52.
8. Woods, R.P., M. Iacoboni, and J.C. Mazziotta, Brief report: bilateral spreading cerebral hypoperfusion during spontaneous migraine headache. *N Engl J Med*, 1994. 331(25): p. 1689-92.
9. Lauritzen, M., et al., Changes in regional cerebral blood flow during the course of classic migraine attacks. *Ann Neurol*, 1983. 13(6): p. 633-41.
10. Hadjikhani, N., et al., Mechanisms of migraine aura revealed by functional MRI in human visual cortex. *Proc Natl Acad Sci U S A*, 2001. 98(8): p. 4687-92.
11. Fox, A.W. and R.L. Davis, Migraine chronobiology. *Headache*, 1998. 38(6): p. 436-41.
12. van Oosterhout, W., et al., Chronotypes and circadian timing in migraine. *Cephalalgia*, 2018. 38(4): p. 617-625.
13. Kelman, L. and J.C. Rains, Headache and sleep: examination of sleep patterns and complaints in a large clinical sample of migraineurs. *Headache*, 2005. 45(7): p. 904-10.
14. Pietrobon, D. and M.A. Moskowitz, Chaos and commotion in the wake of cortical spreading depression and spreading depolarizations. *Nat Rev Neurosci*, 2014. 15(6): p. 379-93.
15. Capuani, C., et al., Defective glutamate and K+ clearance by cortical astrocytes in familial hemiplegic migraine type 2. *EMBO Mol Med*, 2016. 8(8): p. 967-86.
16. Parker, P.D., et al., Non-canonical glutamate signaling in a genetic model of migraine with aura. *Neuron*, 2021. 109(4): p. 611-628 e8.
17. Somjen, G.G., Mechanisms of spreading depression and hypoxic spreading depression-like depolarization. *Physiol Rev*, 2001. 81(3): p. 1065-96.
18. Vitale, M., et al., Mechanisms of initiation of cortical spreading depression. *J Headache Pain*, 2023. 24(1): p. 105.
19. Mei, Y.-Y., et al., NMDA receptors sustain but do not initiate neuronal depolarization in spreading depolarization. *Neurobiology of Disease*, 2020. 145: p. 105071.
20. Herreras, O., et al., Role of neuronal synchronizing mechanisms in the propagation of spreading depression in the in vivo hippocampus. *J Neurosci*, 1994. 14(11 Pt 2): p. 7087-98.

21. Rosenblueth, A. and J. García Ramos, Some phenomena usually associated with spreading depression. *Acta physiol. latinoam*, 1966: p. 141-79.
22. Homayoun, H. and B. Moghaddam, NMDA receptor hypofunction produces opposite effects on prefrontal cortex interneurons and pyramidal neurons. *J Neurosci*, 2007. 27(43): p. 11496-500.
23. Yao, L., et al., Higher ambient synaptic glutamate at inhibitory versus excitatory neurons differentially impacts NMDA receptor activity. *Nat Commun*, 2018. 9(1): p. 4000.
24. Grafstein, B., Mechanism of spreading cortical depression. *Journal of neurophysiology*, 1956. 19(2): p. 154-171.
25. Segall, L., et al., Kinetic alterations due to a missense mutation in the Na,K-ATPase alpha2 subunit cause familial hemiplegic migraine type 2. *J Biol Chem*, 2004. 279(42): p. 43692-6.
26. Kahlig, K.M., et al., Divergent sodium channel defects in familial hemiplegic migraine. *Proc Natl Acad Sci U S A*, 2008. 105(28): p. 9799-804.
27. Desroches, M., et al., Modeling cortical spreading depression induced by the hyperactivity of interneurons. *J Comput Neurosci*, 2019.
28. Chever, O., et al., Initiation of migraine-related cortical spreading depolarization by hyperactivity of GABAergic neurons and NaV1.1 channels. *J Clin Invest*, 2021. 131(21).
29. Ding, F., et al., Changes in the composition of brain interstitial ions control the sleep-wake cycle. *Science*, 2016. 352(6285): p. 550-555.
30. Rasmussen, R., et al., Cortex-wide changes in extracellular potassium ions parallel brain state transitions in awake behaving mice. *Cell reports*, 2019. 28(5): p. 1182-1194. e4.
31. Somjen, G.G. and M. Muller, Potassium-induced enhancement of persistent inward current in hippocampal neurons in isolation and in tissue slices. *Brain Res*, 2000. 885(1): p. 102-10.
32. Taylor, C.P., Na+ currents that fail to inactivate. *Trends in neurosciences*, 1993. 16(11): p. 455-460.
33. Hammarström, A. and P. Gage, Inhibition of oxidative metabolism increases persistent sodium current in rat CA1 hippocampal neurons. *The Journal of physiology*, 1998. 510(3): p. 735-741.
34. Petzold, G.C., et al., Increased extracellular K+ concentration reduces the efficacy of N-methyl-D-aspartate receptor antagonists to block spreading depression-like depolarizations and spreading ischemia. *Stroke*, 2005. 36(6): p. 1270-7.
35. Baker, E.M., et al., The novel sodium channel modulator GS-458967 (GS967) is an effective treatment in a mouse model of SCN8A encephalopathy. *Epilepsia*, 2018. 59(6): p. 1166-1176.
36. Auffenberg, E., et al., Hyperexcitable interneurons trigger cortical spreading depression in an Scn1a migraine model. *J Clin Invest*, 2021. 131(21).
37. Vanmolkot, K.R., et al., The novel p.L1649Q mutation in the SCN1A epilepsy gene is associated with familial hemiplegic migraine: genetic and functional studies. Mutation in brief #957. Online. *Hum Mutat*, 2007. 28(5): p. 522.
38. Smith, S.E., et al., Astrocyte deletion of alpha2-Na/K ATPase triggers episodic motor paralysis in mice via a metabolic pathway. *Nat Commun*, 2020. 11(1): p. 6164.
39. Kudo, C., et al., Anesthetic effects on susceptibility to cortical spreading depression. *Neuropharmacology*, 2013. 67: p. 32-6.

40. van den Maagdenberg, A.M., et al., High cortical spreading depression susceptibility and migraine-associated symptoms in Ca(v)2.1 S218L mice. *Ann Neurol*, 2010. 67(1): p. 85-98.
41. Bureš, J., O. Burešová, and J. Křivánek, The mechanism and applications of Leao's spreading depression of electroencephalographic activity. 1974: *Academic Press*.
42. Andrew, R.D., Y.T. Hsieh, and C.D. Brisson, Spreading depolarization triggered by elevated potassium is weak or absent in the rodent lower brain. *J Cereb Blood Flow Metab*, 2016: p. 271678X16657344.
43. Richter, F., et al., Spreading depression can be elicited in brain stem of immature but not adult rats. *J Neurophysiol*, 2003. 90(4): p. 2163-70.
44. Richter, F., et al., Spreading depression in the brainstem of the adult rat: electrophysiological parameters and influences on regional brainstem blood flow. *J Cereb Blood Flow Metab*, 2008. 28(5): p. 984-94.
45. Ogiwara, I., et al., Nav1.1 localizes to axons of parvalbumin-positive inhibitory interneurons: a circuit basis for epileptic seizures in mice carrying an Scn1a gene mutation. *J Neurosci*, 2007. 27(22): p. 5903-14.
46. Smith, J.C., et al., Pre-Bötzinger complex: a brainstem region that may generate respiratory rhythm in mammals. *Science*, 1991. 254(5032): p. 726-729.
47. Schwarzacher, S.W., U. Rub, and T. Deller, Neuroanatomical characteristics of the human pre-Botzinger complex and its involvement in neurodegenerative brainstem diseases. *Brain*, 2011. 134(Pt 1): p. 24-35.
48. Gray, P.A., et al., Normal breathing requires preBotzinger complex neurokinin-1 receptor-expressing neurons. *Nat Neurosci*, 2001. 4(9): p. 927-30.
49. McKay, L.C., W.A. Janczewski, and J.L. Feldman, Sleep-disordered breathing after targeted ablation of preBotzinger complex neurons. *Nat Neurosci*, 2005. 8(9): p. 1142-4.
50. McKay, L.C. and J.L. Feldman, Unilateral ablation of pre-Botzinger complex disrupts breathing during sleep but not wakefulness. *American journal of respiratory and critical care medicine*, 2008. 178(1): p. 89-95.
51. Jansen, N.A., et al., Apnea associated with brainstem seizures in Cacna1a (S218L) mice is caused by medullary spreading depolarization. *J Neurosci*, 2019. 39(48): p. 9633-9644.
52. Bastany, Z.J.R., et al., Association of cortical spreading depression and seizures in patients with medically intractable epilepsy. *Clin Neurophysiol*, 2020. 131(12): p. 2861-2874.
53. Zakharov, A., et al., Segregation of seizures and spreading depolarization across cortical layers. *Epilepsia*, 2019. 60(12): p. 2386-2397.
54. Tamim, I., et al., Spreading depression as an innate antiseizure mechanism. *Nat Commun*, 2021. **12**(1): p. 2206.
55. Jasper, H.H., *Basic Mechanisms of the Epilepsies*. 1969.
56. Rossi, L.F., et al., Focal cortical seizures start as standing waves and propagate respecting homotopic connectivity. *Nat Commun*, 2017. 8(1): p. 217.
57. Pospelov, A.S., et al., Forebrain-independent generation of hyperthermic convulsions in infant rats. *Epilepsia*, 2016. 57(1): p. e1-6.
58. Derera, I.D., B.P. Delisle, and B.N. Smith, Functional Neuroplasticity in the Nucleus Tractus Solitarius and Increased Risk of Sudden Death in Mice with Acquired Temporal Lobe Epilepsy. *eNeuro*, 2017. **4**(5).
59. Shmuely, S., et al., Mortality in Dravet syndrome: A review. *Epilepsy Behav*, 2016. 64(Pt A): p. 69-74.

60. Brownstein, C.A., et al., SCN1A variants associated with sudden infant death syndrome. *Epilepsia*, 2018. 59(4): p. e56-e62.
61. Koh, H.Y., et al., Genetic Determinants of Sudden Unexpected Death in Pediatrics. *Genet Med*, 2022. 24(4): p. 839-850.
62. Rochtus, A.M., et al., The role of sodium channels in sudden unexpected death in pediatrics. *Mol Genet Genomic Med*, 2020. 8(8): p. e1309.
63. Cestele, S., et al., Nonfunctional NaV1.1 familial hemiplegic migraine mutant transformed into gain of function by partial rescue of folding defects. *Proc Natl Acad Sci U S A*, 2013. 110(43): p. 17546-51.
64. Guerrini, R., et al., Lamotrigine and seizure aggravation in severe myoclonic epilepsy. *Epilepsia*, 1998. 39(5): p. 508-12.
65. Hawkins, N.A., et al., Screening of conventional anticonvulsants in a genetic mouse model of epilepsy. *Ann Clin Transl Neurol*, 2017. 4(5): p. 326-339.
66. Wenker, I.C., et al., Postictal Death Is Associated with Tonic Phase Apnea in a Mouse Model of Sudden Unexpected Death in Epilepsy. *Ann Neurol*, 2021. 89(5): p. 1023-1035.
67. Devinsky, O., et al., Sudden unexpected death in epilepsy: epidemiology, mechanisms, and prevention. *Lancet Neurol*, 2016. 15(10): p. 1075-88.
68. Ryvlin, P., et al., Incidence and mechanisms of cardiorespiratory arrests in epilepsy monitoring units (MORTEMUS): a retrospective study. *Lancet Neurol*, 2013. 12(10): p. 966-77.
69. Kalume, F., et al., Sudden unexpected death in a mouse model of Dravet syndrome. *J Clin Invest*, 2013. 123(4): p. 1798-808.
70. Kim, Y., et al., Severe peri-ictal respiratory dysfunction is common in Dravet syndrome. *J Clin Invest*, 2018. 128(3): p. 1141-1153.
71. Buchanan, G.F., Impaired CO2-Induced Arousal in SIDS and SUDEP. *Trends Neurosci*, 2019. 42(4): p. 242-250.
72. Massey, C.A., et al., Mechanisms of sudden unexpected death in epilepsy: the pathway to prevention. *Nat Rev Neurol*, 2014. 10(5): p. 271-82.
73. Leiter, J. and I. Böhm, Mechanisms of pathogenesis in the sudden infant death syndrome. *Respiratory physiology & neurobiology*, 2007. 159(2): p. 127-138.
74. Nakase, K., et al., Laryngospasm, central and obstructive apnea during seizures: Defining pathophysiology for sudden death in a rat model. *Epilepsy Res*, 2016. 128: p. 126-139.
75. Stewart, M., et al., Obstructive apnea due to laryngospasm links ictal to postictal events in SUDEP cases and offers practical biomarkers for review of past cases and prevention of new ones. *Epilepsia*, 2017.
76. Symonds, J.D., et al., Incidence and phenotypes of childhood-onset genetic epilepsies: a prospective population-based national cohort. *Brain*, 2019. 142(8): p. 2303-2318.
77. Wolff, M., C. Casse-Perrot, and C. Dravet, Severe myoclonic epilepsy of infants (Dravet syndrome): natural history and neuropsychological findings. *Epilepsia*, 2006. 47 Suppl 2: p. 45-8.
78. Cetica, V., et al., Clinical and genetic factors predicting Dravet syndrome in infants with SCN1A mutations. *Neurology*, 2017. 88(11): p. 1037-1044.
79. Brunklaus, A., et al., Development and Validation of a Prediction Model for Early Diagnosis of SCN1A-Related Epilepsies. *Neurology*, 2022.

80. Devinsky, O., et al., Trial of Cannabidiol for Drug-Resistant Seizures in the Dravet Syndrome. *N Engl J Med*, 2017. 376(21): p. 2011-2020.
81. Lagae, L., et al., Fenfluramine hydrochloride for the treatment of seizures in Dravet syndrome: a randomised, double-blind, placebo-controlled trial. *Lancet*, 2019. 394(10216): p. 2243-2254.
82. Han, Z., et al., Antisense oligonucleotides increase Scn1a expression and reduce seizures and SUDEP incidence in a mouse model of Dravet syndrome. *Sci Transl Med*, 2020. 12(558).
83. Richards, K.L., et al., Selective NaV1.1 activation rescues Dravet syndrome mice from seizures and premature death. *Proc Natl Acad Sci U S A*, 2018. 115(34): p. E8077-E8085.
84. Colasante, G., et al., dCas9-Based Scn1a Gene Activation Restores Inhibitory Interneuron Excitability and Attenuates Seizures in Dravet Syndrome Mice. *Mol Ther*, 2020. 28(1): p. 235-253.
85. Fadila, S., et al., Viral vector-mediated expression of NaV1.1, after seizure onset, reduces epilepsy in mice with Dravet syndrome. *J Clin Invest*, 2023. 133(12).
86. Yu, F.H., et al., Reduced sodium current in GABAergic interneurons in a mouse model of severe myoclonic epilepsy in infancy. *Nat Neurosci*, 2006. 9(9): p. 1142-9.
87. Sun, Y., et al., A deleterious Nav1.1 mutation selectively impairs telencephalic inhibitory neurons derived from Dravet Syndrome patients. *Elife*, 2016. 5.
88. Lorincz, A. and Z. Nusser, Cell-type-dependent molecular composition of the axon initial segment. *J Neurosci*, 2008. 28(53): p. 14329-40.
89. Cheah, C.S., et al., Specific deletion of NaV1.1 sodium channels in inhibitory interneurons causes seizures and premature death in a mouse model of Dravet syndrome. *Proc Natl Acad Sci U S A*, 2012. 109(36): p. 14646-51.
90. Favero, M., et al., A Transient Developmental Window of Fast-Spiking Interneuron Dysfunction in a Mouse Model of Dravet Syndrome. *J Neurosci*, 2018. 38(36): p. 7912-7927.
91. Valassina, N., et al., Scn1a gene reactivation after symptom onset rescues pathological phenotypes in a mouse model of Dravet syndrome. *Nat Commun*, 2022. 13(1): p. 161.
92. Berecki, G., et al., *SCN1A* gain of function in early infantile encephalopathy. *Ann Neurol*, 2019. 85(4): p. 514-525.
93. Kaplan, J.S., et al., Cannabidiol attenuates seizures and social deficits in a mouse model of Dravet syndrome. P*roc Natl Acad Sci U S A*, 2017. 114(42): p. 11229-11234.
94. Canolty, R.T., et al., High gamma power is phase-locked to theta oscillations in human neocortex. *Science*, 2006. 313(5793): p. 1626-8.
95. Gerbrandt, L.K., et al., Origin of the neocortically monitored theta rhythm in the curarized rat. Electroencephalogr Clin Neurophysiol, 1978. 45(4): p. 454-67.
96. Sirota, A., et al., Entrainment of neocortical neurons and gamma oscillations by the hippocampal theta rhythm. Neuron, 2008. 60(4): p. 683-97.
97. Andrade-Valenca, L.P., et al., Interictal scalp fast oscillations as a marker of the seizure onset zone. *Neurology*, 2011. 77(6): p. 524-31.
98. Cai, Z., et al., Noninvasive high-frequency oscillations riding spikes delineates epileptogenic sources. *Proc Natl Acad Sci U S A*, 2021. 118(17).

99. Roux, F., et al., The phase of thalamic alpha activity modulates cortical gamma-band activity: evidence from resting-state MEG recordings. *J Neurosci*, 2013. 33(45): p. 17827-35.
100. Krishnaswamy, P., et al., Sparsity enables estimation of both subcortical and cortical activity from MEG and EEG. *Proc Natl Acad Sci U S A*, 2017. 114(48): p. E10465-E10474.
101. Seeber, M., et al., Subcortical electrophysiological activity is detectable with high-density EEG source imaging. *Nature communications*, 2019. 10(1): p. 1-7.
102. Freund, T.F. and I. Katona, Perisomatic inhibition. *Neuron*, 2007. 56(1): p. 33-42.
103. Buzsaki, G. and X.J. Wang, Mechanisms of gamma oscillations. *Annu Rev Neurosci*, 2012. 35: p. 203-25.
104. Lopez-Pigozzi, D., et al., Altered Oscillatory Dynamics of CA1 Parvalbumin Basket Cells during Theta-Gamma Rhythmopathies of Temporal Lobe Epilepsy. *eNeuro*, 2016. 3(6).
105. Verret, L., et al., Inhibitory interneuron deficit links altered network activity and cognitive dysfunction in Alzheimer model. *Cell*, 2012. 149(3): p. 708-21.
106. Ittner, A.A., et al., p38 MAP kinase-mediated NMDA receptor-dependent suppression of hippocampal hypersynchronicity in a mouse model of Alzheimer's disease. *Acta Neuropathol Commun*, 2014. 2: p. 149.
107. Zhang, X., et al., Impaired theta-gamma coupling in APP-deficient mice. *Sci Rep*, 2016. 6: p. 21948.
108. Romoli, M., et al., Amyloid-β: a potential link between epilepsy and cognitive decline. *Nature Reviews Neurology*, 2021. 17(8): p. 469-485.
109. Scarmeas, N., et al., Seizures in Alzheimer disease: who, when, and how common? *Archives of neurology*, 2009. 66(8): p. 992-997.
110. Vossel, K.A., et al., Incidence and impact of subclinical epileptiform activity in Alzheimer's disease. *Ann Neurol*, 2016. 80(6): p. 858-870.
111. Lam, A.D., et al., Silent hippocampal seizures and spikes identified by foramen ovale electrodes in Alzheimer's disease. *Nat Me*d, 2017. 23(6): p. 678-680.
112. Hanson, J.E., et al., GluN2A NMDA Receptor Enhancement Improves Brain Oscillations, Synchrony, and Cognitive Functions in Dravet Syndrome and Alzheimer's Disease Models. *Cell Rep*, 2020. 30(2): p. 381-396 e4

Appendix

Summary
Samenvatting
Curriculum Vitae
List of publications
Dankwoord

SUMMARY

In this thesis, animal models are developed and characterized to study the mechanisms and potential lethal outcome of spontaneous seizures and spreading depolarizations (SDs).

In **Part I**, two new familial hemiplegic migraine (FHM) mouse models are described. Spontaneous SDs occurred in a subset of mice expressing the FHM3-related L263V mutation in α1 subunits of voltage-gated $Na_V1.1$ sodium channels (**Chapter 2**). These events invariably spread from the visual to the motor cortex. A similar caudal-to-rostral spreading pattern was noted for spontaneous SDs in mice expressing the FHM2-related T345A mutation in α2 subunits of the Na^+/K^+ adenosine triphosphatase pump (**Chapter 3**). These SDs were found to originate mostly from the hippocampus in markedly regular intervals with a diurnal rhythm. Despite increased hippocampal excitability as evidenced by SD susceptibility, seizure expression was in fact decreased. NMDA receptor and sodium channel modulation differentially affected SD initiation and propagation in these animals. As opposed to previous studies that induced SDs via an external trigger, these findings allow differentiation of SD initiation and propagation mechanisms.

In **Part II**, disease mechanisms of sudden death in the presence (**Chapters 4 and 5**) or absence (**Chapter 6**) of epilepsy are described. Fatal seizures, occurring in mice expressing a homozygous S218L missense mutation in the α1A subunit of $Ca_V2.1$ P/Q-type $Ca2^+$ channels, were associated with global neuronal suppression and respiratory arrest that coincided with changes in diffusion-weighted MRI signal in the brainstem, which preceded cardiac arrest (**Chapter 4**). Further studies of neuronal activity in the brainstem's regions critical for respiratory functioning show that suppression of neuronal activity in these regions occurred during fatal seizures, as well as during non-fatal seizures associated with prolonged apnea (**Chapter 5**). Such suppression of neuronal activity was caused by brainstem SD, and death could be prevented by timely respiratory resuscitation. Importantly, prevention of seizure-related SD using NMDA receptor antagonists also prevented fatal apnea. In **Chapter 6**, events of sudden apnea are described that occurred in the absence of seizure activity in an infant with a homozygous $SCN1A^{L263V}$ missense mutation. Similar non-seizure apneic events occurred in mice carrying the same mutation, which were associated with a large brainstem DC-shift. Sudden suppression of neuronal activity occurred during the DC-shift, which was associated with fatal apnea onset. These neuronal dynamics – brought about by gain-of-function effects in sodium channel functioning – could be prevented by sodium channel blockade, which prevented brainstem DC-shifts and fatal apnea in the mice. Similarly, apneic events in the infant decreased following treatment with a sodium channel blocker. Together, these studies substantiate brainstem SD as a potential mechanism for fatal apnea even in the absence of seizure activity.

In **Part III**, the epileptogenic potential and neuronal dynamics in brain-wide (global) *versus* local $Na_V1.1$ channel ablation are studied in the context of Dravet syndrome, an epileptic encephalopathy. Both hippocampal and focal cortical ablation of *Scn1a*, a gene affected in the majority of Dravet syndrome patients which encodes the α1 subunit of voltage-gated $Na_V1.1$ sodium channels, was sufficient to induce spontaneous seizures in mice (**Chapter 7**). Global knock-out of *Scn1a* resulted in an early decrease in theta-gamma cross-frequency coupling which only persisted in mice that developed spontaneous seizures (**Chapter 8**). Decreases in theta-gamma cross-frequency coupling – associated with impaired functioning of inhibitory interneurons in modeling experiments – preceded seizures following local ablation of *Scn1a*. As such, these data suggest theta-gamma cross-frequency coupling as an early indicator of epileptogenesis in Dravet syndrome.

SAMENVATTING

Dit proefschrift beschrijft de ontwikkeling en karakteristieken van diermodellen teneinde de oorzaken en de mogelijk dodelijke gevolgen van spontane epileptische aanvallen en spreidende depolarizaties (SDs) beter te begrijpen.

In **Deel I** worden twee nieuwe muismodellen voor familiaire hemiplegische migraine (FHM) beschreven. Spontane SDs werden gezien in een deel van de muizen met de FHM3-gerelateerde L263V mutatie in α1 subunits van voltage-afhankelijke $Na_V1.1$ natrium kanalen (**Hoofdstuk 2)**. Deze SDs toonden een karakteristiek spreidingspatroon vanuit de visuele naar de motorische cortex. Een vergelijkbaar caudaal-naar-rostraal spreidingspatroon werd gezien bij sponane SDs in muizen met de FHM2-gerelateerde T345A mutatie in α2 subunits van de Na^+/K^+ adenosine trifosfatase (ATPase) pomp. SDs in deze muizen initieerden in de hippocampus en traden met regelmaat op met een herkenbaar dag/nachtritme. Hoewel de spontane SDs blijk geven van een toegenomen hippocampale exciteerbaarheid, bleken de dieren juist minder gevoelig te zijn voor het induceren van een epileptische aanval. De initiatie en voortgeleiding van de SD bleek verschillend te kunnen worden beïnvloed door middel van farmacologische modulatie van NMDA receptoren en natriumkanalen in deze dieren. Deze bevindingen tonen daarmee aan dat de mechanismen van SD initiatie en voortgeleiding van elkaar kunnen worden gedifferentieerd, wat niet mogelijk was in eerdere studies waarin SDs actief geïnduceerd werden.

In **Deel II** worden mechanismen voor plotse dood beschreven, optredend in de aanwezigheid (**Hoofdstukken 4 en 5**) of afwezigheid (**Hoofdstuk 6**) van epilepsie. Muizen met een homozygote S218L mutatie in de **α1**A subunit van $Ca_V2.1$ P/Q-type Ca^{2+} kanalen toonden fatale epileptische aanvallen, welke geassocieerd waren met suppressie van corticale neuronale activiteit, respiratoir falen en veranderingen in diffusie-gewogen MRI signaal in de hersenstam, alvorens hartstilstand optrad (**Hoofdstuk 4**). Monitoring van neuronale activiteit in een hersenstam regio verantwoordelijk voor de regulering van de ademhaling toonde onderdrukking van neuronale acitiviteit tijdens fatale epileptische aanvallen, alsook tijdens niet-fatale aanvallen waarbij langdurige apneu optrad (**Hoofdstuk 5**). Deze onderdrukking van neuronale acitiviteit werd veroorzaakt door een SD in de hersenstam, en tijdige repiratoire ondersteuning middels mechanische ventilatie kon een fatale afloop voorkomen. NMDA receptor antagonisten blokkeerden het optreden van SD tijdens de epileptische aanval, alsook de daarop volgende fatale apneu. In **Hoofdstuk 6** wordt een casus beschreven van een kind met een homozygote *SCN1A*^{L263V} mutatie waarbij plotse en levensgevaarlijke apneus optraden zonder dat er sprake bleek te zijn van epileptische aanvallen. Vergelijkbare plotse apneus in de afwezigheid van epileptische aanvallen werden gezien in muizen met dezelfde genetische mutatie. Deze plotse apneus traden gelijktijdig op met een snelle verandering in DC-potentiaal in de hersenstam, welke geassocieerd waren met een massale neuronale depolarisatie gevolgd door neuronale inacitiveit ter plaatse. Dit phenotype, welke verklaard kon worden door een toegenomen

werking van natriumkanalen in de mutant, kon worden voorkomen door farmacologische blokkade van natriumkanalen, wat preventief werkte op zowel de SD in de hersenstam als de fatale apneu. In het kind leidde een vergelijkbare medicamentueze behandeling tot een afname van levensgevaarlijke apneus. Tezamen tonen deze studies aan dat SDs in de hersenstam overwogen moeten worden als een mechanisme voor het optreden van fatale apneus, zelfs in de afwezigheid van epileptische aanvallen.

In **Deel III** van dit proefschrift wordt het epileptogene effect van globale (gehele hersenparenchym) *versus* lokale ablatie van $Na_V1.1$ kanalen onderzocht in de context van het syndroom van Dravet, een epileptische encephalopathie. Zowel hippocampale als focale corticale ablatie van *Scn1a* – het gen dat codeert voor de **α**1 subunit van voltage-afhankelijke $Na_V1.1$ natriumkanalen en wat is aangedaan in de meerderheid van de patiënten met het syndroom van Dravet – was voldoende om spontane epileptische aanvallen te veroorzaken in muizen (**Hoofdstuk 7**). Globale deletie van *Scn1a* in muizen resulteerde in een vroege afname van de modulatie van gamma-frequentie amplitude door theta-frequentie fase (*theta-gamma cross-frequency coupling*) (**Hoofdstuk 8**). Deze afname bleef op latere leeftijd alleen bestaan in muizen die spontane epileptische aanvallen ontwikkelden. Afnames in *theta-gamma cross-frequency coupling* – geassocieerd met een dysfunctie van inhibitoire interneuronen in een computermodel – na lokale ablatie van *Scn1a,* gingen vooraf aan de ontwikkeling van epileptische aanvallen. Deze bevindingen impliceren dat *theta-gamma cross-frequency coupling* als een mogelijke vroege indicator van epileptogenese kan fungeren bij patiënten met het syndroom van Dravet.

CURRICULUM VITAE

Nico Adrian Jansen was born in Town of Urbana, New York, USA, on February 28, 1991. He grew up in Leende, The Netherlands, and finished his secondary education in 2009 from Were Di college, Valkenswaard. After obtaining his BSc in medicine at the Erasmus Medical Center, Rotterdam, he continued with the MSc in Medicine, and a Research MSc in Neuroscience, initially also at the Erasmus Medical Center. During the MSc Neuroscience, he performed anatomical tracing studies to map potential pathways involved in the central mechanisms of itch under the supervision of Dr. J. Holstege. He continued these studies at the laboratory of Prof. G.J. Giesler at the University of Minnesota, USA, where he performed electrophysiological experiments to study the involvement of trigeminoparabrachial tract neurons in itch and pain neurotransmission. While continuing with his clinical rotations, a research project on cerebellar interference with seizure activity, in the group of Prof. F.E. Hoebeek, Erasmus Medical Center, piqued his interest in epilepsy research. After obtaining both Master's degrees, he joined the group of Prof. A.M.J.M. van den Maagdenberg and Dr. E.A. Tolner at the Department of Human Genetics at Leiden University Medical Center in 2016 to work on a PhD project on the mechanisms of Sudden Unexpected Death in Epilepsy, which was complemented by studies on sudden death, spreading depolarizations and epileptogenesis in other transgenic mouse models. In 2021, he resumed his clinical work as a radiology resident at Maasstad Hospital and the Erasmus Medical Center, Rotterdam. During his clinical work, he finished and published the final manuscripts presented in this thesis. After completion of his radiology residency in 2026, he will work as an interventional radiologist at Maasstad Hospital.

LIST OF PUBLICATIONS

Jansen NA, Linnenbank C, Schenke M, Voskuyl RA, Jorge MS, Krivoshein G, Breukel C, Linssen MM, Claassens JW, Brouwers C, van Heiningen SH, Heuck A, Lykke-Hartmann K, Tolner EA, van den Maagdenberg AM. Spontaneous spreading depolarizations originate subcortically in a novel mouse model of familial hemiplegic migraine type 2.
Neurobiology of Disease. 2024 Nov 1;202:106714.

Jansen NA, Cestèle S, Marco SS, Schenke M, Stewart K, Patel J, Tolner EA, Brunklaus A, Mantegazza M, van den Maagdenberg AM. Brainstem depolarization–induced lethal apnea associated with gain-of-function *SCN1A* ^{L263V} is prevented by sodium channel blockade.
Proceedings of the National Academy of Sciences. 2024 Apr 2;121(14):e2309000121.

Jansen NA, van den Maagdenberg AM. Spatial and temporal manipulation of the Scn1a gene affect adult brain function.
Brain. 2024 Apr;147(4):e29-30.

Rooda OH, Kros L, Faneyte SJ, Holland PJ, Gornati SV, Poelman HJ, **Jansen NA**, Tolner EA, van den Maagdenberg AM, De Zeeuw CI, Hoebeek FE. Single-pulse stimulation of cerebellar nuclei stops epileptic thalamic activity.
Brain Stimulation. 2021 Jul 1;14(4):861-72.

Jansen NA, Perez C, Schenke M, van Beurden AW, Dehghani A, Voskuyl RA, Thijs RD, Ullah G, van den Maagdenberg AM, Tolner EA. Impaired θ-γ coupling indicates inhibitory dysfunction and seizure risk in a Dravet syndrome mouse model.
Journal of Neuroscience. 2021 Jan 20;41(3):524-37.

Jansen NA, Dehghani A, Breukel C, Tolner EA, van den Maagdenberg AM. Focal and generalized seizure activity after local hippocampal or cortical ablation of Na_V1. 1 channels in mice.
Epilepsia. 2020 Apr;61(4):e30-6.

Jansen NA, Dehghani A, Linssen MM, Breukel C, Tolner EA, van den Maagdenberg AM. First FHM3 mouse model shows spontaneous cortical spreading depolarizations.
Annals of Clinical and Translational Neurology. 2020 Jan;7(1):132-8.

Jansen NA, Schenke M, Voskuyl RA, Thijs RD, van den Maagdenberg AM, Tolner EA. Apnea associated with brainstem seizures in *Cacna1a*^{S218L} mice is caused by medullary spreading depolarization.
Journal of Neuroscience. 2019 Nov 27;39(48):9633-44.

Loonen IC*, **Jansen NA***, Cain SM*, Schenke M, Voskuyl RA, Yung AC, Bohnet B, Kozlowski P, Thijs RD, Ferrari MD, Snutch TP. Brainstem spreading depolarization and cortical dynamics during fatal seizures in *Cacna1a* ^{S218L} mice.
*Brain. 2019 Feb 1;142(2):412-25. (*Shared first authors)*

Jansen NA, Giesler Jr GJ. Response characteristics of pruriceptive and nociceptive trigeminoparabrachial tract neurons in the rat.
Journal of Neurophysiology. 2015 Jan 1;113(1):58-70.

DANKWOORD

Punt. Het afronden van een thesis tijdens andere (klinische) werkzaamheden valt soms tegen, maar bij vlagen kon ik ervan genieten. Dit resultaat was er nooit geweest zonder onderstaanden, met wie ik heb samengewerkt, gediscusseerd en gestreden. Maar ook dat laatste kan motiveren.

Arn, onderzoek doen in jouw groep betekende voor mij regelmatig zwemmen, aftasten, discussiëren, even escaleren en weer terug aan tafel. Jouw passie voor onderzoek, je openheid en je humor maakte altijd veel goed. *Else*, als co-promotor heb jij niet zelden ons drieën (weer) aan die tafel gekregen. Ik wil jullie beiden bedanken voor het grote vertrouwen en de vrijheid die ik de afgelopen jaren heb gekregen.

Maarten, zonder jou was dit een heel kort proefschrift geworden. Ik weet dat ik veel van jouw (vaste) handen heb gevraagd. Meermaals heb ik collega's met bewondering voor de lastige experimenten naar jou mogen verwijzen. En dan waren er nog die perioden waarin mijn plannen wekelijks veranderden, en ik je vroeg om de agenda van je werkelijke werkgever maar even te parkeren. Je snapt dat sinds mijn vaderschap, mijn bewondering voor jou – als vader van 4 dochters – natuurlijk alleen maar groter is geworden.

Ook de andere collega's op de afdeling Humane Genetica ben ik dank verschuldigd: *Sandra*, jouw organisatiekracht vertaalde zich in uitgebreide excel-sheets, maar ook in een fantastische winstersport met het lab. Je bent een stabiele kracht die zich niet gek laat maken. *Rob*, bedankt voor al je hulp met de gedragsanalyses. Je geduld is bewonderenswaardig (ik hoop dat dat met de jaren komt). *Ludo* († 2022), je was een man met een waanzinnig groot hart. Een grote inspirator voor hoe het leven geleefd kan worden. *Inge, Inge, Thijs, Thijs,* als (vroege) collega's hebben jullie me uitgelegd hoe de hazen in het lab liepen. *Thijs*, zonder jouw Matlab-enthousiasme was dat van mij wellicht (te) laat op gang gekomen, signaalanalyse werd daarna zowaar een passie. Daarbij bedank ik ook graag de (LUMC en TU Delft) studenten die ik heb mogen begeleiden; *Anouk*, speciale dank voor jouw waardevolle bijdrage aan de signaalanalyses. *Susana, Danesh, Michel, Thas,* overige collega's op de afdeling, bedankt voor de gezelligheid en positieve sfeer op de afdeling en tijdens de borrels en kerstlunches.
Collega's van de radiologie, ook al is het aandeel radiologie in dit proefschrift vrij beperkt, bedankt dat ik er soms met jullie over kon praten. Daarmee bedank ik ook graag de opleiders in het *Maasstad* en *Erasmus MC* voor het geduld.

Andreas, Massimo, Ghanim, Roland, it was great to collaborate with you. Thank you for the scientific discussions, constructive feedback and support during the completion of the work presented here.

A

Lieve *vrienden*, bedankt voor de afleiding, maar ook voor de (ongetwijfeld soms geveinsde) interesse in dit werk. *DVC'ers*, wat zijn de fysieke en mentale uitstapjes, discussies over artsenleed, wetenschap en vaderschap met jullie toch heerlijk. *Kay*, als studievriend van het eerste uur heb je me geënthousiasmeerd voor de interventieradiologie, een keuze waar ik tot op heden weinig spijt van heb. Jouw vindingrijkheid en onderzoeksdrang maakt je een hele fijne paranymph. *Pelle*, nog zo'n studievriend van het eerste uur, stiekem heb ik heel veel van dit werk met je besproken. Je zal jezelf een complete leek noemen, maar ik ben dankbaar dat je jouw kijk op de zaken met me deelt. *Tinus* (over complete leken gesproken), zo langzamerhand zijn we wel vanzelfsprekendheden (of antithesen) voor elkaar geworden, en wat is het toch heerlijk om samen met de mannen te kunnen baden in de zelfspot.

Lieve *familie*, veel dank voor de interesse, steun en liefde deze jaren. *Mam*, *pap, Iris* en *Geert, Yvette* en *Chris*: misschien doe ik het liever allemaal zelf, maar als nood aan de man is weet ik waar ik moet zijn. Afgelopen jaar begon voor ons, maar ook voor jullie, loodzwaar en dat heeft de gesprekken er niet makkelijker op gemaakt, maar wel betekenisvol. Lieve *schoonfamilie*, bedankt voor de steun, met name ook het afgelopen jaar.

Lieve *Eva*, mijn beste vriend. Geduchte rivaal geworden tot medestrever. We zijn al lang een paartje, inmiddels zijn we covalent gebonden. Ik moet mezelf er soms aan herinneren dat het uniek is om zoveel gedeelde interesses met je partner te hebben. De creativiteit en daadkracht voor het academische werk kunnen we beiden goed opbrengen, maar met je pragmatische en verbindende benadering zie ik jouw academische carrière rooskleuriger in (het gat is lang geleden al geslagen). We hebben een fantastische dochter, die al jouw vuur heeft. Begin afgelopen jaar zijn we diep beschadigd geraakt door de stilgeboorte van onze zoon. Die onvoorstelbare pijn had ik je nooit willen laten ervaren, maar wat voel ik me sterk met zo'n vrouw. Je ziet jezelf misschien niet als een moederlijk figuur, maar wat ben je een fantastisch veelzijdige moeder. Er komen spannende tijden aan, gelukkig kunnen we samen alles hebben.